

# Study of Peristaltic Flows of non-Newtonian Fluids



*By*

**Arshad Riaz**

*Supervised by*

**Dr. Rahmat Ellahi**

*Co-Supervised by*

**Dr. Sohail Nadeem**

**Department of Mathematics and Statistics  
Faculty of Basic and Applied Sciences  
International Islamic University, Islamabad  
Pakistan  
2014**

Accession No. TH-13681

K  
ds

phd  
510  
ARS

size  
paper  
11x14  
small

**DATA ENTERED** \*

Mathematics

Finite mathematics

# **Study of Peristaltic Flows of non-Newtonian Fluids**



*By*

**Arshad Riaz**

**Department of Mathematics and Statistics  
Faculty of Basic and Applied Sciences  
International Islamic University, Islamabad  
Pakistan  
2014**

# **Study of Peristaltic Flows of non-Newtonian Fluids**

*By*

**Arshad Riaz**

*A Thesis  
Submitted in the Partial Fulfillment of the  
Requirements for the Degree of  
DOCTOR OF PHILOSOPHY IN  
MATHEMATICS*

*Supervised by*

**Dr. Rahmat Ellahi**

*Co-Supervised by*

**Dr. Sohail Nadeem**

**Department of Mathematics and Statistics  
Faculty of Basic and Applied Sciences  
International Islamic University, Islamabad  
Pakistan  
2014**

# Certificate

## Study of Peristaltic Flows of non-Newtonian Fluids


By


**Arshad Riaz**

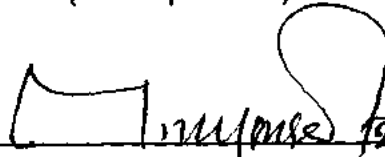
A THESIS SUBMITTED IN THE PARTIAL FULFILLMENT OF THE REQUIREMENTS FOR  
THE DEGREE OF THE **DOCTOR OF PHILOSOPHY IN MATHEMATICS**


We accept this thesis as conforming to the required standard


1.   
Dr. Rahmat Ellahi  
(Supervisor) 29/8/2014

2.   
Dr. Sohail Nadeem  
(Co-Supervisor)

3.   
Prof. Dr. Azad Akhter Siddiqui  
(External Examiner)

4.   
Prof. Dr. Malik Muhammad Yousaf  
(External Examiner) 19/8/2014

5.   
Dr. Ambreen Afsar Khan  
(Internal Examiner)

6.   
Dr. Irshad Ahmad Arshad  
(Chairman)

**Department of Mathematics and Statistics**  
**Faculty of Basic and Applied Sciences**  
**International Islamic University, Islamabad**  
**Pakistan**  
**2014**

## Declaration

I hereby declare and affirm that this research work neither as a whole nor as a part has been copied out from any source. It is further declared that I have developed this research work entirely on the basis of my personal efforts. If any part of this thesis is proven to be copied out or found to be a reproduction of some other, I shall stand by the consequences.

Moreover, no portion of the work presented in this thesis has been submitted in support of an application for other degree or qualification in this or any other university or institute of learning.

Name and signature of student: \_\_\_\_\_



Arshad Riaz  
PhD (Mathematics)

# **Dedication**

*I dedicate my thesis*

*To*

*My family*

*Especially*

*My mother,*

*My beloved uncle Prof. hafiz Maqbool Hussain*

*And*

*Respected Prof. Husain Ahmad Malik.*

## Acknowledgements

First of all, I pay my special thanks to the creator of mankind, the everlasting Allah, who gave us this life, taught us everything we did not know, granted us health, knowledge and intelligence to extract the hidden realities in the universe through scientific and critical approach. I just want to add this verse ﴿أَقْرَأْ بِاسْمِ رَبِّكَ الَّذِي خَلَقَ﴾, start learning with the name of Almighty Allah and you will find the right way you even never expected. I thank the lord Almighty with whose kindness I have achieved this very important goal in my life. I offer salutations upon the Holy Prophet, Hazrat Muhammad (PBUH) who has lightened the life of all mankind with His guidance. He is a source of knowledge and blessings for the entire creations. His teachings make us to ponder and to explore this world with directions of Islam.

I express my profound gratitude to my respectable supervisor Dr. Rahmat Ellahi and co-supervisor Dr. Sohail Nadeem, who helped me through my PhD with his cooperative guidance and guide me to complete my thesis. Their many valuable comments and suggestions put me on the straight path when I was led astray. I also pay my regards to all my teachers who always directed me to right dimensions and made it possible for me to achieve an attractive goal.

I would like to thank all my friends specially Dr. Ahmad Zeeshan, Mr. Shafiq ur Rahman, Mr. Arshad Siddiqui, Mr. Tahir Shabbir, Mr. Nouman Ejaz, Mr. Irfan Mustafa, Dr. Noreen Sher Akbar, Mr. Tayyab Hussain, Mr. Rashid, Mr. Rizwan, Mr. Aziz ur Rahman, Mr. Salman, Mr. Bilal Ashraf, Mr. Fahad Abbasi, Mr. Azad Hussain and Mr. Ashfaq who always helped me during my studies in all respects.

I cannot forget the most affectionate and loving personality my Mamoo Prof. Hafiz Maqbool Hussain who contributed a lot to made my life prosperous and to arrive at such a tremendous stage. His valuable guidance and financial support are the foundations of my career. May he live long....Aameen.

I offer my obligations to my dear uncle Prof. Hussain Ahmad Malik who always motivates me to look forward and achieve my destination. His kindness and love will always be the pivot of my thoughts.

I extend my gratitude to my family for encouragement and support, even in the gloomiest of times. I cannot express enough love and appreciation to my mother who showered her everlasting love, care and support throughout her life trying to remove the hurdles of my life. Her prayers have always been my driving source and whose sustained hope led me to where I am today.

I am also very thankful to Higher Education Commission, Pakistan for providing me scholarship through Indigenous 5000 PhD Fellowship Program without which it would not be possible for me to complete my higher studies.

*Arshad Riaz*



# Preface

Peristalsis accounts for pumping fluids that deals with the propagation of sinusoidal waves which enforces the food to protrude from mouth to esophagus. In the urinary system, peristaltic procedure occurs due to inadvertently muscular contractions of the ureteral wall which pumps urine from kidneys to bladder through ureters. It includes general propulsive and mixing movements and pumps the fluids against pressure rise. In physiology, peristaltic phenomenon is an immanent adjective of smooth muscle contraction. The mechanism of peristalsis is instructive in large number of biological schemes comprising the movement of chyme in the gastrointestinal tract, blood circulation in small blood vessels and in the ducts efferent of the male reproductive tract. In industrial field, the phenomenon of peristaltic pumping suggests various suitable applications such as transfer of sanitary fluids, blood pump in heart lung machine etc. A most prominent application of peristaltic pumping is in the manufacturing of roller pumps in order to pumping fluids without being distorted in contact with the pumping apparatus. Keeping all above valuable applications in mind, mathematical analysis of peristaltic flows of various non-Newtonian fluid models are presented in this thesis. All problems are solved in dimensionless form with the help of exact, analytical and numerical methods. Governing equations are reduced under the implementation of long wavelength and low Reynolds number. Solutions for streamlines are found analytically and discussed through graphs. Obtained results are also compared with the existing literature through tables and graphs. All pertinent parameters are discussed through graphs of velocity, pressure rise, pressure gradient and streamlines. To intertwine above discussion, the present thesis is organized in the following manner.

Chapter one is based on the brief introduction of peristaltic flows. The mathematical models of various non-Newtonian fluids are presented. Some basic definitions, governing equations and analytical schemes are also incorporated.

In Chapter two, the series solutions of magnetohydrodynamic peristaltic flow of Jeffrey fluid in eccentric cylinders are discussed. This chapter comprises the mathematical modelling of magnetohydrodynamic peristaltic flow of Jeffrey fluid in the gap between two eccentric tubes in the presence of applied magnetic field. The Navier-Stokes equations for Jeffrey fluid in three dimensional flows are discussed in a cylindrical coordinates. The analytical solutions are obtained with the help of homotopy perturbation method along with eigen function expansion method. The graphs of pressure rise, pressure gradient and velocity are drawn. The streamlines are presented to discuss the trapping bolus discipline.

Chapter three contains mathematical and theoretical analysis of peristaltic flow of Jeffrey fluid in a rectangular duct having compliant walls. The constitutive equations are solved by using eigen function expansion method. The graphical aspects of all pertinent parameters are analyzed. The graphs of velocity for two and three dimensional flow are plotted. The trapping bolus phenomenon is discussed through streamlines.

Chapter four deals with exact solution for peristaltic flow of Jeffrey fluid in a cross section of three dimensional rectangular duct in the presence of slip at the boundaries. Exact solutions of obtained

linear boundary value problem are presented. However, the expression for pressure rise is calculated by numerical integration. All pertinent parameters are discussed through graphs.

Chapter five is devoted to the study of unsteady peristaltic flow of an incompressible Carreau fluid in eccentric cylinders. The problem is measured in cylindrical coordinates. The obtained highly nonlinear second order partial differential equations are solved by perturbation technique. The relation for pressure rise is evaluated numerically. As a special case, present results are compared with the existing results. The obtained results are plotted to see the influence of different physical parameters on velocity, pressure gradient and pressure rise expressions. The velocity profile is drawn both for two and three dimensions. The trapping boluses are also discussed through streamlines.

In chapter six, heat and mass transfer analysis for peristaltic flow of nanofluid through eccentric cylinders is discussed under the approximations of long wavelength and low Reynolds number. The resulting governing equations are solved analytically by employing the homotopy perturbation method. The obtained expressions for velocity, temperature and nanoparticle phenomenon are discussed through graphs for two and three dimensions. The resulting relations for pressure gradient and pressure rise are plotted for various pertinent parameters. The streamlines are drawn for sundry quantities to discuss the trapping phenomenon.

In chapter seven, the study of chapter six is extended by importing the porous medium effects. Analytical solutions are calculated through homotopy perturbation method. The expression of pressure rise is obtained through numerical integration. The problems under consideration are made dimensionless not only to reduce the complication of the analysis but also to merge the extra parameters. The effects of all emerging parameters are measured through sketching graphs. Trapping bolus scheme is also presented through streamlines for various pertinent quantities.

Chapter eight contains the final results of the whole study.

# Contents

<b>1</b>	<b>Introduction</b>	<b>7</b>
1.1	Some historical background . . . . .	7
1.2	Governing equations for fluid motion . . . . .	14
1.2.1	Law of conservation of mass . . . . .	14
1.2.2	Law of conservation of momentum . . . . .	15
1.3	Governing equations for nanofluid . . . . .	16
1.3.1	Law of conservation of mass . . . . .	16
1.3.2	Law of conservation of momentum . . . . .	17
1.3.3	Energy equation . . . . .	17
1.4	Jeffrey fluid . . . . .	18
1.5	Carreau fluid . . . . .	18
1.6	Porosity . . . . .	19
1.7	Boundary slip . . . . .	19
1.8	Magnetohydrodynamics . . . . .	20
1.9	Methods for solutions . . . . .	21
1.9.1	Eigen function expansion method . . . . .	22
1.9.2	Homotopy perturbation method . . . . .	24
<b>2</b>	<b>Magnetohydrodynamic peristaltic flow of a Jeffrey fluid in eccentric cylinders</b>	<b>26</b>
2.1	Mathematical formulation of the problem . . . . .	27
2.2	Solution of the problem . . . . .	30
2.3	Graphical results and discussion . . . . .	33

<b>3</b>	<b>Peristaltic flow of a Jeffrey fluid in a rectangular duct having compliant walls</b>	<b>49</b>
3.1	Mathematical formulation of the problem . . . . .	49
3.2	Solution of the problem . . . . .	53
3.3	Graphical results and discussion . . . . .	54
<b>4</b>	<b>Exact solution for peristaltic flow of Jeffrey fluid model in a three dimensional rectangular duct having slip at the walls</b>	<b>64</b>
4.1	Mathematical formulation of the problem . . . . .	65
4.2	Solution of the problem . . . . .	67
4.3	Graphical results and discussion . . . . .	68
<b>5</b>	<b>Series solution of unsteady peristaltic flow of a Carreau fluid in eccentric cylinders</b>	<b>83</b>
5.1	Mathematical formulation of the problem . . . . .	83
5.2	Solution of the problem . . . . .	85
5.3	Graphical results and discussion . . . . .	89
<b>6</b>	<b>Effects of heat and mass transfer on peristaltic flow of a nanofluid between eccentric cylinders</b>	<b>98</b>
6.1	Mathematical formulation of the problem . . . . .	98
6.2	Solution of the problem . . . . .	100
6.3	Graphical results and discussion . . . . .	104
<b>7</b>	<b>Mathematical treatment for the peristaltic flow of nanofluid through eccentric tubes comprising porous medium</b>	<b>121</b>
7.1	Mathematical formulation of the problem . . . . .	122
7.2	Solution of the problem . . . . .	122
7.3	Graphical results and discussion . . . . .	127
<b>8</b>	<b>Conclusions</b>	<b>139</b>
8.1	Concluding remarks of chapter two . . . . .	139
8.2	Concluding remarks of chapter three . . . . .	140

8.3	Concluding remarks of chapter four . . . . .	140
8.4	Concluding remarks of chapter five . . . . .	141
8.5	Concluding remarks of chapter six . . . . .	142
8.6	Concluding remarks of chapter seven . . . . .	142
	<b>Bibliography</b>	<b>144</b>

## Nomenclature

### English symbols

$a$	Height of rectangular duct
$a_1$	Radius of outer tube
$B$	Magnetic field
$B_0$	Magnetic field strength
$B_1$	Flexural rigidity of plate
$b$	Amplitude of wave
$b$	Body force
$c$	Velocity of propagation
$c_f$	Specific heat of fluid
$c_p$	Specific heat of nanoparticles
$D_1$	Coefficient of viscous damping membrane
$d$	Width of rectangular duct
$E$	Electric field
$E_1, E_2, E_3, E_4, E_5$	Elasticity parameters
$F$	Lorentz force
$G_r$	Local temperature Grashof number
$g$	Gravitational force
$h_p$	Specific enthalpy of nanoparticle material
$J$	Electrical current density
$j_p$	Diffusion mass flux for nanoparticles
$K_1$	Spring stiffness
$k$	Dimensionless porosity
$k_1$	Permeability of porous medium
$M$	Magnetohydrodynamics parameter
$m_1$	Mass per unit area
$N_b$	Brownian motion parameter
$N_t$	Thermophoresis parameter

$n$	Power law index
$P$	Pressure in fixed frame
$P_r$	Prandtl number
$p$	Pressure in wave frame
$Q$	Mean volume flow rate
$\bar{Q}$	Instantaneous volume flow rate
$q$	Embedding parameter
$R$	Radial direction in fixed frame
Re	Reynolds number
$r$	Radial direction in wave frame
$S$	Stress tensor
$T_1$	Elastic tension in membrane
$t$	Time
$U, V, W$	Velocity components in fixed frame
$V_1$	Velocity of inner tube
$We$	Weissenberg number
$u, v, w$	Velocity components in wave frame
$X, Y, Z$	Cartesian coordinates in fixed frame
$x, y, z$	Cartesian coordinates in wave frame

### Greek symbols

$\beta_1$	Boundary slip parameter
$\mu$	Viscosity
$\lambda$	Wavelength
$\rho_f$	Density of fluid
$\rho_p$	Density of nanoparticle
$\lambda_1$	Ratio of relaxation time to retardation time
$\lambda_2$	Delay time

$\gamma$	Symmetric part of velocity gradient
$\beta$	Aspect ratio
$\phi$	Amplitude ratio
$\psi$	Stream function
$\delta_0$	Dimensionless wave number
$\mathcal{L}_i, (i = 1 - 5)$	Linear operators
$\Gamma$	Time constant
$\Pi$	Second invariant strain tensor
$\tilde{H}$	Homotopy function
$\rho_p$	Density of nanoparticles
$\theta$	Cylindrical coordinate
$\bar{\theta}$	Temperature profile
$\sigma$	Nanoparticles concentration
$\delta$	Radius of inner tube
$\epsilon$	Inner tube position
$\mu_0$	Permeability of free space
$\hat{\sigma}$	Conductivity



# Chapter 1

## Introduction

### 1.1 Some historical background

Peristalsis is a pattern of pumping fluids in ducts in which a progressive wave of area contraction or expansion propagates along the length of a distensible tube containing fluid. It instigates in general propulsive and mixing movements and pumps the fluids against pressure rise. Physiologically, peristaltic phenomenon is an intrinsic attribute of smooth muscle contraction. It is an automatic and valuable scheme that drives the urine from the kidney to the bladder, food through the digestive tract, bile from the gall-bladder into the duodenum, movement of ovum in the fallopian tube and many other situations.

The process of peristalsis in human body states that after food is chewed into a swallowed bolus and travelled through the esophagus. Smooth muscles blench behind the bolus to prevent it from being followed back into the mouth, and then successive, unidirectional waves of contractions will work to quickly pushes the food into the stomach. This manner works in one direction only and its main task is to move food from the mouth into the stomach. Peristalsis is a discriminatory discipline of smooth muscle contractions that propels nutriment distally through the esophagus and intestines. It was first presented by Bayliss and Starling [1] as a type of motility in which there is contraction above and relaxation below a transported. Peristalsis is entirely unaffected by vagotomy or sympathetomy, describing its mediation by the intestine's local, intrinsic nervous system.

Peristalsis is a explanation of two particular reflexes within the enteric nervous system

that are stimulated by a bolus of foodstuff in the lumen. Mechanical distension and perhaps mucosal irritation induce afferent enteric neurons. These sensory neurons coincide with two sets of cholinergic interneurons, which exhibit two peculiar symptoms:

- (i) One group of interneurons activates excitatory motor neurons above the bolus. These neurons, which contain acetylcholine and substance, stimulate contraction of smooth muscle above the bolus.
- (ii) Another group of interneurons activates inhibitory motor neurons that stimulate relaxation of smooth muscle below the bolus. These inhibitor neurons appear to use nitric oxide, vasoactive intestinal peptide and ATP as neurotransmitters.

The mechanism of peristalsis is applicable in many biological systems including the movement of chyme in the gastrointestinal tract, blood circulation in the small blood vessels and in the ducts afferents of the male reproductive tract. Also in industry, the phenomenon of peristaltic pumping is employed in various suitable applications as transfer of sanitary fluids, blood pump in heart lung machines and also in transportation of internecine and toxic liquids to prevent inclusion with the surrounding environment. A major industrial application of peristaltic phenomenon is described in the design of roller pumps, which are used in pumping fluids without being corrupted due to the connection with the pumping equipment. A peristaltic pump (usually known as a roller pump) can be specified as positive displacement pump used for pumping a variety of fluids. Peristaltic pumps are normally applied to isolate aggressive/corrosive or sterile/clean fluids from exposed pump segments to prevent cross infectedness. They can pump problematic fluids comprising viscous, shear-sensitive and aggressive fluids. The design of the pump restrains reverse flow and syphoning without valves. Due to their isolationistic design, they are ideal for a wide range of industries and applications like aseptic filling, biopharmaceutical, brewing, ceramics, chemical, food and beverage, industrial process, mining, paint and pigments, print and packaging, pulp and paper, science and research, water & waste applications. Peristaltic tube pumps endow conscionable and programmable dosing of pharmaceuticals and chemicals, as well as in industrial printing and packaging. Incorporating accurate dosing and repeatability enable the tube pump to account the proficient addition to your manufacturing plant or laboratory. There is a smaller variety of panel mounted peristaltic

tube pumps and hose pumps for use in Original Equipment Manufacture (OEM). These are manufactured to suffice fairly into your own machinery and are found extensively in vending instruments, print presses, dish washes and chemical dosing systems. However, the peristalsis is a prominent mechanism in biological system, the first theoretical and experimental investigation of its fluid dynamics aspects was disclosed four decades ago. In real problems, the peristaltic flow problems are unsteady with moving free boundary value problems where the shape of the wave on flexible tube wall is not known a priori. But the mathematical studies on peristaltic transport presented in the literature deal with a proposed train of waves moving with successive speed on the flexible boundaries and they are analyzed either in a fixed frame or a wave frame travelling with constant velocity of the wave. In a wave frame, the moving walls represent stationary wavy walls. Moreover, the problem could be treated steady under the assumptions that the peristaltic wave train is periodic, the pressure difference about the length of the tube is consistent and the tube length is an integral multiple of the wavelength.

Due to the wide range of biological, medical and industrial applications, the peristaltic flows have been succeeded in getting more interest of many researchers including physicists, mathematicians, biologists etc. In order to sort out the analytical aspect of such flows, peristaltic transport of some basic and applicable fluids has achieved immense consideration in literature. The major obligatories were to characterize the primary fluid phenomenon of the peristaltic transport and, especially, to work out the pressure gradients generated by the wave, the flow behavior in the tube or channel due to peristalsis and the conditions for trapping. In fluid mechanics, the study of peristaltic transport starts with the assumption that the fluid is either Newtonian or non-Newtonian. This reveals that a constitutive relation is employed which deals in relating the stress tensor with pressure and velocity gradients. The equations concerning the law of conservation of mass and momentum with the constitutive equation for a Newtonian fluid provide the well known Navier-Stokes equations, which justifies the mathematical treatment of a motion of fluid after deformation by applied stress/stresses. Some studies on the topic of Newtonian and non-Newtonian fluid can be cited in [2 – 33]. In the beginning, analyses of peristaltic flows were incorporated by theoretical assumptions such as periodic, sinusoidal wave trains in infinitely long tubes or channels, having long wavelength or low Reynolds number.

Yin and Fung [34] have analyzed the peristaltic waves in circular cylindrical tubes by taking

a viscous fluid flow problem induced by an axisymmetric traveling sinusoidal wave of moderate amplitude imposed on the wall of a flexible tube and presented the perturbation solution by taking the amplitude ratio (ratio of wave amplitude to radius of the tube) as a small parameter. They have shown that the mean axial velocity is dominated by two terms. One term corresponds to a parabolic profile which is due to the mean pressure gradient imposed by the wall motion. The other term comes from meeting the no-slip boundary condition at the wavy wall rather than at the mean position of the wall. They also revealed that if the mean pressure gradient approaches a certain positive critical value, the velocity diminishes to zero on the axis and relatively larger values of the mean pressure gradient will account for reverse flow in the fluid. After one year later, Burns and Parkes [35] have investigated the peristaltic flow of a viscous fluid through axial symmetric pipes and symmetrical channels with the approximations of low Reynolds number and long wavelength. The solutions are obtained by an asymptotic expansion, used for the stream function in powers of the amplitude ratio by assuming the amplitude ratio to be small. They described the effects of pressure gradient in their work. Srivastava and Srivastava [36] studied the problem of peristaltic transport of a fluid under the same assumptions as employed in above studies. They distributed the study in three parts. In first part, they presented a solution for a fluid with variable viscosity in a tapered tube. In second part, the solution was applied for plane and axisymmetric geometry, while in third one, the solution is extended to model biological fluid problems. In the present century, the researchers are also keen to enhance the theoretical and experimental investigations of peristaltic flows as these flows have become essential part in the progress and development of biomedical and industrial fields. Afifi and Gad [37] have described the interaction of peristaltic flow with pulsatile magneto-fluid through a porous medium. They considered the viscous incompressible fluid under the effect of a transverse magnetic field through a porous medium between infinite parallel walls with the imposition of a sinusoidal wave travelling on the walls. Later on, Misra and Pandey [38] have presented the mathematical model for the peristaltic transport of blood in small vessels by treating blood as a two-layer fluid where the core region is described by Casson model and the peripheral region is taken to be Newtonian. They found that the viscosity of the peripheral layer increases the flow rate. They also extracted that a thinner peripheral layer enhances the flow rate, while it starts decreasing when the yield stress increases and the flow-rate in the case

of a single layer is higher than the two layer flow-rate provided that the peripheral layer has more viscosity than the core layer. After a couple of years, Mekheimer [39] has investigated the peristaltic flow of blood under effect of a magnetic field in a non-uniform channels with the conditions of low Reynolds number along with long wavelength. He has considered the blood as viscous, incompressible and electrically conducting couple-stress fluid and given that the pressure rise for a couple stress fluid (as a blood model) is larger than that for a viscous Newtonian fluid and seen smaller for a magnetohydrodynamic fluid than for a fluid which is not electrically conducting. Nadeem and Akbar [40] have observed the effects of heat transfer on the peristaltic transport of MHD Newtonian fluid with variable viscosity. They have obtained the exact solution for temperature profile and velocity field is achieved by Adomian decomposition method (ADM) along with the numerical solutions as well.

In all above mentioned studies, the flow problems are considered in two dimensional geometries (tube/channels). However, the studies regarding the three dimensional peristaltic flows have a very little amount of literature due to the complexity of highly nonlinear partial differential equations which often occur for the case of non-Newtonian models in three dimensional geometries (channel/tube). Only a small number of researchers are keen to work on peristaltic flow problems which deal with the three dimensional investigation. Reddy et al. [41] have introduced the influence of lateral walls on peristaltic flow in a rectangular duct under the same theoretical restrictions as taken by the researchers in above mentioned studies. They have taken the concept that the sagittal cross section of the uterus may be better approximated by a tube of rectangular cross section than a two-dimensional channel. The experimental investigation has been taken into account by Aranda et al. [42] in which they presented the Stokesian peristaltic pumping in a three-dimensional tube with a phase shifted asymmetry. They employed a computational model of peristaltic pumping of a viscous fluid in three dimensions based upon the method of regularized Stokeslets. They evaluated the result that the maximum mean flow rate is achieved for the parameter that results in an axisymmetric tube. They also made a comparison of their computational results with classical long-wavelength theory for the three-dimensional axisymmetric tube to work out the validity of the technique. Two years ago, Mekheimer et al. [43] have made analysis regarding effect of lateral walls on peristaltic flow through an asymmetric rectangular duct. They have found the exact solutions of the problem

under the constraints of long wave length and low Reynolds number and measured the effects of aspect ratio (relating variation of lateral walls) on the rheological aspects of the viscous fluid. More recently, Akram et al. [44] have presented the influence of lateral walls on peristaltic flow of a couple stress fluid in a non-uniform rectangular duct to sort out the theoretical study of peristaltic flow in a three dimensional enclosure and got the exact series solution. They considered the flow in a wave frame of reference moving with the uniform velocity away from the fixed frame and peristaltic waves produced on the horizontal walls of a non-uniform rectangular duct are justified under lubrication approach. They have illustrated the graphical results for the flow phenomenon and also discussed the circulating bolus scheme. Some more studies on the topic of peristaltic flows of Newtonian and non-Newtonian fluids are given in [45 – 56].

A material having pores (voids) is described as porous medium filled with fluid (liquid or gas). Some of the nature provided porous media include beach sand, sandstone, lime stone, rye bread, wood, and the human lung. However, foams are often also characterized using theme of porous media. Most of the time, a porous medium is described by its porosity and some times the other properties like permeability, tensile strength and electrical conductivity are also measured as a respective aspects of its constituents (solid matrix and fluid) and the pores structure. The porosity of the porous medium is stated as the fraction of the volume of pores to the volume of the medium. The mathematical expression regarding porosity has been described by Henry Darcy and known as Darcy's law after an experimental investigation. He has evaluated a mathematical relationship between flow rate and applied pressure gradient. A lot of literature is available which deals with the study of porous medium. Mekheimer and Elmaboud [57] have discussed the theoretical analysis for peristaltic flow through a porous medium in an annulus under the constraints of low Reynolds number and long wavelength approximation. They considered the flow phenomenon in a wave frame of reference moving with constant velocity. They have concluded from their analysis that the peristaltic pumping rate and pressure gradient vary inversely with the corresponding increase in the numerical value of permeability of porous medium. They also found that the velocity of the fluid increases as permeability of the porous medium increases. Three years later, Vasudev et al. [58] have presented the peristaltic flow of a Newtonian fluid through a porous medium in a vertical tube under the effect of a magnetic field. They found the effects of heat transfer and magnetic field

of viscous incompressible Newtonian fluid by calculating closed form analytical solutions under same assumptions as employed by Mekheimer and Elamaboud [57]. They revealed that the pumping region, the time-averaged volume flux decreases with an increase in Darcy number. In the same year, Mahmoud et al. [59] have published the work on effect of porous medium and magnetic field on peristaltic transport of a Jeffrey fluid in an asymmetric channel. The expressions for the stream function and pressure gradient are found analytically while numerical investigation is used to analyze the pumping phenomenon.

In nanotechnology, a particle means a small object presenting a whole unit according to its movement and attributes. Particles are again recognized with diameter, as coarse particles have a range between 10,000 and 2,500 nanometers, fine particles are measured between 2,500 and 100 nanometers and nanoparticles or ultrafine particles lie between size of 1 and 100 nanometers. A base fluid comprising the particles of nano-meter sized is identified as nanofluid (NF). Nanotechnology has immense contribution in industry since materials of nanometers dimension examine incomparable physical and chemical characteristics. Water, ethylene glycol and oil are common examples of base fluids used for the nanofluid phenomenon. Nanofluids have their enormous applications in heat transfer, like microelectronics, fuel cells, pharmaceutical processes, and hybrid-powered engines, domestic refrigerator, chiller, nuclear reactor coolant, grinding and space technology etc. Nanofluids explore enhanced thermal conductivity and the convective heat transfer coefficient counter balanced to the base fluid. Nanofluid have attracted the attention of many researchers for new production of heat transfer fluids in heat exchangers, in plants and in automotive cooling significations, due to their extensive thermal properties. A large amount of literature is available which deals with the study of nanofluid and its applications [60, 61]. In the recent time, the interaction of nanoparticles phenomenon in peristaltic flows has become the core of attention for many researchers, engineers, mathematicians, modelers and scientists due to the wide range of applications of nanoparticles in the field of peristaltic pumping. Nadeem and Maraj [62] have investigated the mathematical analysis for peristaltic flow of nanofluid in a curved channel with compliant walls. They reduced the highly nonlinear, partial differential equations by using the wave frame transformation, long wave length and low Reynolds number assumptions. Peristaltic flow of a nanofluid in a non-uniform tube have been produce by Akbar et al. [63]. They have found the numerical data for the graphical results of

pressure rise and frictional forces with the help of numerical integration.

## 1.2 Governing equations for fluid motion

In order to describe the physical behavior of the fluid flow, one needs to have some mathematical relations. In fluid mechanics, we have three basic laws which account for the motion of the fluid and those are recognized as law of conservation of mass, momentum and energy. These laws in their mathematical form gives the relations for rate of change of mass, momentum and energy at a point and are explained as below.

### 1.2.1 Law of conservation of mass

This law states that the mass of the closed system always remains constant with time, as mass of the system cannot change quantity except being added or removed. It means that the quantity of mass is conserved over time. The mathematical relation expressing law of conservation of mass is known as continuity equation. For compressible fluid, it is defined as

$$\frac{d\rho}{dt} + \rho_f \nabla \cdot \mathbf{V} = 0. \quad (1.1)$$

Here,  $\rho_f$  is the density of the fluid,  $d/dt$  is the material time derivative,  $\mathbf{V}$  is the velocity field and  $\nabla$  is the gradient operator. In Cartesian coordinates, material time derivative is defined as

$$\frac{d}{dt} = \frac{\partial}{\partial t} + \mathbf{V} \cdot \nabla. \quad (1.2)$$

So the Eq. (1.1) will take the following form

$$\frac{\partial \rho_f}{\partial t} + \nabla \cdot \rho_f \mathbf{V} = 0. \quad (1.3)$$

For an incompressible fluid, the density remains stable and therefore, the continuity equation becomes

$$\nabla \cdot \mathbf{V} = 0. \quad (1.4)$$



In Cartesian coordinates, the above equations is written as

$$\frac{\partial U}{\partial X} + \frac{\partial V}{\partial Y} + \frac{\partial W}{\partial Z} = 0. \quad (1.5)$$

In which  $U, V, W$  are the velocity components in  $X, Y, Z$  directions, respectively.

### 1.2.2 Law of conservation of momentum

This law is defined as the total momentum of an isolated system is always conserved. The equations which describe this law mathematically are called as Navier–Stokes equations. In general, these equation are composed in the subsequent form

$$\rho_f \left( \frac{\partial \mathbf{V}}{\partial t} + \mathbf{V} \cdot \nabla \mathbf{V} \right) = -\nabla P + \nabla \cdot \mathbf{S}_1 + \rho_f \mathbf{b}, \quad (1.6)$$

where,  $P$  is the pressure,  $\mathbf{S}_1$  denotes the Cauchy stress tensor and  $\mathbf{b}$  represents the body force. It is to important to mention that the Cauchy stress tensor implies the nature of the fluid.

For Newtonian fluid,  $\mathbf{S}_1$  is defined as

$$\mathbf{S}_1 = \mu \mathbf{A}_1, \quad (1.7)$$

where

$$\mathbf{A}_1 = \nabla \mathbf{V} + (\nabla \mathbf{V})^t. \quad (1.8)$$

In component form

$$\mathbf{S}_1 = \begin{pmatrix} S_{1XX} & S_{1XY} & S_{1XZ} \\ S_{1YX} & S_{1YY} & S_{1YZ} \\ S_{1ZX} & S_{1ZY} & S_{1ZZ} \end{pmatrix}. \quad (1.9)$$

In above expression,  $S_{1XX}, S_{1YY}, S_{1ZZ}$  are normal stresses and  $S_{1XY}, S_{1XZ}, S_{1YX}, S_{1YZ}, S_{1ZX}, S_{1ZY}$  are the shear stresses regarded as components of  $\mathbf{S}_1$ . In Cartesian coordinates, for Newtonian fluid, Navier–Stokes equations (neglecting body forces) take the following form

$$\rho_f \left( \frac{\partial U}{\partial t} + U \frac{\partial U}{\partial X} + V \frac{\partial U}{\partial Y} + W \frac{\partial U}{\partial Z} \right) = -\frac{\partial P}{\partial X} + \mu \left( \frac{\partial^2 U}{\partial X^2} + \frac{\partial^2 U}{\partial Y^2} + \frac{\partial^2 U}{\partial Z^2} \right), \quad (1.10)$$

$$\rho_f \left( \frac{\partial V}{\partial t} + U \frac{\partial V}{\partial X} + V \frac{\partial V}{\partial Y} + W \frac{\partial V}{\partial Z} \right) = -\frac{\partial P}{\partial Y} + \mu \left( \frac{\partial^2 V}{\partial X^2} + \frac{\partial^2 V}{\partial Y^2} + \frac{\partial^2 V}{\partial Z^2} \right), \quad (1.11)$$

$$\rho_f \left( \frac{\partial W}{\partial t} + U \frac{\partial W}{\partial X} + V \frac{\partial W}{\partial Y} + W \frac{\partial W}{\partial Z} \right) = -\frac{\partial P}{\partial Z} + \mu \left( \frac{\partial^2 W}{\partial X^2} + \frac{\partial^2 W}{\partial Y^2} + \frac{\partial^2 W}{\partial Z^2} \right). \quad (1.12)$$

For non-Newtonian fluid, there are a lot of models having different forms of Cauchy tensor which represents the physical properties of the corresponding fluid.

### 1.3 Governing equations for nanofluid

We can measure the nanofluid phenomenon with the help of four equations (two mass equations, one momentum equation and one energy equation).

#### 1.3.1 Law of conservation of mass

This law is defined by the equation of continuity which for nanofluid is defined in [64] and is described as

$$\left( \frac{\partial C}{\partial t} + \mathbf{V} \cdot \nabla C \right) = -\frac{1}{\rho_p} \nabla \cdot \mathbf{j}_p, \quad (1.13)$$

where  $C$  is the nanoparticle concentration,  $t$  is time,  $\mathbf{j}_p$  is the diffusion mass flux for the nanoparticles ( $kg/m^2s$ ), and denotes the nanoparticle flux relative to the nanofluid velocity  $\mathbf{V}$  and  $\rho_p$  is the density of nanoparticles. If the external forces are assumed to be negligible,  $\mathbf{j}_p$  can be given as the sum of only two diffusion terms i.e., Brownian diffusion and thermophoresis

$$\mathbf{j}_p = \mathbf{j}_{p,B} + \mathbf{j}_{p,T} = -\rho_p D_B \nabla C - \rho_p D_T \frac{\nabla T}{T_0}. \quad (1.14)$$

Substituting Eq. (1.14) into (1.13), one finds

$$\left( \frac{\partial C}{\partial t} + \mathbf{V} \cdot \nabla C \right) = \nabla \cdot \left( D_B \nabla C + D_T \frac{\nabla T}{T_0} \right). \quad (1.15)$$

Eq. (1.15) describes that the nanoparticles can move homogeneously with the fluid (second term on the left-hand side), but they also follow a slip velocity relative to the fluid (right-hand side), which is due to Brownian diffusion and thermophoresis.

### 1.3.2 Law of conservation of momentum

This law gives the equation of momentum which for nanofluid is similar to that of usual Navier-Stokes equations but in the presence of external forces which are due to heat and mass convection of nanoparticles. So the Navier-Stokes equation for nanofluid in the presence of body forces take the following form [64]

$$\rho_f \left( \frac{\partial \mathbf{V}}{\partial t} + \mathbf{V} \cdot \nabla \mathbf{V} \right) = -\nabla P + \nabla \cdot \mathbf{S}_1 + \rho_f \mathbf{g} \alpha_f (T - T_0) + \rho_f \mathbf{g} \alpha_f (C - C_0), \quad (1.16)$$

where  $\mathbf{g}$  is the gravitational force and  $\alpha_f$  represents the volumetric volume expansion coefficient of the nanofluid.

### 1.3.3 Energy equation

The energy equation for nanofluid are expressed as [64]

$$(\rho c)_f \left( \frac{dT}{dt} \right) = \nabla \cdot K \nabla T - \nabla \cdot (h_p \mathbf{j}_p) + h_p \nabla \cdot \mathbf{j}_p. \quad (1.17)$$

If we put

$$\nabla \cdot (h_p \mathbf{j}_p) = h_p \nabla \cdot \mathbf{j}_p + \mathbf{j}_p \cdot \nabla h_p \quad (1.18)$$

and

$$\nabla h_p = c_p \nabla P, \quad (1.19)$$

then the Eq. (1.17) gets the following form

$$(\rho c)_f \left( \frac{dT}{dt} \right) = \nabla \cdot K \nabla T - c_p \mathbf{j}_p \cdot \nabla T, \quad (1.20)$$

where  $c_p$  is the specific heat of nanoparticles. In above relation, when we set  $\mathbf{j}_p = 0$ , it becomes the familiar heat equation for the pure fluid. By incorporating Eq. (1.14) into Eq. (1.20), we arrive at the final form of energy equation for nanofluid

$$(\rho c)_f \left( \frac{\partial T}{\partial t} + \mathbf{V} \cdot \nabla T \right) = \nabla \cdot K \nabla T + (\rho c)_p \left( D_B (\nabla C \cdot \nabla T) + \frac{D_T}{T_0} (\nabla T \cdot \nabla T) \right), \quad (1.21)$$

in which  $(\rho c)_f$  denotes the heat capacity of the fluid,  $(\rho c)_p$  accounts for effective heat capacity of the nanoparticle. Eq. (1.21) states that heat can be transmitted in a nanofluid by convection (second term on the left-hand side), by conduction (first term on the right-hand side) and also by means of nanoparticle diffusion (second and third terms on the right-hand side). Moreover, the last two terms on the right-hand side simply stand for the additional contribution of nanoparticle motion relative to the fluid. It is to be noted that mass, momentum and energy equations for nanofluid are coupled with each other. Once the boundary and initial conditions are known we can calculate the coefficients of velocity, temperature and nanoparticle mass concentration.

## 1.4 Jeffrey fluid

The Cauchy stress tensor for Jeffrey fluid is represented as [65]

$$\mathbf{S}_2 = \frac{\mu}{1 + \lambda_1} (\dot{\boldsymbol{\gamma}} + \lambda_2 \ddot{\boldsymbol{\gamma}}), \quad (1.22)$$

where  $\lambda_1$  is the ratio of relaxation to retardation times,  $\lambda_2$  is the delay time,  $\dot{\boldsymbol{\gamma}}$  gives the symmetric part of velocity gradient and double dots denote the differentiation with respect to time.

## 1.5 Carreau fluid

The Cauchy stress tensor for Carreau fluid is defined as [66]

$$\mathbf{S}_3 = \mu \left( 1 + (\Gamma |\dot{\boldsymbol{\gamma}}|)^2 \right)^{\frac{n-1}{2}} \dot{\boldsymbol{\gamma}}, \quad (1.23)$$

in above relation,  $\Gamma$  represents the time constant,  $n$  shows the power law index and  $|\dot{\boldsymbol{\gamma}}|$  is defined as

$$|\dot{\boldsymbol{\gamma}}| = \sqrt{\frac{1}{2} \sum_i \sum_j \dot{\gamma}_{ij} \dot{\gamma}_{ji}} = \sqrt{\frac{1}{2} \Pi}. \quad (1.24)$$

Here  $\Pi$  is the second invariant strain tensors.

## 1.6 Porosity

A material having pores (voids) is described as porous medium filled with fluid (liquid or gas). Porosity measures the empty spaces in a porous medium and comes from the ratio of volume of voids over the total volume. Examples of porous media are beach sand, sandstone, lime stone, rye bread, wood, and the human lung. However, foams are often also characterized using theme of porous media. Most of the time, a porous medium is described by its porosity and some times the other properties like permeability, tensile strength and electrical conductivity are also measured as a respective aspects of its constituents (solid matrix and fluid) and the pores structure [67]. The mathematical expression regarding porosity has been described by Henry Darcy and known as Darcy's law after an experimental investigation. He has evaluated a mathematical relationship between flow rate and applied pressure gradient. Mathematically, this law is expressed as

$$\mathbf{V} = -\frac{k_1}{\mu} \nabla P, \quad (1.25)$$

where,  $\mu$  gives the dynamic viscosity of the fluid,  $k_1$  is the permeability of the medium having dimensions (length)<sup>2</sup> and in general, it describes the second order tensor. After revising the above expression, we obtain the following relation

$$\nabla P = -\frac{\mu}{k_1} \mathbf{V}. \quad (1.26)$$

## 1.7 Boundary slip

In practical engineering problems, the no-slip condition does not always hold in reality. For instance, at very low pressure (e.g., at high altitude), there may be some molecules at the wall of the surface that they bounce along down the surface. A mathematical expression for fluid slip is

$$u - u_{\text{wall}} = \beta_1 \frac{\partial u}{\partial z}, \quad (1.27)$$

where  $\beta_1$  gives the slip parameter.

## 1.8 Magnetohydrodynamics

Magnetohydrodynamics (MHD) (magneto fluid dynamics or hydromagnetics) deals with the attributes of electrically conducting fluids [68]. Plasmas, liquid metals, and salt water or electrolytes are the common examples of such fluids. The word magnetohydrodynamics (MHD) comes from magneto- meaning magnetic field, "hydro" means liquid and "dynamics" means movement. The concept of MHD was given by Hannes Alfvén [69] for which he was granted with the Nobel Prize in Physics in 1970.

The fundamental theme of MHD is that magnetic fields can induce currents in a moving conductive fluid, which in response impose forces on the fluid and also effects the magnetic field itself. The basic equations which describe MHD are a combination of the Navier-Stokes equations of fluid dynamics and Maxwell's equations of electromagnetism.

In the presence of MHD, the momentum equation will be

$$\rho_f \left( \frac{\partial \mathbf{V}}{\partial t} + \mathbf{V} \cdot \nabla \mathbf{V} \right) = -\nabla P + \nabla \cdot \mathbf{S} + \mathbf{J} \times \mathbf{B}, \quad (1.28)$$

where the term  $\mathbf{J} \times \mathbf{B}$  is the Lorentz force and can be written as

$$\mathbf{J} \times \mathbf{B} = \frac{(\mathbf{B} \cdot \nabla) \mathbf{B}}{\mu_0} - \nabla \left( \frac{B_0^2}{2\mu_0} \right). \quad (1.29)$$

Maxwell's equations can be described by the following expressions.

Solenoidal nature of magnetic field  $\mathbf{B}$

$$\nabla \cdot \mathbf{B} = 0. \quad (1.30)$$

Faraday's law

$$\nabla \times \mathbf{E} = -\frac{\partial \mathbf{B}}{\partial t}. \quad (1.31)$$

Ampere equation

$$\nabla \times \mathbf{B} = \mu_0 \mathbf{J}. \quad (1.32)$$

Charge conservation

$$\nabla \cdot \mathbf{J} = 0. \quad (1.33)$$

Lorentz force

$$\mathbf{F} = \mathbf{J} \times \mathbf{B}. \quad (1.34)$$

Ohm's law

$$\mathbf{J} = \hat{\sigma} (\mathbf{E} + \mathbf{V} \times \mathbf{B}). \quad (1.35)$$

In above equations,  $\mathbf{B}$  is the total magnetic field,  $B_0$  is the magnetic field strength,  $\mathbf{E}$  is the electric field,  $\mu_0$  is the permeability of the free space,  $\mathbf{J}$  is the current density and  $\hat{\sigma}$  is the conductivity.

## 1.9 Methods for solutions

Most of the natural processes can be effectual well elaborated on the macroscopic level, without considering the single attitude of molecules, atoms, electrons or other particles. The common properties like deformation, density, velocity, pressure, temperature, concentration or electromagnetic field are expressed by partial differential equations (PDEs) which deal with the formulation of many engineering and scientific problems. We can include some processes in which PDEs are employed to predict and control the static and dynamic attributes of constructions, blood flow in human body, flow of air past cars and airplanes, weather, thermal inhibition of tumors, heating and melting of metals, cleaning of air and water in urban facilities, burning of gas in vehicle engines, magnetic resonance imaging and computer tomography in medicine etc. Second order partial differential equations are widely used in practical problems.

In physical phenomena, PDEs (second order) occurred in three forms i.e., elliptic, parabolic or hyperbolic. The general form of a PDE of a function  $u(x_1, \dots, x_n)$  can be expressed as

$$F \left( x_1, \dots, x_n, u, \frac{\partial u}{\partial x_1}, \dots, \frac{\partial u}{\partial x_n}, \frac{\partial^2 u}{\partial x_1 \partial x_1}, \dots, \frac{\partial^2 u}{\partial x_1 \partial x_n}, \dots \right) = 0. \quad (1.36)$$

In the present thesis, the emphasize will be given on the properties and solution of hyperbolic PDEs. Most common example of hyperbolic PDE is a wave equation. A wave equation can either be linear or nonlinear depending upon the nature of the physical problem. To solve a linear PDE, several methods are available in literature; like method of separation of variable, Laplace and Fourier transform methods, Green's functions and eigen function expansion meth-

ods etc. Although, solutions of nonlinear PDEs is not an easy task. The nonlinear PDEs have a less chances to have an exact or closed form solutions. For that reason, one has to seek some approximate numerical or analytical techniques. However, the analytical solutions have more significance than numerical because they provide a way of checking the convergence and validity by getting number of approximate solutions either numerical or empirical [70, 71]. There exists a number of analytical techniques which can solve nonlinear PDEs encountered in almost all branches of science and engineering. Some of them are listed as: perturbation method, homotopy analysis method, homotopy perturbation method, Optimal homotopy method, Adomian decomposition method, Variational iteration method. But here, we will only explain the eigen function expansion method and the homotopy perturbation method which are employed in the subsequent chapters.

### 1.9.1 Eigen function expansion method

Let us consider a non-homogeneous wave equation of the form

$$\frac{\partial^2 u}{\partial y^2} + \frac{\partial^2 u}{\partial z^2} = f(z) \quad (1.37)$$

with non-homogeneous boundary conditions

$$u(\pm a, z) = -1, u(y, 0) = 0, u(y, L) = 0. \quad (1.38)$$

To solve this method, we use eigen function expansion method. We express the unknown function  $u(y, z)$  into the following series [72]

$$u(y, z) = \sum_{n=1}^{\infty} Y_n(y) \phi_n(z), \quad (1.39)$$

where  $\phi_n(z) = \sin \frac{n\pi z}{L}$ ,  $n = 1, 2, 3, \dots$  are eigen functions which satisfy the solution of Sturm-Livoilue system of homogeneous part of the given equation i.e.,

$$\frac{d^2 \phi_n(z)}{dz^2} = -\lambda_n \phi_n(z). \quad (1.40)$$



Now, using the Eq. (1.39) into Eq. (1.37) and applying term by term differentiation, one obtain the relations as

$$\sum_{n=1}^{\infty} \frac{d^2 Y_n''(y)}{dy^2} \phi_n(z) + \sum_{n=1}^{\infty} Y_n(y) \frac{d^2 \phi_n(z)}{dz^2} = f(z) \quad (1.41)$$

or

$$\sum_{n=1}^{\infty} \frac{d^2 Y_n''(y)}{dy^2} \phi_n(z) - \sum_{n=1}^{\infty} Y_n(y) \lambda_n \phi_n(z) = f(z). \quad (1.42)$$

Now we write  $f(z)$  as a Fourier series of eigen function

$$f(z) = \sum_{n=1}^{\infty} a_n \phi_n(z), \quad (1.43)$$

where the Fourier series coefficients are given by

$$a_n = \frac{2}{L} \int_0^L f(z) \phi_n(z) dz. \quad (1.44)$$

After replacing Eq. (1.43) into Eq. (1.42) and equating the coefficients, we achieve the following differential equations for the coefficients

$$\frac{d^2 Y_n''(y)}{dy^2} - \lambda_n Y_n(y) = a_n, \quad n = 1, 2, 3, \dots \quad (1.45)$$

To obtain the conditions for the differential Eq. (1.45), we utilize conditions given in Eq. (1.38) and obtain

$$-1 = \sum_{n=1}^{\infty} Y_n(\pm a) \phi_n(z), \quad (1.46)$$

such that

$$Y_n(\pm a) = -\frac{2}{L} \int_0^L \phi_n(z) dz, \quad n = 1, 2, 3, \dots \quad (1.47)$$

Now Eq. (1.45) can easily be solved along with above boundary conditions and then the final solution is obtained after using the expressions of  $Y_n(y)$  and  $\phi_n(z)$  into Eq. (1.39).

### 1.9.2 Homotopy perturbation method

The homotopy perturbation method (HPM) is a series expansion method works to evaluate solution of nonlinear partial differential equations. Main idea of the method comes from the construction homotopy function a topic from topology to generate a convergent series solution of differential equations. The HPM was first introduced by Ji-Huan He of Shanghai University in 1998. This method provides flexibility in the choice of basis functions for the solution and the linear inversion operators [73 – 76].

Let us describe the basic idea of HPM by considering the following general nonlinear differential equation

$$\mathcal{L}(u) + N(u) = f(r), \quad r \in \Omega \quad (1.48)$$

having boundary conditions

$$B(u, \partial u / \partial s) = 0, \quad r \in \tilde{\Pi}, \quad (1.49)$$

where  $\mathcal{L}$  is the linear operator,  $N$  is the nonlinear operator,  $B$  is a boundary operator,  $\tilde{\Pi}$  is the boundary of the domain  $\Omega$  and  $f(r)$  is a known analytic function.

According to the theme of homotopy process, He suggests the homotopy

$\tilde{u}(r, q) : \Omega \rightarrow \Omega \times [0, 1] \rightarrow \Re$  which satisfies

$$\tilde{H}(\tilde{u}, q) = (1 - q) [\mathcal{L}(\tilde{u}) - \mathcal{L}(u_0)] + q [\mathcal{L}(\tilde{u}) + N(\tilde{u}) - f(r)] = 0 \quad (1.50)$$

or

$$\tilde{H}(\tilde{u}, q) = \mathcal{L}(\tilde{u}) - \mathcal{L}(u_0) + q \mathcal{L}(u_0) + q [N(\tilde{u}) - f(r)] = 0, \quad (1.51)$$

in which  $q \in [0, 1]$  stands for embedding parameter and  $u_0$  is an initial approximation which obey the defined boundary conditions. Now from Eqs. (1.51), we can simply describe that for  $q \rightarrow 0$

$$\tilde{H}(\tilde{u}, 0) = \mathcal{L}(\tilde{u}) - \mathcal{L}(u_0) = 0 \quad (1.52)$$

and for  $q \rightarrow 1$

$$\tilde{H}(\tilde{u}, 1) = \mathcal{L}(\tilde{u}) + N(\tilde{u}) - f(r) = 0. \quad (1.53)$$

From above two expressions, we can obviously mention that by changing  $q$  from 0 to 1, we

convert  $\tilde{u}(r, q)$  from  $u_0(r)$  to  $u(r)$  and this process is recognized as deformation in topology. The basic approximation implies that the solution of Eq. (1.51) can be composed in a power series of the embedding parameter  $q$  i.e.,

$$\tilde{u} = \tilde{u}_0 + q\tilde{u}_1 + q^2\tilde{u}_2 + \dots \quad (1.54)$$

Now setting  $q = 1$ , one gets the final approximate solution of Eq. (1.48) i.e.,

$$u = \lim_{q \rightarrow 1} \tilde{u} = \tilde{u}_0 + \tilde{u}_1 + \tilde{u}_2 + \dots \quad (1.55)$$

## Chapter 2

# Magnetohydrodynamic peristaltic flow of a Jeffrey fluid in eccentric cylinders

In this chapter, the series solutions for magnetohydrodynamic peristaltic flow of Jeffrey fluid in the gap between two eccentric tubes has been discussed in the presence of applied magnetic field. Geometrically, two eccentric tubes are considered in which the inner tube is rigid while the tube at the outer side has a sinusoidal wave propagating along the wall. The governing equations for Jeffrey fluid in a cylindrical coordinates for three dimensional flow are given. The approximations of low Reynolds number and long wavelength have been employed to reduce the highly nonlinear partial differential equations. The problem has been solved with the help of homotopy perturbation method along with eigen function expansion method. The graphs of pressure rise, pressure gradient and velocity for two and three dimensional flow have been drawn. The streamlines have also been presented to discuss the trapping bolus discipline. Findings of this chapter are published in the journal of "*Applied Mathematics and Information Sciences*", 7 (2013) 1441–1449.

## 2.1 Mathematical formulation of the problem

The flow geometry is described as the inner tube is rigid and sinusoidal wave is travelling at the outer tube down its wall. The radius of the inner tube is  $\delta$  but we require to consider the fluid motion to the centre of the outer tube. The centre of the inner tube is now at the position  $R = \epsilon$ ,  $Z = 0$ , where  $R$  and  $Z$  are coordinates in the cross-section of the pipe. The radially varying magnetic field is applied normally to the direction of the flow. The boundary of the inner tube is described of order  $\epsilon$  by  $r_1 = \delta + \epsilon \cos \theta$ , where  $\epsilon$  is the parameter that controls the eccentricity of the inner tube position. The geometry of the walls is visualized in Fig. 2.1.

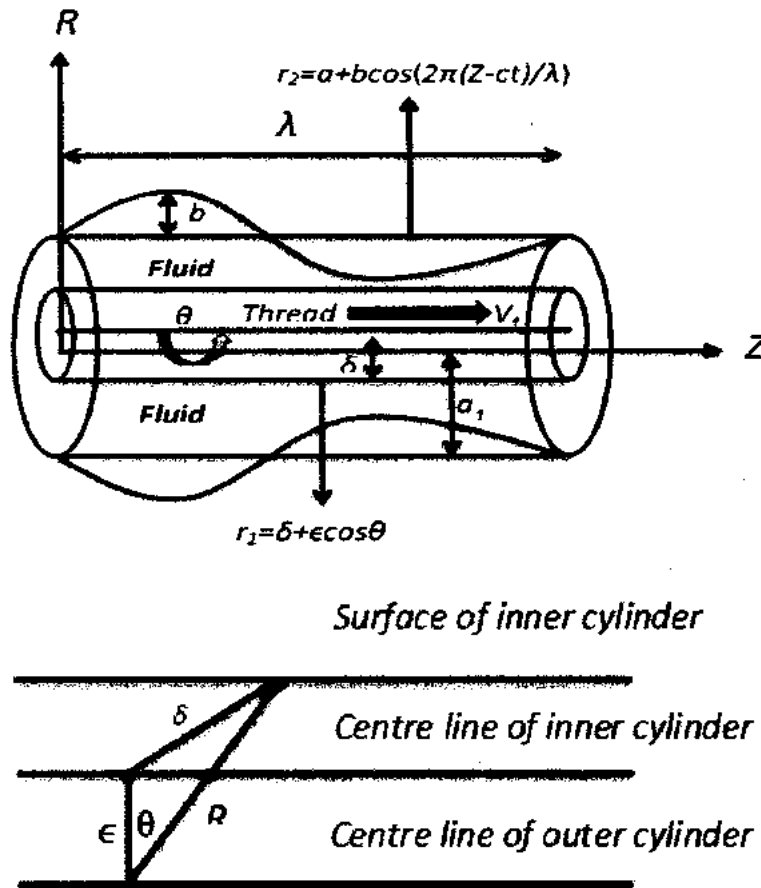


Fig. 2.1: The simplified model of geometry of the problem.

The equations for the radii are

$$r_1 = \delta + \epsilon \cos \theta, \quad (2.1)$$

$$r_2 = a_1 + b \cos \left[ \frac{2\pi}{\lambda} (Z - ct) \right], \quad (2.2)$$

where  $\delta$  and  $a_1$  are the radii of the inner and outer tubes,  $b$  is amplitude of the wave,  $\lambda$  is the wavelength,  $c$  is the propagation velocity and  $t$  is the time. The problem is considered in the system of cylindrical coordinates  $(R, \theta, Z)$  as radial, azimuthal and axial coordinates, respectively.

In the presence of MHD, the governing Eqs. (1.4) and (1.6) in component notation are as follow

$$\frac{\partial U}{\partial Z} + \frac{\partial V}{\partial R} + \frac{V}{R} + \frac{1}{R} \frac{\partial W}{\partial \theta} = 0, \quad (2.3)$$

$$\rho_f \left[ \frac{\partial V}{\partial t} + U \frac{\partial V}{\partial Z} + V \frac{\partial V}{\partial R} + \frac{W}{R} \frac{\partial V}{\partial \theta} - \frac{W^2}{R} \right] = -\frac{\partial P}{\partial R} + \frac{1}{R} \frac{\partial}{\partial R} (RS_{2RR}) + \frac{1}{R} \frac{\partial}{\partial \theta} (S_{2R\theta}) + \frac{\partial}{\partial Z} (S_{2RZ}) - \frac{S_{2\theta\theta}}{R} \quad (2.4)$$

$$\rho_f \left[ \frac{\partial W}{\partial t} + U \frac{\partial W}{\partial Z} + V \frac{\partial W}{\partial R} + \frac{W}{R} \frac{\partial W}{\partial \theta} - \frac{WV}{R} \right] = -\frac{1}{R} \frac{\partial P}{\partial \theta} + \frac{1}{R^2} \frac{\partial}{\partial R} (R^2 S_{2\theta R}) + \frac{1}{R} \frac{\partial}{\partial \theta} (S_{2\theta\theta}) + \frac{\partial}{\partial Z} (S_{2\theta Z}) \quad (2.5)$$

$$\rho_f \left[ \frac{\partial U}{\partial t} + U \frac{\partial U}{\partial Z} + V \frac{\partial U}{\partial R} + \frac{W}{R} \frac{\partial U}{\partial \theta} \right] = -\frac{\partial P}{\partial Z} + \frac{1}{R} \frac{\partial}{\partial R} (RS_{2RZ}) + \frac{1}{R} \frac{\partial}{\partial \theta} (S_{2\theta Z}) + \frac{\partial}{\partial Z} (S_{2ZZ}) - \sigma_2 B_0^2 U \quad (2.6)$$

here,  $V$ ,  $W$  and  $U$  are the velocity components in  $R$ ,  $\theta$  and  $Z$ -directions, respectively, whereas  $S_{2RR}$ ,  $S_{2R\theta}$ ,  $S_{2RZ}$ ,  $S_{2\theta\theta}$ ,  $S_{2\theta Z}$  and  $S_{2ZZ}$  are stresses for Jeffrey fluid.

According to the flow geometry, the boundary conditions are defined as

$$U = 0, \quad \text{at } R = r_2, \quad (2.7)$$

$$U = V_1, \quad \text{at } R = r_1, \quad (2.8)$$

where  $V_1$  is the uniform velocity of the inner tube. The velocity component in the azimuthal direction is assumed to be unaffected, so the velocity field is taken as  $(V, 0, U)$ .

By using the following non-dimensional parameters

$$\left. \begin{aligned} P' &= \frac{a_1^2}{\mu c \lambda} P, \quad U' = \frac{U}{c}, \quad V' = \frac{\lambda}{a_1 c} V, \quad t' = \frac{c}{\lambda} t, \quad r_1' = \frac{r_1}{a_1}, \quad \phi = \frac{b}{a_1}, \quad \delta' = \frac{\delta}{a_1}, \\ \epsilon' &= \frac{\epsilon}{a_1}, \quad \delta_0 = \frac{a_1}{\lambda}, \quad Z' = \frac{Z}{\lambda}, \quad r_2' = \frac{r_2}{a_1}, \quad \text{Re} = \frac{\rho c a_1}{\mu}, \quad M^2(r) = \frac{\sigma_2 B_0^2(r) a_1^2}{\mu}, \\ \theta' &= \theta, \quad V_1' = \frac{V_1}{c} \end{aligned} \right\}, \quad (2.9)$$

the governing Eqs. (2.3) to (2.6) (after dropping dashes) are reduced to the following form

$$\frac{\partial V}{\partial R} + \frac{V}{R} + \frac{\partial U}{\partial Z} = 0, \quad (2.10)$$

$$\left. \begin{aligned} \text{Re} \delta_0^3 \left[ \frac{\partial V}{\partial t} + U \frac{\partial V}{\partial Z} + V \frac{\partial V}{\partial R} \right] &= -\frac{\partial P}{\partial R} + \frac{\delta_0}{R} \frac{\partial}{\partial R} (R S_{2RR}) + \frac{\delta_0}{R} \frac{\partial}{\partial \theta} (S_{2R\theta}) \\ &\quad + \delta_0^2 \frac{\partial}{\partial Z} (S_{2RZ}) - \delta_0 \frac{S_{2\theta\theta}}{R} \end{aligned} \right\}, \quad (2.11)$$

$$0 = -\frac{1}{R} \frac{\partial P}{\partial \theta} + \frac{\delta_0}{R^2} \frac{\partial}{\partial R} (R^2 S_{2R\theta}) + \frac{\delta_0}{R} \frac{\partial}{\partial \theta} (S_{2\theta\theta}) + \delta_0^2 \frac{\partial}{\partial Z} (S_{2\theta Z}), \quad (2.12)$$

$$\left. \begin{aligned} \text{Re} \delta_0 \left[ \frac{\partial U}{\partial t} + U \frac{\partial U}{\partial Z} + V \frac{\partial U}{\partial R} \right] &= -\frac{\partial P}{\partial Z} + \frac{1}{R} \frac{\partial}{\partial R} (R S_{2RZ}) + \frac{1}{R} \frac{\partial}{\partial \theta} (S_{2\theta Z}) \\ &\quad + \delta_0 \frac{\partial}{\partial Z} (S_{2ZZ}) - M^2(r) U \end{aligned} \right\}. \quad (2.13)$$

where  $\phi$  is the amplitude ratio,  $\text{Re}$  is the Reynolds number,  $\delta_0$  is the dimensionless wave number and  $M(r)$  represents the radially varying MHD.

The components of non-dimensional stresses for Jeffrey fluid are evaluated as

$$\left. \begin{aligned} S_{2RR} &= \frac{2\delta_0}{1+\lambda_1} \left( 1 + \frac{\lambda_2 c \delta_0}{a_1} \left( \frac{\partial}{\partial t} + V \frac{\partial}{\partial R} + U \frac{\partial}{\partial Z} \right) \right) \frac{\partial V}{\partial R} \\ S_{2R\theta} &= \frac{\delta_0}{1+\lambda_1} \left( 1 + \frac{\lambda_2 c \delta_0}{a_1} \left( \frac{\partial}{\partial t} + V \frac{\partial}{\partial R} + U \frac{\partial}{\partial Z} \right) \right) \frac{1}{R} \frac{\partial V}{\partial \theta} \\ S_{2RZ} &= \frac{1}{1+\lambda_1} \left( 1 + \frac{\lambda_2 c \delta_0}{a_1} \left( \frac{\partial}{\partial t} + V \frac{\partial}{\partial R} + U \frac{\partial}{\partial Z} \right) \right) \left( \delta_0^2 \frac{\partial V}{\partial Z} + \frac{\partial U}{\partial R} \right) \\ S_{2\theta\theta} &= \frac{2\delta_0}{1+\lambda_1} \left( 1 + \frac{\lambda_2 c \delta_0}{a_1} \left( \frac{\partial}{\partial t} + V \frac{\partial}{\partial R} + U \frac{\partial}{\partial Z} \right) \right) \frac{V}{R} \\ S_{2\theta Z} &= \frac{1}{1+\lambda_1} \left( 1 + \frac{\lambda_2 c \delta_0}{a_1} \left( \frac{\partial}{\partial t} + V \frac{\partial}{\partial R} + U \frac{\partial}{\partial Z} \right) \right) \frac{1}{R} \frac{\partial U}{\partial \theta} \\ S_{2ZZ} &= \frac{2\delta_0}{1+\lambda_1} \left( 1 + \frac{\lambda_2 c \delta_0}{a_1} \left( \frac{\partial}{\partial t} + V \frac{\partial}{\partial R} + U \frac{\partial}{\partial Z} \right) \right) \frac{\partial U}{\partial Z} \end{aligned} \right\}. \quad (2.14)$$

Using the long wavelength approximation ( $\delta_0 \rightarrow 0$ ) and taking  $M(r) = M/R$ , Eqs. (2.11) to (2.13) are simplified to the following form

$$\frac{\partial P}{\partial R} = 0, \quad (2.15)$$

$$\frac{\partial P}{\partial \theta} = 0, \quad (2.16)$$

$$(1 + \lambda_1) \frac{\partial P}{\partial Z} = \frac{\partial^2 U}{\partial R^2} + \frac{1}{R} \frac{\partial U}{\partial R} + \frac{1}{R^2} \frac{\partial^2 U}{\partial \theta^2} - (1 + \lambda_1) \frac{M^2}{R^2} U, \quad (2.17)$$

or

$$(1 + \lambda_1) \frac{\partial P}{\partial Z} = \frac{\partial^2 U}{\partial R^2} + \frac{1}{R} \frac{\partial U}{\partial R} + \frac{1}{R^2} \frac{\partial^2 U}{\partial \theta^2} - \frac{M^2 (1 + \lambda_1)}{R^2} U. \quad (2.18)$$

where  $M$  is the MHD parameter. From Eqs. (2.15) and (2.16) it is clear that  $P$  is not a function of  $r$  and  $\theta$ .

The corresponding boundary conditions in non-dimensional form are as given below

$$U = 0, \quad \text{at } R = r_2 = 1 + \phi \cos 2\pi(Z - t), \quad (2.19)$$

$$U = V_1, \quad \text{at } R = r_1 = \delta + \epsilon \cos \theta. \quad (2.20)$$

## 2.2 Solution of the problem

Solution of Eq. (2.18) is evaluated by using homotopy perturbation method. The homotopy equation for the given problem is defined as

$$\tilde{H}(\tilde{u}, q) = (1 - q) (\mathcal{L}_1[\tilde{u}] - \mathcal{L}_1[\tilde{u}_0]) + q \left( \mathcal{L}_1[\tilde{u}] + \frac{1}{R^2} \frac{\partial^2 \tilde{u}}{\partial \theta^2} - (1 + \lambda_1) \frac{\partial P}{\partial Z} \right) = 0, \quad (2.21)$$

where  $\mathcal{L}_1$ , the linear operator which is assumed to be

$$\mathcal{L}_1 = \frac{\partial^2}{\partial R^2} + \frac{1}{R} \frac{\partial}{\partial R} - \frac{M^2 (1 + \lambda_1)}{R^2}. \quad (2.22)$$

We define the following initial guess

$$\tilde{u}_0 = V_1 \sinh \left( M \sqrt{1 + \lambda_1} \left( \ln \frac{R}{r_2} \right) \right) \operatorname{csc} h \left( M \sqrt{1 + \lambda_1} \left( \ln \frac{r_1}{r_2} \right) \right). \quad (2.23)$$

Now we choose

$$\tilde{u}(R, \theta, Z, t, q) = u_0 + qu_1 + \dots \quad (2.24)$$



Using the above equation into Eq. (2.21) and then taking the terms upto first two orders, we get the following problems along with corresponding boundary conditions.

**Zeroth order system**

$$\mathcal{L}_1 [u_0] - \mathcal{L}_1 [\tilde{u}_0] = 0, \quad (2.25)$$

$$u_0 = 0, \quad \text{at } R = r_2, \quad (2.26)$$

$$u_0 = V_1, \quad \text{at } R = r_1. \quad (2.27)$$

The solution of the above zeroth order system can be obtained by using Eq. (2.23) and is directly written as

$$u_0(R, \theta, Z, t, q) = \tilde{u}_0 = V_1 \sinh \left( M\sqrt{1+\lambda_1} \left( \ln \frac{R}{r_2} \right) \right) \operatorname{csch} \left( M\sqrt{1+\lambda_1} \left( \ln \frac{r_1}{r_2} \right) \right). \quad (2.28)$$

**First order system**

$$\mathcal{L}_1 [u_1] + \mathcal{L}_1 [\tilde{u}_0] + \frac{1}{R^2} \frac{\partial^2 u_0}{\partial \theta^2} - (1 + \lambda_1) \frac{\partial P}{\partial Z} = 0, \quad (2.29)$$

or

$$\frac{\partial^2 u_1}{\partial R^2} + \frac{1}{R} \frac{\partial u_1}{\partial R} - \frac{M^2(1+\lambda_1)}{R^2} u_1 = (1 + \lambda_1) \frac{\partial P}{\partial Z} - \frac{1}{R^2} \frac{\partial^2 u_0}{\partial \theta^2}, \quad (2.30)$$

$$u_1 = 0, \quad \text{at } R = r_2, \quad (2.31)$$

$$u_1 = 0, \quad \text{at } R = r_1. \quad (2.32)$$

The solution of the above system is directly defined as

$$u_1 = \left. \begin{aligned} & \frac{1}{4M\sqrt{1+\lambda_1}((M\sqrt{1+\lambda_1})^2-4)} \left( \operatorname{csch} \left( M\sqrt{1+\lambda_1} \ln \frac{r_1}{r_2} \right) \left( (-4M\sqrt{1+\lambda_1} \frac{\partial P}{\partial Z} r_2^2 \right. \right. \\ & + C_2 (M^2(1+\lambda_1) - 4) \ln \frac{R r_1}{r_2^2} \right) \sinh \left( M\sqrt{1+\lambda_1} \ln \frac{R}{r_1} \right) - C_2 M^2(1+\lambda_1) - 4 \\ & \ln \frac{R}{r_1} \sinh \left( M\sqrt{1+\lambda_1} \ln \frac{R r_1}{r_2^2} \right) + 4M\sqrt{1+\lambda_1} \frac{\partial P}{\partial Z} \left( r_1^2 \sinh \left( M\sqrt{1+\lambda_1} \ln \frac{R}{r_2} \right) \right. \\ & - R^2 \sinh \left( M\sqrt{1+\lambda_1} \ln \frac{r_1}{r_2} \right) \left. \right) - 4M\sqrt{1+\lambda_1} \frac{\partial P}{\partial Z} \left( r_2^2 \sinh \left( M\sqrt{1+\lambda_1} \ln \frac{R}{r_1} \right) \right. \\ & \left. \left. - r_1^2 \sinh \left( M\sqrt{1+\lambda_1} \ln \frac{R}{r_2} \right) + R^2 \sinh \left( M\sqrt{1+\lambda_1} \ln \frac{r_1}{r_2} \right) \right) \lambda_1 \right) \end{aligned} \right\}, \quad (2.33)$$

where

$$C_2 = \frac{1}{(\delta + \epsilon \cos \theta)^2} \left( M\sqrt{1 + \lambda_1} V_1 \epsilon \operatorname{csch} \left( M\sqrt{1 + \lambda_1} \ln \frac{\delta + \epsilon \cos \theta}{r_2} \right) \right. \\ \left. \left( (\epsilon + \delta \cos \theta) \coth \left( M\sqrt{1 + \lambda_1} \left( \ln \frac{\delta + \epsilon \cos \theta}{r_2} \right) \right) + M\sqrt{1 + \lambda_1} \epsilon \right. \right. \\ \left. \left. \left( 1 + 2 \operatorname{csch}^2 \left( M\sqrt{1 + \lambda_1} \left( \ln \frac{\delta + \epsilon \cos \theta}{r_2} \right) \right) \right) \sin^2 \theta \right) \right) \quad (2.34)$$

Now for  $q \rightarrow 1$ , we approach the final solution. So from Eq. (2.24), we get

$$U(R, \theta, Z, t) = u_0 + u_1, \quad (2.35)$$

here  $u_0$  and  $u_1$  are defined in Eqs. (2.28) and (2.33). The instantaneous volume flow rate  $\bar{Q}(z, t)$  is given by

$$\bar{Q}(z, t) = 2\pi \int_{r_1}^{r_2} RU dR, \quad (2.36)$$

$$\bar{Q}/2\pi = \frac{1}{4M\sqrt{1+\lambda_1}((M\sqrt{1+\lambda_1})^2-4)^2} \left( (M^2(1+\lambda_1)+4)(2C_2r_2^2+M\sqrt{1+\lambda_1}\frac{\partial P}{\partial Z} \right. \\ (r_1^4-r_2^4)) + 8M\sqrt{1+\lambda_1}(M^2(1+\lambda_1)-4)r_1^2V_1 - 2C_2(M^2(1+\lambda_1)+4r_1^2) \\ \left. \cosh \left( M\sqrt{1+\lambda_1} \ln \frac{r_1}{r_2} \right) + 2M\sqrt{1+\lambda_1} \operatorname{csch} \left( M\sqrt{1+\lambda_1} \ln \frac{r_1}{r_2} \right) (2M \right. \\ \left. \sqrt{1+\lambda_1} r_2^2 (2\frac{\partial P}{\partial Z} r_1^2 + (M^2(1+\lambda_1)-4)V_1) - C_2(M^2(1+\lambda_1)-4) \right. \\ \left. r_1^2 \ln \frac{r_1}{r_2} \right) - 2M\sqrt{1+\lambda_1} \coth \left( M\sqrt{1+\lambda_1} \ln \frac{r_1}{r_2} \right) (2M\sqrt{1+\lambda_1} (\frac{\partial P}{\partial Z} \times \\ (r_1^4+r_2^4) + (M^2(1+\lambda_1)-4)r_1^2V_1) - C_2(M^2(1+\lambda_1)-4)r_2^2 \ln \frac{r_1}{r_2}) \\ + 8C_2M\sqrt{1+\lambda_1}r_1^2 \sinh \left( M\sqrt{1+\lambda_1} \ln \frac{r_1}{r_2} \right) + M\sqrt{1+\lambda_1} \frac{\partial P}{\partial Z} ((M^2 \times \\ (1+\lambda_1)+4)(r_1^4-r_2^4) - 4M\sqrt{1+\lambda_1}(r_1^4+r_2^4) \coth \left( M\sqrt{1+\lambda_1} \ln \frac{r_1}{r_2} \right) \\ \left. + 8M\sqrt{1+\lambda_1}r_1^2r_2^2 \operatorname{csch} \left( M\sqrt{1+\lambda_1} \ln \frac{r_1}{r_2} \right)) \lambda_1 \right) \quad (2.37)$$

The mean volume flow rate  $Q$  over one period is given by Shapiro et al. [77] and is defined as

$$Q(Z, t) = \frac{\bar{Q}}{\pi} - \frac{\phi^2}{2} + 2\phi \cos 2\pi(Z-t) + \phi^2 \cos^2 2\pi(Z-t). \quad (2.38)$$

Now we can evaluate pressure gradient  $\partial P/\partial Z$  by solving Eqs. (2.37) and (2.38) and is obtained

as

$$\left. \begin{aligned}
\frac{\partial P}{\partial Z} = & \left( 2 \left( -4C_2\pi r_2^2 + M\sqrt{1+\lambda_1} \left( 2(M^2(1+\lambda_1)-4)^2 Q + \pi \times \right. \right. \right. \\
& C_2M\sqrt{1+\lambda_1}r_2^2 - 4(M^2(1+\lambda_1)-4)r_1^2V_1 + M\sqrt{1+\lambda_1} \\
& (M^2(1+\lambda_1)-4)^2\pi\phi(4\cos[2\pi(Z-t)] + \phi\cos[4\pi(Z-t)]) + \\
& C_2(M^2(1+\lambda_1)+4)\pi r_1^2\cosh\left(M\sqrt{1+\lambda_1}\ln\frac{r_1}{r_2}\right) + M\sqrt{1+\lambda_1}\pi \\
& \csc h\left(M\sqrt{1+\lambda_1}\ln\frac{r_1}{r_2}\right) (2C_2r_1^2 - 2M\sqrt{1+\lambda_1}(M^2(1+\lambda_1)-4) \\
& r_2^2V_1 + C_2r_1^2 \left( 2\cosh\left(2M\sqrt{1+\lambda_1}\ln\frac{r_2}{r_1}\right) + \left( (M\sqrt{1+\lambda_1})^2 - 4 \right) \right. \\
& \left. \ln\frac{r_1}{r_2} \right) + (M^2(1+\lambda_1)-4)\cosh\left(M\sqrt{1+\lambda_1}\ln\frac{r_1}{r_2}\right) \times (2M \\
& \left. \sqrt{1+\lambda_1}r_1^2V_1 + C_2r_2^2\ln\frac{r_2}{r_1} \right) \left. \right) / (M\sqrt{1+\lambda_1}\pi((M^2(1+\lambda_1) \\
& +4)(r_1^4 - r_2^4) - 4M\sqrt{1+\lambda_1}(r_1^4 + r_2^4)\coth\left(M\sqrt{1+\lambda_1}\ln\frac{r_1}{r_2}\right) + 8M \\
& \left. \sqrt{1+\lambda_1}r_1^2r_2^2\csc h\left(M\sqrt{1+\lambda_1}\ln\frac{r_1}{r_2}\right)(1+\lambda_1)) \right)
\end{aligned} \right\} \quad (2.39)$$

The pressure rise  $\Delta P(t)$  in non-dimensional form is defined as

$$\Delta P(t) = \int_0^1 \frac{\partial P}{\partial Z} dZ, \quad (2.40)$$

in which  $\partial P/\partial Z$  is defined in Eq. (2.39).

### 2.3 Graphical results and discussion

The analytical and numerical results obtained for the given analysis are discussed graphically in this section. The comparison table and graph are presented to compare the results found in the present case with that of already available in literature. The graphical results for the data of pressure rise  $\Delta P$ , pressure gradient  $\partial P/\partial Z$  and velocity profile  $U(R, \theta, Z, t)$  with the variation of all emerging dimensionless parameters flow rate  $Q$ , amplitude ratio  $\phi$ , the velocity of the inner tube  $V_1$ , the eccentricity parameter  $\epsilon$ , Jeffrey fluid parameter  $\lambda_1$  and the MHD parameter  $M$  have been analyzed. At the end, the stream lines observing the peristaltic flow are drawn for the parameters  $M$ ,  $Q$ ,  $\lambda_1$  and  $\phi$  while other parameters remain fixed.

Table 2.1 is shown to see the matching of results for the current case and the Mekheimer et al. [78]. The comparison graph for the values obtained in present work with the results of [78] is displayed in Fig. 2.2. The graphs for the pressure rise  $\Delta P(t)$  versus flow rate  $Q$  under the effects

of given parameters are drawn in Figs. 2.3 to 2.7. These graphs show the pumping regions, that is, the peristaltic pumping ( $Q > 0, \Delta P > 0$ ), the augmented pumping ( $Q > 0, \Delta P < 0$ ) and the retrograde pumping ( $Q < 0, \Delta P > 0$ ). The pressure gradient  $\partial P/\partial Z$  against the the coordinate  $Z$  with the variation of pertinent parameters are shown in Figs. 2.8 to 2.12. The velocity field  $U(R, \theta, Z, t)$  versus the radial coordinate  $r$  is plotted in Figs. 2.13 to 2.17 for both two and three dimensions. The stream line graphs are shown in Figs. 2.18 to 2.21.

It is observed from Fig. 2.2 that the results obtained in the present case are in good agreement with that of [78] in most part of the domain. It is also observed that the presence of magnetic field for Jeffrey fluid causes to slow down the flow. Fig. 2.3 is plotted to see the variation of pressure rise for different values of the eccentricity parameter  $\epsilon$  and the angle  $\theta$  while all other parameters are kept fixed. It is observed that peristaltic pumping region is in between  $Q \in [0, 0.9]$ , augmented pumping is in  $Q \in [0.9, 2]$  and retrograde pumping part is  $Q \in [-1, 0]$ . It is also observed from this graph that the pressure rise increases with the variation of  $\epsilon$  but decreases with the angle  $\theta$  in between the region  $Q \in [-1, 0.9]$  and opposite behavior is seen in the remaining part. The graph of pressure rise for the parameter  $M$  and  $\delta$  is plotted in Fig. 2.4. The peristaltic pumping occurs in the region  $Q \in [0, 0.6]$ , augmented pumping is in  $Q \in [0.6, 2]$  and retrograde pumping part is  $Q \in [-1, 0]$ . It is clear that the similar behavior is seen in this case for the parameter  $M$  but the opposite attitude is observed with the variation of  $\delta$  as compared to that of  $\epsilon$  and  $\theta$ . It tells that the flow rate decreases with  $M$  while increases with  $\delta$ , this shows that the back flow increases and decreases with  $M$  and  $\delta$ , respectively. Fig. 2.5 shows that the peristaltic pumping part is  $Q \in [0, 0.3]$ , while augmented and retrograde pumping regions are  $Q \in [0.3, 2]$  and  $Q \in [-1, 0]$  respectively. The variation of pressure rise  $\Delta P$  for  $V_1$  is similar to that of  $M$  (see Fig. 2.6). Fig. 2.7 indicates the effect of the parameters  $\lambda_1$  and  $\delta$  upon pressure rise. This plot reveals that the peristaltic pumping area lies in between  $Q \in [0, 0.6]$ , the retrograde pumping appears in the part  $Q \in [-1, 0]$  and the augmented pumping region is  $Q \in [0.6, 2]$ . The pressure gradient  $\partial P/\partial Z$  for the parameters  $M$  and  $\delta$  is drawn in Fig. 2.8. It is measured from this figure that pressure gradient is in linear relation with both of the parameters in narrowest parts of the cylinders but inverse relation is seen in the wider parts. The variation of pressure gradient with the parameters  $\phi$  and  $\epsilon$  is very much similar to that of the parameters  $M$  and  $\delta$  and is shown in Fig. 2.9. The only difference is

that the pressure gradient is minimum on the left and right sides of the cylinder while appears maximum at the centre. It means that flow can easily pass without imposition of large pressure gradient in the two sides of the channel while much pressure gradient is required to maintain the flux in the central part near  $Z = 0.8$ . This is in good agreement with the physical condition. It can be observed from Figs. 2.10 and 2.11 that the pressure gradient increases with the parameters  $Q$  and  $V_1$ , while when  $\delta$  is increased the pressure gradient decreases on the left and right sides but increases at the centre of the cylinders. It is also seen that the variation of pressure gradient remains same in the two sides of the channel and become different at the central part with changing  $V_1$  but this variation remains same throughout for the parameter  $Q$ . The pressure gradient graph for the parameters  $\lambda_1$  and  $\delta$  is drawn in the Fig. 2.12. It is seen here that the pressure gradient increases with  $\delta$  at the middle but decreases at the two sides of the cylinders. However, the effect of the parameter  $\lambda_1$  is totally opposite with that of  $\delta$ . The Fig. 2.13 shows that the velocity field is an increasing function of the parameter  $\delta$  while decreasing with the parameter  $M$ . The velocity field is in inverse relation with  $Q$  but have a direct variation with  $\epsilon$  (see Fig. 2.14). It is observed from Fig. 2.15 that the velocity distribution is increasing with  $\delta$  and  $\phi$  while reducing for  $t$ . Fig. 2.16 shows that the velocity profile is linearly changing with  $\phi$  and  $V_1$ . From Fig. 2.17, it is measured that velocity is lessened with the increasing effect of the parameter  $\lambda_1$ . It is also observed that velocity is decreasing function of  $\delta$  in the region  $R \in [0.2, 0.4]$ , while increasing on the rest of the domain. Fig. 2.18 is drawn to see the stream lines for the parameter  $M$ . It is measured from this figure that numbers of bolus are not changing but size is increasing with the increasing effects of  $M$  in the bottom of the cylinder, while bolus are lessened in number when seen in the upper part. The boluses are reduced both in size and number when seen for the parameter  $Q$  in both parts of the geometry (see Fig. 2.19). It is seen from Fig. 2.20 that the numbers of bolus are decreasing with different values of the parameter  $\phi$  in both sides of the cylinder but in the lower half of the channel, the bolus becomes smaller with increasing magnitude of the parameter  $\phi$ . Fig. 2.21 reveals the fact that when we increase the value of the parameter  $\lambda_1$ , the boluses decreased in number but expanded in size.

	Mekheimer et al. [78]	Present work	
$R$	$U(R, \theta, Z, t)$	$U(R, \theta, Z, t)$ for $M = 0, \lambda_1 = 0$	$U(R, \theta, Z, t)$ for $M = 0.5, \lambda_1 = 1$
0.20	0.1000	0.1000	0.1000
0.25	0.1093	0.1081	0.0969
0.30	0.1119	0.1116	0.0944
0.35	0.1119	0.1120	0.0918
0.40	0.1096	0.1099	0.0887
0.45	0.1054	0.1057	0.0848
0.50	0.0995	0.0997	0.0801
0.55	0.0919	0.0920	0.0743
0.60	0.0829	0.0829	0.0674
0.65	0.0724	0.0723	0.0593
0.70	0.0606	0.0604	0.0501

Table 2.1: Comparison of variation of velocity distribution in present work with [78].

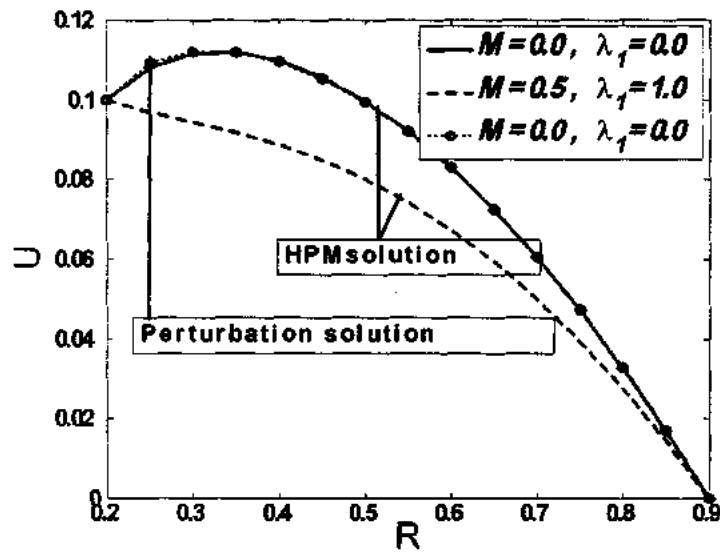


Fig. 2.2: Comparison of velocity profile  $U$  with [78] for fixed values of  $\delta = 0.1$ ,  $\theta = 0.87$ ,  $\phi = 0.1$ ,  $Z = 0$ ,  $t = 0.5$ ,  $V_1 = 0.1$ ,  $\epsilon = 0.1$ ,  $Q = 0.6$ .

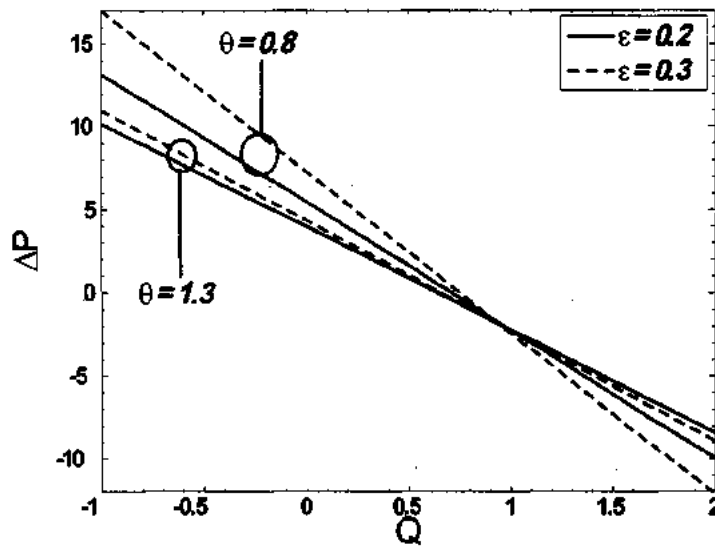


Fig. 2.3: Variation of pressure rise  $\Delta P$  with  $\epsilon$  and  $\theta$  for fixed values of  $\delta = 0.1$ ,  $\phi = 0.2$ ,  $t = 0.1$ ,  $M = 0.5$ ,  $V_1 = 0.5$ ,  $\lambda_1 = 1.5$ .

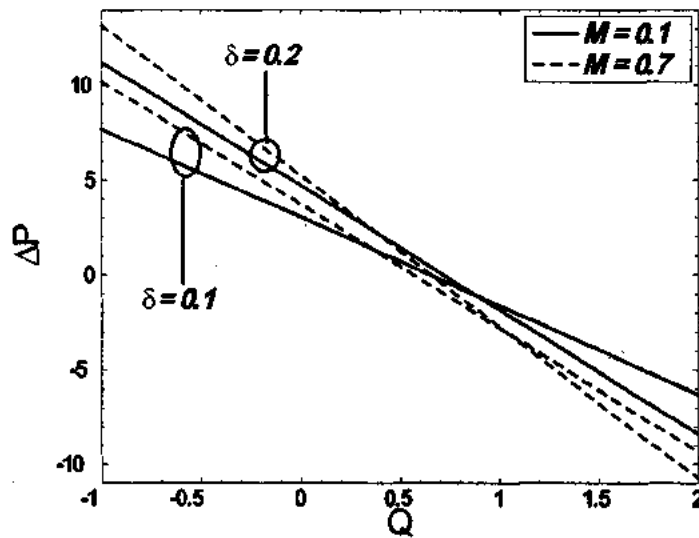


Fig. 2.4: Variation of pressure rise  $\Delta P$  with  $M$  and  $\delta$  for fixed values of  $\epsilon = 0.01$ ,  $\phi = 0.2$ ,  $t = 0.1$ ,  $\theta = 0.87$ ,  $V_1 = 0.5$ ,  $\lambda_1 = 1.5$ .

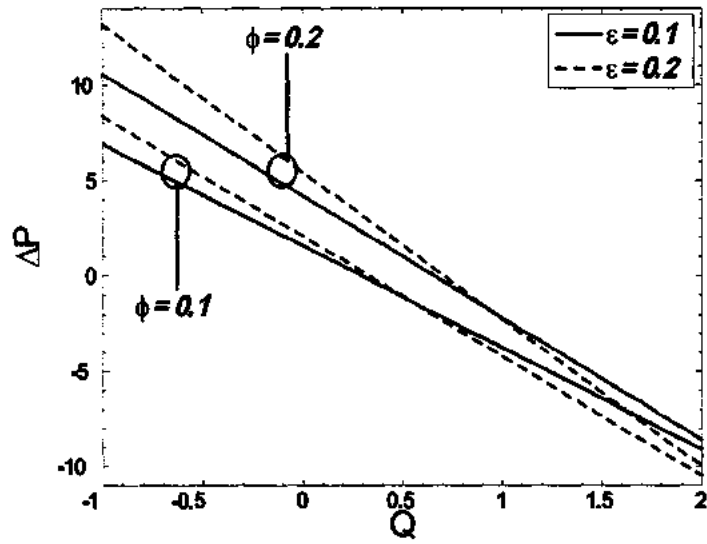


Fig. 2.5: Variation of pressure rise  $\Delta P$  with  $\epsilon$  and  $\phi$  for fixed values of  $\delta = 0.1$ ,  $M = 0.5$ ,  $t = 0.1$ ,  $\theta = 0.87$ ,  $V_1 = 0.5$ ,  $\lambda_1 = 1.5$ .

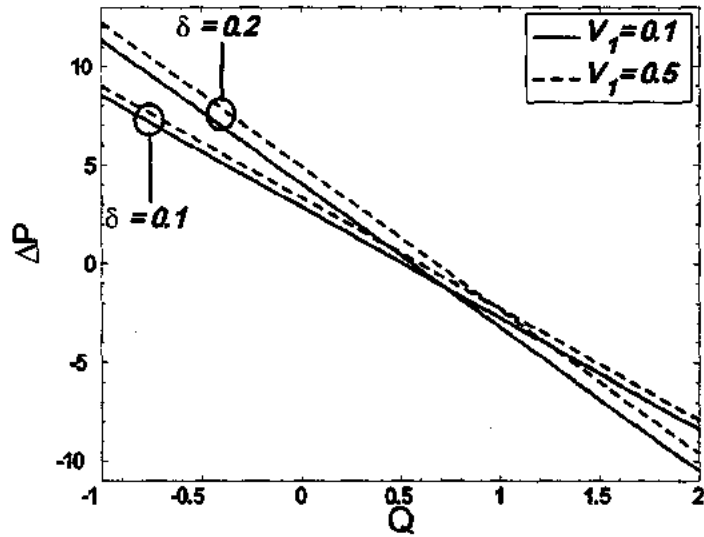


Fig. 2.6: Variation of pressure rise  $\Delta P$  with  $V_1$  and  $\delta$  for fixed values of  $\epsilon = 0.01$ ,  $M = 0.5$ ,  $t = 0.1$ ,  $\theta = 0.87$ ,  $\phi = 0.2$ ,  $\lambda_1 = 1.5$ .



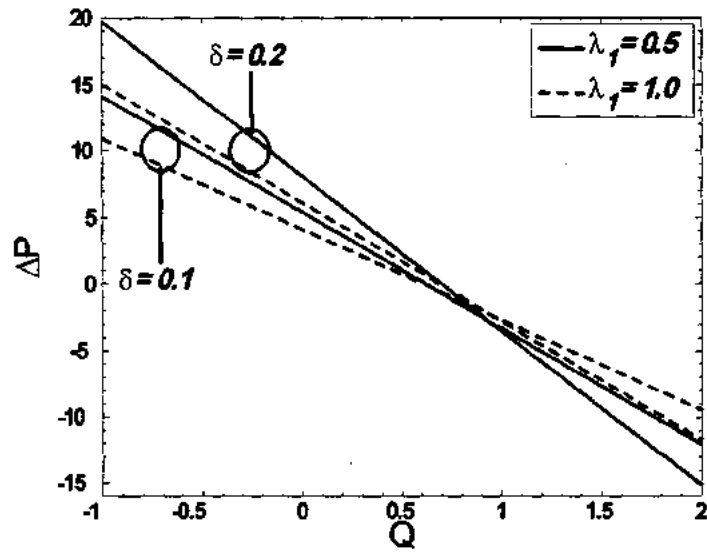


Fig. 2.7: Variation of pressure rise  $\Delta P$  with  $V_1$  and  $\delta$  for fixed values of  $\epsilon = 0.01$ ,  $M = 0.5$ ,  $t = 0.1$ ,  $\theta = 0.87$ ,  $\phi = 0.2$ ,  $V_1 = 0.5$ .

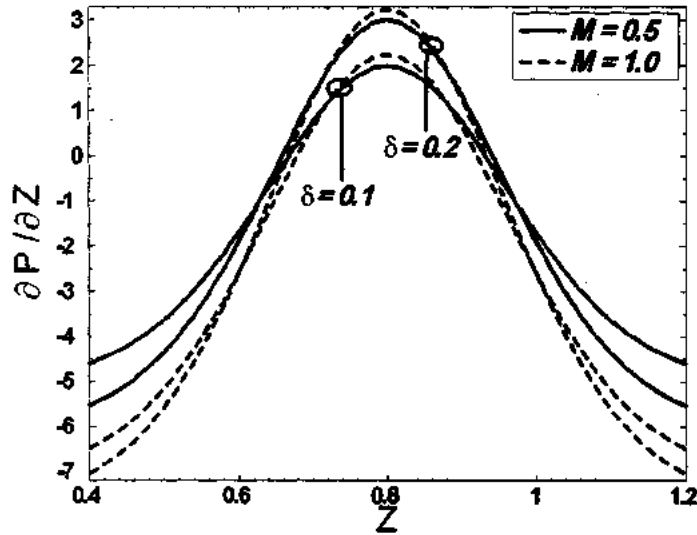


Fig. 2.8: Variation of pressure gradient  $\partial P/\partial Z$  with  $M$  and  $\delta$  for fixed values of  $\epsilon = 0.01$ ,  $V_1 = 0.3$ ,  $t = 0.3$ ,  $\theta = 0.87$ ,  $\phi = 0.1$ ,  $Q = 0.5$ ,  $\lambda_1 = 1.5$ .

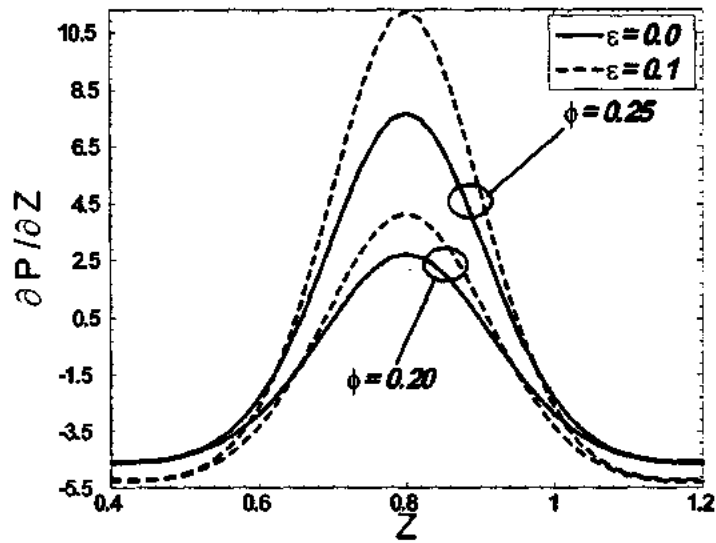


Fig. 2.9: Variation of pressure gradient  $\partial P / \partial Z$  with  $\epsilon$  and  $\phi$  for fixed values of  $\delta = 0.1$ ,  $V_1 = 0.3$ ,  $t = 0.3$ ,  $\theta = 0.87$ ,  $M = 0.5$ ,  $Q = 1$ ,  $\lambda_1 = 1.5$ .

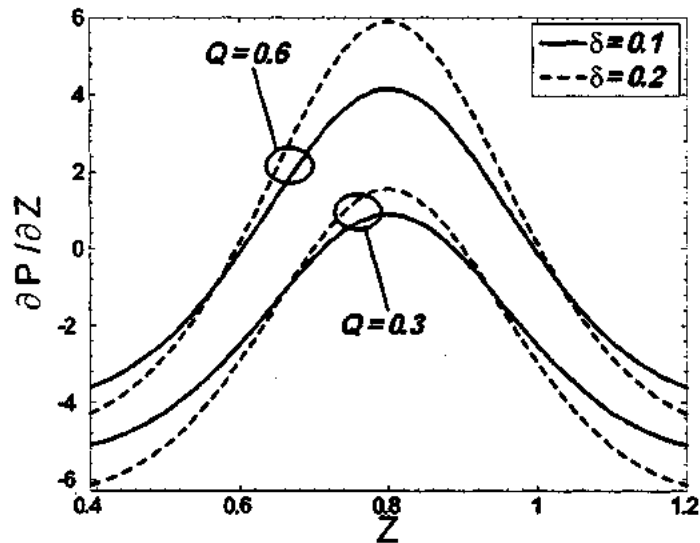


Fig. 2.10: Variation of pressure gradient  $\partial P / \partial Z$  with  $Q$  and  $\delta$  for fixed values of  $\epsilon = 0.01$ ,  $V_1 = 0.3$ ,  $t = 0.3$ ,  $\theta = 0.87$ ,  $M = 0.5$ ,  $\phi = 0.1$ ,  $\lambda_1 = 0.5$ .

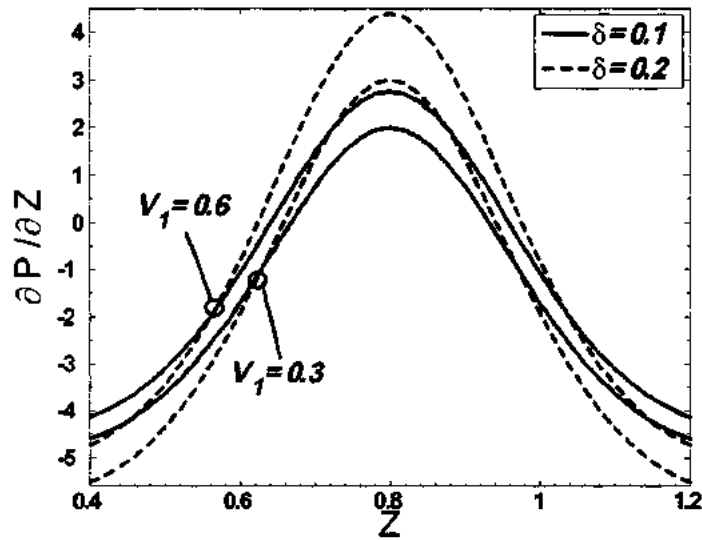


Fig. 2.11: Variation of pressure gradient  $\partial P / \partial Z$  with  $V_1$  and  $\delta$  for fixed values of  $\epsilon = 0.01$ ,  $Q = 0.5$ ,  $t = 0.3$ ,  $\theta = 0.87$ ,  $M = 0.5$ ,  $\phi = 0.1$ ,  $\lambda_1 = 0.5$ .

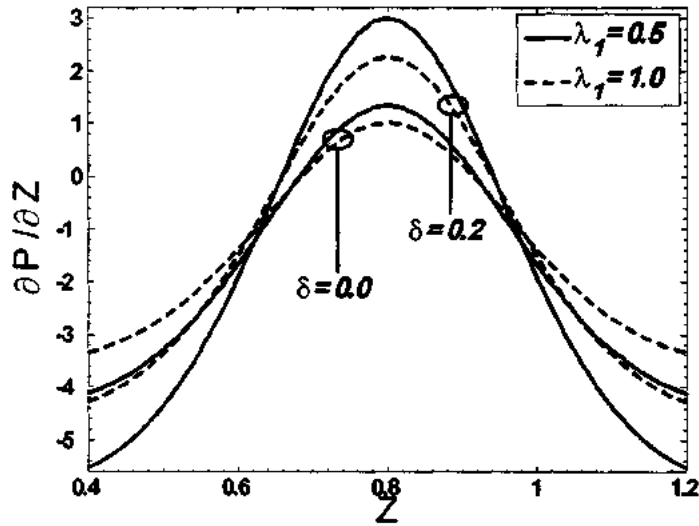
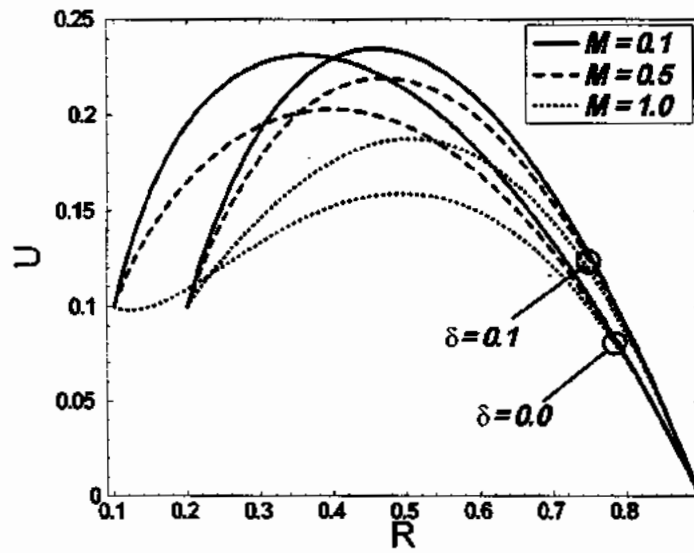
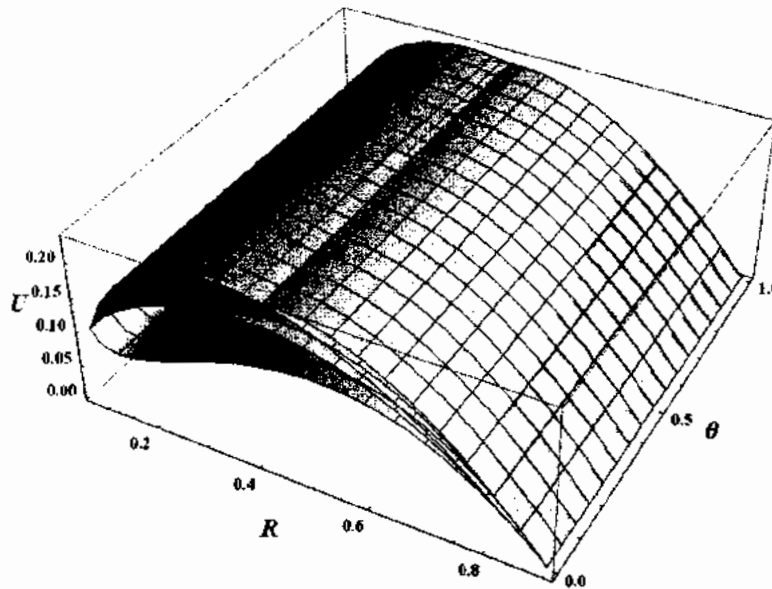


Fig. 2.12: Variation of pressure gradient  $\partial P / \partial Z$  with  $\lambda_1$  and  $\delta$  for fixed values of  $\epsilon = 0.01$ ,  $Q = 0.5$ ,  $t = 0.3$ ,  $\theta = 0.87$ ,  $M = 0.5$ ,  $\phi = 0.1$ ,  $V_1 = 0.3$ .

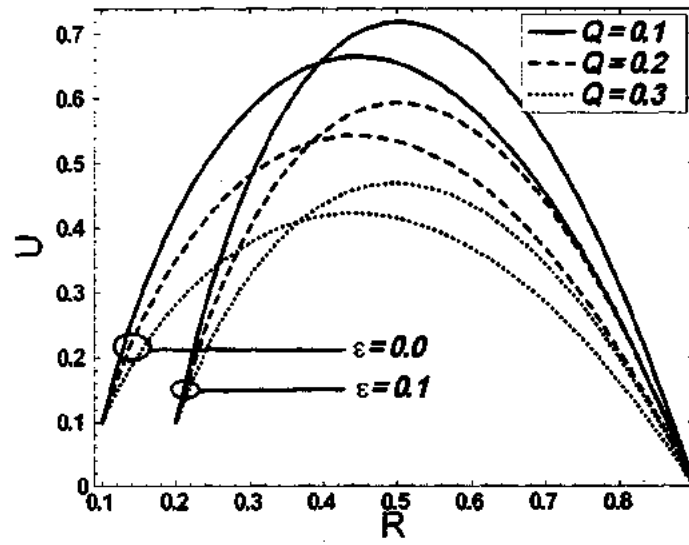


(a)

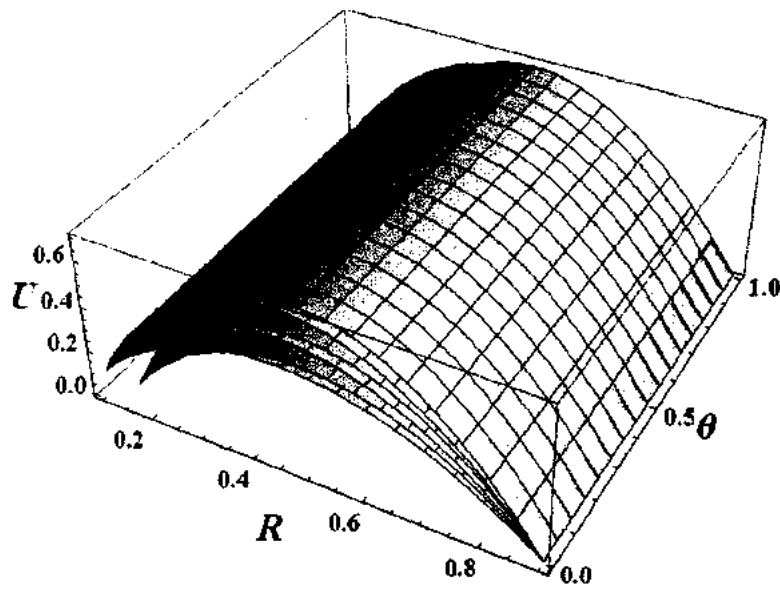


(b)

Fig. 2.13: Variation of velocity profile  $U$  with  $M$  and  $\delta$  for fixed values of  $\epsilon = 0.1$ ,  $Q = 0.5$ ,  $t = 0.5$ ,  $Z = 0$ ,  $V_1 = 0.1$ ,  $\theta = 0.87$ ,  $\phi = 0.1$ ,  $\lambda_1 = 1.5$ .

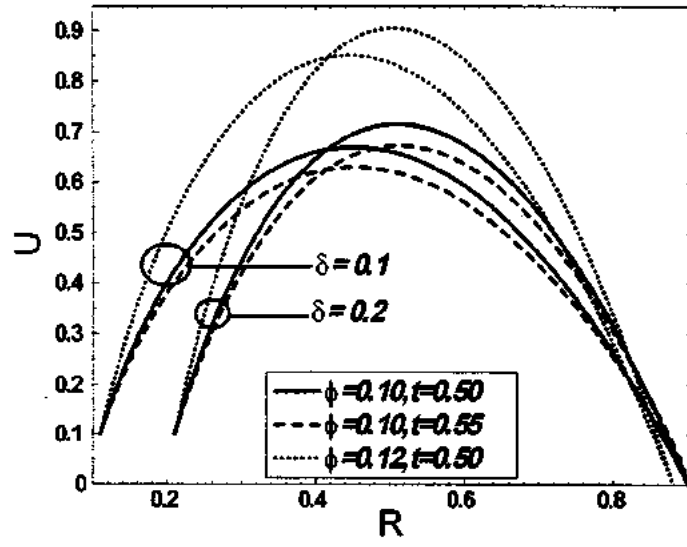


(a)

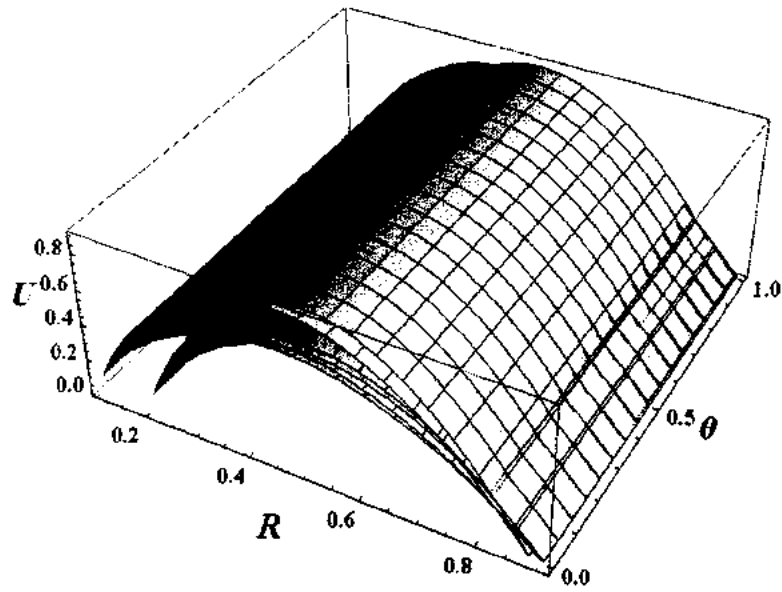


(b)

Fig. 2.14: Variation of velocity profile  $U$  with  $Q$  and  $\epsilon$  for fixed values of  $\delta = 0.1$ ,  $M = 0.5$ ,  $t = 0.5$ ,  $Z = 0$ ,  $V_1 = 0.1$ ,  $\theta = 0.87$ ,  $\phi = 0.1$ ,  $\lambda_1 = 1.5$ .

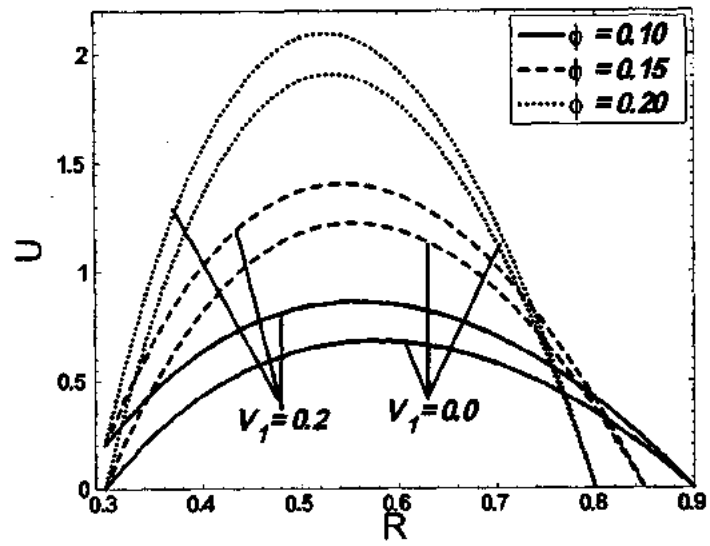


(a)

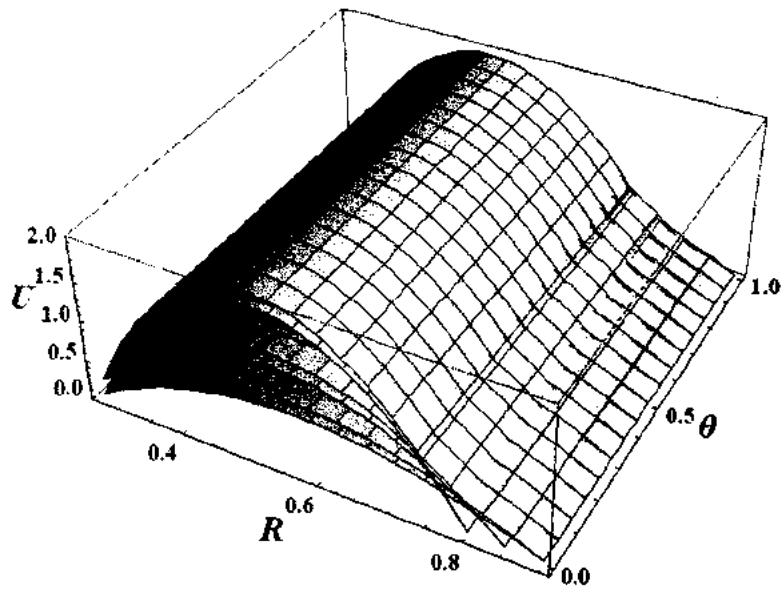


(b)

Fig. 2.15: Variation of velocity profile  $U$  with  $t$ ,  $\phi$  and  $\delta$  for fixed values of  $Q = 0.1$ ,  $M = 0.5$ ,  $\epsilon = 0.01$ ,  $Z = 0$ ,  $V_1 = 0.1$ ,  $\theta = 0.87$ ,  $\lambda_1 = 1.5$ .

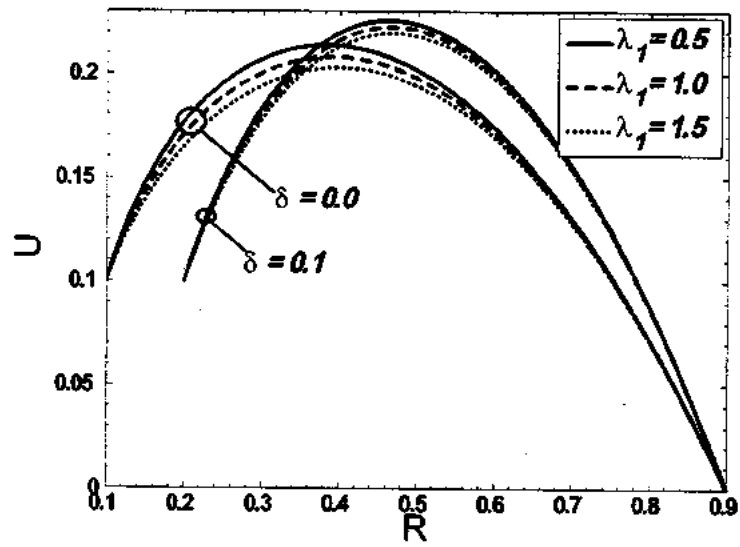


(a)

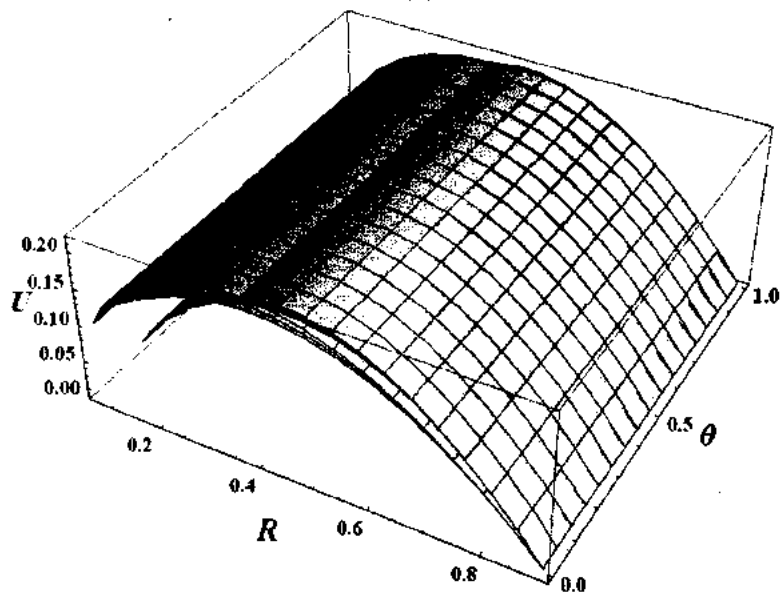


(b)

Fig. 2.16: Variation of velocity profile  $U$  with  $V_1$  and  $\phi$  for fixed values of  $Q = 0.1$ ,  $M = 0.5$ ,  $t = 0.5$ ,  $\epsilon = 0.1$ ,  $Z = 0$ ,  $\delta = 0.2$ ,  $\theta = 0.87$ ,  $\lambda_1 = 1.5$ .



(a)



(b)

Fig. 2.17: Variation of velocity profile  $U$  with  $\lambda_1$  and  $\delta$  for fixed values of  $Q = 0.5$ ,  $M = 0.5$ ,  $t = 0.5$ ,  $\epsilon = 0.1$ ,  $Z = 0$ ,  $\theta = 0.87$ ,  $\phi = 0.1$ ,  $V_1 = 0.1$ .



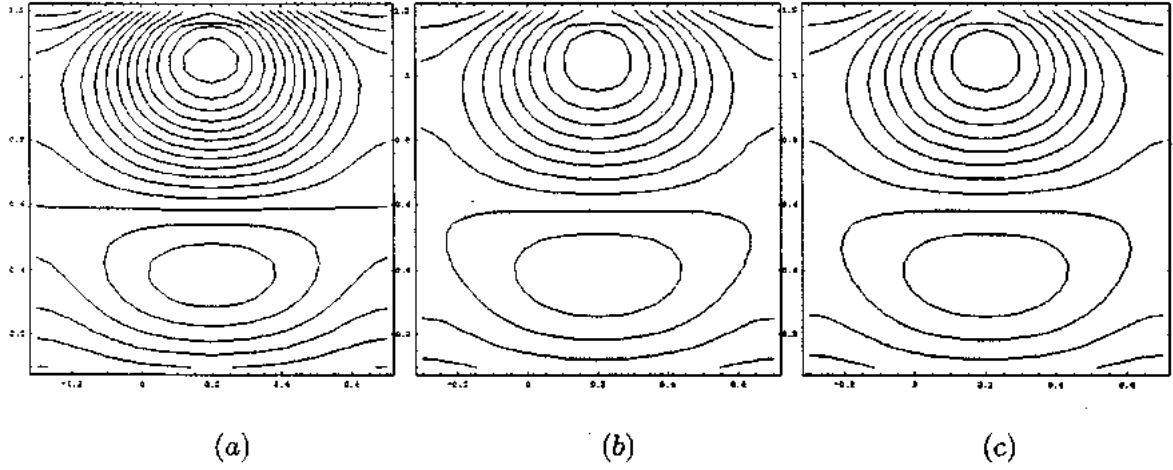


Fig. 2.18: Stream lines for different values of  $M$ , (a) for  $M = 0.3$ , (b) for  $M = 0.4$ , (c) for  $M = 0.5$ . The other parameters are  $\epsilon = 0.4$ ,  $V_1 = 0.3$ ,  $t = 0.2$ ,  $\theta = 0.87$ ,  $\phi = 0.05$ ,  $Q = 0.6$ ,  $\delta = 0.05$ ,  $\lambda_1 = 1$ .

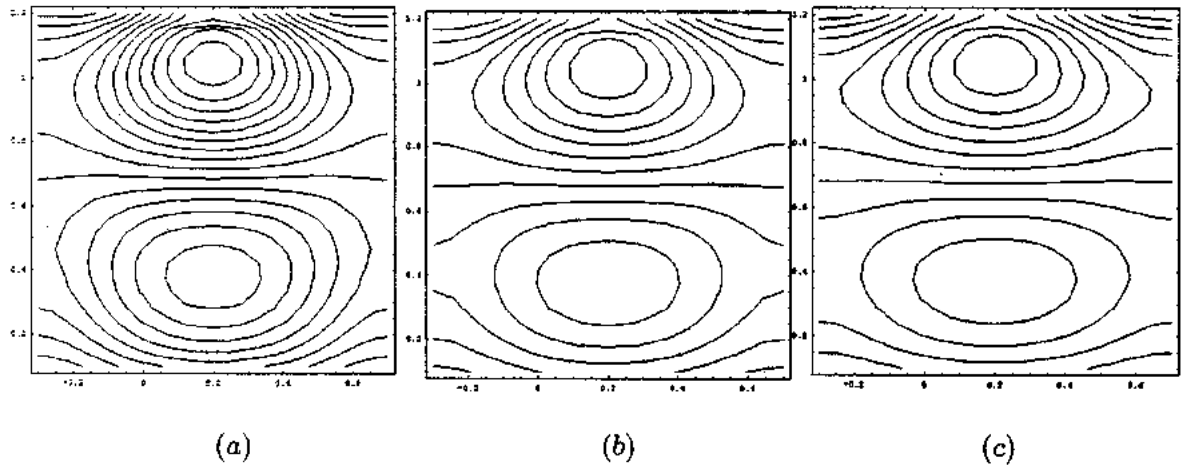


Fig. 2.19: Stream lines for different values of  $Q$ , (a) for  $Q = 0.6$ , (b) for  $Q = 0.7$ , (c) for  $Q = 0.8$ . The other parameters are  $\epsilon = 0.4$ ,  $V_1 = 0.3$ ,  $t = 0.2$ ,  $\theta = 0.87$ ,  $\phi = 0.05$ ,  $M = 1$ ,  $\delta = 0.05$ ,  $\lambda_1 = 1$ .

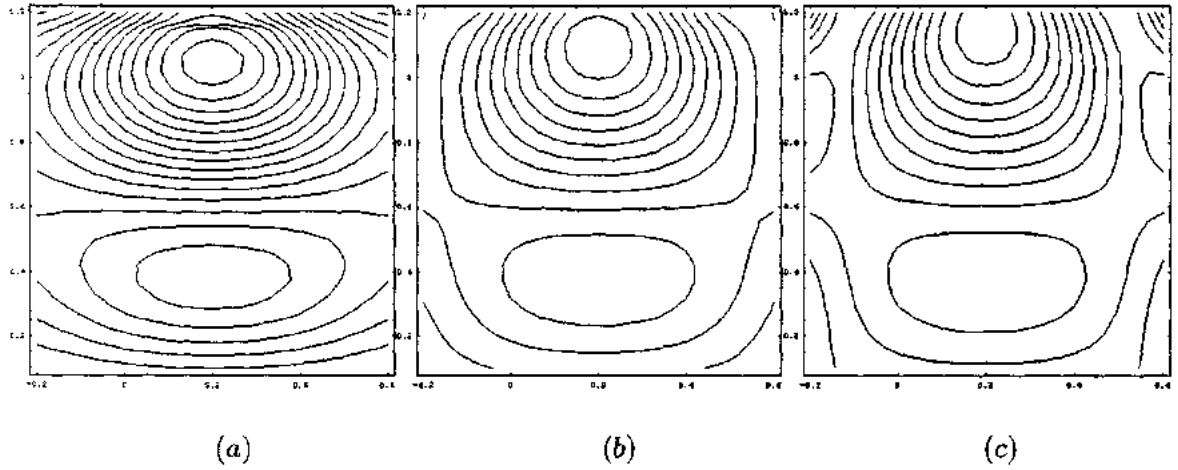


Fig. 2.20: Stream lines for different values of  $\phi$ , (a) for  $\phi = 0.05$ , (b) for  $\phi = 0.1$ , (c) for  $\phi = 0.15$ . The other parameters are  $\epsilon = 0.4$ ,  $V_1 = 0.3$ ,  $t = 0.2$ ,  $\theta = 0.87$ ,  $Q = 0.6$ ,  $M = 0.4$ ,  $\delta = 0.05$ ,  $\lambda_1 = 1$ .

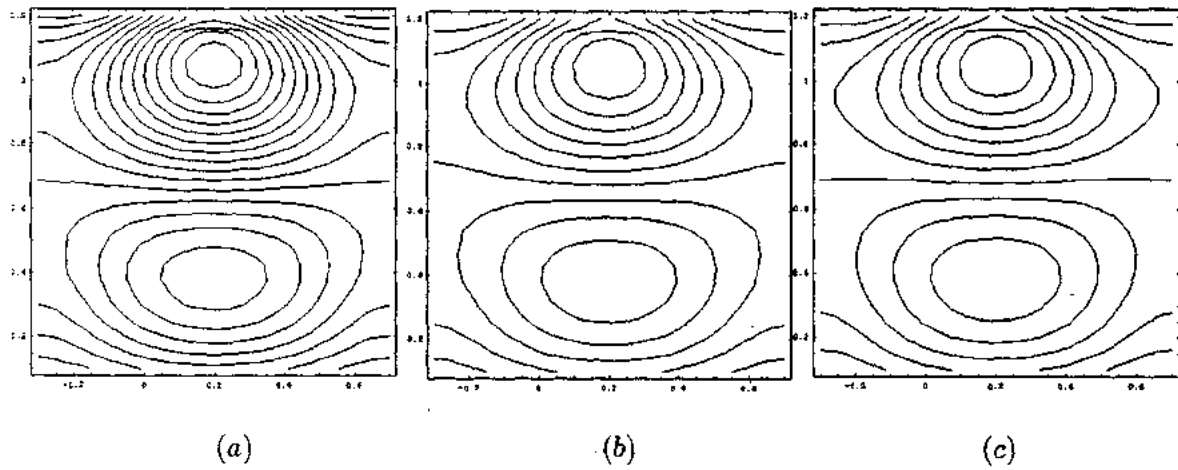


Fig. 2.21: Stream lines for different values of  $\lambda_1$ , (a) for  $\lambda_1 = 0.5$ , (b) for  $\lambda_1 = 0.7$ , (c) for  $\lambda_1 = 0.9$ . The other parameters are  $\epsilon = 0.4$ ,  $V_1 = 0.3$ ,  $t = 0.2$ ,  $\theta = 0.87$ ,  $Q = 0.6$ ,  $M = 1$ ,  $\delta = 0.05$ ,  $\phi = 0.05$ .

## Chapter 3

# Peristaltic flow of a Jeffrey fluid in a rectangular duct having compliant walls

The theme of this chapter is to analyze the theoretical and mathematical study of peristaltic transport of a Jeffrey fluid in a rectangular duct with compliant walls. The constitutive equations have been simplified under the implementation of low Reynolds number and long wavelength approximations. The analytical solution of the resulting equation has been evaluated by eigen function expansion method. The graphical aspects of all the parameters of interest have also been analyzed. The graphs of velocity for two and three dimensional flow are plotted. The trapping bolus phenomenon has also been discussed through streamlines. These observations are published in the journal of "*Chemical Industry and Chemical Engineering Quarterly*", 19 (2013) 399–409.

### 3.1 Mathematical formulation of the problem

Consider the peristaltic flow of an incompressible non-Newtonian Jeffrey fluid in a cross section of rectangular channel having the width  $2d$  and height  $2a$ . In the present geometry, the Cartesian coordinate system is taken in such a way that  $X$ -axis is taken along the axial direction,  $Y$ -axis is taken along the lateral direction and  $Z$ -axis is along the vertical direction of rectangular

channel (see Fig. 3.1). The walls of the channel are assumed to be flexible and are taken as compliant, on which waves with small amplitude and long wavelength are considered.

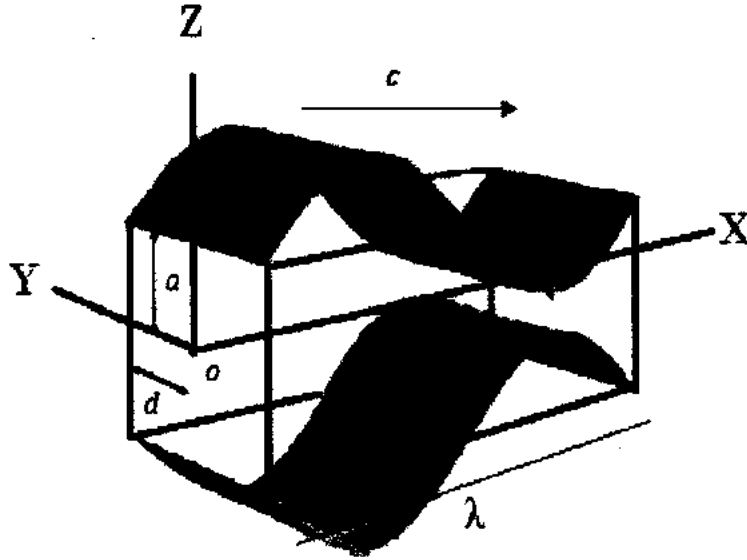


Fig. 3.1: Schematic diagram for peristaltic flow in a rectangular duct.

The geometry of the channel wall is given by [79]

$$Z = H(X, t) = \pm a \pm b \cos \left[ \frac{2\pi}{\lambda} (X - ct) \right], \quad (3.1)$$

where  $a$  and  $b$  are the amplitudes of the waves and  $x$  is the direction of wave propagation. The walls parallel to  $XZ$ -plane remain undisturbed and do not measure any peristaltic wave motion. We assume that the lateral velocity is zero as there is no change in lateral direction of the duct cross section. Let  $(U, 0, W)$  be the velocity for a rectangular duct. Then the continuity and momentum Eqs. (1.4) and (1.6) in Cartesian coordinates become

$$\frac{\partial U}{\partial X} + \frac{\partial W}{\partial Z} = 0, \quad (3.2)$$

$$\rho_f \left( \frac{\partial U}{\partial t} + U \frac{\partial U}{\partial X} + W \frac{\partial U}{\partial Z} \right) = -\frac{\partial P}{\partial Z} + \frac{\partial}{\partial X} S_{XX} + \frac{\partial}{\partial Y} S_{XY} + \frac{\partial}{\partial Z} S_{XZ}, \quad (3.3)$$

$$0 = -\frac{\partial P}{\partial Y} + \frac{\partial}{\partial X} S_{YX} + \frac{\partial}{\partial Y} S_{YY} + \frac{\partial}{\partial Z} S_{YZ}, \quad (3.4)$$

$$\rho_f \left( \frac{\partial W}{\partial t} + U \frac{\partial W}{\partial X} + W \frac{\partial W}{\partial Z} \right) = -\frac{\partial P}{\partial Z} + \frac{\partial}{\partial X} S_{ZX} + \frac{\partial}{\partial Y} S_{ZY} + \frac{\partial}{\partial Z} S_{ZZ}. \quad (3.5)$$

Let us introduce the following dimensionless parameters

$$\left. \begin{aligned} \bar{X} &= \frac{X}{\lambda}, \bar{Y} = \frac{Y}{d}, \bar{Z} = \frac{Z}{a}, \bar{U} = \frac{U}{c}, \bar{W} = \frac{W}{cb_0}, \bar{t} = \frac{ct}{\lambda}, \bar{H} = \frac{H}{a}, \\ \bar{P} &= \frac{a^2 P}{\mu c \lambda}, \text{Re} = \frac{\rho a c}{\mu}, \delta_0 = \frac{a}{\lambda}, \phi = \frac{b}{a}, \bar{S}_{2\bar{X}\bar{X}} = \frac{a}{\mu c} S_{2XX}, \\ \bar{S}_{2\bar{X}\bar{Y}} &= \frac{d}{\mu c} S_{2XY}, \bar{S}_{2\bar{X}\bar{Z}} = \frac{a}{\mu c} S_{2XZ}, \bar{S}_{2\bar{Y}\bar{Z}} = \frac{d}{\mu c} S_{2YZ}, \\ \bar{S}_{2\bar{Z}\bar{Z}} &= \frac{\lambda}{\mu c} S_{2ZZ}, \bar{S}_{2\bar{Y}\bar{Y}} = \frac{\lambda}{\mu c} S_{2YY}, \bar{\gamma} = \frac{\gamma a}{c}, \beta = \frac{a}{d} \end{aligned} \right\} \quad (3.6)$$

Using the above dimensionless quantities, the Eqs. (3.2) and (3.5) (after omitting bars) take the following form

$$\frac{\partial U}{\partial X} + \frac{\partial W}{\partial Z} = 0, \quad (3.7)$$

$$\text{Re } \delta_0 \left( \frac{\partial U}{\partial t} + U \frac{\partial U}{\partial X} + W \frac{\partial U}{\partial Z} \right) = -\frac{\partial P}{\partial Z} + \delta_0 \frac{\partial}{\partial X} S_{2XX} + \beta^2 \frac{\partial}{\partial Y} S_{2XY} + \frac{\partial}{\partial Z} S_{2XZ}, \quad (3.8)$$

$$0 = -\frac{\partial P}{\partial Y} + \delta_0^2 \frac{\partial}{\partial X} S_{2YX} + \delta_0^2 \frac{\partial}{\partial Y} S_{2YY} + \delta_0 \frac{\partial}{\partial Z} S_{2YZ}, \quad (3.9)$$

$$\text{Re } \delta_0^2 \left( \frac{\partial W}{\partial t} + U \frac{\partial W}{\partial X} + W \frac{\partial W}{\partial Z} \right) = -\frac{\partial P}{\partial Z} + \delta_0^2 \frac{\partial}{\partial X} S_{2ZX} + \delta_0 \beta^2 \frac{\partial}{\partial Y} S_{2ZY} + \delta_0^2 \frac{\partial}{\partial Z} S_{2ZY}. \quad (3.10)$$

The components of stress tensor for Jeffrey fluid are

$$\left. \begin{aligned} S_{2XX} &= \frac{2\delta_0}{1+\lambda_1} \left( 1 + \frac{\lambda_2 c \delta_0}{a} \left( \frac{\partial}{\partial t} + U \frac{\partial}{\partial X} + W \frac{\partial}{\partial Z} \right) \right) \frac{\partial U}{\partial X} \\ S_{2XY} &= \frac{1}{1+\lambda_1} \left( 1 + \frac{\lambda_2 c \delta_0}{a} \left( \frac{\partial}{\partial t} + U \frac{\partial}{\partial X} + W \frac{\partial}{\partial Z} \right) \right) \frac{\partial U}{\partial Y} \\ S_{2XZ} &= \frac{1}{1+\lambda_1} \left( 1 + \frac{\lambda_2 c \delta_0}{a} \left( \frac{\partial}{\partial t} + U \frac{\partial}{\partial X} + W \frac{\partial}{\partial Z} \right) \right) \left( \frac{\partial U}{\partial Z} + \delta_0^2 \frac{\partial W}{\partial X} \right) \\ S_{2YY} &= 0 \\ S_{2YZ} &= \frac{\delta_0}{1+\lambda_1} \left( 1 + \frac{\lambda_2 c \delta_0}{a} \left( \frac{\partial}{\partial t} + U \frac{\partial}{\partial X} + W \frac{\partial}{\partial Z} \right) \right) \frac{\partial W}{\partial Y} \\ S_{2ZZ} &= \frac{2}{1+\lambda_1} \left( 1 + \frac{\lambda_2 c \delta_0}{a} \left( \frac{\partial}{\partial t} + U \frac{\partial}{\partial X} + W \frac{\partial}{\partial Z} \right) \right) \frac{\partial W}{\partial Z} \end{aligned} \right\} \quad (3.11)$$

Under the assumption of long wave length and low Reynolds number, the governing equations in non-dimensional form for the considered flow problem are stated as

$$\frac{\partial P}{\partial X} = \frac{\beta^2}{1+\lambda_1} \frac{\partial^2 U}{\partial Y^2} + \frac{1}{1+\lambda_1} \frac{\partial^2 U}{\partial Z^2}, \quad (3.12)$$

$$\frac{\partial P}{\partial Y} = 0, \quad (3.13)$$

$$\frac{\partial P}{\partial Z} = 0. \quad (3.14)$$

The corresponding non-dimensional boundary conditions for compliant walls are stated as

$$U = 0 \text{ at } Y = \pm 1, \quad (3.15)$$

$$U = 0 \text{ at } Z = \pm H(X, t) = \pm 1 \pm \eta(X, t), \quad (3.16)$$

where  $\eta(X, t) = \phi \cos 2\pi(X - t)$  and  $0 \leq \phi \leq 1$ .

The governing equation for the flexible wall may be specified as

$$\mathcal{L}_2(\eta) = P - P_0, \quad (3.17)$$

in which  $\mathcal{L}_2$  is linear operator, which is used to represent the motion of stretched membrane with viscosity damping forces [80] such that

$$\mathcal{L}_2 = m_1 \frac{\partial^2}{\partial t^2} + D_1 \frac{\partial}{\partial t} + B_1 \frac{\partial^4}{\partial X^4} - T_1 \frac{\partial^2}{\partial X^2} + K_1. \quad (3.18)$$

In the above equation,  $m_1$  is the mass per unit area,  $D_1$  is the coefficient of the viscous damping forces,  $B_1$  is the flexural rigidity of the plate,  $T_1$  is the elastic tension per unit width in the membrane,  $K_1$  is spring stiffness and  $P_0$  is the pressure on the outside surface of the wall due to tension in the muscle, which is assumed to be zero here. The continuity of stress at  $Z = \pm 1 \pm \eta$  and using  $X$ -momentum Eq. (3.9), yield

$$\frac{\partial P}{\partial X} = E_1 \frac{\partial^3 \eta}{\partial t^2 \partial X} + E_2 \frac{\partial^2 \eta}{\partial t \partial X} + E_3 \frac{\partial^5 \eta}{\partial X^5} - E_4 \frac{\partial^3 \eta}{\partial X^3} + E_5 \frac{\partial \eta}{\partial X}, \quad (3.19)$$

$$\left. \begin{aligned} E_1 \frac{\partial^3 \eta}{\partial t^2 \partial X} + E_2 \frac{\partial^2 \eta}{\partial t \partial X} + E_3 \frac{\partial^5 \eta}{\partial X^5} - E_4 \frac{\partial^3 \eta}{\partial X^3} \\ + E_5 \frac{\partial \eta}{\partial X} = \frac{\beta^2}{1+\lambda_1} \frac{\partial^2 U}{\partial Y^2} + \frac{1}{1+\lambda_1} \frac{\partial^2 U}{\partial Z^2} \end{aligned} \right\} \text{ at } Z = \pm 1 \pm \eta, \quad (3.20)$$

in which  $E_1 = m_1 a^3 c / \lambda^3 \mu$ ,  $E_2 = D_1 a^3 / \mu \lambda^2$ ,  $E_3 = B_1 a^3 / c \mu \lambda^5$ ,  $E_4 = T_1 a^3 / c \mu \lambda^3$  and  $E_5 = K_1 a^3 / c \mu \lambda$  are the non-dimensional elasticity parameters.

Eliminating the pressure from Eqs. (3.12) and (3.14), we obtain

$$\frac{\beta^2}{1 + \lambda_1} \frac{\partial^3 U}{\partial Z \partial Y^2} + \frac{1}{1 + \lambda_1} \frac{\partial^3 U}{\partial Z^3} = 0. \quad (3.21)$$

### 3.2 Solution of the problem

We use the method of eigen function expansion to solve the above boundary value problem. Now let us introduce a transformation

$$U(X, Y, Z, t) = v_1(X, Y, Z, t) + w_1(Y). \quad (3.22)$$

After using the above equation in Eqs. (3.15), (3.16), (3.20) and (3.21), we get the system of two equations

$$\frac{d^2 w_1}{dY^2} = 0 \quad (3.23)$$

with

$$w_1(\pm 1) = 0 \quad (3.24)$$

and

$$\frac{\beta^2}{1 + \lambda_1} \frac{\partial^2 v_1}{\partial Y^2} + \frac{1}{1 + \lambda_1} \frac{\partial^2 v_1}{\partial Z^2} = F(X, Y, T). \quad (3.25)$$

The corresponding boundary conditions

$$v_1(X, \pm 1, Z, t) = 0, v_1(X, Y, \pm H, t) = -w_1(Y). \quad (3.26)$$

$$\left. \begin{aligned} E_1 \frac{\partial^3 \eta}{\partial t^2 \partial X} + E_2 \frac{\partial^2 \eta}{\partial t \partial X} + E_3 \frac{\partial^5 \eta}{\partial X^5} - E_4 \frac{\partial^3 \eta}{\partial X^3} \\ + E_5 \frac{\partial \eta}{\partial X} = \frac{\beta^2}{1 + \lambda_1} \frac{\partial^2 v_1}{\partial Y^2} + \frac{1}{1 + \lambda_1} \frac{\partial^2 v_1}{\partial Z^2} \end{aligned} \right\} \text{at } Z = \pm 1 \pm \eta, \quad (3.27)$$

where  $F(X, Y, T)$  is a constant of integration. The solution of Eq. (3.23) can be easily found by using the boundary conditions defined in Eq. (3.24). Now we solve Eq. (3.25) with boundary conditions (3.26) and (3.27) by eigen function expansion method. The eigen functions can be defined as

$$\phi_n(Y) = \cos(2n - 1) \frac{\pi}{2} Y, \quad n = 1, 2, 3, \dots \quad (3.28)$$

Now we define a series solution of the form

$$v_1 = \sum_{n=1}^{\infty} \phi_n(Y) \varphi_n(Z). \quad (3.29)$$

Using Eq. (3.29) into Eq. (3.25) and after using the orthogonality condition, we found

$$\varphi_n(Z) = \left(1 - \frac{\cosh \alpha_n Z}{\cosh \alpha_n H}\right) \frac{16F(-1)^n}{(2n-1)^3 \pi^3 \beta^2}. \quad (3.30)$$

From Eq. (3.22), the final solution is evaluated below

$$U(X, Y, Z, t) = \sum_{n=1}^{\infty} \left[ \left(1 - \frac{\cosh \alpha_n Z}{\cosh \alpha_n H}\right) \frac{16F(-1)^n}{(2n-1)^3 \pi^3 \beta^2} \right] \cos(2n-1) \frac{\pi}{2} Y, \quad (3.31)$$

where  $\alpha_n$  and  $F$  are defined as

$$\alpha_n = (2n-1) \frac{\pi}{2} \beta, \quad (3.32)$$

$$F(X, Y, t) = \left. \begin{aligned} &2\pi(1 + \lambda_1) \phi(2E_2\pi \cos 2\pi(X-t) - \\ &(E_5 + 4\pi^2(-E_1 + E_4 + 4E_3\pi^2)) \sin 2\pi(X-t)) \end{aligned} \right\}. \quad (3.33)$$

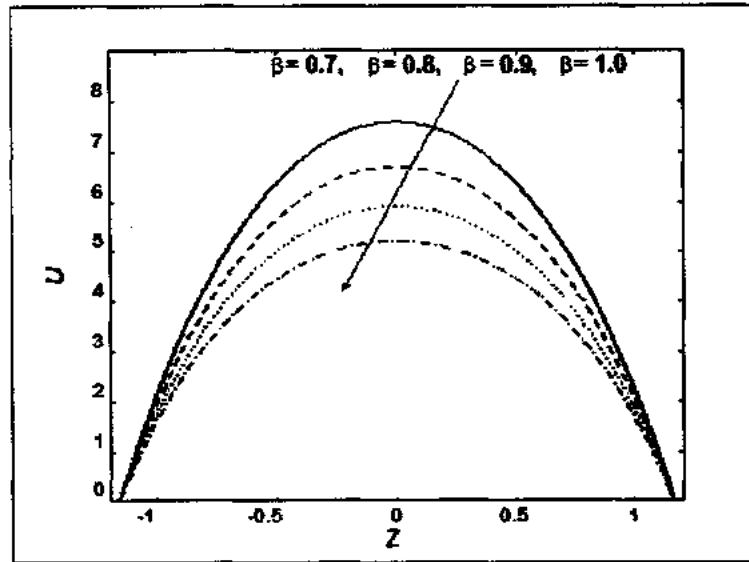
It is noted that limiting  $\lambda_1 \rightarrow 0$  results in reversing the present problem to the viscous fluid case. It can also be observed from the above analysis that employing  $\beta \rightarrow 0$  and  $\beta \rightarrow 1$ , reduces the discussed geometry to the two dimensional channel and square duct, respectively.

### 3.3 Graphical results and discussion

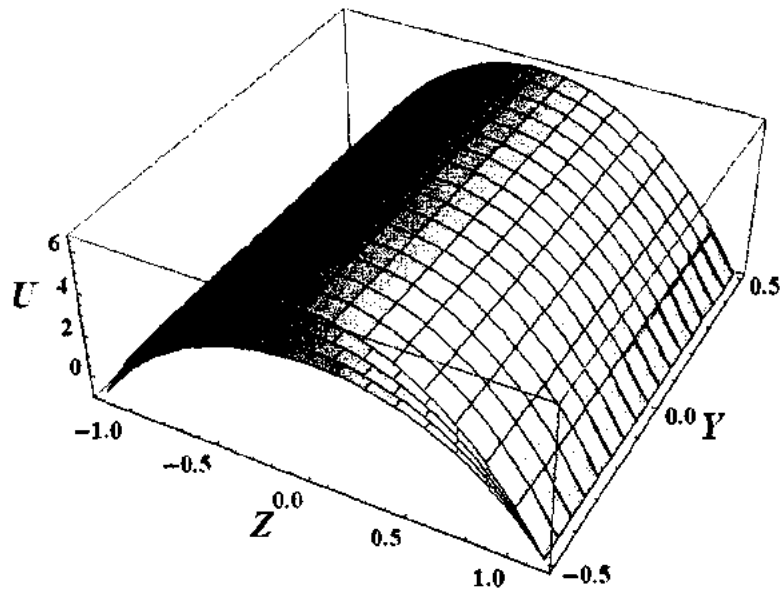
In this section, the effects of different physical parameters of Jeffrey fluid model on velocity profile of the fluid under discussion are examined graphically and the trapping phenomenon is also illustrated by plotting stream lines for different pertinent parameters. Figs. 3.2 to 3.6 are plotted to see the variation of velocity profile with the emerging parameters  $\beta$ ,  $E_1$ ,  $E_2$ ,  $E_3$  and  $E_4$ . The stream lines are sketched in Figs. 3.7 to 3.12, which observe the flow behavior with various values of all the observing parameters. In Figs. 3.2, 3.3 and 3.4, the velocity profile is plotted with different values of the parameters  $\beta$ ,  $E_1$  and  $E_2$ . From these figures, one can observe that magnitude of the velocity profile is a decreasing function of the above three parameters.



The effects of different values of the physical parameters  $E_3$  and  $E_4$  are mentioned in Figs. 3.5 and 3.6. From these plots, it is seen that velocity profile rises directly with increasing the magnitude of  $E_3$  and  $E_4$ . From Figs. 3.2 to 3.6, it can also be seen that the velocity attains its maximum value at the centre of the channel and remains symmetric throughout the channel. The stream lines for different values of the emerging parameters are drawn in Figs. 3.7 to 3.12 to lookout for the trapping bolus phenomenon. From Fig. 3.7, it can be seen that number of the trapped bolus are reduced with increasing the value of the parameter  $\beta$ . Fig. 3.8 is plotted to show the stream lines with the  $\lambda_1$  being raised. From this plot, it is clear that the number and size of the trapping bolus rises on left side but reduce in the opposite side of the channel with increasing magnitude of  $\lambda_1$ . The stream lines for different values of the parameter  $\phi$  are shown in Fig. 3.9. It is clear from this graph that the number of bolus are increasing monotonically with increasing  $\phi$  in left hand side and the size is decreasing on that side while the inverse behavior is seen on the right side of the channel. Fig. 3.10 reveals that the number of trapped bolus remain same but size is increasing on the left side while decreasing on the other side of the channel with the variation of  $E_1$ . It is measured from Fig. 3.11 that the trapped bolus do not change in number but increase in size with increasing value of  $E_2$  on left side of the channel and have opposite behavior on the different side. The stream lines for  $E_3$  are shown in Fig. 3.12. It is easy to see from this figure that more trapped bolus appear when one increases the value of  $E_3$  while size of the bolus changes randomly in both sides of the channel.

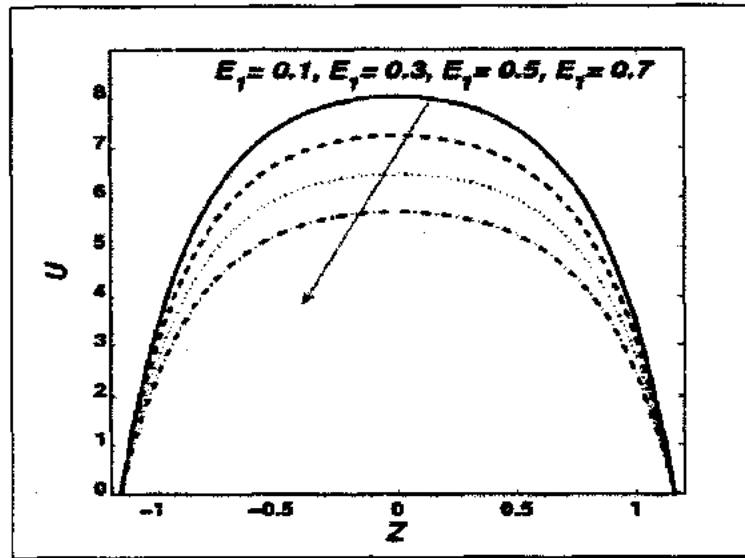


(a)

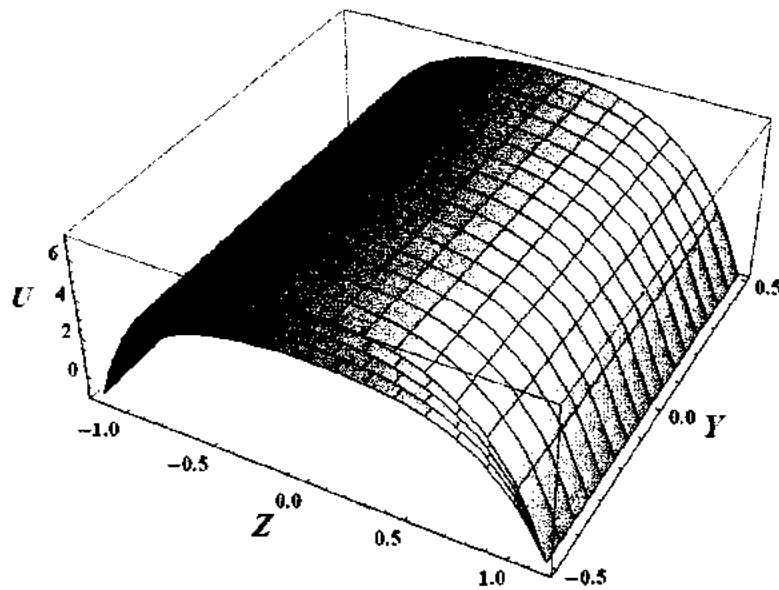


(b)

Fig. 3.2: Variation of velocity profile  $U$  with  $\beta$  for fixed values of  $\phi = 0.2$ ,  $X = 0.5$ ,  $t = 0.4$ ,  $\lambda_1 = 0.5$ ,  $E_1 = 0.1$ ,  $E_2 = 0.2$ ,  $E_3 = 0.01$ ,  $E_4 = 0.2$ ,  $E_5 = 0.3$  (a) for 2-dimensional, (b) For 3-dimensional.

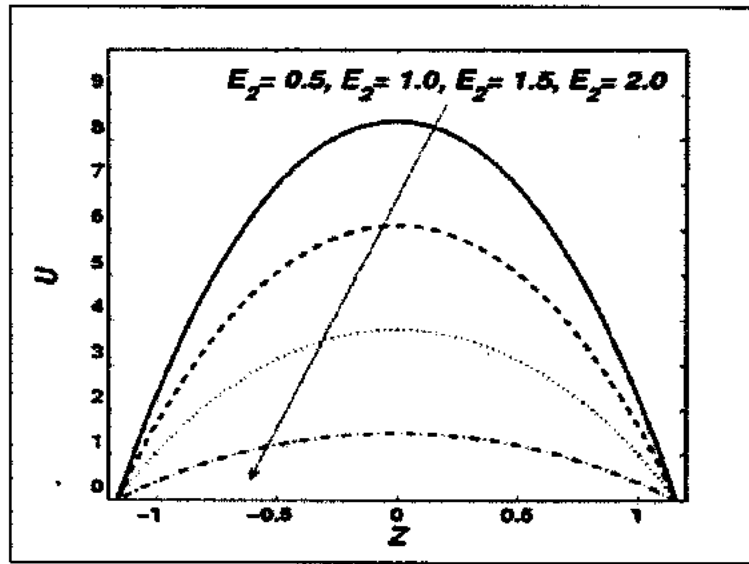


(a)

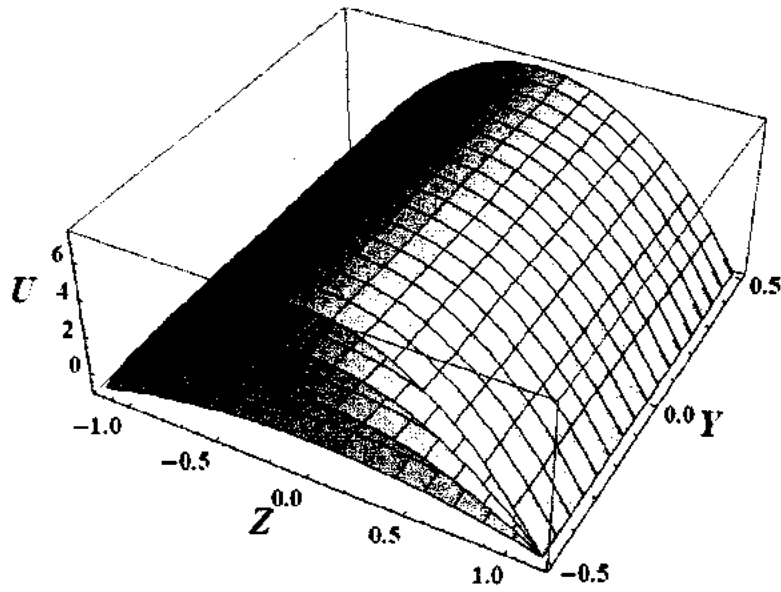


(b)

Fig. 3.3: Variation of velocity profile  $U$  with  $E_1$  for fixed values of  $\phi = 0.2$ ,  $X = 0.5$ ,  $t = 0.4$ ,  $\lambda_1 = 0.5$ ,  $\beta = 1.5$ ,  $E_2 = 0.1$ ,  $E_3 = 0.05$ ,  $E_4 = 0.2$ ,  $E_5 = 0.5$  (a) for 2-dimensional, (b) For 3-dimensional.

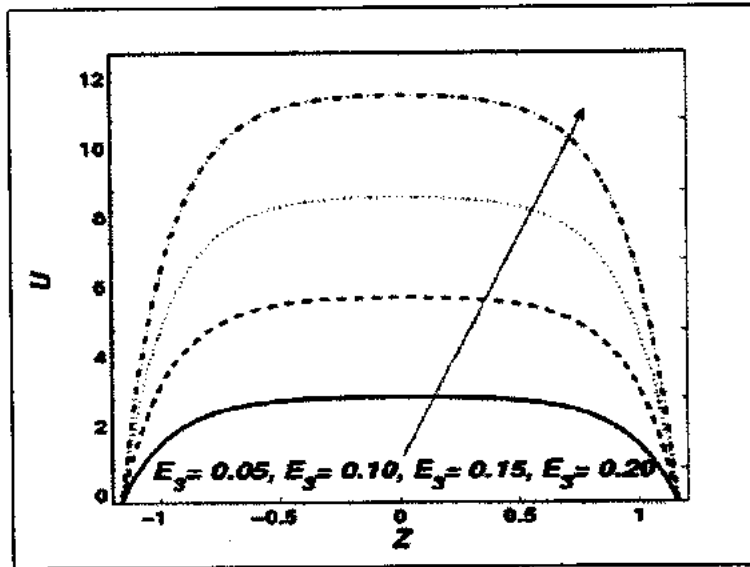


(a)

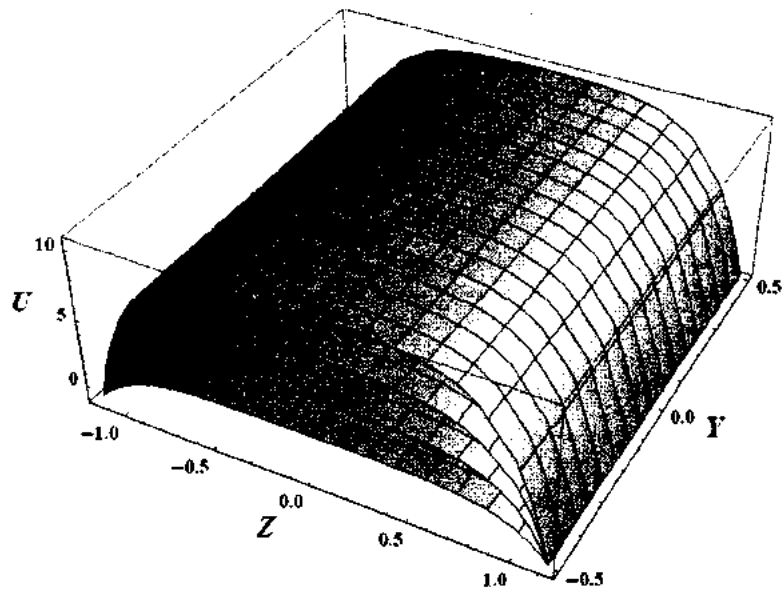


(b)

Fig. 3.4: Variation of velocity profile  $U$  with  $E_2$  for fixed values of  $\phi = 0.2$ ,  $X = 0.5$ ,  $t = 0.4$ ,  $\beta = 1.5$ ,  $\lambda_1 = 0.5$ ,  $E_1 = 0.1$ ,  $E_3 = 0.01$ ,  $E_4 = 0.2$ ,  $E_5 = 0.5$  (a) for 2-dimensional, (b) For 3-dimensional.

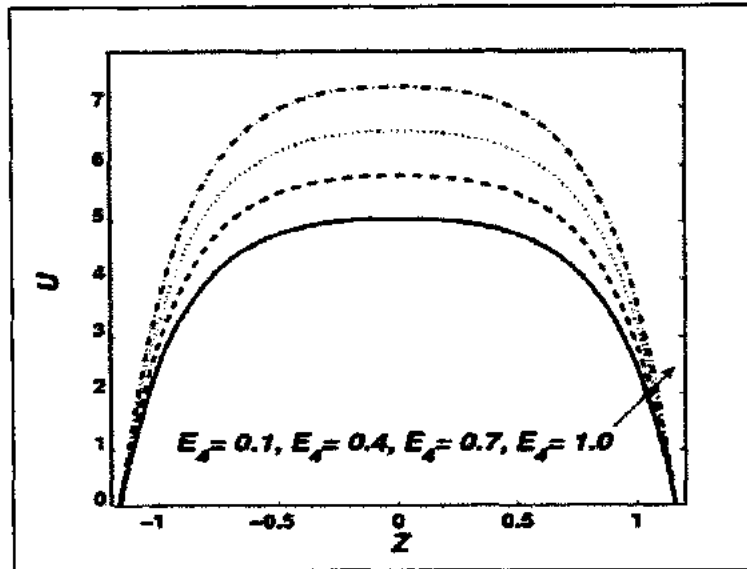


(a)

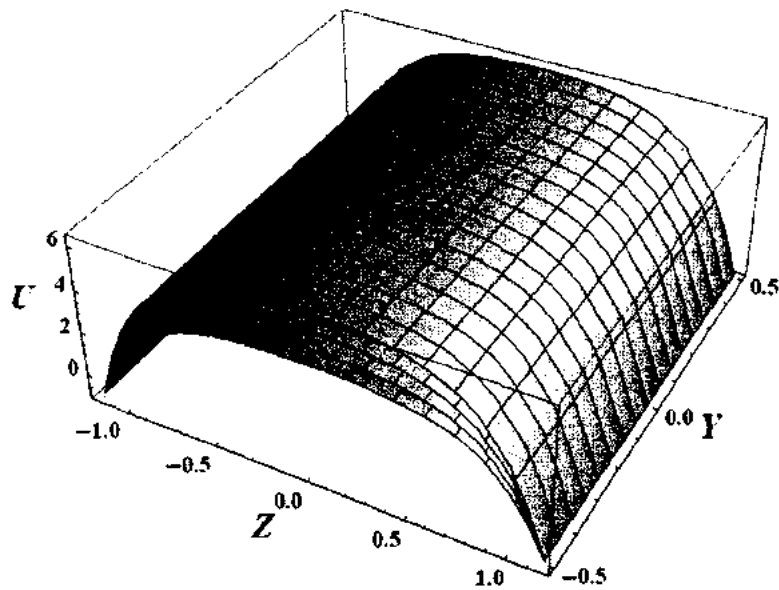


(b)

Fig. 3.5: Variation of velocity profile  $U$  with  $E_3$  for fixed values of  $\phi = 0.2$ ,  $X = 0.5$ ,  $t = 0.4$ ,  $\beta = 2.7$ ,  $\lambda_1 = 0.5$ ,  $E_1 = 0.1$ ,  $E_2 = 0.1$ ,  $E_4 = 0.2$ ,  $E_5 = 0.5$  (a) for 2-dimensional, (b) For 3-dimensional.



(a)



(b)

Fig. 3.6: Variation of velocity profile  $U$  with  $E_4$  for fixed values of  $\phi = 0.2$ ,  $X = 0.5$ ,  $t = 0.4$ ,  $\beta = 3$ ,  $\lambda_1 = 0.5$ ,  $E_1 = 0.1$ ,  $E_2 = 0.1$ ,  $E_3 = 0.2$ ,  $E_5 = 0.5$  (a) for 2-dimensional, (b) For 3-dimensional.

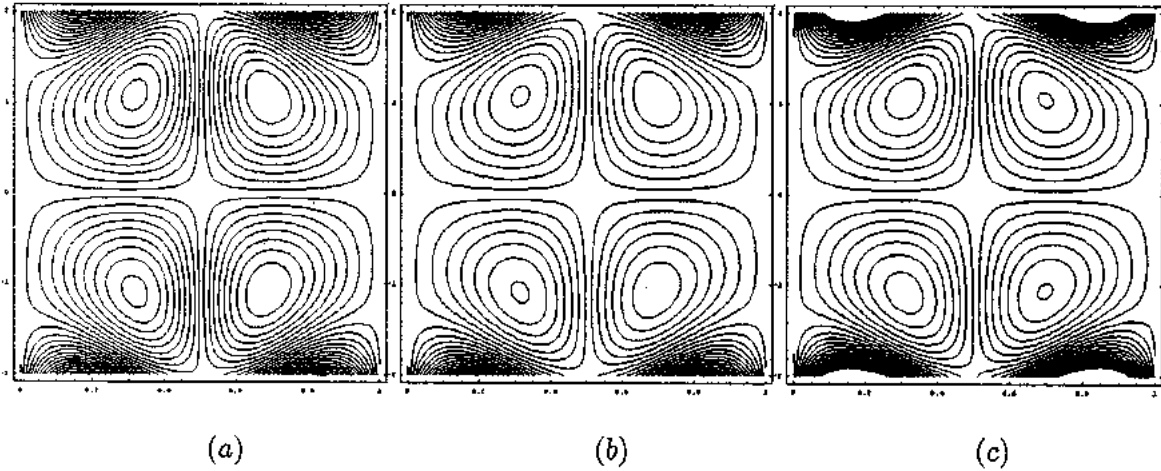


Fig. 3.7: Stream lines for different values of  $\beta$ , (a) for  $\beta = 0.4$ , (b) for  $\beta = 0.6$ , (c) for  $\beta = 0.8$ . The other parameters are  $Y = 0.5$ ,  $\lambda_1 = 1$ ,  $\phi = 0.2$ ,  $t = 0.5$ ,  $E_1 = 1$ ,  $E_2 = 0.2$ ,  $E_3 = 0.05$ ,  $E_4 = 0.1$ ,  $E_5 = 0.3$ .

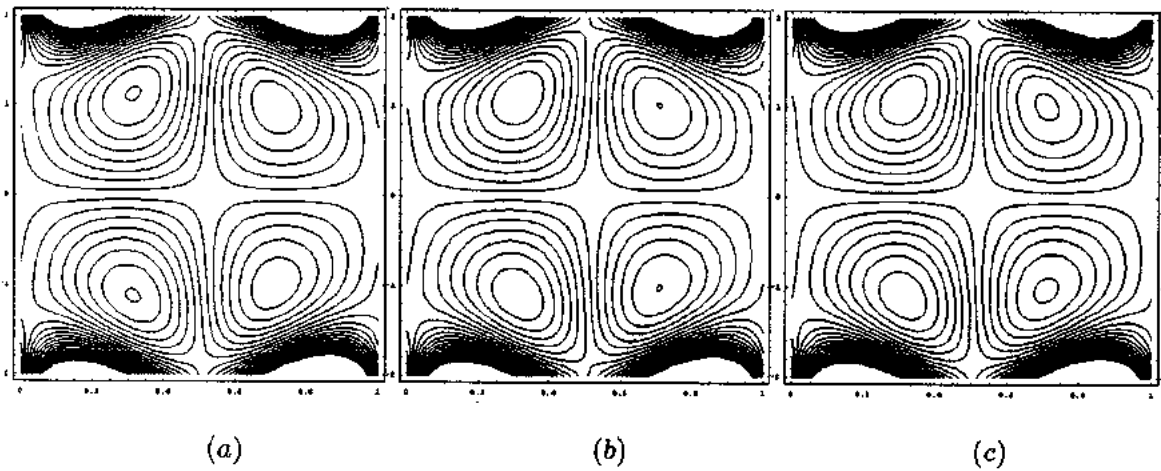


Fig. 3.8: Stream lines for different values of  $\lambda_1$ , (a) for  $\lambda_1 = 0.5$ , (b) for  $\lambda_1 = 1.0$ , (c) for  $\lambda_1 = 1.5$ . The other parameters are  $Y = 0.5$ ,  $\beta = 1.1$ ,  $\phi = 0.2$ ,  $t = 0.5$ ,  $E_1 = 1$ ,  $E_2 = 0.2$ ,  $E_3 = 0.01$ ,  $E_4 = 0.2$ ,  $E_5 = 0.3$ .

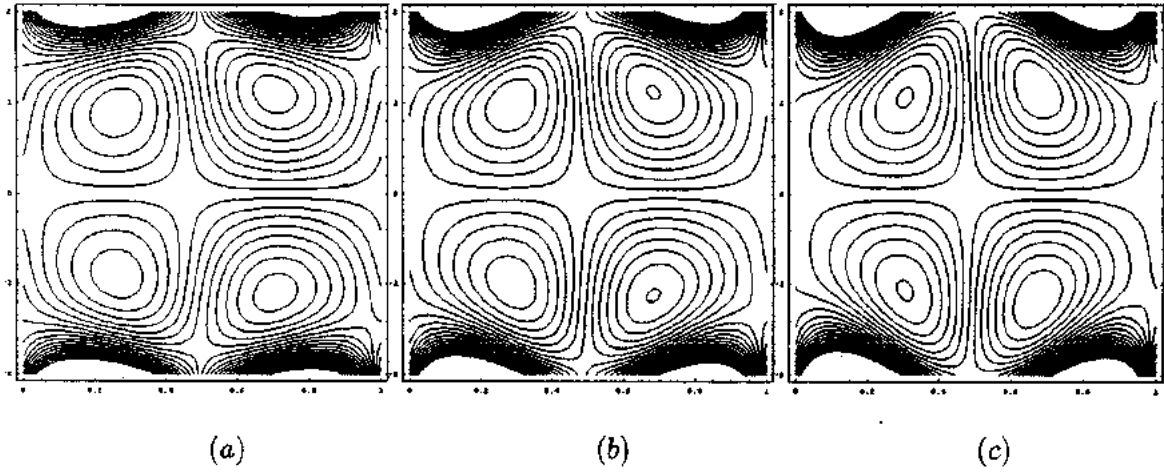


Fig. 3.9: Stream lines for different values of  $\phi$ , (a) for  $\phi = 0.1$ , (b) for  $\phi = 0.2$ , (c) for  $\phi = 0.3$ . The other parameters are  $Y = 0.5$ ,  $\lambda_1 = 1$ ,  $\beta = 1.1$ ,  $t = 0.5$ ,  $E_1 = 1$ ,  $E_2 = 0.2$ ,  $E_3 = 0.01$ ,  $E_4 = 0.2$ ,  $E_5 = 0.3$ .

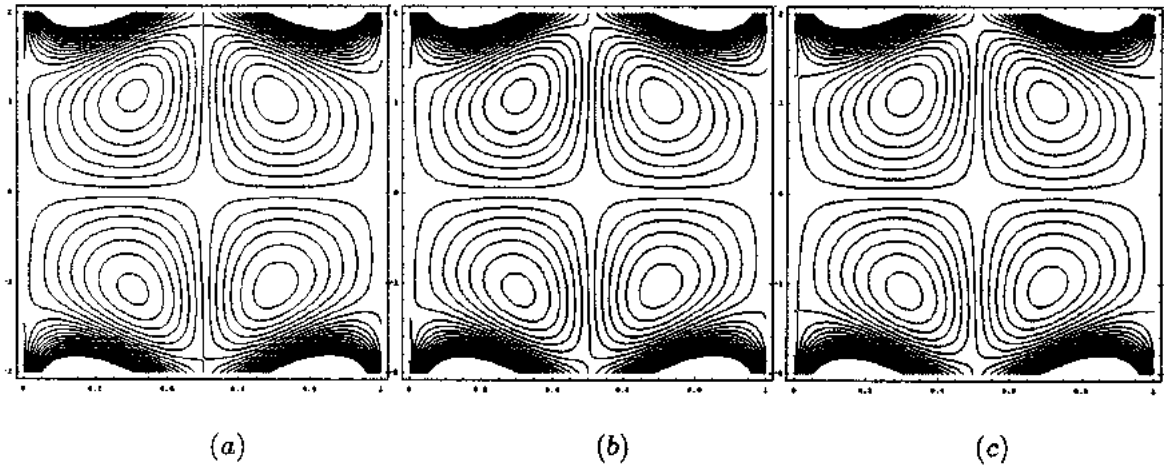


Fig. 3.10: Stream lines for different values of  $E_1$ , (a) for  $E_1 = 1$ , (b) for  $E_1 = 2$ , (c) for  $E_1 = 3$ . The other parameters are  $Y = 0.5$ ,  $\lambda_1 = 1$ ,  $\phi = 0.2$ ,  $t = 0.5$ ,  $\beta = 1$ ,  $E_2 = 0.2$ ,  $E_3 = 0.05$ ,  $E_4 = 0.2$ ,  $E_5 = 0.3$ .



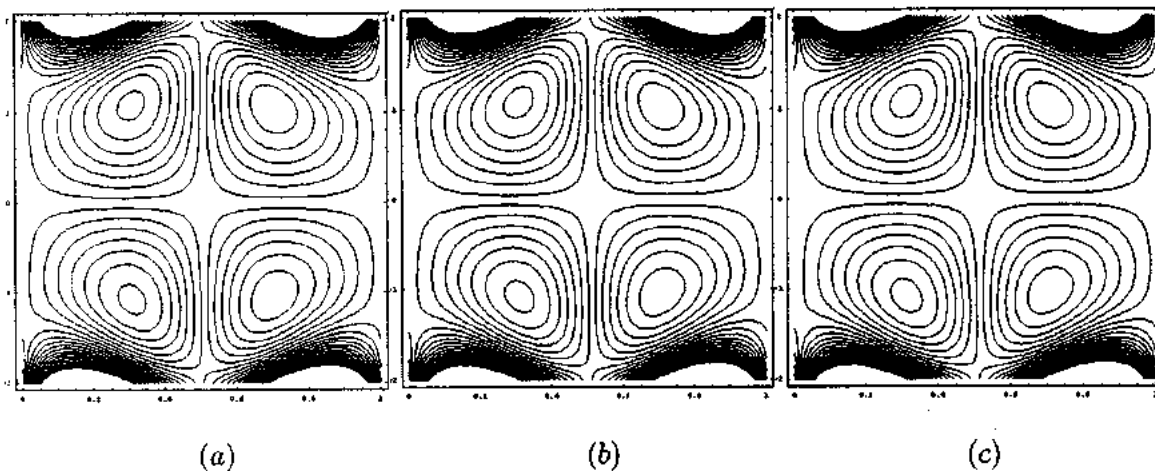


Fig. 3.11: Stream lines for different values of  $E_2$ , (a) for  $E_2 = 0.5$ , (b) for  $E_2 = 1$ , (c) for  $E_2 = 1.5$ . The other parameters are  $Y = 0.5$ ,  $\lambda_1 = 1$ ,  $\phi = 0.2$ ,  $t = 0.5$ ,  $\beta = 1.1$ ,  $E_1 = 0.2$ ,  $E_3 = 0.05$ ,  $E_4 = 0.2$ ,  $E_5 = 0.3$ .

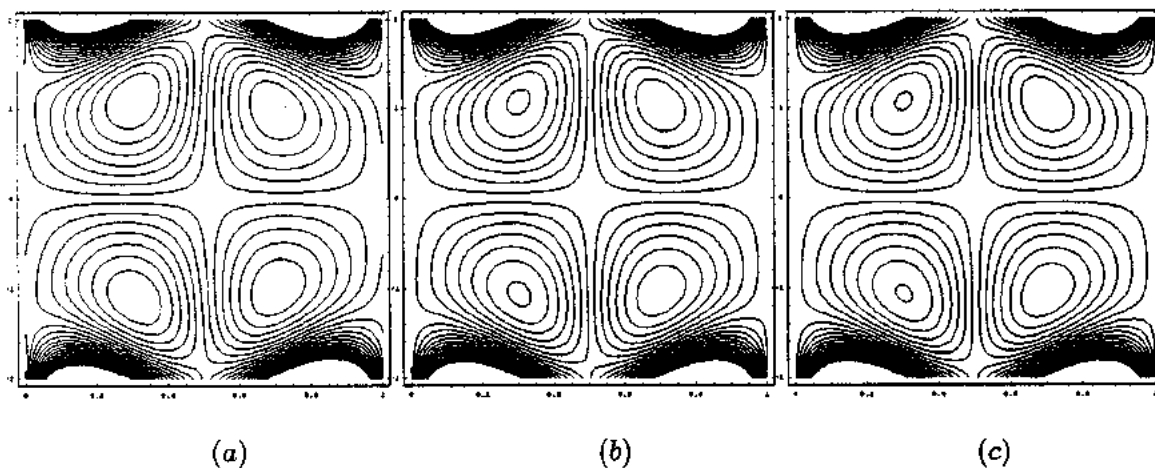


Fig. 3.12: Stream lines for different values of  $E_3$ , (a) for  $E_3 = 0.01$ , (b) for  $E_3 = 0.05$ , (c) for  $E_3 = 0.09$ . The other parameters are  $Y = 0.5$ ,  $\lambda_1 = 1$ ,  $\phi = 0.2$ ,  $t = 0.5$ ,  $\beta = 1$ ,  $E_1 = 0.2$ ,  $E_2 = 0.05$ ,  $E_4 = 0.2$ ,  $E_5 = 0.3$ .

## Chapter 4

# Exact solution for peristaltic flow of Jeffrey fluid model in a three dimensional rectangular duct having slip at the walls

This chapter deals with the exact solutions for the peristaltic flow of Jeffrey fluid model in a cross section of three dimensional rectangular channel having slip at the peristaltic boundaries. The equation of motion and boundary conditions are made dimensionless by introducing some suitable non-dimensional parameters. The flow is considered under the approximations of low Reynolds number and long wavelength. Exact solution of the obtained linear boundary value problem is evaluated. However, the expression for pressure rise is calculated numerically with the help of numerical integration. All pertinent parameters are discussed through graphs of pressure rise, pressure gradient, velocity and stream functions. This study has been accepted for publication in the journal of "*Applied Bionics and Biomechanics*", 11 (2014) 81–90.

## 4.1 Mathematical formulation of the problem

Let us consider the slip effects at the peristaltic walls for peristaltic flow of an incompressible Jeffrey fluid in a rectangular channel (see Fig. 3.1). The flow is induced by the propagation of sinusoidal waves travelling in the direction parallel to the flow.

Let us analyze the flow in a wave frame  $(x, y, z)$  moving with a constant velocity  $c$  away from the fixed frame  $(X, Y, Z)$  by the transformation

$$x = X - ct, \quad y = Y, \quad z = Z, \quad u = U - c, \quad w = W, \quad p(x, z) = p(X, Z, t). \quad (4.1)$$

We define the following non-dimensional quantities along with the already defined in Eq. (3.6)

$$\left. \begin{aligned} \bar{x} &= \frac{x}{\lambda}, \quad \bar{y} = \frac{y}{d}, \quad \bar{z} = \frac{z}{a}, \quad \bar{u} = \frac{u}{c}, \quad \bar{w} = \frac{w}{\frac{c}{\delta_0}}, \quad \bar{h} = \frac{H}{a}, \quad \bar{p} = \frac{a^2 p}{\mu c \lambda}, \quad \beta_1 = \frac{L}{a}, \\ \bar{S}_{2\bar{x}\bar{x}} &= \frac{a}{\mu c} S_{2xx}, \quad \bar{S}_{2\bar{x}\bar{y}} = \frac{d}{\mu c} S_{2xy}, \quad \bar{S}_{2\bar{x}\bar{z}} = \frac{a}{\mu c} S_{2xz}, \quad \bar{S}_{2\bar{y}\bar{z}} = \frac{d}{\mu c} S_{2yz}, \\ \bar{S}_{2\bar{z}\bar{z}} &= \frac{\lambda}{\mu c} S_{2zz}, \quad \bar{S}_{2\bar{y}\bar{y}} = \frac{\lambda}{\mu c} S_{2yy}, \quad \bar{\gamma} = \frac{\gamma a}{c}, \quad \beta = \frac{a}{d} \end{aligned} \right\}. \quad (4.2)$$

Under the assumption of long wavelength and low Reynolds number, the non-dimensional governing Eqs. (1.4) to (1.6) in wave frame for the considered flow problem (after exempting the prime symbols) are simplified as

$$\frac{\partial u}{\partial x} + \frac{\partial w}{\partial z} = 0, \quad (4.3)$$

$$\text{Re } \delta_0 \left( u \frac{\partial u}{\partial x} + w \frac{\partial u}{\partial z} \right) = -\frac{\partial p}{\partial x} + \delta_0 \frac{\partial}{\partial x} S_{2xx} + \beta^2 \frac{\partial}{\partial y} S_{2xy} + \frac{\partial}{\partial z} S_{2xz}, \quad (4.4)$$

$$0 = -\frac{\partial p}{\partial y} + \delta_0^2 \frac{\partial}{\partial x} S_{2yx} + \delta_0^2 \frac{\partial}{\partial y} S_{2yy} + \delta_0 \frac{\partial}{\partial z} S_{2yz}, \quad (4.5)$$

$$\text{Re } \delta_0^2 \left( u \frac{\partial w}{\partial x} + w \frac{\partial w}{\partial z} \right) = -\frac{\partial p}{\partial z} + \delta_0^2 \frac{\partial}{\partial x} S_{2zx} + \delta_0 \beta^2 \frac{\partial}{\partial y} S_{2zy} + \delta_0^2 \frac{\partial}{\partial z} S_{2zz}, \quad (4.6)$$

where the components of stress tensor  $S_{2xx}$ ,  $S_{2xy}$ ,  $S_{2xz}$ ,  $S_{2yy}$ ,  $S_{2yz}$  and  $S_{2zz}$  for Jeffrey fluid are

evaluated as

$$\left. \begin{aligned}
 S_{2xx} &= \frac{2\delta_0}{1+\lambda_1} \left( 1 + \frac{\lambda_2 c \delta_0}{a} \left( \frac{\partial}{\partial t} + u \frac{\partial}{\partial x} + w \frac{\partial}{\partial z} \right) \right) \frac{\partial u}{\partial x} \\
 S_{2xy} &= \frac{1}{1+\lambda_1} \left( 1 + \frac{\lambda_2 c \delta_0}{a} \left( \frac{\partial}{\partial t} + u \frac{\partial}{\partial x} + w \frac{\partial}{\partial z} \right) \right) \frac{\partial u}{\partial y} \\
 S_{2xz} &= \frac{1}{1+\lambda_1} \left( 1 + \frac{\lambda_2 c \delta_0}{a} \left( \frac{\partial}{\partial t} + u \frac{\partial}{\partial x} + w \frac{\partial}{\partial z} \right) \right) \left( \frac{\partial u}{\partial z} + \delta_0^2 \frac{\partial w}{\partial x} \right) \\
 S_{2yy} &= 0 \\
 S_{2yz} &= \frac{\delta_0}{1+\lambda_1} \left( 1 + \frac{\lambda_2 c \delta_0}{a} \left( \frac{\partial}{\partial t} + u \frac{\partial}{\partial x} + w \frac{\partial}{\partial z} \right) \right) \frac{\partial w}{\partial y} \\
 S_{2zz} &= \frac{2}{1+\lambda_1} \left( 1 + \frac{\lambda_2 c \delta_0}{a} \left( \frac{\partial}{\partial t} + u \frac{\partial}{\partial x} + w \frac{\partial}{\partial z} \right) \right) \frac{\partial w}{\partial z}
 \end{aligned} \right\} \quad (4.7)$$

Under the long wavelength and low Reynolds number approximations, Eqs. (4.4) to (4.6) have the form

$$\beta^2 \frac{\partial^2 u}{\partial y^2} + \frac{\partial^2 u}{\partial z^2} = (1 + \lambda_1) \frac{\partial p}{\partial x}, \quad (4.8)$$

$$\frac{\partial p}{\partial y} = 0 = \frac{\partial p}{\partial z}. \quad (4.9)$$

The corresponding slip boundary conditions at the walls are described as [80]

$$\left. \begin{aligned}
 u &= -1 \text{ at } y = \pm 1, u = -\frac{\beta_1}{1+\lambda_1} \frac{\partial u}{\partial z} - 1 \text{ at } z = h(x) = 1 + \phi \cos(2\pi x), \\
 u &= \frac{\beta_1}{1+\lambda_1} \frac{\partial u}{\partial z} - 1 \text{ at } z = -h(x) = -1 - \phi \cos(2\pi x)
 \end{aligned} \right\} \quad (4.10)$$

From Eq. (4.9), it is obvious that  $p \neq p(y, z)$ . Therefore, the Eq. (4.8) can be written in more precise form as

$$\beta^2 \frac{\partial^2 u}{\partial y^2} + \frac{\partial^2 u}{\partial z^2} = (1 + \lambda_1) \frac{dp}{dx}. \quad (4.11)$$

**Special cases:** There are some special cases which can be derived from the above discussion i.e., for  $\beta = 0$ , we retrieve the case for peristaltic flow of Jeffrey fluid in two dimensional channel,  $\lambda_1 = 0$  gives the peristaltic flow of viscous fluid in three dimensional channel and  $\beta_1 = 0$  leads to the no-slip conditions.

## 4.2 Solution of the problem

The exact solution of the Eq. (4.11) along with boundary conditions defined in Eq. (4.10) are evaluated by adopting the eigen function expansion method and is found as

$$u(x, y, z) = \left. \begin{aligned} & -\frac{dp}{dx} \frac{(1-y^2+\lambda_1-y^2\lambda_1)-2\beta^2}{2\beta^2} + \sum_{n=1}^{\infty} \cos\left(y \frac{\alpha_n}{\beta}\right) \\ & \left( \cosh(z\alpha_n) \left( -\frac{8\frac{dp}{dx}(1+\lambda_1)(2\cos n\pi)}{(-1+2n)^3 \pi^3 \beta^2 \left( \cosh(h\alpha_n) + \frac{\alpha_n \beta_1 \sinh(h\alpha_n)}{1+\lambda_1} \right)} \right. \right. \\ & - \left. \left. \left( 8(1+\lambda_1) \operatorname{sech}(h\alpha_n) \left( \frac{\alpha_n \beta_1 \cosh(h\alpha_n)}{1+\lambda_1} + \sinh(h\alpha_n) \right) \right) \right) / \left( (-1+2n)^3 \pi^3 \beta^2 \right. \right. \\ & \left. \left. \left( \alpha_n \beta_1 \cosh(h\alpha_n) + \sinh(h\alpha_n) + \lambda_1 \sinh(h\alpha_n) \right) \right) \right) \\ & \left. \left( \cosh(h\alpha_n) + \frac{\alpha_n \beta_1 \sinh(h\alpha_n)}{1+\lambda_1} \right) \right) + (8(1+\lambda_1) \operatorname{Sech}(h\alpha_n) \\ & \left. \left( 2\frac{dp}{dx} \alpha_n \beta_1 \cos n\pi \sinh(h\alpha_n) \right) \sinh(z\alpha_n) \right) / \left( (-1+2n)^3 \right. \\ & \left. \left. \pi^3 \beta^2 \left( \alpha_n \beta_1 \cosh(h\alpha_n) + \sinh(h\alpha_n) + \lambda_1 \sinh(h\alpha_n) \right) \right) \right) \end{aligned} \right\}, \quad (4.12)$$

where  $\alpha_n = (2n-1)\frac{\pi}{2}\beta$ ,  $n = 1, 2, 3, \dots$

The volumetric flow rate  $\bar{Q}$  is calculated as

$$\bar{Q} = \int_0^{h(x)} \int_0^1 u(x, y, z) dy dz. \quad (4.13)$$

The average volume flow rate over one period ( $T = \lambda/c$ ) of the peristaltic wave is defined as

$$Q = \int_0^{h(x)} \int_0^1 (u(x, y, z) + 1) dy dz = \bar{Q} + h(x). \quad (4.14)$$

The pressure gradient  $dp/dx$  is obtained after solving Eqs. (4.13) and (4.14) and is found as

$$\frac{dp}{dx} = - \left. \sum_{n=1}^{\infty} \left( Q / \left( \frac{h}{3\beta^2} + \frac{h\lambda_1}{3\beta^2} + \left( 8(1+\lambda_1) 2\cos n\pi \sin \frac{\alpha}{\beta} \left( \alpha_n \beta_1 + \right. \right. \right) \right. \right. \right. \right. \\ \left. \left. \left. \left. \left. (1+\lambda_1) \sinh(h\alpha_n) \right) \tanh(h\alpha_n) \right) / \left( (-1+2n)^3 \pi^3 \alpha_n^2 \beta \left( \alpha_n \beta_1 \right. \right. \right. \right. \right. \\ \left. \left. \left. \left. \left. \cosh(h\alpha_n) + (1+\lambda_1) \sinh(h\alpha_n) \right) \right) \right) \right) \right) \right\}. \quad (4.15)$$

The pressure rise  $\Delta p$  is evaluated by numerically integrating the pressure gradient  $dp/dx$  over

one wavelength, i.e.,

$$\Delta p = \int_0^1 \frac{dp}{dx} dx. \quad (4.16)$$

### 4.3 Graphical results and discussion

We have obtained the exact analytical solutions for the peristaltic flow of Jeffrey fluid model in a rectangular channel having slip at the peristaltic walls. In this section, the effects of physical parameters on the rheological aspects of the flow phenomenon are described. All the pertinent quantities are described through graphical treatment. Numerical variation of pressure rise and velocity profile is also described through Tables 4.1 and 4.2. Figs. 4.1 to 4.4 are drawn to show the effect of different parameters such as  $\beta$ ,  $\beta_1$ ,  $\lambda_1$  and  $\phi$  on pressure rise per unit wavelength  $\Delta p$  against the mean flux  $Q$ . The fluid flow can be classify on the basis of coordinate system generated by taking  $\Delta p$  along y-axis and  $Q$  along x-axis in to three major regions: Quadrant (I) displays  $Q > 0$  and  $\Delta p > 0$  is called peristaltic pumping region, Quadrant (II) where  $Q > 0$  and  $\Delta p < 0$  is augmented flow region and Quadrant (IV) contains  $Q < 0$  and  $\Delta p > 0$  is known as backward pumping region. If  $\Delta p = 0$  it is called free pumping. Fig. 4.1 indicates free pumping at  $Q = 0$ , an increase in  $\beta$  rises the magnitude of pressure change in quadrant IV while reduces in II. Fig. 4.2 shows the behavior of  $\Delta p$  with changing values of  $\beta_1$ . It is observed an increase in the values of  $\beta_1$  gives opposite behavior as compared with  $\beta$ . Figs. 4.3 and 4.4 are drawn to show for the variation of  $\lambda_1$  and  $\phi$  respectively. It is noted that with the increase in  $\lambda_1$  pressure rise suppresses in augmented part while increased in backward pumping and for rising  $\phi$  pressure change inversely.

The variation in pressure gradient  $dp/dx$  for different parameters  $\beta$ ,  $\beta_1$ ,  $\lambda_1$ ,  $\phi$  and  $Q$  can be observed from Figs. 4.5 to 4.9. Figs. 4.5 and 4.6 display the effects of  $\beta$  and  $\beta_1$  respectively. Increase in  $\beta$  decreases the magnitude of pressure gradient  $dp/dx$  in the wavelength  $x \in [0, 1]$  whereas, increase in  $\beta_1$  increases pressure gradient. In both the graphs the pressure at  $x < 0.2$  and  $x > 0.8$  attains a much smaller value indicating a low resistance to the flow and at about  $x = 0.5$  the maximum resistance to the flow is anticipated. Fig. 4.7 Shows a similar behavior for  $\lambda_1$  as observed for  $\beta_1$ . Fig. 4.8 indicates that in the central region increase in amplitude ratio  $\phi$  decreases the pressure but this behavior reverse itself in the region  $x < 0.2$  and  $x > 0.8$ .

Fig. 4.9 shows decrease in pressure gradient with mean flow rate  $Q$ .

Next we examine the graphical aspects of the different parameters of interest on the velocity distribution through Figs. 4.10 to 4.14. The two and three dimensional analysis is submitted in these figures for all the observing parameters  $\beta$ ,  $\beta_1$ ,  $\lambda_1$ ,  $\phi$  and  $Q$ . The variation of  $\beta$  is shown in Fig. 4.10. It is observed that velocity decreases with the increasing effects of  $\beta$ . Fig. 4.11 shows the variation of velocity for different fixed values of  $\beta_1$ . It is noted that in the part  $z \in (-1, 0.5)$ , velocity decreases with the increase of  $\beta_1$  while the situation is opposite in the rest of the region. The maximum velocity is at the centre of the duct but for smaller values of  $\beta_1$  velocity decreases rapidly. The theoretical effects of  $\lambda_1$  are displayed in Fig. 4.12. An increase in velocity profile is observed when the values of  $\lambda_1$  increases. Figs. 4.13 and 4.14 show decrease in velocity when  $\phi$  increases and increase when  $Q$  increases respectively.

The stream lines are drawn in Figs. 4.15 to 4.18 to see the trapping bolus behavior with the variation of emerging parameters  $\beta$ ,  $\lambda_1$ ,  $\phi$ , and  $Q$ . From Fig. 4.15, it is seen that numbers of the trapped bolus are reduced with increasing the values of the parameter  $\beta$  where as the size increases. Fig. 4.16 is for stream lines versus wavelength constructed for  $\lambda_1$ . It is measured here that number of bolus is reduced with the increase of  $\lambda_1$ . The stream lines for different values of the parameter  $\phi$  are shown in Fig. 4.17. It is evident that the size of the trapped bolus increases with increasing  $\phi$ . It is measured from Fig. 4.18 that the size of trapped bolus

decreases with mean flux  $Q$ , however the boluses are increased in number.

$Q$	$\Delta p$ when $\beta_1 = 0$	$\Delta p$ when $\beta_1 = 0.3$	$\Delta p$ when $\beta_1 = 0.5$
-2.0	7.87572	6.13742	5.60602
-1.6	6.30057	4.90993	4.48482
-1.2	4.72543	3.68245	3.36361
-0.8	3.15029	2.45497	2.24241
-0.4	1.57514	1.22748	1.12120
0.0	0.00000	0.00000	0.00000
0.4	-1.5751	-1.2274	-1.1212
0.8	-3.1502	-2.4549	-2.2424
1.2	-4.7254	-3.6824	-3.3636
1.6	-6.3005	-4.9099	-4.4848
2.0	-7.8757	-6.1374	-5.6060

Table 4.1: Variation of pressure rise  $\Delta p$  for fixed values of  $\lambda_1 = 0.1$ ,  $\beta = 0.5$ ,  $\phi = 0.1$ .



$z$	$u$ when $\beta_1 = 0$	$u$ when $\beta_1 = 0.3$	$u$ when $\beta_1 = 0.5$
-1.0	0.77306	0.52413	0.39374
-0.8	0.99314	0.75071	0.62376
-0.6	1.15593	0.92096	0.79799
-0.4	1.26801	1.04190	0.92366
-0.2	1.33366	1.11816	1.00559
0.0	1.35529	1.15257	1.04679
0.2	1.33366	1.14633	1.04872
0.4	1.26801	1.09923	1.01143
0.6	1.15593	1.00954	0.93353
0.8	0.99314	0.87388	0.81212
1.0	0.77306	0.68690	0.64245

Table 4.2: Variation of velocity profile  $u$  for fixed values of  $\lambda_1 = 3$ ,  $\beta = 0.5$ ,  $\phi = 0.2$ ,  $Q = 0.5$ ,  $x = 0$ ,  $y = 0.5$ .

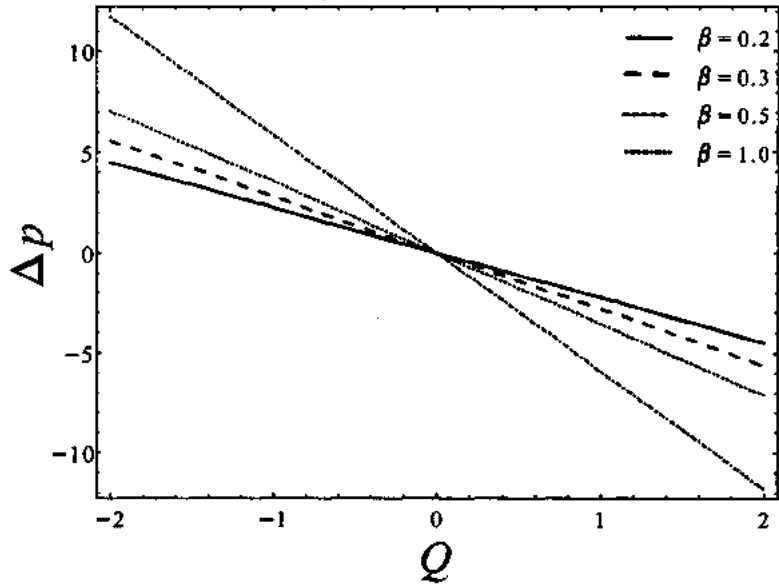


Fig. 4.1: Variation of pressure rise  $\Delta p$  with  $\beta$  for fixed values of  $\lambda_1 = 0.1$ ,  $\beta_1 = 0.1$ ,  $\phi = 0.1$ .

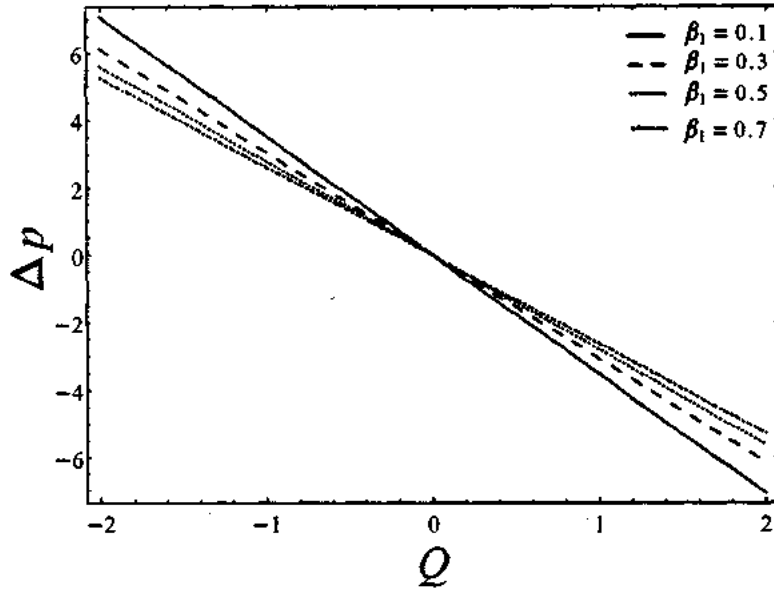


Fig. 4.2: Variation of pressure rise  $\Delta p$  with  $\beta_1$  for fixed values of  $\lambda_1 = 0.1$ ,  $\beta = 0.5$ ,  $\phi = 0.1$ .

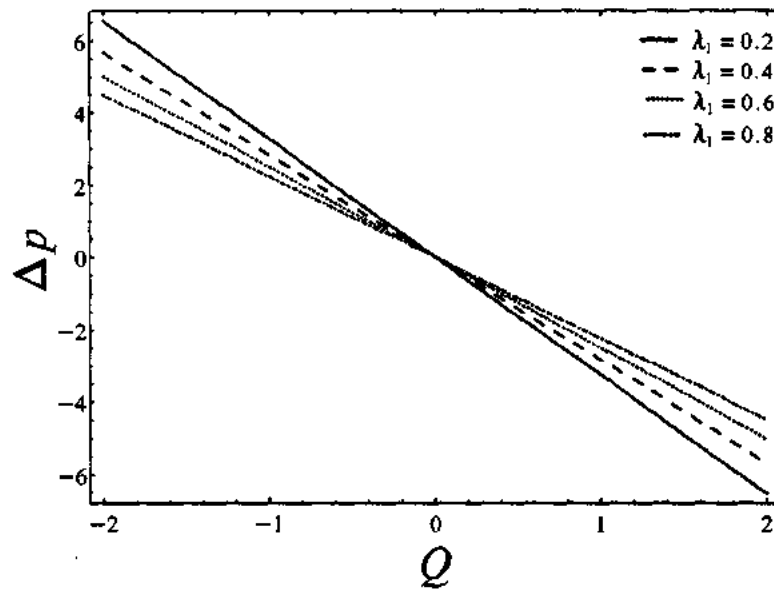


Fig. 4.3: Variation of pressure rise  $\Delta p$  with  $\lambda_1$  for fixed values of  $\beta = 0.5$ ,  $\beta_1 = 0.1$ ,  $\phi = 0.1$ .

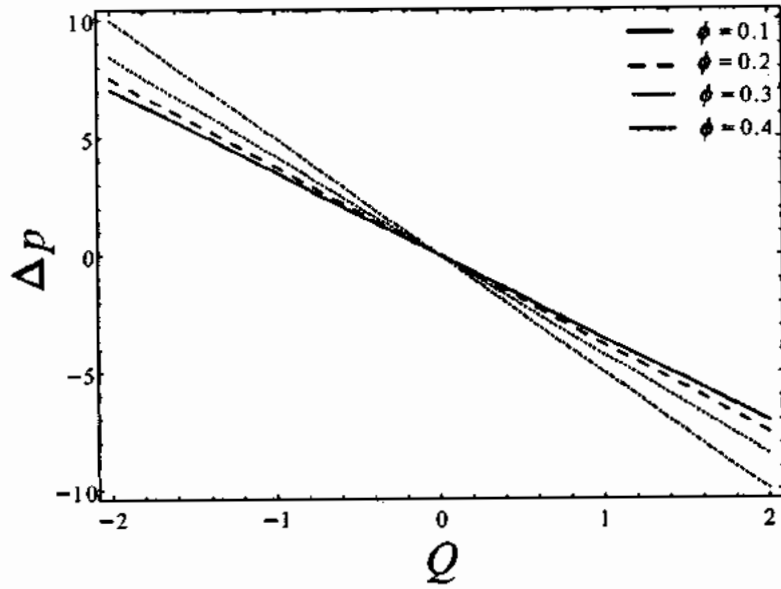


Fig. 4.4: Variation of pressure rise  $\Delta p$  with  $\phi$  for fixed values of  $\lambda_1 = 0.1$ ,  $\beta = 0.5$ ,  $\beta_1 = 0.1$ .

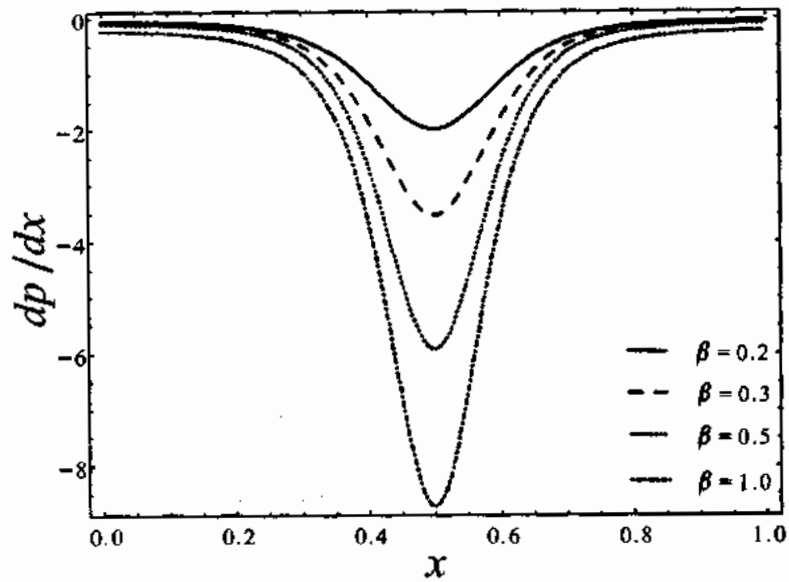


Fig. 4.5: Variation of pressure rise  $dp/dx$  with  $\beta$  for fixed values of  $\lambda_1 = 0.1$ ,  $\beta_1 = 0.1$ ,  $\phi = 0.7$ ,  $Q = 0.1$ .

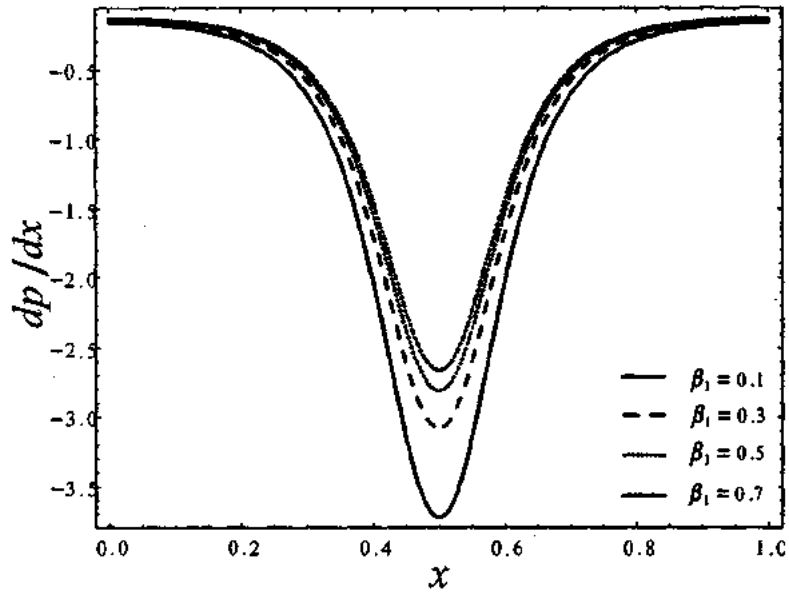


Fig. 4.6: Variation of pressure rise  $dp/dx$  with  $\beta_1$  for fixed values of  $\lambda_1 = 0.1$ ,  $\beta = 0.7$ ,  $\phi = 0.6$ ,  $Q = 0.1$ .

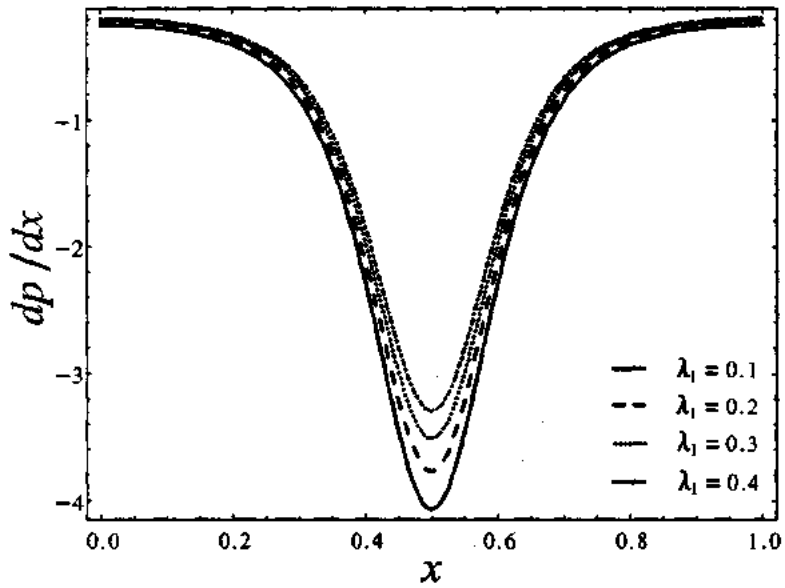


Fig. 4.7: Variation of pressure rise  $dp/dx$  with  $\lambda_1$  for fixed values of  $\beta = 0.7$ ,  $\beta_1 = 0.1$ ,  $\phi = 0.6$ ,  $Q = 0.1$ .

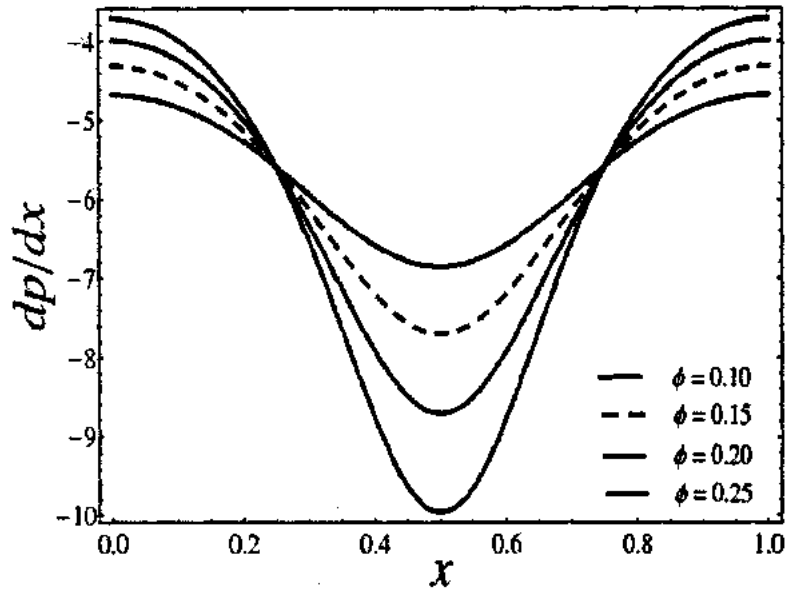


Fig. 4.8: Variation of pressure rise  $dp/dx$  with  $\phi$  for fixed values of  $\lambda_1 = 0.1$ ,  $\beta = 0.7$ ,  $\beta_1 = 0.1$ ,  $Q = 0.1$ .

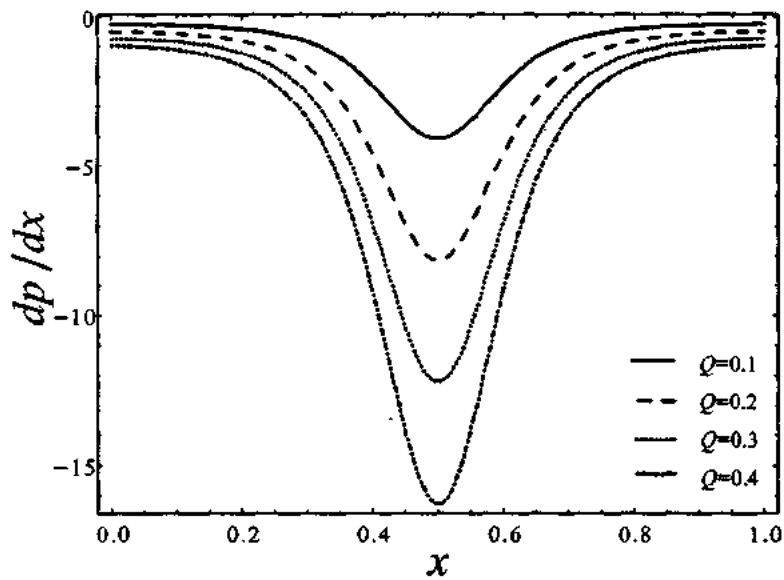
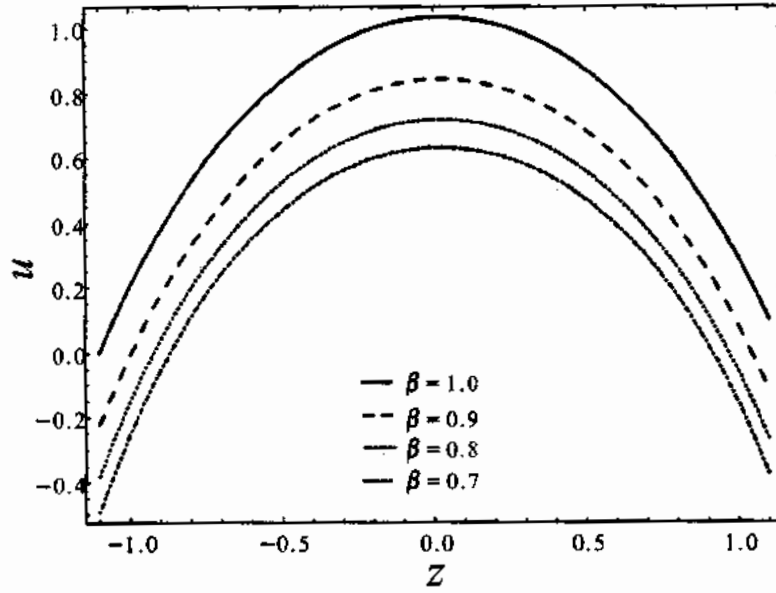
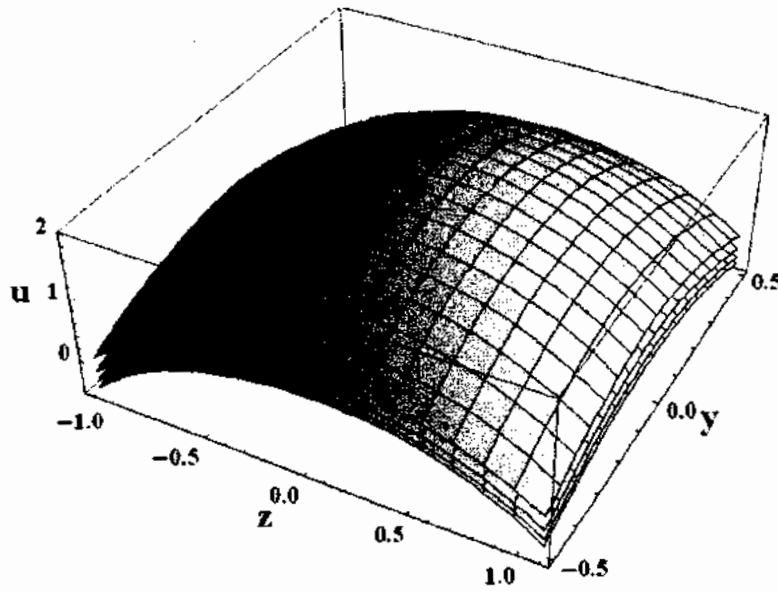


Fig. 4.9: Variation of pressure rise  $dp/dx$  with  $Q$  for fixed values of  $\beta = 0.7$ ,  $\beta_1 = 0.1$ ,  $\phi = 0.6$ ,  $\lambda_1 = 0.1$ .

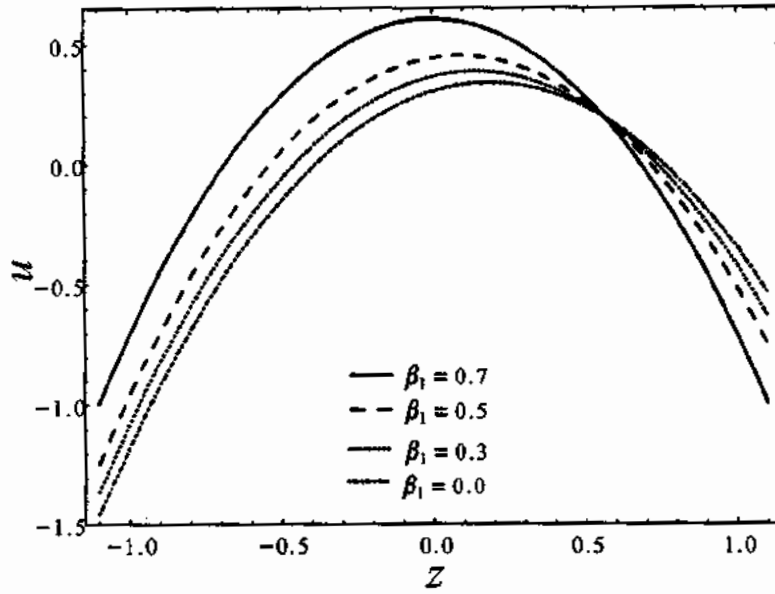


(a)

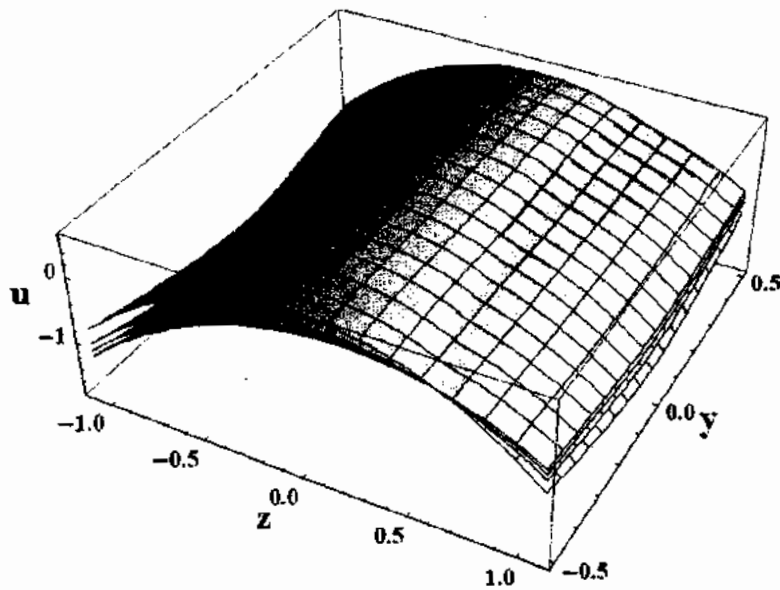


(b)

Fig. 4.10: Variation of velocity profile  $u$  with  $\beta$  for fixed values of  $\phi = 0.1$ ,  $x = 0$ ,  $y = 0.5$ ,  $\beta_1 = 0.1$ ,  $\lambda_1 = 3$ ,  $Q = 0.5$ , (a) for 2-dimensional, (b) For 3-dimensional.

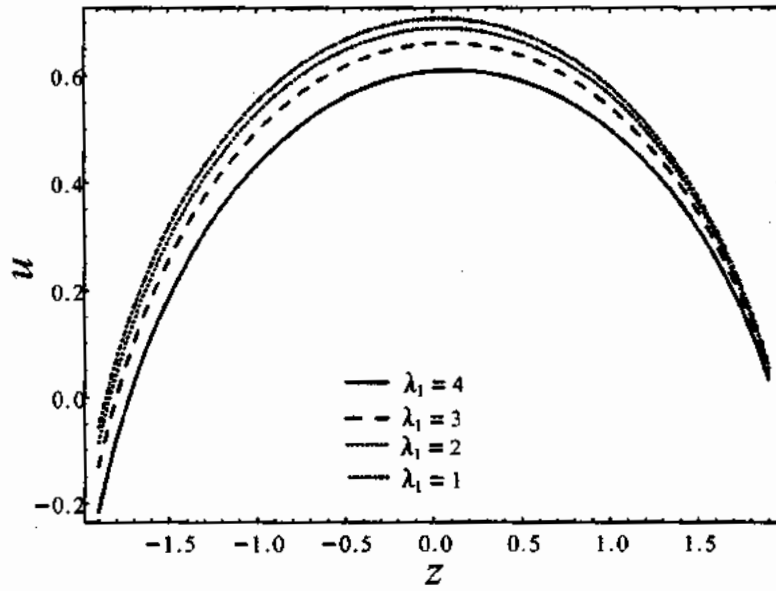


(a)

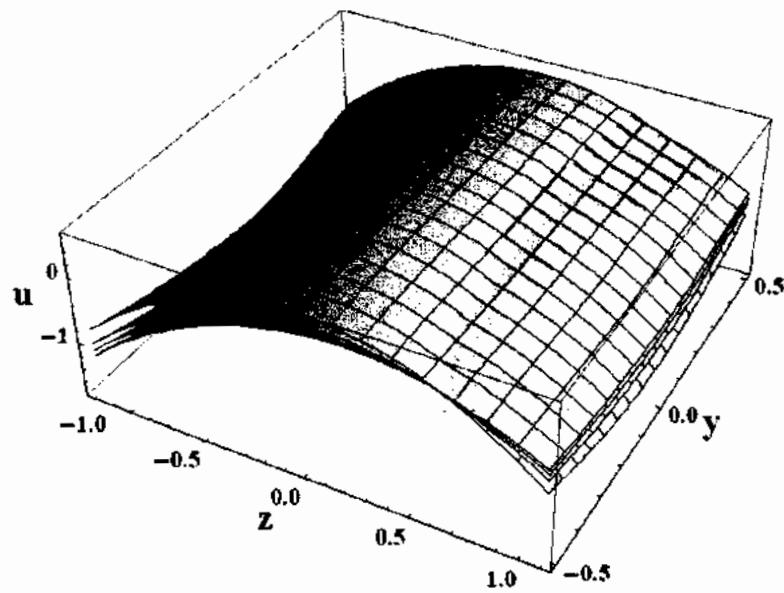


(b)

Fig. 4.11: Variation of velocity profile  $u$  with  $\beta_1$  for fixed values of  $\phi = 0.1$ ,  $x = 0$ ,  $y = 0.37$ ,  $\beta = 0.4$ ,  $\lambda_1 = 2$ ,  $Q = 1$ , (a) for 2-dimensional, (b) For 3-dimensional.



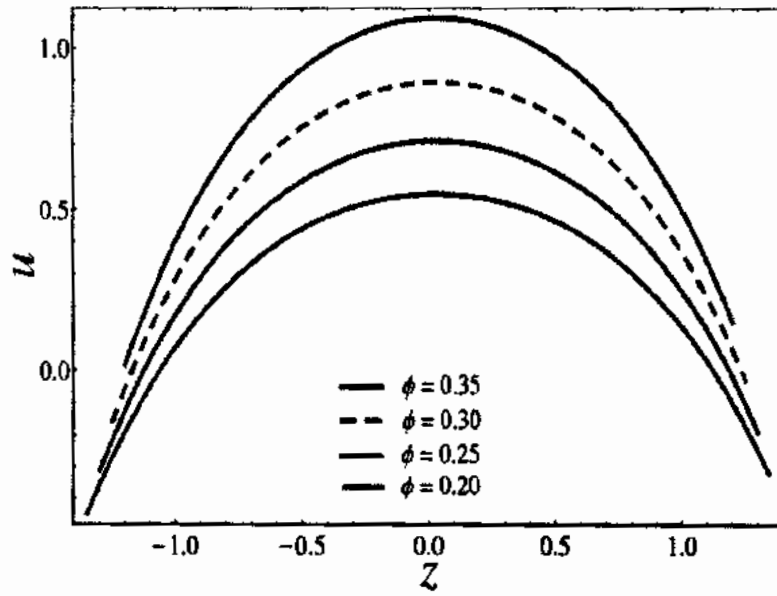
(a)



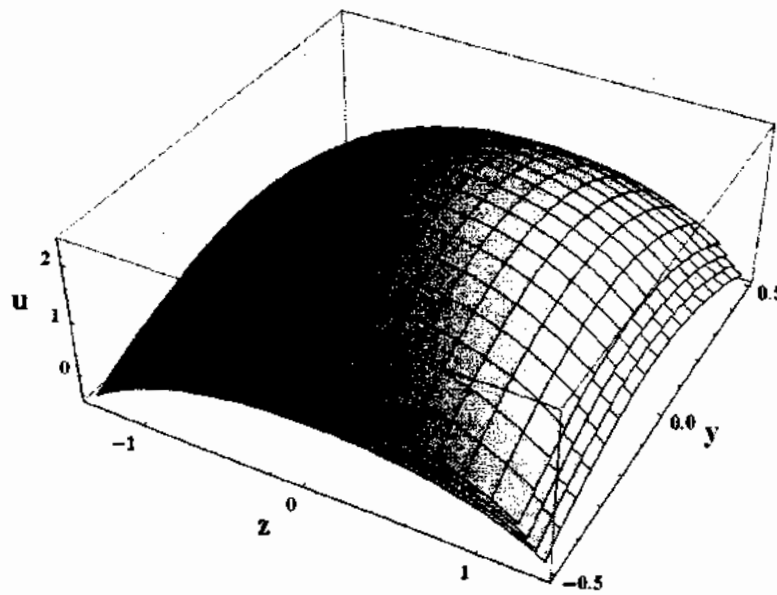
(b)

Fig. 4.12: Variation of velocity profile  $u$  with  $\lambda_1$  for fixed values of  $\phi = 0.9$ ,  $x = 0$ ,  $y = 0.9$ ,  $\beta_1 = 0.25$ ,  $\beta = 0.5$ ,  $Q = 0.65$ , (a) for 2-dimensional, (b) For 3-dimensional.



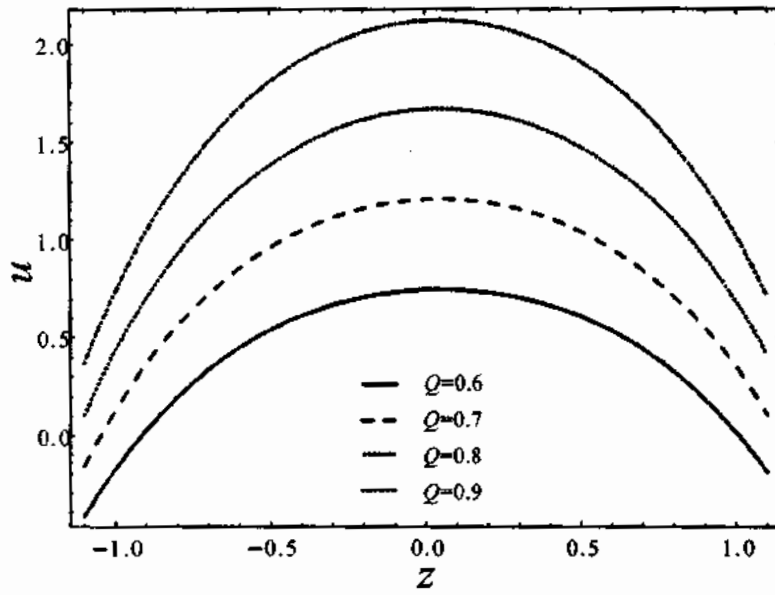


(a)

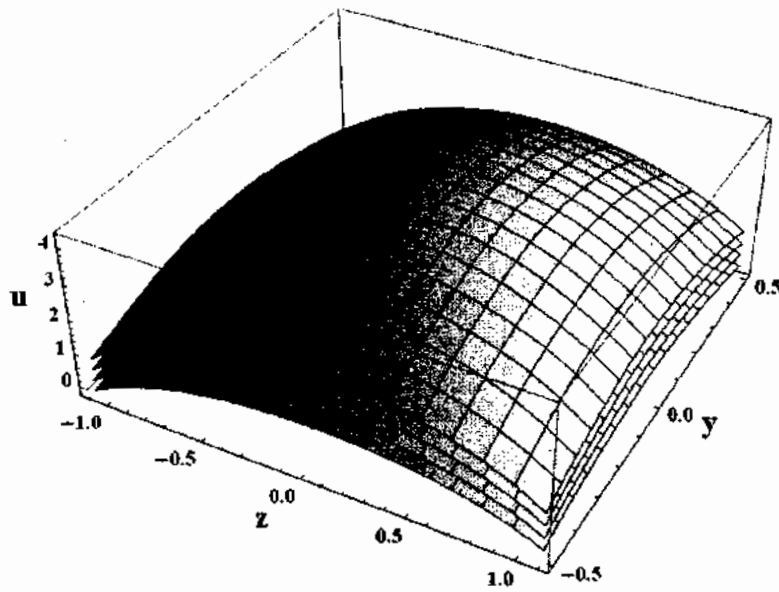


(b)

Fig. 4.13: Variation of velocity profile  $u$  with  $\phi$  for fixed values of  $\beta = 0.9$ ,  $x = 0$ ,  $y = 0.5$ ,  $\beta_1 = 0.1$ ,  $\lambda_1 = 2$ ,  $Q = 0.5$ , (a) for 2-dimensional, (b) For 3-dimensional.



(a)



(b)

Fig. 4.14: Variation of velocity profile  $u$  with  $Q$  for fixed values of  $\phi = 0.1$ ,  $x = 0$ ,  $y = 0.5$ ,  $\beta_1 = 0.15$ ,  $\lambda_1 = 2$ ,  $\beta = 0.9$ , (a) for 2-dimensional, (b) For 3-dimensional.

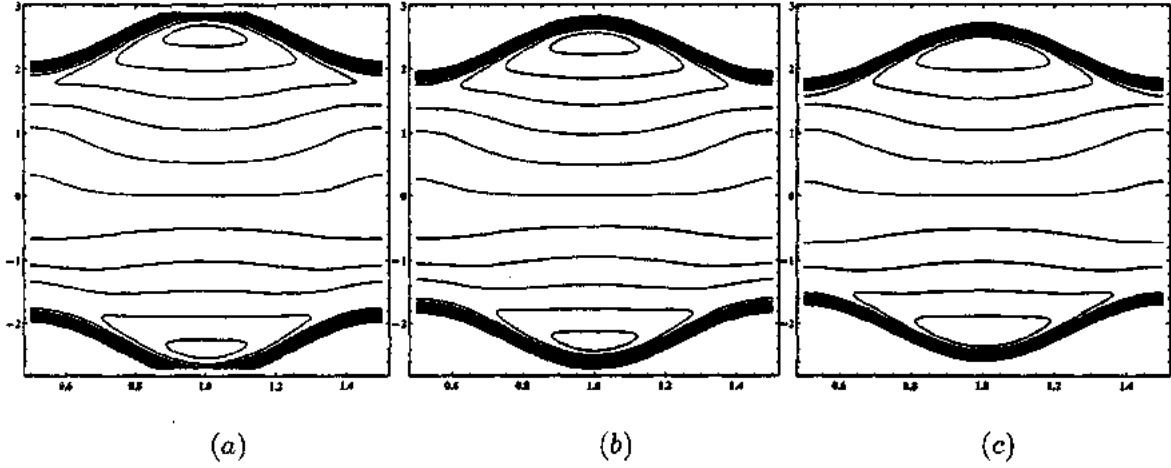


Fig. 4.15: Stream lines for different values of  $\beta$ , (a) for  $\beta = 0.8$ , (b) for  $\beta = 0.9$ , (c) for  $\beta = 1$ . The other parameters are  $y = 0.1$ ,  $Q = 0.3$ ,  $\lambda_1 = 0.1$ ,  $\phi = 0.4$ ,  $\beta_1 = 0.2$ .

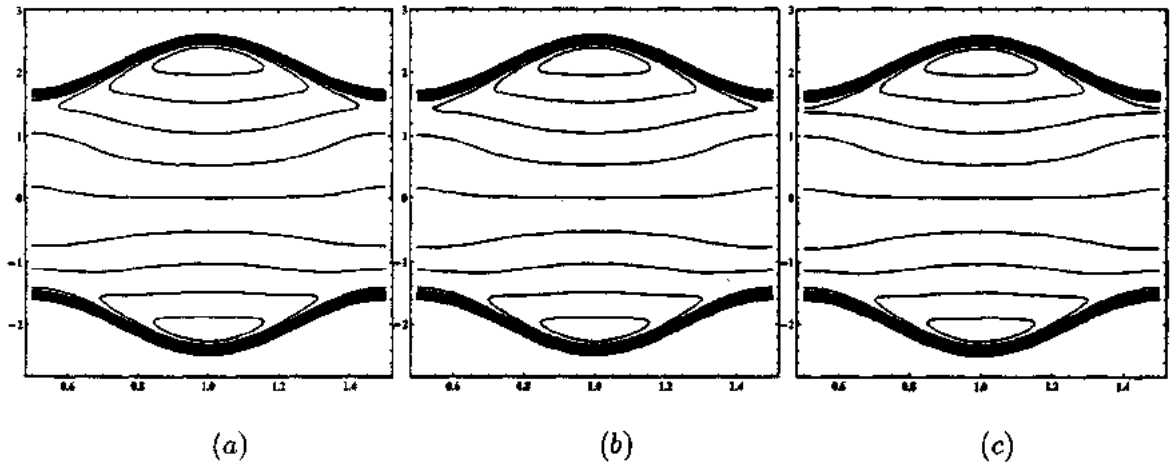


Fig. 4.16: Stream lines for different values of  $\lambda_1$ , (a) for  $\lambda_1 = 0.1$ , (b) for  $\lambda_1 = 0.5$ , (c) for  $\lambda_1 = 0.9$ . The other parameters are  $y = 0.1$ ,  $Q = 0.3$ ,  $\beta = 1.1$ ,  $\phi = 0.4$ ,  $\beta_1 = 0.2$ .

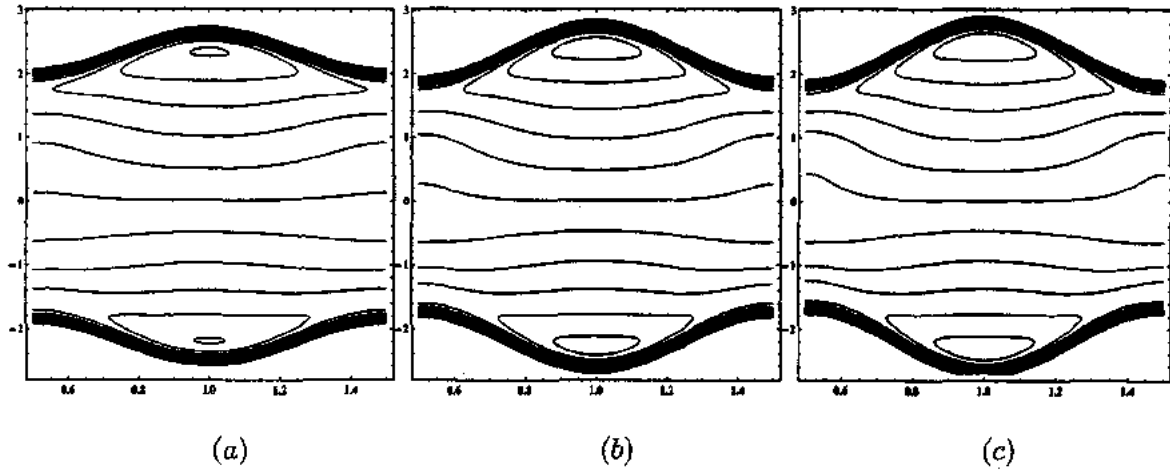


Fig. 4.17: Stream lines for different values of  $\phi$ , (a) for  $\phi = 0.3$ , (b) for  $\phi = 0.4$ , (c) for  $\phi = 0.45$ . The other parameters are  $y = 0.1$ ,  $Q = 0.3$ ,  $\beta = 0.9$ ,  $\lambda_1 = 0.1$ ,  $\beta_1 = 0.2$ .

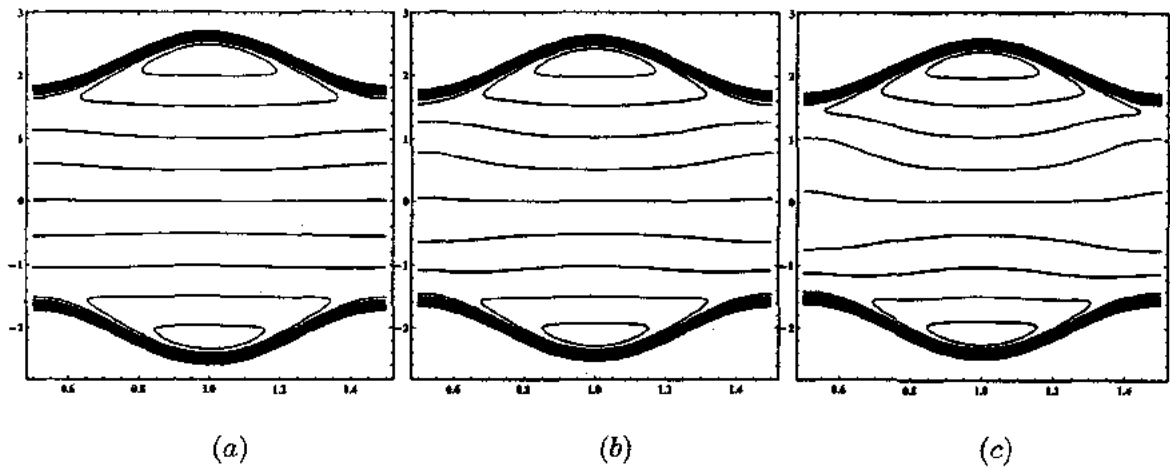


Fig. 4.18: Stream lines for different values of  $Q$ , (a) for  $Q = 0.1$ , (b) for  $Q = 0.2$ , (c) for  $Q = 0.3$ . The other parameters are  $y = 0.1$ ,  $\phi = 0.4$ ,  $\beta = 1.1$ ,  $\lambda_1 = 0.3$ ,  $\beta_1 = 0.2$ .

## Chapter 5

# Series solution of unsteady peristaltic flow of a Carreau fluid in eccentric cylinders

This chapter is devoted to the study of unsteady peristaltic flow of an incompressible Carreau fluid in eccentric cylinders. The problem is measured in cylindrical coordinates. The governing equations are observed under the conditions of long wavelength and low Reynolds number approximations. The resulting highly non-linear second order partial differential equations are solved by series solution technique. The relation for pressure rise is evaluated numerically by built-in technique with the help of mathematics software. As a special case, the present results are compared with the existing results given in the literature. The obtained results are then plotted to see the influence of different physical parameters on the velocity, pressure gradient and pressure rise expressions. The velocity profile is drawn both for two and three dimensions. The trapping boluses are also discussed through streamlines. This work is published in the journal of "*Ain Shams Engineering Journal*", 5 (2014) 293–304.

### 5.1 Mathematical formulation of the problem

Let us observe the peristaltic flow of incompressible Carreau fluid flowing between the two eccentric cylinders. The problem has been considered in the system of cylindrical coordinates

( $R, \theta, Z$ ) as radial, azimuthal and axial coordinates, respectively (see Fig. 2.1). According to the nature of the flow, the velocity field is taken as  $\mathbf{V} = (V, 0, U)$ . The Cauchy stress tensor for Carreau fluid is defined in Eq. (1.23). Now using the above velocity field, the continuity equation remains same as in Eq. (2.10) while momentum Eq. (1.6) takes the following form

$$\rho_f \left[ \frac{\partial V}{\partial t} + U \frac{\partial V}{\partial Z} + V \frac{\partial V}{\partial R} + \frac{W}{R} \frac{\partial V}{\partial \theta} - \frac{W^2}{R} \right] = -\frac{\partial P}{\partial R} + \frac{1}{R} \frac{\partial}{\partial R} (RS_{3RR}) + \frac{1}{R} \frac{\partial}{\partial \theta} (S_{3R\theta}) + \frac{\partial}{\partial Z} (S_{3RZ}) - \frac{S_{3\theta\theta}}{R} \quad \left. \right\}, \quad (5.1)$$

$$\rho_f \left[ \frac{\partial W}{\partial t} + U \frac{\partial W}{\partial Z} + V \frac{\partial W}{\partial R} + \frac{W}{R} \frac{\partial W}{\partial \theta} - \frac{WV}{R} \right] = -\frac{1}{R} \frac{\partial P}{\partial \theta} + \frac{1}{R^2} \frac{\partial}{\partial R} (R^2 S_{3\theta R}) + \frac{1}{R} \frac{\partial}{\partial \theta} (S_{3\theta\theta}) + \frac{\partial}{\partial Z} (S_{3\theta Z}) \quad \left. \right\}, \quad (5.2)$$

$$\rho_f \left[ \frac{\partial U}{\partial t} + U \frac{\partial U}{\partial Z} + V \frac{\partial U}{\partial R} + \frac{W}{R} \frac{\partial U}{\partial \theta} \right] = -\frac{\partial P}{\partial Z} + \frac{1}{R} \frac{\partial}{\partial R} (RS_{3RZ}) + \frac{1}{R} \frac{\partial}{\partial \theta} (S_{3\theta Z}) + \frac{\partial}{\partial Z} S_{3ZZ} \quad \left. \right\}. \quad (5.3)$$

Let us introduce non-dimensional parameters as defined in Eq. (2.9) along with the following additional quantities

$$We = \frac{\Gamma c}{a_1}, \quad \gamma' = \frac{a_1}{c} \dot{\gamma}. \quad (5.4)$$

The components of non-dimensional stresses for Carreau fluid are defined as

$$\left. \begin{aligned} S_{3RR} &= 2\delta_0 \left( 1 + \frac{n-1}{2} We^2 \dot{\gamma}^2 \right) \frac{\partial V}{\partial R} \\ S_{3R\theta} &= \delta_0 \left( 1 + \frac{n-1}{2} We^2 \dot{\gamma}^2 \right) \frac{1}{R} \frac{\partial V}{\partial \theta} \\ S_{3RZ} &= \left( 1 + \frac{n-1}{2} We^2 \dot{\gamma}^2 \right) \left( \delta_0^2 \frac{\partial V}{\partial Z} + \frac{\partial U}{\partial R} \right) \\ S_{3\theta\theta} &= 2\delta_0 \left( 1 + \frac{n-1}{2} We^2 \dot{\gamma}^2 \right) \frac{V}{R} \\ S_{3\theta Z} &= \left( 1 + \frac{n-1}{2} We^2 \dot{\gamma}^2 \right) \frac{1}{R} \frac{\partial U}{\partial \theta} \\ S_{3ZZ} &= 2\delta_0 \left( 1 + \frac{n-1}{2} We^2 \dot{\gamma}^2 \right) \frac{\partial U}{\partial Z} \end{aligned} \right\}, \quad (5.5)$$

$$\dot{\gamma}^2 = 2\delta_0^2 \left( \frac{\partial V}{\partial R} \right)^2 + \frac{\delta_0^2}{R^2} \left( \frac{\partial V}{\partial \theta} \right)^2 + \left( \delta_0^2 \frac{\partial V}{\partial Z} + \frac{\partial U}{\partial R} \right)^2 + \frac{2\delta_0^2 V^2}{R^2} + \frac{1}{R^2} \left( \frac{\partial U}{\partial \theta} \right)^2 + 2\delta_0^2 \left( \frac{\partial U}{\partial Z} \right)^2 \quad \left. \right\}. \quad (5.6)$$

Using the assumptions of long wavelength and low Reynolds number, the non-dimensional form

of the Eqs. (2.11) to (2.13) (without MHD effects) is simplified as

$$\left. \begin{aligned} \frac{\partial P}{\partial Z} = & \frac{\partial^2 U}{\partial R^2} + \frac{1}{R} \frac{\partial U}{\partial R} + \frac{1}{R^2} \frac{\partial^2 U}{\partial \theta^2} + \frac{n-1}{2} W e^2 \frac{\partial}{\partial R} \left( \frac{\partial U}{\partial R} \right)^3 + \frac{n-1}{2} W e^2 \frac{\partial}{\partial R} \left( \frac{1}{R^2} \frac{\partial U}{\partial R} \left( \frac{\partial U}{\partial \theta} \right)^2 \right) \\ & + \frac{(n-1) W e^2}{2R} \left( \left( \frac{\partial U}{\partial R} \right)^3 + \frac{1}{R^2} \frac{\partial U}{\partial R} \left( \frac{\partial U}{\partial \theta} \right)^2 \right) + \frac{(n-1) W e^2}{2R^2} \left( \frac{\partial}{\partial \theta} \left( \frac{\partial U}{\partial \theta} \left( \frac{\partial U}{\partial R} \right)^2 \right) \right. \\ & \left. + \frac{1}{R^2} \frac{\partial}{\partial \theta} \left( \frac{\partial U}{\partial \theta} \right)^3 \right) \end{aligned} \right\} \quad (5.7)$$

The corresponding boundary conditions in non-dimensional form are defined in Eqs. (2.20) and (2.21).

## 5.2 Solution of the problem

Solution of the boundary value problem defined in (5.7) is obtained by homotopy perturbation method. The deformation equation for the given problem is defined as

$$\left. \begin{aligned} \tilde{H}(\tilde{u}, q) = & (1 - q) (\mathcal{L}_3 [\tilde{u}] - \mathcal{L}_3 [\tilde{u}_0]) + q \left( \mathcal{L}_3 [\tilde{u}] + \frac{1}{R} \frac{\partial \tilde{u}}{\partial R} + \frac{1}{R^2} \frac{\partial^2 \tilde{u}}{\partial \theta^2} + \frac{n-1}{2} W e^2 \right. \\ & \left. \frac{\partial}{\partial R} \left( \frac{\partial \tilde{u}}{\partial R} \right)^3 + \frac{n-1}{2} W e^2 \frac{\partial}{\partial R} \left( \frac{1}{R^2} \frac{\partial \tilde{u}}{\partial R} \left( \frac{\partial \tilde{u}}{\partial \theta} \right)^2 \right) + \frac{(n-1) W e^2}{2R} \left( \left( \frac{\partial \tilde{u}}{\partial R} \right)^3 + \right. \right. \\ & \left. \left. \frac{1}{R^2} \frac{\partial \tilde{u}}{\partial R} \left( \frac{\partial \tilde{u}}{\partial \theta} \right)^2 \right) + \frac{(n-1) W e^2}{2R^2} \left( \frac{\partial}{\partial \theta} \left( \frac{\partial \tilde{u}}{\partial \theta} \left( \frac{\partial \tilde{u}}{\partial R} \right)^2 \right) + \frac{1}{R^2} \frac{\partial}{\partial \theta} \left( \frac{\partial \tilde{u}}{\partial \theta} \right)^3 \right) - \frac{\partial P}{\partial Z} \right) = 0 \end{aligned} \right\} \quad (5.8)$$

where  $\mathcal{L}_3$ , the linear operator is assumed to be  $\mathcal{L}_3 = \partial^2 / \partial R^2$ .

We define the following initial guess satisfying the boundary conditions

$$\tilde{u}_0 = \frac{V_1 (R - r_2)}{r_1 - r_2} \quad (5.9)$$

After employing the homotopy perturbation scheme, we have the following systems of equations.

**Zeroth order system**

$$\mathcal{L}_3 [u_0] - \mathcal{L}_3 [\tilde{u}_0] = 0, \quad (5.10)$$

with boundary conditions mentioned in Eqs. (2.27) and (2.28). The solution of the above zeroth order system can be obtained by using Eqs. (5.9) and (5.10) and is simply found as

$$u_0(R, \theta, Z, t, q) = \tilde{u}_0 = \frac{V_1 (R - r_2)}{r_1 - r_2} \quad (5.11)$$

First order system

$$\left. \begin{aligned} & \frac{\partial^2 u_1}{\partial R^2} + \frac{1}{R} \frac{\partial u_0}{\partial R} + \frac{1}{R^2} \frac{\partial^2 u_0}{\partial \theta^2} + \frac{n-1}{2} W e^2 \frac{\partial}{\partial R} \left( \frac{\partial u_0}{\partial R} \right)^3 + \frac{n-1}{2} W e^2 \frac{\partial}{\partial R} \left( \frac{1}{R^2} \frac{\partial u_0}{\partial R} \left( \frac{\partial u_0}{\partial \theta} \right)^2 \right) + \\ & \frac{(n-1)W e^2}{2R} \left( \left( \frac{\partial u_0}{\partial R} \right)^3 + \frac{1}{R^2} \frac{\partial u_0}{\partial R} \left( \frac{\partial u_0}{\partial \theta} \right)^2 \right) + \frac{(n-1)W e^2}{2R^2} \left( \frac{\partial}{\partial \theta} \left( \frac{\partial u_0}{\partial \theta} \left( \frac{\partial u_0}{\partial R} \right)^2 \right) + \right. \\ & \left. \frac{1}{R^2} \frac{\partial}{\partial \theta} \left( \frac{\partial u_0}{\partial \theta} \right)^3 \right) - \frac{\partial P}{\partial Z} = 0 \end{aligned} \right\}, \quad (5.12)$$

The related boundary conditions are mentioned in Eqs. (2.32) and (2.33). The solution of Eq. (5.12) is calculated as

$$\begin{aligned} u_1 = & -\frac{1}{384R^2r_1^2m_3m_5^7} (288R^2r_1^2 m_7m_5V_1m_{11}\epsilon (8m_1^4 + 20m_1^2\epsilon^2 + 5\epsilon^4) \cos \theta - 3\frac{\partial P}{\partial Z} R^2 \\ & m_8r_1^2m_7m_5\epsilon^7 \cos 7\theta + 3R^2r_1^2m_7 - m_5\epsilon^5 \cos 5\theta(48V m_1 + 7\frac{\partial P}{\partial Z} m_8(12m_1^2 + \epsilon^2) + \\ & 24V m_1 \ln \frac{R}{r_1}) + 6R^2r_1^2\epsilon^6 \cos 6\theta(m_7m_5 (-2V + 7\frac{\partial P}{\partial Z} m_8 m_{11}) + 2r_2V_1(-m_5 \ln R + \\ & m_7 \ln r_1 + -m_8 \ln r_2) + 4\epsilon^4 \cos 4\theta(m_7m_5 (21\frac{\partial P}{\partial Z} R^2 m_8 r_1^2 (r_2 m_{11}(10m_1^2 + 3\epsilon^2) + \\ & V_1(m_2 r_1^2 r_2(1 + 3r_2)m_4 - 5m_2 r_1(1 + 6r_2)m_4 + 18 r_1^2(10m_1^2 + \epsilon^2)))) + 6R^2 \\ & r_1^2 V_1(m_5(26Rm_1^2 + 4R\epsilon^2 + r_2(8m_2V_1m_4 - 4 m_{11} + \epsilon^2)) \ln R - m_7(26r_1m_{11} + \\ & 4R\epsilon^2 + r_2(8m_2V_1 W e^2 - 4m_1^2 + \epsilon^2)) \ln r_1 + m_8r_2(8m_2m_4 + 22m_1^2 + 5\epsilon^2) \\ & \ln r_2)) + 2\epsilon^2 \cos 2\theta (m_7m_5 (21\frac{\partial P}{\partial Z} R^2 m_8 r_1^2 m_{11}(48m_1^4 + 80m_1^2\epsilon^2 + 15\epsilon^4) + \\ & 2V(-4m_2Rr_1^2m_4((5 + 6r_2)m_{11} - 48r_2\epsilon^2) + 4m_2r_1r_2m_4(m_{11} - 6r_2\epsilon^2) - R^2 \\ & (4m_2r_2m_4(m_{11} - 6r_2\epsilon^2) + 4m_2r_1V_1W e^2(-5 + 6r_2)m_{11} + 48r_2\epsilon^2) + 45r_1^2 \\ & (16m_1^4 + 16m_1^2\epsilon^2 + \epsilon^4)))) - 6r_2r_1V_1(-m_5(8(-5m_2m_4 + r_2(m_2V_1 \times \\ & W e^2 + 6m_1^2)) m_{11} + 8(-m_2m_4 + r_2(-17m_2m_4 + 20 \times m_{11})) \epsilon^2 + 17r_2\epsilon^4 \\ & + 8r_1((-m_2m_4 + 36m_1^2) m_{11} + 5(-m_2 m_4 + 10m_1^2) \epsilon^2 + 4\epsilon^4)) \ln R + m_7(8 \\ & (-5m_2m_4 + r_2(m_2W e^2 + 6m_1^2))m_{11} + 8(-m_2m_4 + r_2(-17m_2m_4 + 20m_1^2)) \\ & \epsilon^2 + 17r_2\epsilon^4 + 8r_1((-m_2V_1W e^2 + 36m_1^2)m_{11} + 5(-m_2m_4 + 10m_1^2)\epsilon^2 + 4\epsilon^4)) \\ & \ln r_1 + m_8(-8(5 - m_2m_4 + 42r_2m_{11})m_{11} - 8(-m_2m_4 + 2r_2(-11m_2m_4 + \\ & 35m_1^2)) \epsilon^2 - 49r_2\epsilon^4) \ln r_2)) + \epsilon \cos \theta((r_1 - R)m_7m_5(8m_2(-10rr_1 + 2 \\ & m_4 + 44m_1^2))m_{11}\epsilon^2 + 2(2 - m_2m_4 + 2r_2(17m_2(R + r_1 + 6rr_1)r_2 - 3(R \\ & + r_1r_2) m_4m_{11}\epsilon^2 + 21\frac{\partial P}{\partial Z} R^2r_1(64m_1^6 + 240m_1^4\epsilon^2 + 120m_1^2\epsilon^4 + 5\epsilon^6)) - 48 \\ & r_2r_1V_1m_{11}(m_5(4(4 - m_2m_4 + r_2(m_2m_4 + 2m_1^2)) m_{11} + 2(-7m_2m_4 + r_2 \end{aligned}$$



$$\begin{aligned}
& (11m_2m_4 + 38m_1^2)) \epsilon^2 + 33r_2\epsilon^4 + R(4(m_2m_4 + 14\ln R + (r_2 - R)(4(4 - m_2m_4 \\
& + r_2(m_2m_4 + 2m_1^2))) m_{11} + 2(7 - m_2m_4 + r_2(11m_2m_4 + 38m_1^2))) \epsilon^2 + 33r_2\epsilon^4 \\
& + r_1(4(m_2m_4 + 14m_1^2)m_{11} + 4(5m_2m_4 + 49m_1^2)\epsilon^2 + 63\epsilon^4))\ln r_1 + 2(r - r_1) \\
& (4(-2m_2m_4 + r_2(m_2m_4 + 8m_1^2))m_{11} + (7 - m_2m_4 + r_2(21m_2m_4 + 136m_1^2)) \\
& \epsilon^2 + 48r_2\epsilon^4)\ln r_2)) + 4((r - r_2)m_5(3\frac{\partial P}{\partial Z} r^2(r - r_1)r_1^2m_{11}(16m_1^6 + 168m_1^4\epsilon^2 \\
& + 210m_1^2\epsilon^4 + 35\epsilon^6) + V_1(m_2r_1^2r_2m_4\epsilon^2(-4m_1^2 + (-1 + 21r_2)\epsilon^2) + r^2(m_2r_2V_1^2 \\
& We^2\epsilon^2(-4(5 + 6r_2)m_{11} + (-5 + 162r_2)\epsilon^2)6r_1^2(-16m_1^6 - 120m_1^4\epsilon^2 - 90m_1^2\epsilon^4 \\
& - 5\epsilon^6)))) + 6r^2r_1^2V_1(m_5(8(-m_2m_4 + 2r_2m_1^2)m_{11} + 4(7 - m_2m_4 + r_2(5m_2m_4 \\
& + 14m_1^2) + r(7m_2V_1^2We^2 + 44m_1^2))m_{11}\epsilon^2 + 2(2 - m_2m_4 + 2r_2(17m_2m_4 + 21m_1^2) \\
& + r(14m_2m_4 + 87m_1^2))\epsilon^4 + (12r + 7r_2)\epsilon^6)\ln r + (r_2 - r)(8(-m_2m_4 + 2r_1m_{11}) \\
& m_{11} + 4(7 - m_2m_4 + r_2(5m_2m_4 + 14m_1^2) + r_1(7m_2m_4 + 21m_1^2) + r_1(14m_2m_4 \\
& + 87m_1^2))\epsilon^4 + (12r_1 + 7r_2)\epsilon^6)\ln r_1 + m_8(8(-m_2m_4 + 2r_2m_{11})m_{11} + 4(7 - m_2m_4 \\
& + 2r_2(6m_2m_4 + 29m_1^2))m_{11}\epsilon^2 + 2(-2m_2m_4 + 3r_2(16m_2m_4 + 43m_1^2))\epsilon^4 + 19r_2 \\
& \epsilon^6)\ln r_2)) + \epsilon^3 \cos 3\theta(m_7 - m_5(21\frac{\partial P}{\partial Z} R^2m_8r_1(80m_1^4 + 60m_1^2\epsilon^2 + 3\epsilon^4) - 8V_1 \\
& m_{11}(m_2r_1r_2(-2 + 3r_2)m_4 + 2 - m_2rr_1^2(-5 + 6r_2)m_4 + R^2(-m_2r_2(-2 + 3r_2)m_4 \\
& + 2m_2r_1(-5 + 6r_2)V_1^2We^2 + 30r_1^2(8m_1^2 + 3\epsilon^2)))) + 24r^2r_1^2V_1m_{11}(-m_5(-4m_2m_4 \\
& + r_2(-20m_2m_4 + 8m_1^2 + 17\epsilon^2) + r(16 - m_2m_4 + 88m_1^2 + 47\epsilon^2))\ln r + (r - r_2) \\
& (4 - m_2m_4 + r_2(-20m_2m_4 + 8m_1^2 + 17\epsilon^2) + r_1(-16m_2m_4 + 88m_1^2 + 47\epsilon^2)) \\
& \ln r_1 - 4(r - r_1)(-m_2m_4 + r_2(9 - m_2m_4 + 24m_1^2 + 16\epsilon^2))\ln(r_2))))
\end{aligned} \tag{5.13}$$

Finally,  $q \rightarrow 1$  approaches the final solution

$$U(R, \theta, Z, t) = u_0 + u_1. \tag{5.14}$$

Now pressure gradient  $\partial P/\partial Z$  will be evaluated by using Eqs. (2.38) and (2.39) and is found as

$$\begin{aligned}
\frac{\partial P}{\partial Z} = & \frac{1}{48\pi r_1^2 m_2^3 m_4 - m_5^7} (2(36Qr_1^2 m_{11}(16m_1^6 + 168m_1^4 \epsilon^2 + 210m_1^2 \epsilon^4 + 35\epsilon^6) - \pi m_5 V_1 \\
& (m_2 r_2^3 m_3(4m_1^2 + (1 - 21r_2)\epsilon^2) + m_2 r_1 r_2^2 m_3(-8(2 + 3r_2)m_{11} + (141r_2 - 4)\epsilon^2) + \\
& 4r_1^4(64m_1^6 + 4(7m_2 m_4 + 134m_1^2)m_{11}\epsilon^2 + 4(7m_2 m_4 + 111m_1^2)\epsilon^4 + 27\epsilon^6) + r_1^2 r_2 \\
& (-8(9m_2 m_4 + 4r_2 m_{11})m_{11} + 4(49 - m_2 m_4 + r_2(85m_2 m_4 + 122 m_{11}))) m_{11}\epsilon^2 + 2 \\
& (-11m_2 m_4 + 2r_2(79m_2 m_4 + 228m_1^2)) \epsilon^4 + 81r_2 \epsilon^6) + r_1^3(-8(9m_2 m_4 + 4r_2 m_{11}) \\
& m_{11} + 4(68 - m_2 m_4 + r_2(67m_2 m_4 + 122m_1^2)))m_{11}\epsilon^2 + (41 - m_2 m_4 + 2r_2(443 \\
& m_2 m_4 + 456m_1^2))\epsilon^4 + 81r_2 \epsilon^6)) + 2304\pi r_1^2 \phi \cos 2\pi(Z - t) - m_5^7 - 9r_1^2 \epsilon^7 \\
& (2Q + \pi \phi^2 \cos 4\pi(Z - t)) \cos 7\theta + 3r_1^2 \epsilon^5 \cos 5\theta(2(\pi(28r_1^3 - 45r_1^2 r_2 + 17r_2^3) V_1 \\
& - 252Qm_1)m_{11} - 42Q\epsilon^2 + 3\pi(-7(12m_1^2 + \epsilon^2)\phi^2 \cos 4\pi(Z - t) + 4r_2^3 V_1 m_{11} \ln \frac{r_1}{r_2})) \\
& + \epsilon \cos \theta(2(63Qr_1^2(-64m_1^6 - 240m_1^4 \epsilon^2 - 120m_1^2 \epsilon^4 - 5\epsilon^6) + 2\pi m_5 V_1 m_{11}(-m_2 r_2^3 \\
& (-2 + 3r_2)m_3 + m_2 r_1 r_2^2(-8 + 9r_2)m_3 + 4r_1^4(4(m_2 m_4 + 50m_1^2)m_{11} + 4(5m_2 m_4 \\
& + 139m_1^2)\epsilon^2 + 153\epsilon^4) + r_1^2 r_2(4(36 - m_2 m_4 + r_2(13m_2 m_4 + 2m_1^2)))m_{11} + 2(49 - \\
& m_2 m_4 + 11r_2(11m_2 m_4 + 34 m_{11}))) \epsilon^2 + 369r_2 \epsilon^4) + r_1^3(4(36 - m_2 m_4 + r_2 \\
& (13m_2 m_4 + 2m_1^2)))m_{11} + 2(68 - m_2 m_4 + r_2(145m_2 m_4 + 374m_1^2))\epsilon^2 + 369r_2 \\
& \epsilon^4)) + 3\pi r_1^2(-21(64m_1^6 + 240m_1^4 \epsilon^2 + 120m_1^2 \epsilon^4 + 5\epsilon^6)\phi^2 \cos 4\pi(Z - t) - 8 \\
& V_1 m_{11}(r_2^2(4(4 - m_2 m_4 + r_2(m_2 m_4 + 2m_1^2)))m_{11} + (12 - m_2 m_4 + 19r_2(m_2 m_4 \\
& + 4m_1^2))\epsilon^2 + 33r_2 \epsilon^4) + 2r_1^2(4(2 - m_2 m_4 + r_2(m_2 m_4 + 8m_1^2)))m_{11} + (7 - m_2 m_4 \\
& + r_2(21m_2 m_4 + 136m_1^2))\epsilon^2 + 48r_2 \epsilon^4)2r_1 r_2(4(2 - m_2 m_4 + r_2(m_2 m_4 + 8m_1^2)) \\
& m_{11} + (7 - m_2 m_4 + r_2(21m_2 m_4 + 136m_1^2))\epsilon^2 + 48r_2 \epsilon^4)) \ln \frac{r_1}{r_2}) + \epsilon^2 \\
& \cos 2\theta(252Qr_1^2 m_{11}(48m_1^4 + 80m_1^2 \epsilon^2 + 15\epsilon^4) - \pi m_5 V_1(16m_2 r_1 r_2^2 m_4((2 + 3r_2) \\
& m_{11} - 21r_2 \epsilon^2) + 8m_2 r_2^3 m_4(-m_{11} + 6r_2 \epsilon^2) + 4r_1^4(8(-m_2 m_4 + 126m_1^2)m_{11} + \\
& 40(-m_2 m_4 + 28m_1^2)\epsilon^2 + 77\epsilon^4) + r_1^3(8(-40m_2 m_4 + r_2(11m_2 m_4 + 18 \times \\
& m_{11})))m_{11} + 8(-9m_2 m_4 + r_2(-221m_2 m_4 + 200m_1^2))\epsilon^2 + 191r_2 \epsilon^4) + \\
& r_1^2 r_2(8(-59m_2 m_4 + r_2(-7m_2 m_4 + 18m_1^2))m_{11} + 8(-9m_2 m_4 + r_2 \\
& (-53m_2 m_4 + 200m_1^2))\epsilon^2 + 191r_2 \epsilon^4)) + 6\pi r_1^2(21m_1(48m_1^4 + 80m_1^2 \epsilon^2 + 15\epsilon^4) \\
& \phi^2 \cos 4\pi(Z - t) + V_1(r_2^2(8(-6m_2 m_4 + r_2(m_2 m_4 + 6m_1^2)))m_{11} + 8(-m_2 m_4 + \\
& r_2(-11m_2 m_4 + 20m_1^2))\epsilon^2 + 17r_2 \epsilon^4) + r_1^2(8(-5m_2 m_4 + 42r_2 m_{11})m_{11} + 8 \\
& (-m_2 m_4 + 2r_2(-11m_2 m_4 + 35m_1^2))\epsilon^2 + 49r_2 \epsilon^4) + r_1 r_2(8(-5m_2 m_4 \\
& + 42r_2 m_{11})m_{11} + 8(-m_2 m_4 + 2r_2(-11m_2 m_4 + 35m_1^2))\epsilon^2 + 49r_2 \epsilon^4)) \ln \frac{r_1}{r_2})
\end{aligned}$$

$$\begin{aligned}
& +2\epsilon^4 \cos 4\theta(252Qr_1^2m_{11}(10m_1^2 + 3\epsilon^2) - \pi m_5V_1(-m_2r_2^3(1 + 3r_2)m_4 + m_2r_1r_2^2 \\
& (4 + 27r_2)m_4 + 4r_1^4(116m_1^2 + 13\epsilon^2) + r_1^3(5m_2m_4 - 2r_2(-51m_2m_4 + 56m_1^2) \\
& + 7r_2\epsilon^2) + 7r_1^2r_2(-2m_2m_4 + r_2(-16m_1^2 + \epsilon^2))) + 6\pi r_1^2(21m_1(10m_1^2 + 3\epsilon^2)\phi^2 \\
& \cos 4\pi(Z - t) + r_2V_1(r_1^2(8m_2m_4 + 22m_1^2 + 5\epsilon^2) + r_1r_2(8m_2m_4 + 22m_1^2 + 5\epsilon^2) + \\
& r_2(-m_2m_4 + r_2(5m_2m_4 - 4m_1^2 + \epsilon^2)))\ln\frac{r_1}{r_2} + \epsilon^3 \cos 3\theta(2(63Qr_1^2(-80m_1^4 - \\
& 60m_1^2\epsilon^2 - 3\epsilon^4) + \pi m_5V_1m_{11}(2m_2r_2^3(-2 + 3r_2)m_4 - 2m_2r_1r_2^2(-8 + 9r_2)m_4 \\
& + 4r_1^4(-16m_2m_4 + 328m_1^2 + 137\epsilon^2) + r_1^3(-4(4m_2m_4 + r_2(67m_2m_4 + 14m_1^2)) \\
& + 161r_2\epsilon^2) + r_1^2r_2(-92m_2m_4 + r_2(-172m_2m_4 - 56m_1^2 + 161\epsilon^2)))) + 3\pi r_1^2 \\
& (-21(80m_1^4 + 60m_1^2\epsilon^2 + 3\epsilon^4)\phi^2 \cos 4\pi(Z - t) - 4Vm_1(4r_1^2(-m_2m_4 + r_2 \\
& (-9m_2m_4 + 24m_1^2 + 16\epsilon^2)) + 4r_1r_2(-m_2m_4 + r_2(-9m_2m_4 + 24m_1^2 + 16\epsilon^2)) \\
& + r_2^2(-8m_2m_4 + r_2(-14m_2m_4 + 8m_1^2 + 17\epsilon^2)))\ln\frac{r_1}{r_2} + 12\pi r_1^2(3m_1(16m_1^6 + \\
& 168m_1^4\epsilon^2 + 210m_1^2\epsilon^4 + 35\epsilon^6)\phi^2 \cos 4\pi(Z - t) + V_1(r_2^2(-8m_2m_4m_{11} + 4 \\
& (-6m_2m_4 + r_2(5m_2m_4 + 14m_1^2))m_{11}\epsilon^2 + (-3m_2m_4 + r_2(47m_2m_4 + 84m_1^2))\epsilon^4 \\
& + 7r_2\epsilon^6) + r_1^2(8(-m_2m_4 + 2r_2m_{11})m_{11} + 4(-7m_2m_4 + 2r_2(6m_2m_4 + 29m_1^2)) \\
& m_{11}\epsilon^2 + 2(-2m_2m_4 + 3r_2(16m_2m_4 + 43m_1^2))\epsilon^4 + 19r_2\epsilon^6) + r_1r_2(8(-m_2m_4 + \\
& 2r_2m_{11})m_{11} + 4(-7m_2m_4 + 2r_2(6m_2m_3 + 29m_1^2))m_{11}\epsilon^2 + 2(-2m_2m_4 \\
& + 3r_2(16m_2V^2We^2 + 43m_1^2))\epsilon^4 + 19r_2\epsilon^6)\ln\frac{r_1}{r_2} + 3r_1^2\epsilon^6 \cos 6\theta(\pi(-4r_1^3 + 9r_1^2r_2 - \\
& 5r_2^3)V + 84Qm_1 + 42\pi m_1\phi^2 \cos 4\pi(z - t) + 2\pi r_2(r_1^2 + r_1r_2 + r_2^2)V_1\ln\frac{r_2}{r_1})))
\end{aligned} \tag{5.15}$$

in which

$$\left. \begin{aligned}
m_{11} &= r_2 - \delta, \quad m_2 = n - 1, \quad m_3 = V_1^2We^2, \quad m_4 = m_3\epsilon^2, \quad m_5 = r_1 - r_2, \\
m_6 &= r_1 + r_2, \quad m_7 = R - r_2, \quad m_8 = R - r_1
\end{aligned} \right\} \tag{5.16}$$

The pressure rise  $\Delta P(t)$  can be evaluated numerically by using the expression given in Eq. (3.41).

### 5.3 Graphical results and discussion

In this section, we have discussed the effects of all the pertinent parameters on pressure rise, pressure gradient, velocity profile and streamlines with the help of graphs. As a special case of this problem, the comparison of the present work with that of Mekheimer et al. [78] is also

manipulated through table and graph as well. The residue error is also presented to see the solution validity by varying certain quantities.

Table 5.1 shows the comparison of velocity variation in this article with the values obtained in [78]. In Table 5.2, the residue error analysis for velocity by varying different parameters is observed. Fig. 5.1 contains the graphs showing the velocity profile variation with emerging parameters for the present analysis and the old one. Figs. 5.2 and 5.3 tell us the variation of pressure rise  $\Delta P$  with the flow rate  $Q$ . We can observe the behavior of pressure gradient  $\partial P/\partial Z$  with space coordinate  $z$  from Figs. 5.4 and 5.5. The graphs for the velocity profile  $U$  are displayed in Figs. 5.6 and 5.7. From Figs. 5.8 and 5.9, the trapping bolus phenomenon is discussed through streamlines for different effective parameters.

If we look at the Table 5.1, we can easily conclude that when we omit the effects of Carreau fluid parameters ( $We = n = 0$ ), the present results are very much similar to that of given in [78]. From Fig. 5.1, it is clear that the present results for neglecting the effects of Carreau fluid overlaps the already produced results. It is also observed from Table. 5.1 and Fig. 5.2 that when we include the Carreau fluid parameters ( $We = 0.5, n = 2$ ), the velocity profile increases in the region  $0.2 \leq R \leq 0.4$  but in the rest of the domain velocity decreases.

Fig. 5.2 has the variation of pressure rise  $\Delta P$  with  $\delta$  and  $We$ . From this figure, it is measured that pressure rise  $\Delta P$  is varying directly with the the increase in the values of  $\delta$  in the retrograde pumping region ( $\Delta P > 0, Q < 0$ ) and peristaltic pumping region ( $\Delta P > 0, Q > 0$ ) but different observations are made for the augmented pumping region ( $\Delta P < 0, Q > 0$ ). It is also revealed from this figure that pressure rise is reduced with the increase in  $We$ . It is observed from Fig. 5.3 that peristaltic pressure rise  $\Delta P$  is varying directly with the rising the magnitude of radius  $\delta$  in retrograde pumping region and peristaltic pumping but reducing when observed in the augmented pumping region but decreasing with the power law index  $n$ .

Fig. 5.4 shows the effects of  $\theta$  and  $We$  on the expression of pressure gradient  $\partial P/\partial Z$ . It is noted here that  $\partial P/\partial Z$  is decreasing with the increase in  $We$  and  $\theta$ . Fig. 5.5 is drawn to see the effects of  $\delta$  and  $n$  on the pressure gradient  $\partial P/\partial Z$  against the coordinate  $Z$ . We can say that pressure gradient gets inverse attitude when someone increases the magnitude of  $n$  but reverse behavior is reported when  $\delta$  gets larger.

The velocity profile  $U$  with  $\delta$  and  $We$  is sketched in Fig. 5.6 both for two and three

dimensions. It is noted from this figure that  $U$  gets lessened with the increase in  $We$  in the part  $0.6 \leq R \leq 0.9$  but in the remaining part  $U$  rises with  $We$  but in the whole region, velocity enlarges when  $\delta$  gains larger values. From Fig. 5.7, it is derived that it gives the similar behavior with the parameter  $\delta$  and  $n$  as that of observed for  $\delta$  and  $We$  in Fig. 5.6.

Fig. 5.8 gives the streamlines for the parameter  $We$ . It is noted from this figure that increasing the magnitude of  $We$  results in decreasing the number of bolus in both the parts of the geometry but size of the bolus is enlarged. Fig. 5.9 shows that the number of bolus is decreased but volume of the bolus expands when someone increases the numerical values of flow rate  $Q$ .

	Mekheimer et al. [78]	Present work	
$R$	$U(R, \theta, Z, t)$	$U(R, \theta, Z, t)$ for $We = 0, n = 0$	$U(R, \theta, Z, t)$ for $We = 0.5, n = 2$
0.20	0.1000	0.1000	0.1000
0.25	0.1093	0.1096	0.1103
0.30	0.1119	0.1119	0.1142
0.35	0.1119	0.1114	0.1137
0.40	0.1096	0.1098	0.1100
0.45	0.1054	0.1056	0.1041
0.50	0.0995	0.0992	0.0964
0.55	0.0919	0.0916	0.0873
0.60	0.0829	0.0827	0.0771
0.65	0.0724	0.0726	0.0659
0.70	0.0606	0.0601	0.0539
0.75	0.0474	0.0478	0.0412
0.80	0.0329	0.0337	0.0280
0.85	0.0171	0.0177	0.0142
0.90	0.0000	0.0000	0.0000

Table 5.1: Comparison of velocity distribution of present work with Mekheimer et al. [78].

$n$	$\delta$	$\phi$	$\theta$	$Z$	$t$	$Q$	$We$	Residue
2	0.1	0.17	0.87	0	0.4	0.9	1.000	-0.246548
							1.043	-0.226122
							1.086	-0.204769
							1.129	-0.182481
							1.172	-0.159250
							1.215	-0.135066
							1.258	-0.109921
							1.301	-0.083805
							1.344	-0.056707
							1.387	-0.028618
							1.430	0.0004728

Table 5.2: Residue error for velocity profile  $U$ .

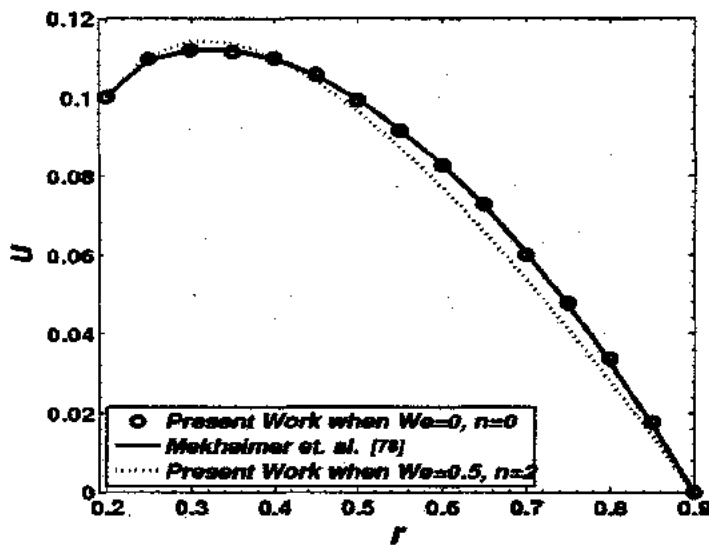


Fig. 5.1: Comparison of velocity profile of present work with [78] for fixed values of  $\delta = 0.1$ ,  $\theta = 0.87$ ,  $\phi = 0.1$ ,  $Z = 0$ ,  $t = 0.5$ ,  $V_1 = 0.1$ ,  $\epsilon = 0.1$ ,  $Q = 0.69$ .

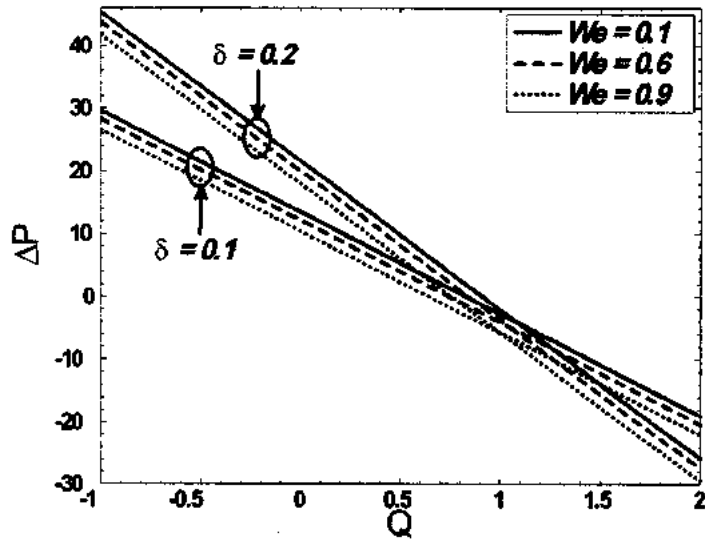


Fig. 5.2: Variation of pressure rise  $\Delta P$  with  $\delta$  and  $We$  for fixed values of  $\epsilon = 0.1$ ,  $\phi = 0.1$ ,  $t = 0.1$ ,  $\theta = 0.87$ ,  $n = 2$ ,  $V_1 = 0.9$ .

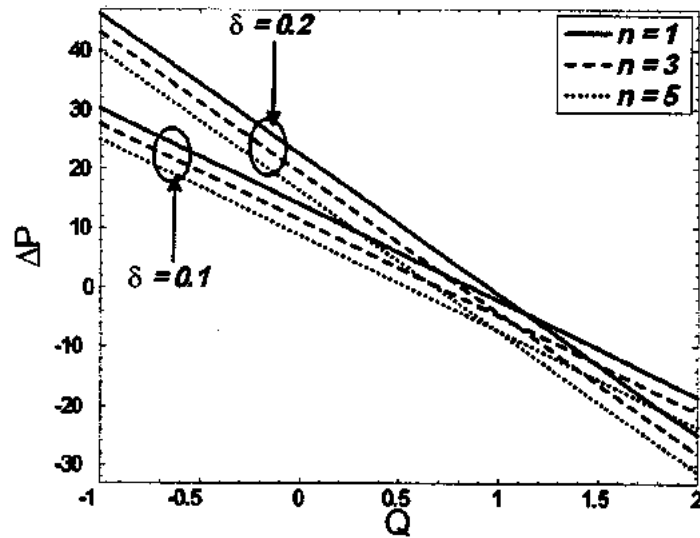


Fig. 5.3: Variation of pressure rise  $\Delta P$  with  $\delta$  and  $n$  for fixed values of  $\epsilon = 0.1$ ,  $We = 0.5$ ,  $t = 0.1$ ,  $\theta = 0.87$ ,  $\phi = 0.2$ ,  $V_1 = 1$ .

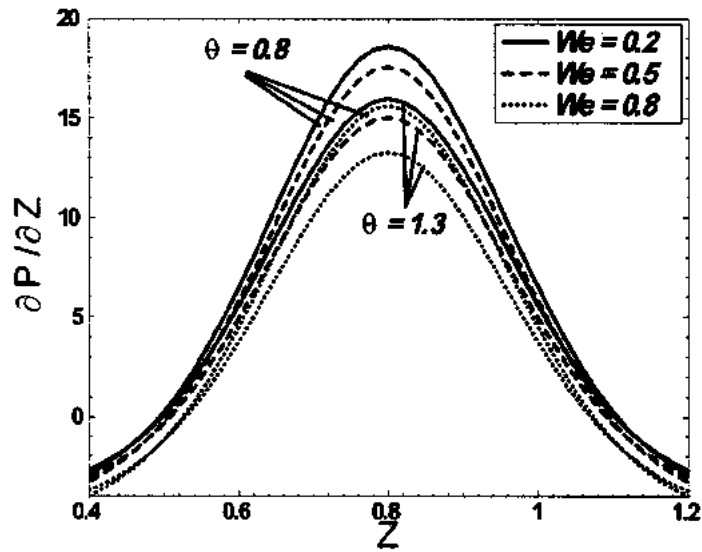


Fig. 5.4: Variation of pressure gradient  $\partial P / \partial Z$  with  $\theta$  and  $We$  for fixed values of  $\epsilon = 0.1$ ,  $V_1 = 0.9$ ,  $t = 0.3$ ,  $n = 2$ ,  $\phi = 0.1$ ,  $Q = 0.2$ ,  $\delta = 0.2$ .

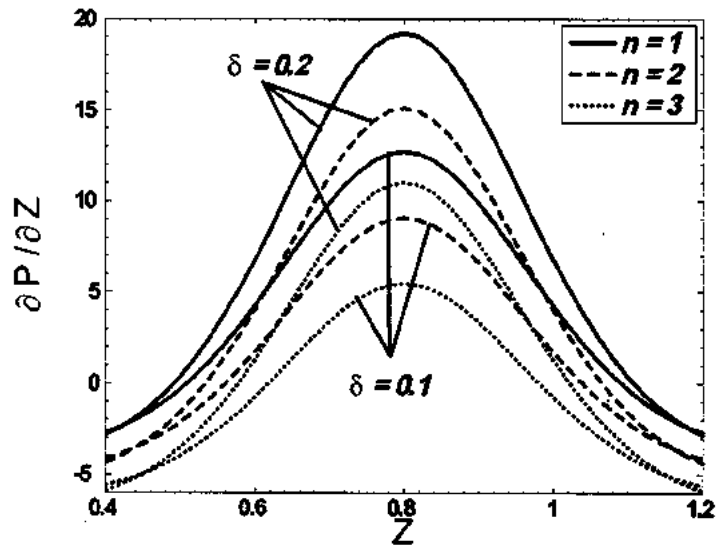
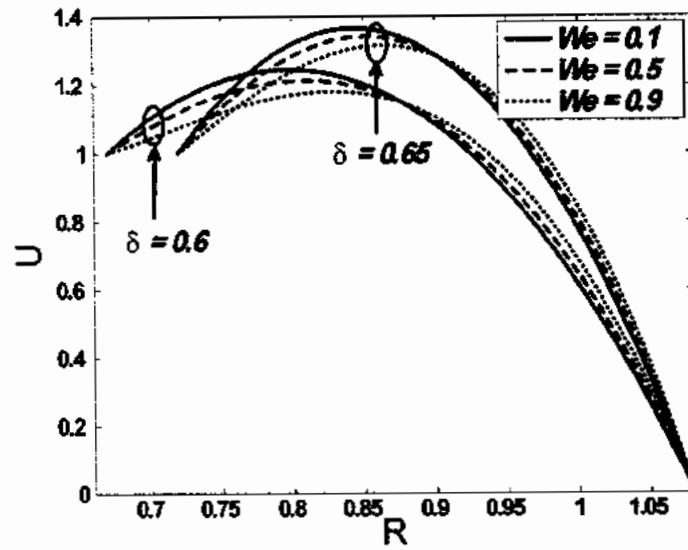
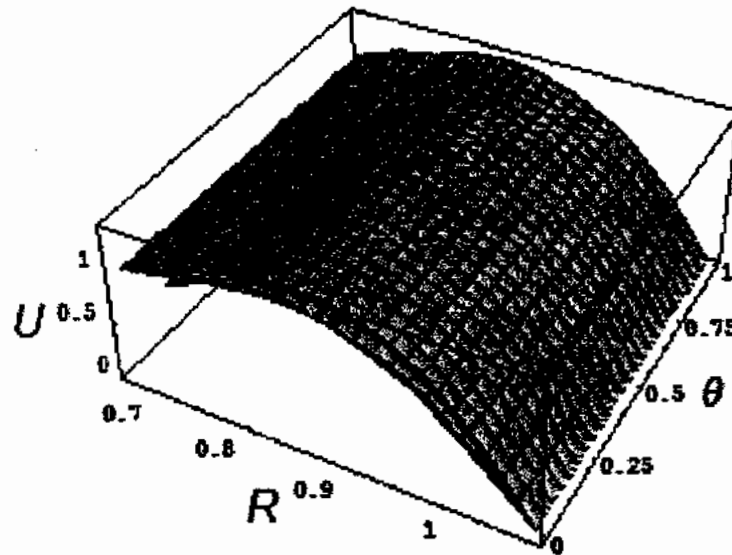


Fig. 5.5: Variation of pressure gradient  $\partial P / \partial Z$  with  $n$  and  $\delta$  for fixed values of  $\epsilon = 0.01$ ,  $Q = 0.5$ ,  $t = 0.3$ ,  $\theta = 0.87$ ,  $M = 0.5$ ,  $\phi = 0.1$ ,  $V_1 = 0.3$ .



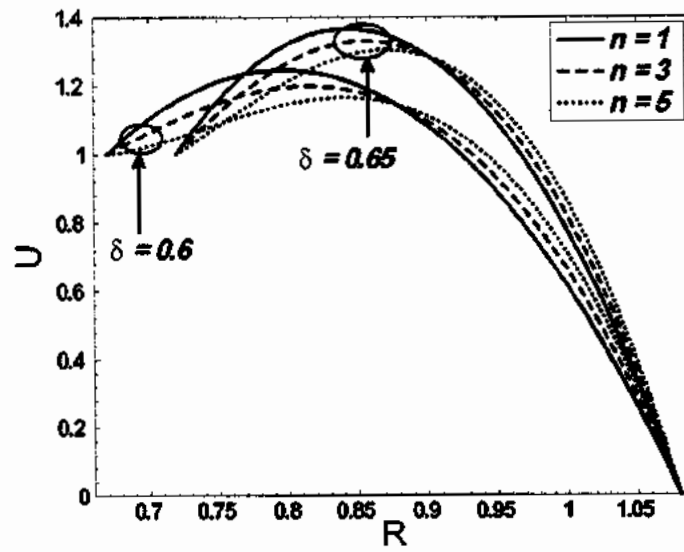


(a)

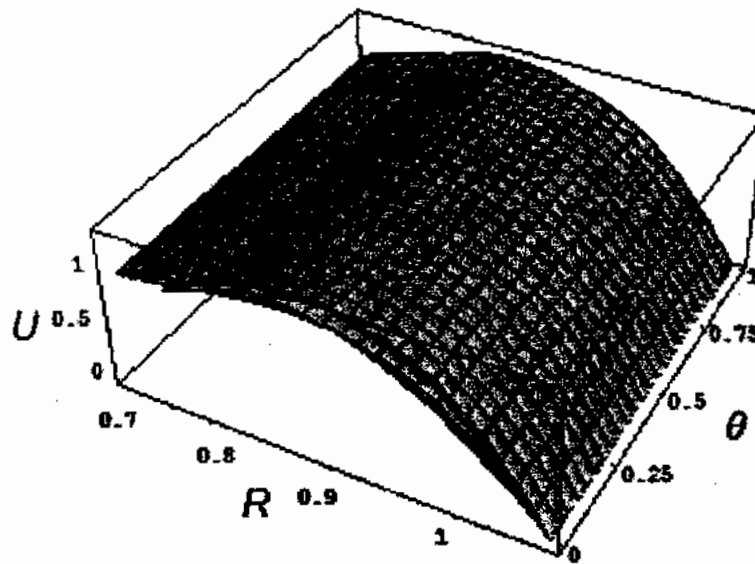


(b)

Fig. 5.6: Variation of velocity profile  $U$  with  $\delta$  and  $We$  for fixed values of  $\epsilon = 0.1$ ,  $Q = 0.5$ ,  $t = 0.1$ ,  $Z = 0$ ,  $V_1 = 1$ ,  $\theta = 0.87$ ,  $\phi = 0.1$ ,  $n = 4$ , (a) for 2-dimensional, (b) for 3-dimensional.



(a)



(b)

Fig. 5.7: Variation of velocity profile  $U$  with  $\delta$  and  $n$  for fixed values of  $Q = 0.5$ ,  $We = 1.5$ ,  $t = 0.2$ ,  $\epsilon = 0.1$ ,  $Z = 0.1$ ,  $\theta = 0.87$ ,  $\phi = 0.1$ ,  $V_1 = 1$ , (a) for 2-dimensional, (b) for 3-dimensional.

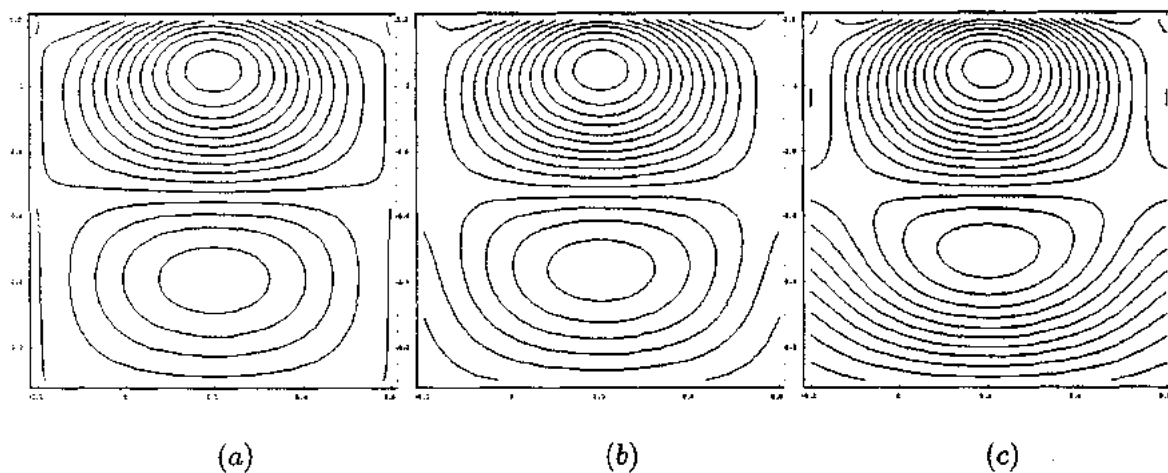


Fig. 5.8: Stream lines for different values of  $We$ , (a) for  $We = 0.1$ , (b) for  $We = 0.5$ , (c) for  $We = 0.9$ . The other parameters are  $\epsilon = 0.3$ ,  $Q = 0.2$ ,  $V_1 = 0.1$ ,  $t = 0.2$ ,  $\theta = 0.87$ ,  $\phi = 0.05$ ,  $\delta = 0.2$ ,  $n = 5$ .

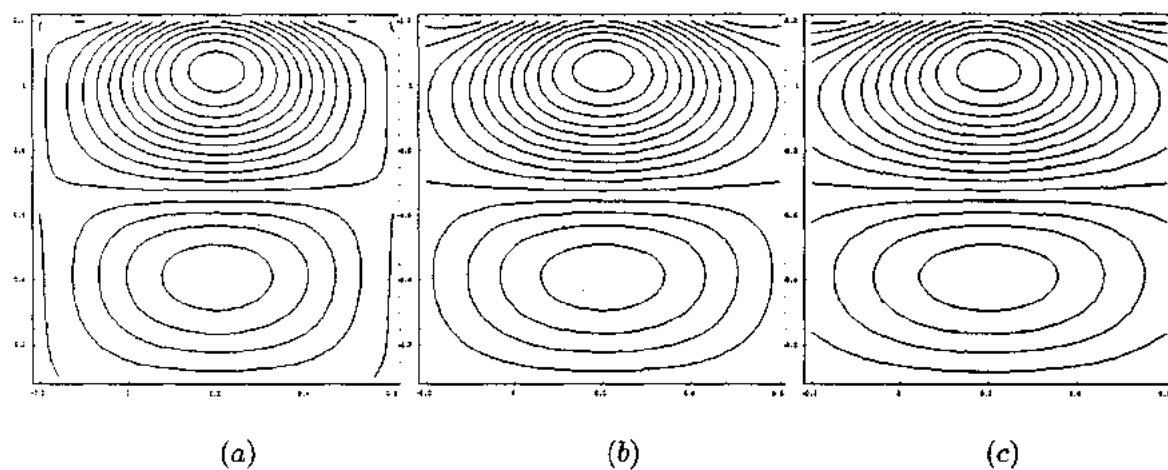


Fig. 5.9: Stream lines for different values of  $Q$ , (a) for  $Q = 0.2$ , (b) for  $Q = 0.3$ , (c) for  $Q = 0.4$ . The other parameters are  $\epsilon = 0.3$ ,  $t = 0.2$ ,  $\theta = 0.87$ ,  $V_1 = 0.2$ ,  $We = 0.3$ ,  $n = 2$ ,  $\delta = 0.2$ ,  $\phi = 0.05$ .

## Chapter 6

# Effects of heat and mass transfer on peristaltic flow of a nanofluid between eccentric cylinders

This chapter examines the heat and mass transfer analysis for the peristaltic flow of nanofluid through eccentric cylinders. The complexity of equations describing the flow of nanofluid is reduced through applying the low Reynolds number and long wavelength approximations. The resulting equations are highly non-linear, coupled and non homogeneous partial differential equations. These complicated governing equations are solved analytically by employing the homotopy perturbation method. The obtained expressions for velocity, temperature and nanoparticle phenomenon are sketched through graphs for two dimensions as well as three dimensions. The resulting relations for pressure gradient and pressure rise are plotted for various pertinent parameters. The streamlines are also drawn for some physical quantities to discuss the trapping phenomenon. This work has been published in the journal of "*Applied Nanoscience*", 4 (2014) 393–404.

### 6.1 Mathematical formulation of the problem

Let us consider the peristaltic flow of an incompressible nanofluid between two vertical eccentric cylinders. The geometry of the flow is described as the inner tube is rigid and sinusoidal wave

is propagating at the outer tube along its length. Further, we assume that boundary of the inner tube is at the temperature  $T_0$  and the outer tube is maintained at temperature  $T_1$ . The nano particles concentration is described as  $C_0$  and  $C_1$  at the walls of inner and outer cylinders, correspondingly. The problem has been considered in the system of cylindrical coordinates.

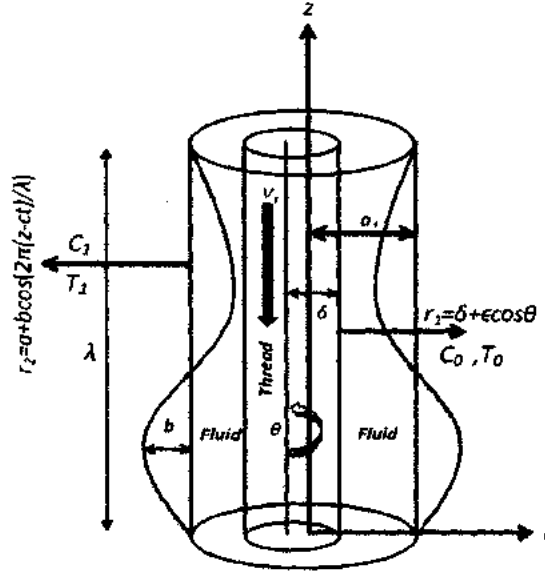


Fig. 6.1: The simplified model of geometry of the problem.

Introducing a wave frame  $(r, z)$  moving with velocity  $c$  away from the fixed frame  $(R, Z)$  by the transformations

$$z = Z - ct, \quad r = R, \quad u = U - c, \quad v = V, \quad p = P. \quad (6.1)$$

Let us assume that the velocity field for the flow is  $\mathbf{V} = (v, 0, u)$ . The dimensionless parameters used in the problem are defined in Eq. (2.9) and some extra quantities are introduced as follow

$$\left. \begin{aligned} \bar{\theta} &= \frac{T-T_0}{T_1-T_0}, \quad \sigma = \frac{C-C_0}{C_1-C_0}, \quad P_r = \frac{\mu}{\rho\alpha}, \quad S_c = \frac{\mu}{\rho D_B}, \quad B_r = \frac{\rho_f g \alpha a^2}{\mu c} (C_1 - C_0), \quad \tau = \frac{(\rho c)_p}{(\rho c)_f}, \\ G_r &= \frac{\rho_f g \alpha a^2}{\mu c} (T_1 - T_0), \quad N_b = \frac{\tau D_B}{\alpha_f} (C_1 - C_0), \quad N_t = \frac{\tau D_T}{T_0 \alpha_f} (T_1 - T_0), \quad \alpha_f = \frac{k}{(\rho c)_f} \end{aligned} \right\}, \quad (6.2)$$

where  $P_r$ ,  $N_b$ ,  $N_t$ ,  $G_r$  and  $B_r$  represent the Prandtl number, Brownian motion parameter, thermophoresis parameter, local temperature Grashof number and local nanoparticle Grashof number, respectively. After using the above non-dimensional parameters and employing the

assumptions of long wavelength ( $\delta_0 \rightarrow 0$ ) and low Reynolds number ( $Re \rightarrow 0$ ), the dimensionless form of governing Eqs. (1.15), (1.16) and (1.21) for nanofluid in the wave frame (without using primes) take the final form as

$$\frac{\partial^2 u}{\partial r^2} + \frac{1}{r} \frac{\partial u}{\partial r} + \frac{1}{r^2} \frac{\partial^2 u}{\partial \theta^2} + B_r \sigma + G_r \theta = \frac{dp}{dz}, \quad (6.3)$$

$$\frac{\partial^2 \bar{\theta}}{\partial r^2} + \frac{1}{r} \frac{\partial \bar{\theta}}{\partial r} + \frac{1}{r^2} \frac{\partial^2 \bar{\theta}}{\partial \theta^2} + N_b \left( \frac{\partial \bar{\theta}}{\partial r} \frac{\partial \sigma}{\partial r} + \frac{1}{r^2} \frac{\partial \bar{\theta}}{\partial \theta} \frac{\partial \sigma}{\partial \theta} \right) + N_t \left( \left( \frac{\partial \bar{\theta}}{\partial r} \right)^2 + \frac{1}{r^2} \left( \frac{\partial \bar{\theta}}{\partial \theta} \right)^2 \right) = 0, \quad (6.4)$$

$$\frac{\partial^2 \sigma}{\partial r^2} + \frac{1}{r} \frac{\partial \sigma}{\partial r} + \frac{1}{r^2} \frac{\partial^2 \sigma}{\partial \theta^2} + \frac{N_t}{N_b} \left( \frac{\partial^2 \bar{\theta}}{\partial r^2} + \frac{1}{r} \frac{\partial \bar{\theta}}{\partial r} + \frac{1}{r^2} \frac{\partial^2 \bar{\theta}}{\partial \theta^2} \right) = 0. \quad (6.5)$$

The corresponding boundary conditions are described as

$$u = V_1 \quad \text{at } r = r_1, \quad u = 0 \quad \text{at } r = r_2, \quad (6.6)$$

$$\bar{\theta} = 0 \quad \text{at } r = r_1, \quad \bar{\theta} = 1 \quad \text{at } r = r_2, \quad (6.7)$$

$$\sigma = 0 \quad \text{at } r = r_1, \quad \sigma = 1 \quad \text{at } r = r_2. \quad (6.8)$$

## 6.2 Solution of the problem

We use homotopy perturbation method to solve the above non-linear, non homogeneous and coupled partial differential equations of second order. The deformation equations for the given problems are manipulated as

$$\tilde{H}(\tilde{u}, q) = (1 - q) (\mathcal{L}_4[\tilde{u}] - \mathcal{L}_4[\tilde{u}_0]) + q \left( \mathcal{L}_4[\tilde{u}] + \frac{1}{r^2} \frac{\partial^2 \tilde{u}}{\partial \theta^2} + B_r \tilde{\sigma} + G_r \tilde{\theta} - \frac{dp}{dz} \right) = 0, \quad (6.9)$$

$$\left. \begin{aligned} & (1 - q) (\mathcal{L}_4[\tilde{\theta}] - \mathcal{L}_4[\tilde{\theta}_0]) + q \left( \mathcal{L}_4[\tilde{\theta}] + \frac{1}{r^2} \frac{\partial^2 \tilde{\theta}}{\partial \theta^2} + \right. \\ & \left. N_b \left( \frac{\partial \tilde{\theta}}{\partial r} \frac{\partial \tilde{\sigma}}{\partial r} + \frac{1}{r^2} \frac{\partial \tilde{\theta}}{\partial \theta} \frac{\partial \tilde{\sigma}}{\partial \theta} \right) + N_t \left( \left( \frac{\partial \tilde{\theta}}{\partial r} \right)^2 + \frac{1}{r^2} \left( \frac{\partial \tilde{\theta}}{\partial \theta} \right)^2 \right) \right) = 0 \end{aligned} \right\}, \quad (6.10)$$

$$(1 - q) (\mathcal{L}_4[\tilde{\sigma}] - \mathcal{L}_4[\tilde{\sigma}_0]) + q \left( \mathcal{L}_4[\tilde{\sigma}] + \frac{1}{r^2} \frac{\partial^2 \tilde{\sigma}}{\partial \theta^2} + \frac{N_t}{N_b} \left( \frac{\partial^2 \tilde{\theta}}{\partial r^2} + \frac{1}{r} \frac{\partial \tilde{\theta}}{\partial r} + \frac{1}{r^2} \frac{\partial^2 \tilde{\theta}}{\partial \theta^2} \right) \right) = 0. \quad (6.11)$$

The linear operator  $\mathcal{L}_4$  is chosen as

$$\mathcal{L}_4 = \frac{1}{r} \frac{\partial}{\partial r} \left( r \frac{\partial}{\partial r} \right). \quad (6.12)$$

We suggest the following initial guesses for  $u$ ,  $\bar{\theta}$  and  $\sigma$

$$\tilde{u}_0 = \frac{V_1 (\ln r - \ln r_2)}{\ln r_1 - \ln r_2}, \quad \tilde{\theta}_0 = \frac{\ln r_1 - \ln r}{\ln r_1 - \ln r_2} = \tilde{\sigma}_0. \quad (6.13)$$

Now we describe

$$\tilde{u}(r, \theta, z, q) = u_0 + qu_1 + \dots \quad (6.14)$$

$$\tilde{\theta}(r, \theta, z, q) = \bar{\theta}_0 + q\bar{\theta}_1 + \dots \quad (6.15)$$

$$\tilde{\sigma}(r, \theta, z, q) = \sigma_0 + q\sigma_1 + \dots \quad (6.16)$$

Making use of Eqs. (6.14) to (6.16) into Eqs. (6.9) to (6.11) and comparing terms of first two orders, we have the following systems

**Zeroth order system**

$$\mathcal{L}_4 [u_0] - \mathcal{L}_4 [\tilde{u}_0] = 0, \quad (6.17)$$

with boundary conditions defined in Eqs. (2.27) and (2.28).

$$\mathcal{L}_4 [\bar{\theta}_0] - \mathcal{L}_4 [\tilde{\theta}_0] = 0, \quad (6.18)$$

$$\bar{\theta}_0 = 1, \quad \text{at } r = r_2, \quad \bar{\theta}_0 = 0, \quad \text{at } r = r_1, \quad (6.19)$$

$$\mathcal{L}_4 [\sigma_0] - \mathcal{L}_4 [\tilde{\sigma}_0] = 0, \quad (6.20)$$

$$\sigma_0 = 1, \quad \text{at } r = r_2, \quad \sigma_0 = 0, \quad \text{at } r = r_1. \quad (6.21)$$

The solutions of the above zeroth order systems can be obtained by using Eqs. (6.13), (6.17) to (6.21) and are found as

$$u_0(r, \theta, z, q) = \frac{V_1 (\ln r - \ln r_2)}{\ln r_1 - \ln r_2}, \quad \bar{\theta}_0 = \frac{\ln r_1 - \ln r}{\ln r_1 - \ln r_2} = \sigma_0. \quad (6.22)$$

First order system

$$\mathcal{L}_4[u_1] + \frac{1}{r^2} \frac{\partial^2 u_0}{\partial \theta^2} + B_r \sigma_0 + G_r \bar{\theta}_0 - \frac{dp}{dz} = 0. \quad (6.23)$$

The corresponding boundary conditions are stated in Eqs. (2.32) and (2.33).

$$\mathcal{L}_4[\bar{\theta}_1] + \frac{1}{r^2} \frac{\partial^2 \bar{\theta}_0}{\partial \theta^2} + N_b \left( \frac{\partial \bar{\theta}_0}{\partial r} \frac{\partial \sigma_0}{\partial r} + \frac{1}{r^2} \frac{\partial \bar{\theta}_0}{\partial \theta} \frac{\partial \sigma_0}{\partial \theta} \right) + N_t \left( \left( \frac{\partial \bar{\theta}_0}{\partial r} \right)^2 + \frac{1}{r^2} \left( \frac{\partial \bar{\theta}_0}{\partial \theta} \right)^2 \right) = 0, \quad (6.24)$$

$$\bar{\theta}_1 = 0, \quad \text{at } r = r_2, \quad \bar{\theta}_1 = 0, \quad \text{at } r = r_1, \quad (6.25)$$

$$\mathcal{L}_4[\sigma_1] + \frac{1}{r^2} \frac{\partial^2 \sigma_0}{\partial \theta^2} + \frac{N_t}{N_b} \left( \frac{\partial^2 \bar{\theta}_0}{\partial r^2} + \frac{1}{r} \frac{\partial \bar{\theta}_0}{\partial r} + \frac{1}{r^2} \frac{\partial^2 \bar{\theta}_0}{\partial \theta^2} \right) = 0, \quad (6.26)$$

$$\sigma_1 = 1, \quad \text{at } r = r_2, \quad \sigma_1 = 0, \quad \text{at } r = r_1. \quad (6.27)$$

The solutions of the above non-linear ordinary differential equations are found as

$$u_1 = \left. \begin{aligned} &(-2(r-r_1)(r-r_2)(r_1-r_2) \left( 2(r_2-\delta)^2 (B_r(r+r_1+r_2-3\delta) + G_r \right. \\ &\quad \left. (r+r_1+r_2-3\delta)G_r(r+r_1+r_2-3\delta) + 3\frac{dp}{dz}(-r_2+\delta) \right) + (B_r(r+r_1 \\ &\quad + 7r_2-9\delta) + G_r(r+r_1+7r_2+G_r(r+r_1+7r_2-9\delta) + 9\frac{dp}{dz}(-r_2+\delta)) \epsilon^2) \\ &\quad + \epsilon \left( 3 \left( B_r + G_r - \frac{dp}{dz} \right) (r-r_1)(r-r_2)(r_1-r_2) \epsilon^2 \cos 3\theta + 36V_1 \epsilon \right. \\ &\quad \left. ((r_1-r_2)(r+r_2) \ln r - (r-r_2)(r_1+r_2) \ln r_1 + 2(r-r_1)r_2 \ln r_2) \right. \\ &\quad \left. + \cos \theta ((r-r_1)(r-r_2)(r_1-r_2) (4(r_2-\delta)(2B_r r + 2G_r r + 2B_r r_1 + 2 \right. \\ &\quad \left. G_r r_1 + 5B_r r_2 + 5G_r r_2 - 9r_2 \frac{dp}{dz} - 9 \left( B_r + G_r - \frac{dp}{dz} \right) \delta) + 9 \right. \\ &\quad \left. \left( B_r + G_r - \frac{dp}{dz} \right) \epsilon^2) + 24V_1(r_2-\delta)(-(r_1-r_2)(r+r_2) \ln r + (r-r_2) \right. \\ &\quad \left. (r_1+r_2) \ln r_1 + 2(-r+r_1)r_2 \ln r_2) - 2\epsilon \cos 2\theta (6(r_1-r_2)(r+r_2) \right. \\ &\quad \left. V_1 \ln r - 6(r-r_2)(r_1+r_2)V_1 \ln r_1 + (r-r_1)((r-r_2)(r_1-r_2)(B_r \right. \\ &\quad \left. (r+r_1+7r_2-9\delta) + G_r(r+r_1+7r_2-9\delta) + 9\frac{dp}{dz}(-r_2+\delta)) \right. \\ &\quad \left. + 12r_2V_1 \ln r_2) \right) / (24(r_1-r_2)(r_2-\delta-\epsilon \cos \theta)^3) \end{aligned} \right\} \quad (6.28)$$



$$\theta_1 = - \left( \begin{aligned} & (\ln r - \ln r_2) (\ln r - \ln r_1) \left( N_b \epsilon^2 (\ln r)^2 + N_t \epsilon^2 (\ln r)^2 + 4 \epsilon^2 \ln r \right. \\ & \ln r_2 - 3 N_b \epsilon^2 \ln r \ln r_2 - 3 N_t \epsilon^2 \ln r \ln r_2 + 12 N_b \delta^2 (\ln r_2)^2 + 12 N_t \delta^2 (\ln r_2)^2 \\ & - 8 \epsilon^2 (\ln r_2)^2 + 9 N_b \epsilon^2 (\ln r_2)^2 + 9 N_t \epsilon^2 (\ln r_2)^2 - 4 \epsilon^2 \ln r (\ln r_2)^2 + 8 \epsilon^2 \ln r_2^3 \\ & + 4 \delta \epsilon \cos \theta (\ln r_2 - \ln r_1)^2 (6 N_b + 6 N_t - \ln r + 2 \ln r_2 - \ln r_1) - 4 \epsilon^2 \ln r \\ & \ln (\delta + \epsilon \cos \theta) + N_b \epsilon^2 \ln r \ln r_1 + N_t \epsilon^2 \ln r \ln r_1 - 24 N_b \delta^2 \ln r_2 \ln r_1 \\ & - 24 N_t \delta^2 \ln r_2 \ln r_1 + 12 \epsilon^2 \ln r_2 \ln r_1 - 15 N_b \epsilon^2 \ln r_2 \ln r_1 - 15 N_t \epsilon^2 \ln r_2 \\ & \ln r_1 + 8 \epsilon^2 \ln r \ln r_2 \ln r_1 - 20 \epsilon^2 \ln r_2^2 \ln r_1 + \epsilon^2 \ln r_2 \ln r_1 - 15 N_t \epsilon^2 \ln r_2 \\ & \ln r_1 + 8 \epsilon^2 \ln r \ln r_2 \ln r_1 - 20 \epsilon^2 \ln r_2^2 \ln r_1 + 12 N_b \delta^2 (\ln r_1)^2 + 12 N_t \delta^2 \\ & (\ln r_1)^2 - 4 \epsilon^2 (\ln r_1)^2 + 7 N_b \epsilon^2 (\ln r_1)^2 + 7 N_t \epsilon^2 (\ln r_1)^2 - 4 \epsilon^2 \ln r \\ & (\ln r_1)^2 + 16 \epsilon^2 \ln r_2 (\ln r_1)^2 - 4 \epsilon^2 (\ln r_1)^3 - \epsilon^2 \cos 2\theta ((N_b + N_t) \\ & (\ln r)^2 - (8 + 3 N_b + 3 N_t) (\ln r_2)^2 + 3(4 + 3 N_b + 3 N_t) \ln r_2 (\ln r_1) \\ & - (4 + 5 N_b + 5 N_t) (\ln r_1)^2 + \ln r ((4 - 3 N_b - 3 N_t) \ln r_2 + \\ & \left. (-4 + N_b + N_t) \ln r_1) \right) \Big/ (24 r_1^2 (\ln r_2 - \ln r_1)^4) \end{aligned} \right) \quad (6.29)$$

$$\sigma_1 = \left( \begin{aligned} & ((N_b + N_t) \epsilon (\ln r - \ln r_2) (-\epsilon + \epsilon \cos 2\theta + (\epsilon + \delta \cos \theta) (\ln r_2 - \ln r_1)) \\ & (\ln r - \ln r_1) (\ln r - 2 \ln r_2 + \ln r_1)) \Big/ 6 N_b r_1^2 (\ln r_2 - \ln r_1)^3 \end{aligned} \right) \quad (6.30)$$

Now for  $q \rightarrow 1$ , Eqs. (6.14) to (6.16) approach the following solutions

$$u(r, \theta, z) = u_0 + u_1, \quad (6.31)$$

$$\bar{\theta}(r, \theta, z) = \theta_0 + \theta_1, \quad (6.32)$$

$$\sigma(r, \theta, z) = \sigma_0 + \sigma_1, \quad (6.33)$$

where  $u_0$ ,  $\theta_0$ ,  $\sigma_0$ ,  $u_1$ ,  $\theta_1$ , and  $\sigma_1$  are defined in Eqs. (6.22) and (6.28) to (6.30) respectively.

The instantaneous volume flow rate  $\bar{Q}$  is given by

$$\bar{Q} = 2\pi \int_{r_1}^{r_2} r u dr. \quad (6.34)$$

The mean volume flow rate  $Q$  over one period is given as

$$Q(z, t) = \frac{\bar{Q}}{\pi} - \frac{\phi^2}{2} + 2\phi \cos 2\pi z + \phi^2 \cos^2 2\pi z. \quad (6.35)$$

Now we can evaluate pressure gradient  $dp/dz$  by solving Eqs. (6.34) and (6.35) and is elaborated

as

$$\frac{dp}{dz} = \frac{1}{60\pi(r_1-r_2)^3(r_1+r_2)(r_2-\delta-\epsilon\cos\theta)^3} (15\epsilon^3(24Q - (B_r + G_r)\pi(r_1 - r_2)^3) \left. \begin{aligned} & (r_1 + r_2) + 12\pi\phi(4\cos 2\pi z + \phi\cos 4\pi z) \cos 3\theta + 2\epsilon^2 \cos 2\theta(2\pi \\ & ((B_r + G_r)(r_1 - r_2)^3(4r_1^2 + 22r_1r_2 + 19r_2^2) - 5(8r_1^3 - 27r_1^2r_2 + \\ & 19r_2^3)V_1) - 1080Q(r_2 - \delta) - 45(B_r + G_r)\pi(r_1 - r_2)^3(r_1 + r_2) \\ & \delta + 60\pi(36(-r_2 + \delta)\phi\cos 2\pi(z - t) + 9(-r_2 + \delta)\phi^2\cos 4\pi z - r_2 \\ & (2r_1^2 + 2r_1r_2 + r_2^2)V_1(\ln r_1 - \ln r_2))) + \epsilon\cos\theta(-B_r\pi(r_1 - r_2)^3 \\ & (4(r_2 - \delta)(16r_1^2 + 43r_1r_2 + 31r_2^2 - 45(r_1 + r_2)\delta) + 45(r_1 + r_2)\epsilon^2) \\ & - G_r\pi(r_1 - r_2)^3(4(r_2 - \delta)(16r_1^2 + 43r_1r_2 + 31r_2^2 - 45(r_1 + r_2)\delta) \\ & + 45(r_1 + r_2)\epsilon^2) + 40(\pi(r_1 - r_2)(28r_1^2 + r_1r_2 + r_2^2)V_1(r_2 - \delta) + \\ & 27Q(4(r_2 - \delta)^2 + \epsilon^2)) + 60\pi(36(4(r_2 - \delta)^2 + \epsilon^2)\phi\cos 2\pi z + \\ & 9(4(r_2 - \delta)^2 + \epsilon^2)\phi^2\cos 4\pi z - 4r_2(2r_1^2 + 2r_1r_2 + r_2^2)V_1 \\ & (r_2 - \delta)(\ln r_1 - \ln r_2))) + 2(-120(\pi(r_1 - r_2)^2(2r_1 + r_2)V_1 \\ & + 6Q(r_2 - \delta))(r_2 - \delta)^2 - 30(\pi(8r_1^3 + 3r_1^2r_2 - 11r_2^3)V_1 + 36 \\ & Q(r_2 - \delta))\epsilon^2 + B_r\pi(r_1 - r_2)^3(2(r_2 - \delta)^2(8r_1^2 + 14r_1r_2 + \\ & 8r_2^2 - 15(r_1 + r_2)\delta) + (8r_1^2 + 44r_1r_2 + 38r_2^2 - 45(r_1 + r_2) \\ & \delta)\epsilon^2) + G_r\pi(r_1 - r_2)^3(2(r_2 - \delta)^2(8r_1^2 + 14r_1r_2 + 8r_2^2 - \\ & 15(r_1 + r_2)\delta) + (8r_1^2 + 44r_1r_2 + 38r_2^2 - 45(r_1 + r_2)\delta)\epsilon^2) + \\ & 180\pi(-4(r_2 - \delta)(2(r_2 - \delta)^2 + 3\epsilon^2)\phi\cos 2\pi(z - t) - (r_2 - \delta) \\ & (2(r_2 - \delta)^2 + 3\epsilon^2)\phi^2\cos 4\pi z + r_2(2r_1^2 + 2r_1r_2 + r_2^2)V_1\epsilon^2 \\ & (\ln r_1 - \ln r_2)))) \end{aligned} \right\} \quad (6.36)$$

The data for pressure rise is obtained by integrating Eq. (2.41) numerically and presented in graphs.

### 6.3 Graphical results and discussion

In this section, we discussed the effects of different physical parameters on the profiles of velocity, temperature and nano particles concentration. Three dimensional analysis is also made to measure the influence of physical quantities on the flow properties in space. The variation

of pressure gradient and peristaltic pumping is also considered for various values of pertinent quantities. The trapping bolus phenomenon observing the flow behavior is also manipulated as well with the help of streamlines graphs. Figs. 6.2 to 6.9 are drawn to see the impact of different parameters on the peristaltic pressure rise  $\Delta p$  and pressure gradient  $dp/dz$ , accordingly. Variation of velocity profile, temperature distribution and nano particle phenomenon under the influence of observing parameters is shown in Figs. 6.10 to 6.15, respectively. The streamlines for the parameters  $B_r$ ,  $G_r$ ,  $N_b$  and  $N_t$  are displayed through the Figs. 6.16 to 6.19.

Fig. 6.2 represents the effects of parameters  $\delta$  and  $G_r$  on the pressure rise  $\Delta p$ . It is noticed here that pressure rise is an increasing function of local temperature Grashof number  $G_r$ , throughout the domain but for  $\delta$ , the pressure rise  $\Delta p$  is increasing in the retrograde pumping region ( $\Delta p > 0$ ,  $Q < 0$ ), while decreasing in the peristaltic pumping region ( $\Delta p > 0$ ,  $Q > 0$ ) and augmented pumping region ( $\Delta p < 0$ ,  $Q > 0$ ). If someone look at the Fig. 6.3, it is observed that  $\Delta p$  gets decreased with the increasing effects of Brownian motion parameter  $N_b$ . From Fig. 6.4, it is measured that pressure rise  $\Delta p$  is varying linearly with local nano particle Grashof number  $B_r$  and the effects of the parameter  $\epsilon$  are same as that of  $\delta$  measured in Figs. 6.2 and 6.3. Similarly, the variation of the parameter thermophoresis parameter  $N_t$  gives the same behavior on pressure rise graph as seen for  $G_r$  (see Fig. 6.5).

We can see the impact of parameters local temperature Grashof number  $G_r$  and local nano particle Grashof number  $B_r$  on the variation of pressure gradient  $dp/dz$  from Fig. 6.6 when all other parameters are kept fixed. It is noted that pressure gradient is directly proportional to both the parameters. It is also depicted from the considered graph that pressure gradient is wider near the walls but closer in the central part of the geometry which means that much pressure gradient is needed at the boundaries to maintain the flow as compared with the middle part for the parameters  $G_r$  and  $B_r$ . To see the influence of radius  $\delta$  and flow rate  $Q$  on the pressure gradient  $dp/dz$ , we prepared the graph shown in Fig. 6.7. It is seen here that pressure gradient is decreasing function of flow rate  $Q$  at all points within the flow but it is also measured from this graph that  $dp/dz$  is reducing in the middle of the flow but rising in the boundaries of the container. Fig. 6.8 presents the effects of velocity of the inner tube  $V_1$  and  $\epsilon$  on the pressure gradient profile. One comes to know from this graph that  $dp/dz$  is changing linearly with  $V_1$  but for  $\epsilon$ , pressure gradient gets reduction in the region  $z \in [0.9, 1.7]$  while observes increment

at walls of the outer cylinder, i.e., in the range  $z \in [0.64, 0.9] \cup [1.7, 1.97]$ . We can observe the variation of pressure gradient with Brownian motion parameter  $N_b$  and thermophoresis parameter  $N_t$  from Fig. 6.9. We can observe that pressure gradient profile rises directly when someone varies the magnitude of both the parameters throughout the flow.

It is observed from Fig. 6.10 that velocity profile decreases in the region  $r \in [0.1, 0.55]$  but increases in the rest of the domain with increasing the value of  $\delta$  while direct variation of velocity is observed in case of flow rate  $Q$  in the every part of the region. We presented the Fig. 6.11 to obtain the variation of velocity profile  $u$  for varying the magnitude of the parameters  $\epsilon$  and  $V_1$ . It is depicted that velocity is directly varying with  $V_1$  when seen in the range  $r \in [0.15, 0.6]$  but inverse behavior is reported in the zone  $r \in [0.6, 1.05]$  while totally reverse investigation is made for the parameter  $\epsilon$ . It is noticed from Fig. 6.12 that velocity profile  $u$  increases when we increase the value of Grashof number  $G_r$  and local nano particle Grashof number  $B_r$  at every point of the flow. The velocity profile gets maximum altitude with the increasing effects of  $N_t$  but rise in the value of  $N_b$  lessened the height of velocity distribution  $u$  (see Fig. 6.13).

To see the behavior of temperature distribution  $\theta$  with the variation of Brownian motion parameter  $N_b$  and thermophoresis parameter  $N_t$ , the Figs. 6.14 (a, b) and 6.15 (a, b) are displayed. It is concluded here that temperature is increasing with the increase in the magnitude of  $N_b$  and  $N_t$ . It is also mentioned here that temperature gets maximum value at the boundary of the outer tube and vanished at the centre of the outer tube. We look at the Figs. 6.16 (a, b) and 6.17 (a, b) in order to observe the impact of  $N_b$  and  $N_t$  on the nano particles concentration  $\sigma$ . From these graphs, we can release the observation that nano particles distribution gets larger with rising  $N_t$  but diminished when we increase the effects of  $N_b$ .

A very interesting phenomenon in the fluid transport is trapping. In the wave frame, streamlines under certain circumstances swell to trap a bolus which travels as an inlet with the wave speed. The occurring of an internally circulating bolus stiffened by closed streamline is called trapping. The bolus described as a volume of fluid bounded by a closed streamlines in the wave frame is moved at the wave pattern. Fig. 6.18 shows the streamlines for the various values of the parameter local nano particle Grashof number  $B_r$  in the upper part of the outer cylinder. It is noted that number of trapping bolus is decreasing with increasing the magnitude of  $B_r$ , while bolus becomes large when we give greater values to the  $B_r$ . From Fig. 6.19, it can be

seen that boluses are increased in counting but size of the bolus is reduced while increasing the values of local temperature Grashof number  $G_r$ . The number of trapping boluses is decreased with the rising effects of  $N_b$  but size of the bolus remains steady with varying  $N_b$  (see Fig. 6.20). Fig. 6.21 reveals the effect of  $N_t$  on the streamlines for wave travelling down the tube. It is noticed here that number of bolus is varying randomly with  $N_t$  but bolus expanded across the wave with increasing the magnitude of  $N_t$ .

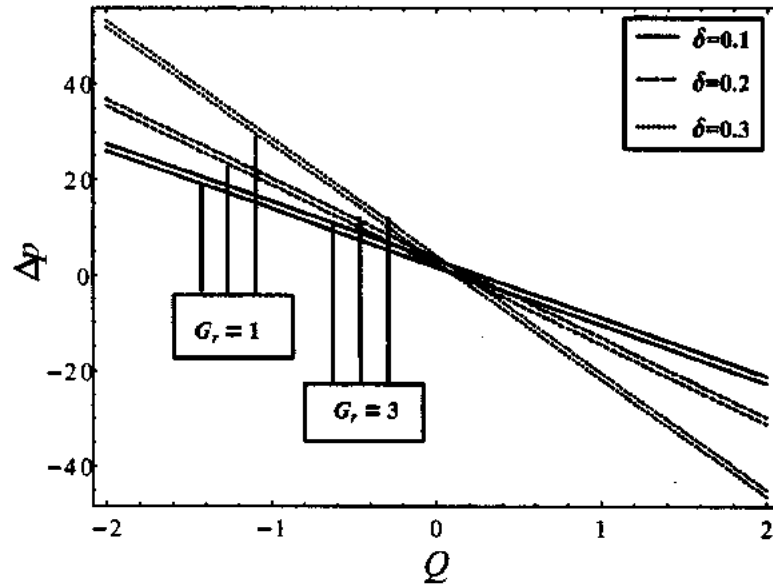


Fig. 6.2: Variation of pressure rise  $\Delta p$  with  $\delta$  and  $G_r$  for fixed values of  $\theta = 0.8$ ,  $\phi = 0.1$ ,  $B_r = 0.2$ ,  $N_b = 0.5$ ,  $N_t = 0.2$ ,  $\epsilon = 0.1$ ,  $V_1 = 0.3$ .

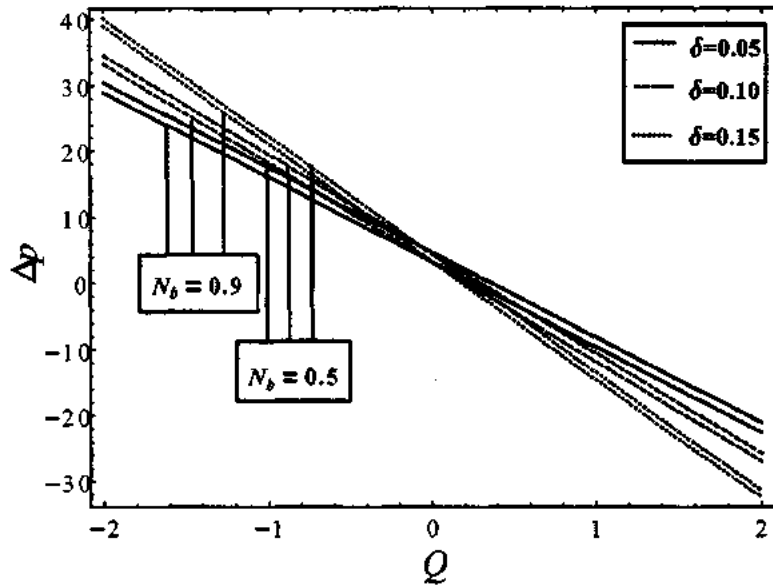


Fig. 6.3: Variation of pressure rise  $\Delta p$  with  $\delta$  and  $N_b$  for fixed values of  $\theta = 0.8$ ,  $\phi = 0.1$ ,  $B_r = 0.2$ ,  $G_r = 0.2$ ,  $N_t = 2$ ,  $\epsilon = 0.2$ ,  $V_1 = 0.3$ .

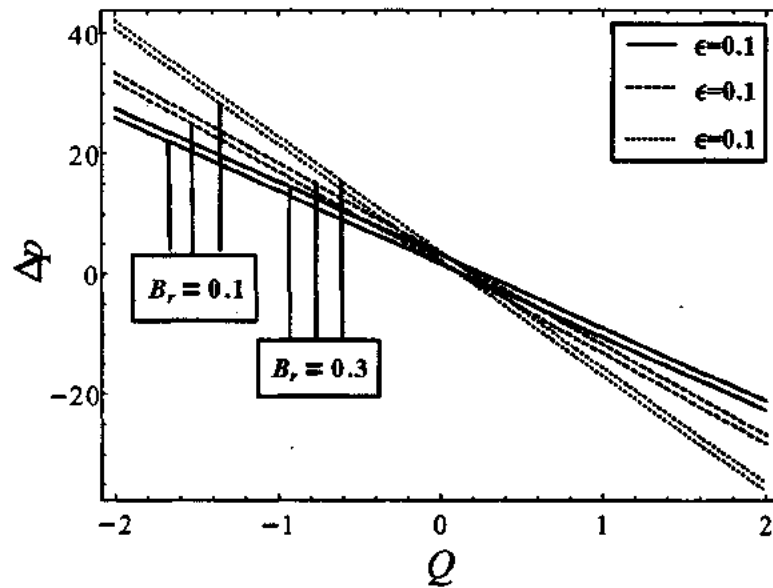


Fig. 6.4: Variation of pressure rise  $\Delta p$  with  $\epsilon$  and  $B_r$  for fixed values of  $\theta = 0.8$ ,  $\phi = 0.1$ ,  $N_b = 0.5$ ,  $G_r = 0.2$ ,  $N_t = 0.2$ ,  $\delta = 0.1$ ,  $V_1 = 0.3$ .

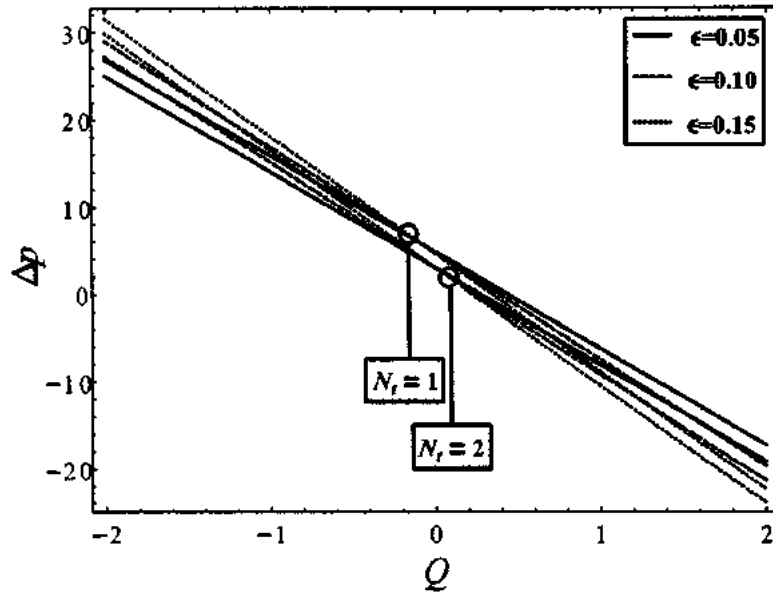


Fig. 6.5: Variation of pressure rise  $\Delta p$  with  $\epsilon$  and  $N_t$  for fixed values of  $\theta = 0.8$ ,  $\phi = 0.1$ ,  $N_b = 0.5$ ,  $G_r = 0.2$ ,  $B_r = 0.5$ ,  $\delta = 0.1$ ,  $V_1 = 0.3$ .

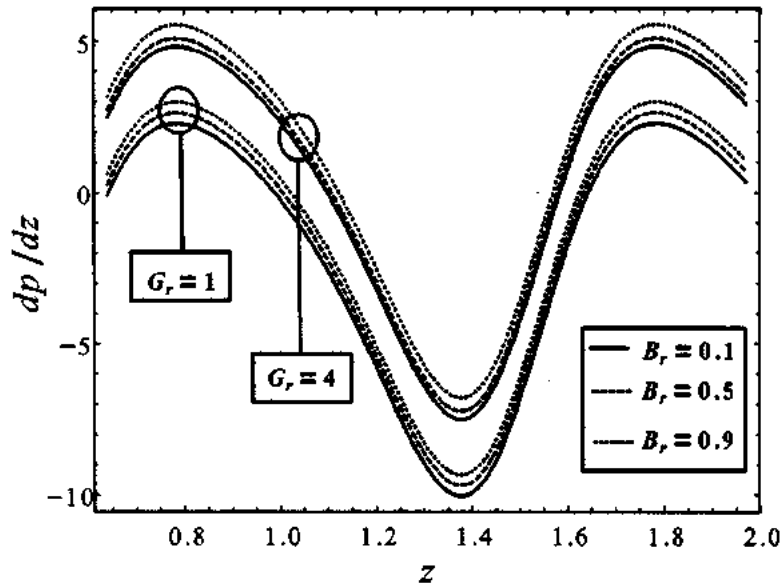


Fig. 6.6: Variation of pressure gradient  $dp/dz$  with  $G_r$  and  $B_r$  for fixed values of  $\epsilon = 0.01$ ,  $\delta = 0.02$ ,  $V_1 = 0.3$ ,  $\theta = 0.8$ ,  $\phi = 0.1$ ,  $Q = 0.5$ ,  $N_b = 0.5$ ,  $N_t = 0.2$ .

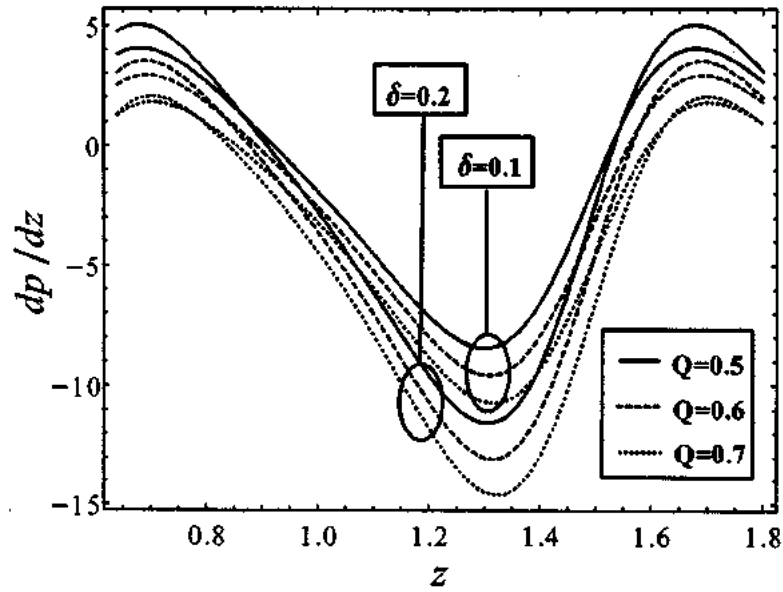


Fig. 6.7: Variation of pressure gradient  $dp/dz$  with  $\delta$  and  $Q$  for fixed values of  $\epsilon = 0.01$ ,  $G_r = 2$ ,  $V_1 = 0.3$ ,  $\theta = 0.8$ ,  $\phi = 0.1$ ,  $B_r = 0.8$ ,  $N_b = 0.5$ ,  $N_t = 0.2$ .

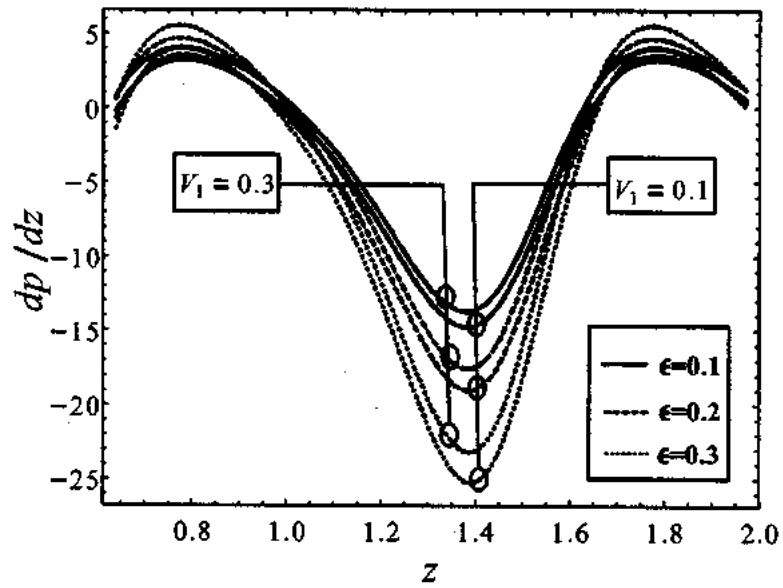


Fig. 6.8: Variation of pressure gradient  $dp/dz$  with  $\epsilon$  and  $V_1$  for fixed values of  $\delta = 0.1$ ,  $G_r = 2$ ,  $Q = 0.5$ ,  $\theta = 0.8$ ,  $\phi = 0.1$ ,  $B_r = 0.2$ ,  $N_b = 0.5$ ,  $N_t = 0.2$ .



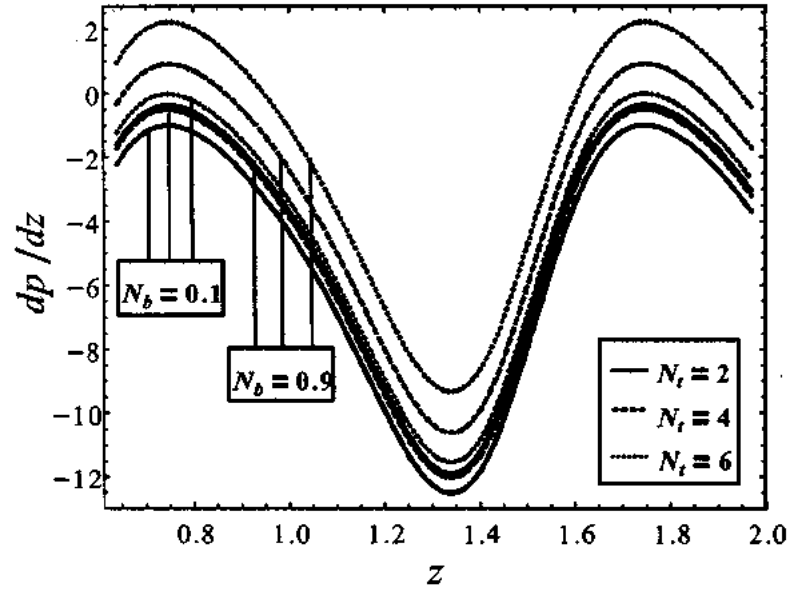
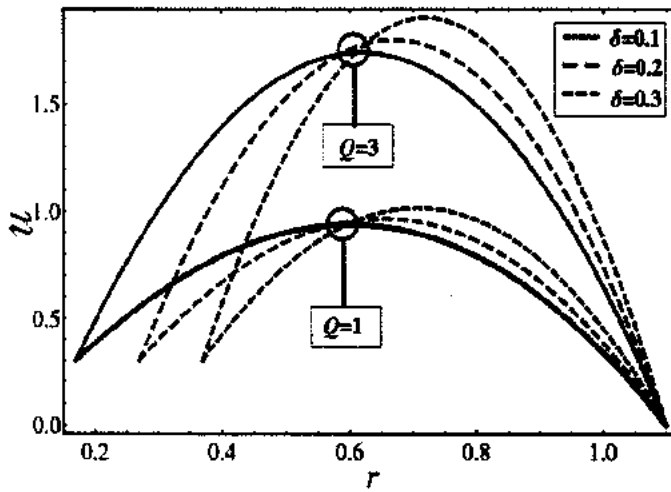
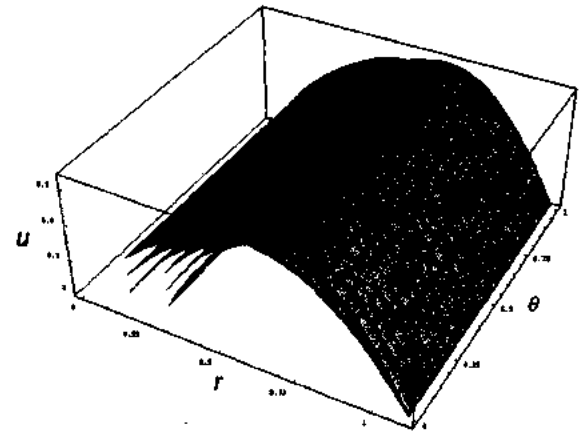


Fig. 6.9: Variation of pressure gradient  $dp/dz$  with  $N_b$  and  $N_t$  for fixed values of  $\delta = 0.05$ ,  $G_r = 2$ ,  $Q = 1$ ,  $\theta = 0.8$ ,  $\phi = 0.1$ ,  $B_r = 0.2$ ,  $\epsilon = 0.01$ ,  $V_1 = 0.1$ .

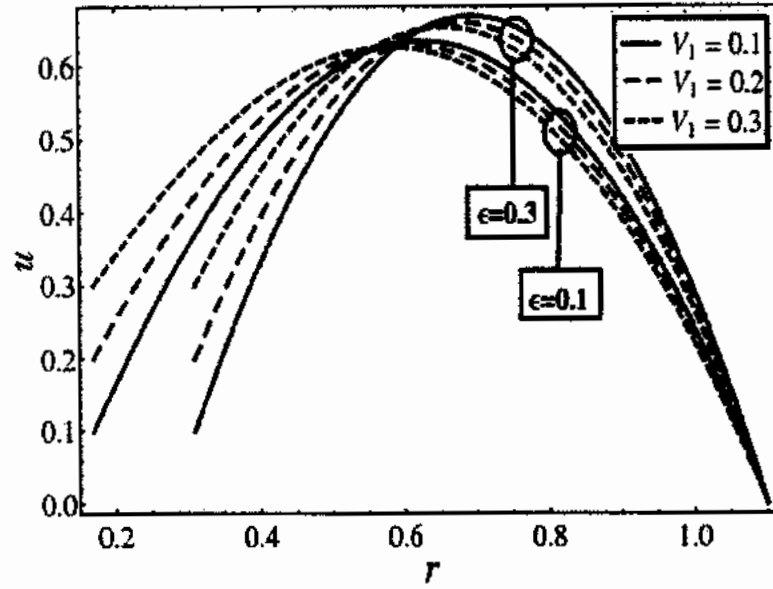


(a)

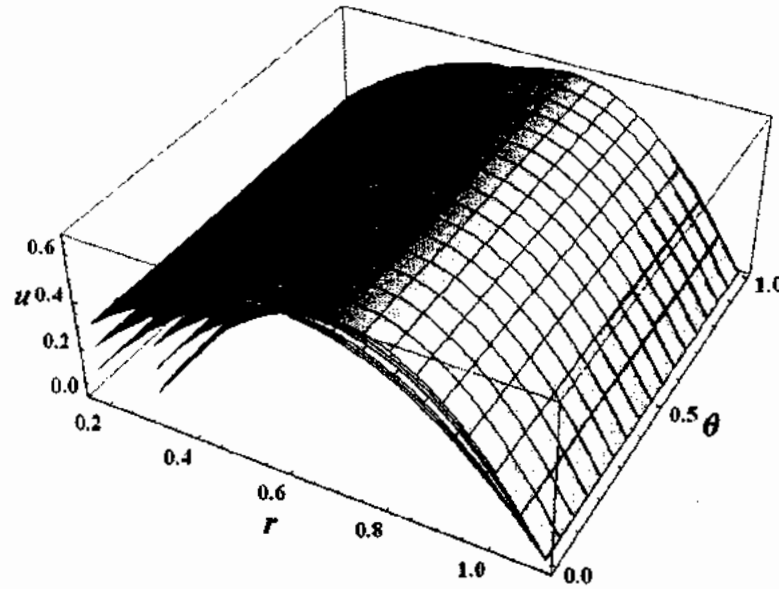


(b)

Fig. 6.10: Variation of velocity profile  $u$  with  $\delta$  and  $Q$  for fixed values of  $\epsilon = 0.1$ ,  $N_t = 0.5$ ,  $N_b = 0.1$ ,  $B_r = 0.3$ ,  $G_r = 1$ ,  $z = 0$ ,  $V_1 = 0.3$ ,  $\theta = 0.8$ ,  $\phi = 0.1$ , (a) for 2-dimensional, (b) for 3-dimensional.

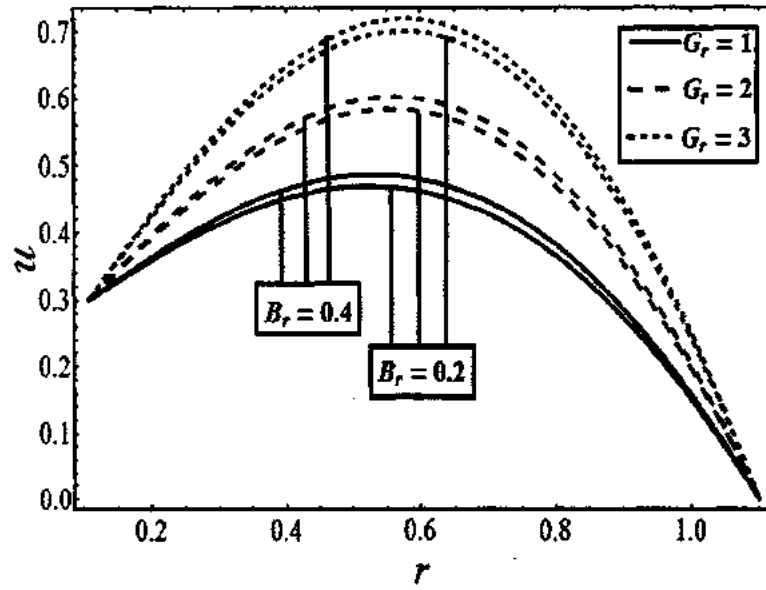


(a)

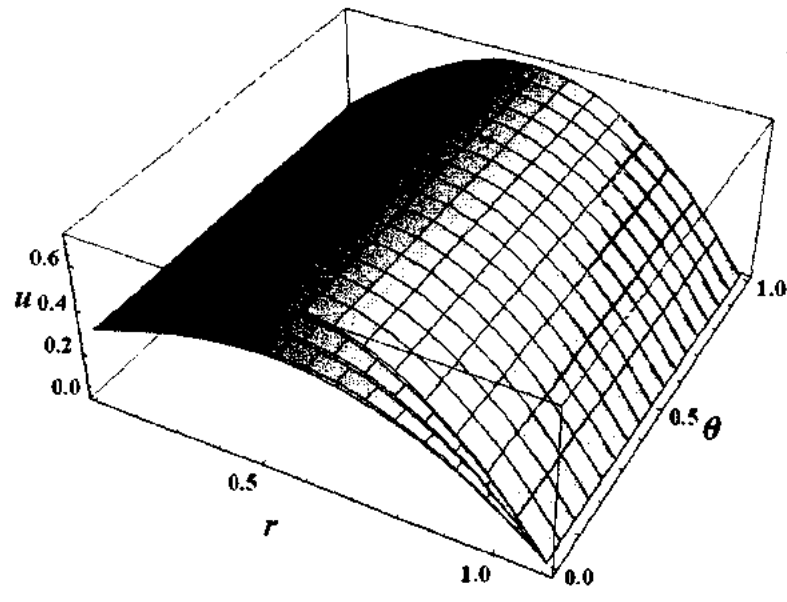


(b)

Fig. 6.11: Variation of velocity profile  $u$  with  $\epsilon$  and  $V_1$  for fixed values of  $\delta = 0.1$ ,  $N_t = 0.5$ ,  $N_b = 0.1$ ,  $B_r = 0.3$ ,  $G_r = 1$ ,  $z = 0$ ,  $Q = 1$ ,  $\theta = 0.8$ ,  $\phi = 0.1$ , (a) for 2-dimensional, (b) for 3-dimensional.

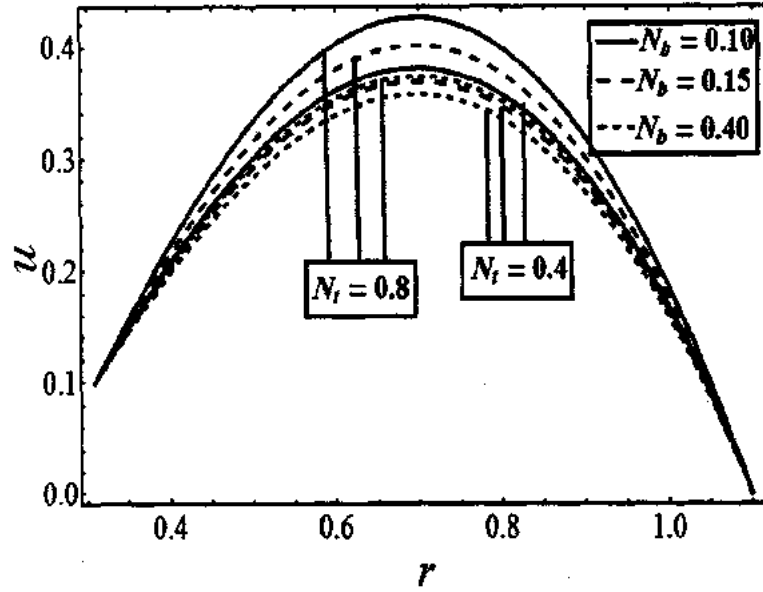


(a)

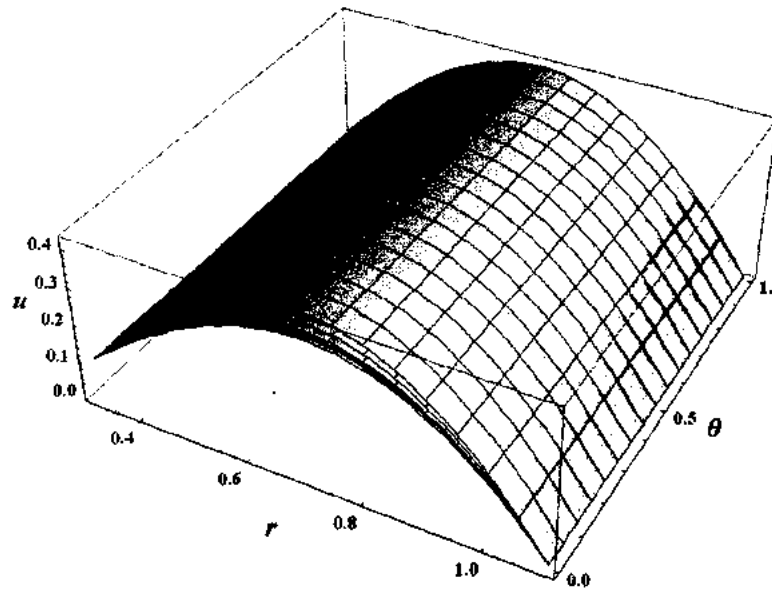


(b)

Fig. 6.12: Variation of velocity profile  $u$  with  $B_r$  and  $G_r$  for fixed values of  $\delta = 0.1$ ,  $N_t = 0.5$ ,  $N_b = 2$ ,  $\epsilon = 0.01$ ,  $V_1 = 0.3$ ,  $z = 0$ ,  $Q = 1$ ,  $\theta = 0.8$ ,  $\phi = 0.1$ , (a) for 2-dimensional, (b) for 3-dimensional.

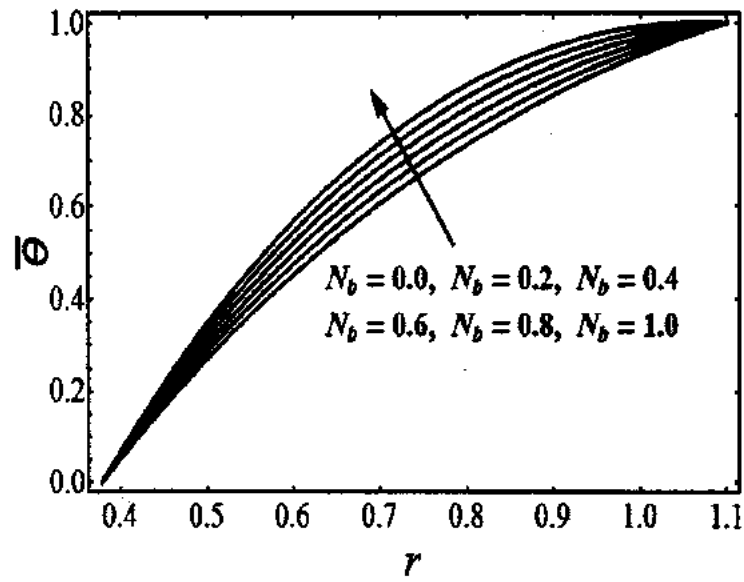


(a)

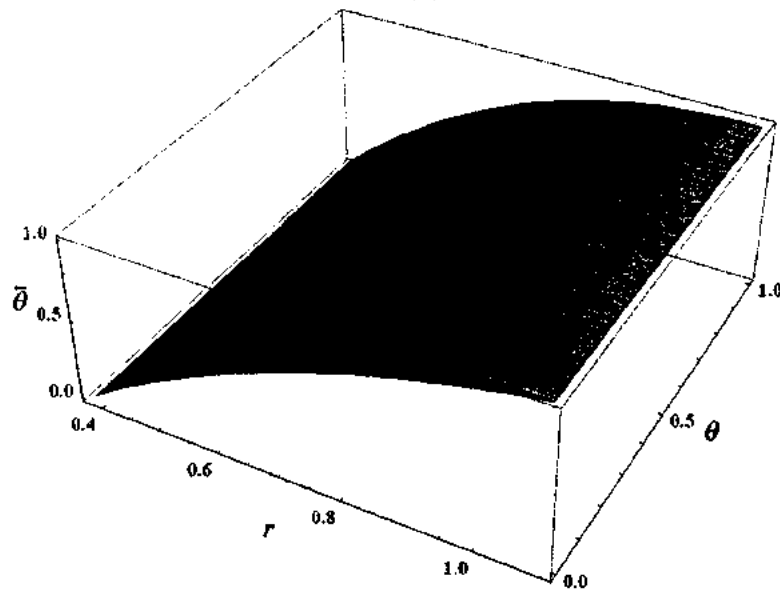


(b)

Fig. 6.13: Variation of velocity profile  $u$  with  $N_b$  and  $N_t$  for fixed values of  $\delta = 0.1$ ,  $B_r = 0.9$ ,  $G_r = 2$ ,  $\epsilon = 0.3$ ,  $V_1 = 0.1$ ,  $z = 0$ ,  $Q = 1$ ,  $\theta = 0.8$ ,  $\phi = 0.1$ , (a) for 2-dimensional, (b) for 3-dimensional.

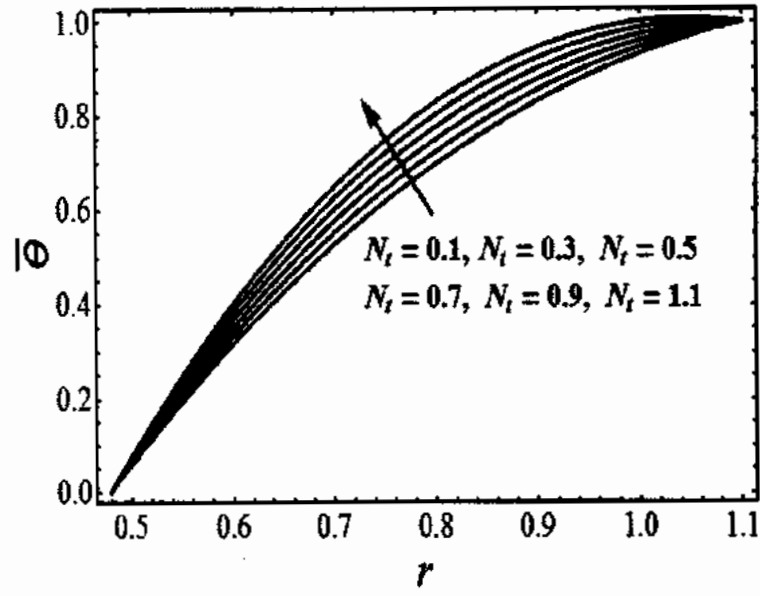


(a)

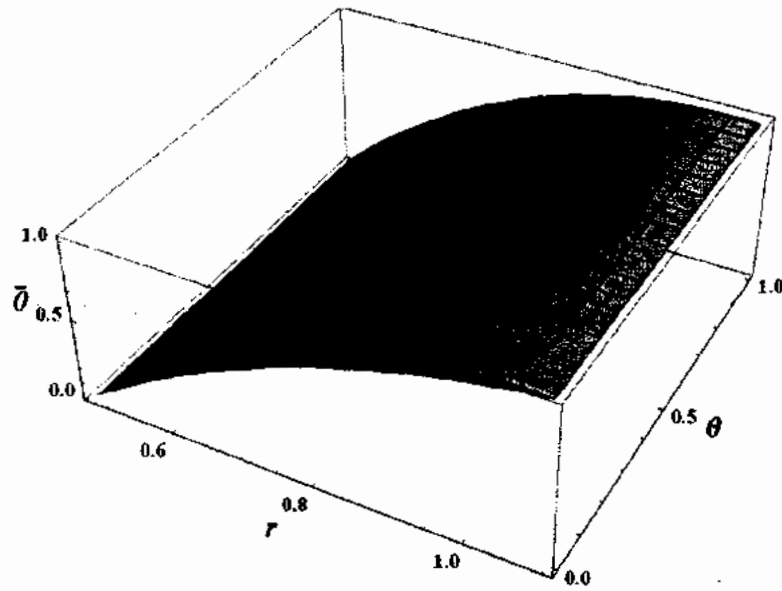


(b)

Fig. 6.14: Variation of temperature profile  $\bar{\theta}$  with  $N_b$  for fixed values of  $\delta = 0.1, \epsilon = 0.4, V_1 = 0.1, N_t = 0.2, z = 0, \theta = 0.8, \phi = 0.1$ , (a) for 2-dimensional, (b) for 3-dimensional.

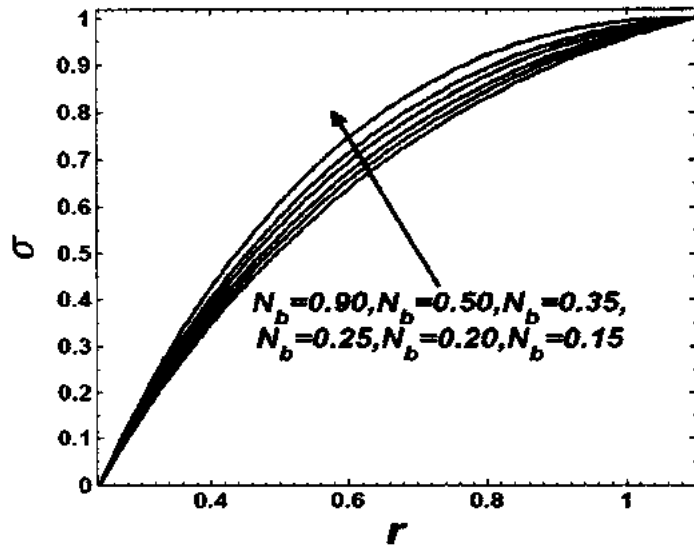


(a)

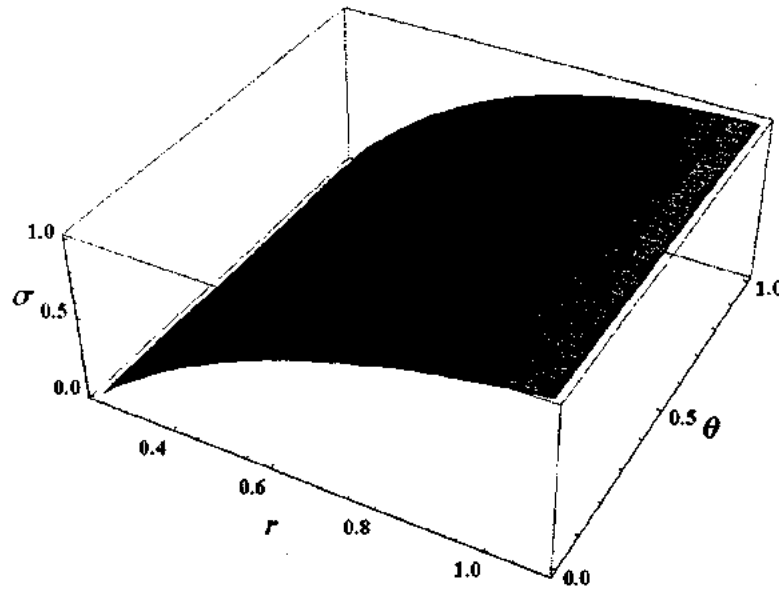


(b)

Fig. 6.15: Variation of temperature profile  $\bar{\theta}$  with  $N_t$  for fixed values of  $\delta = 0.2$ ,  $\epsilon = 0.4$ ,  $V_1 = 0.1$ ,  $N_b = 0.5$ ,  $z = 0$ ,  $\theta = 0.8$ ,  $\phi = 0.1$ , (a) for 2-dimensional, (b) for 3-dimensional.

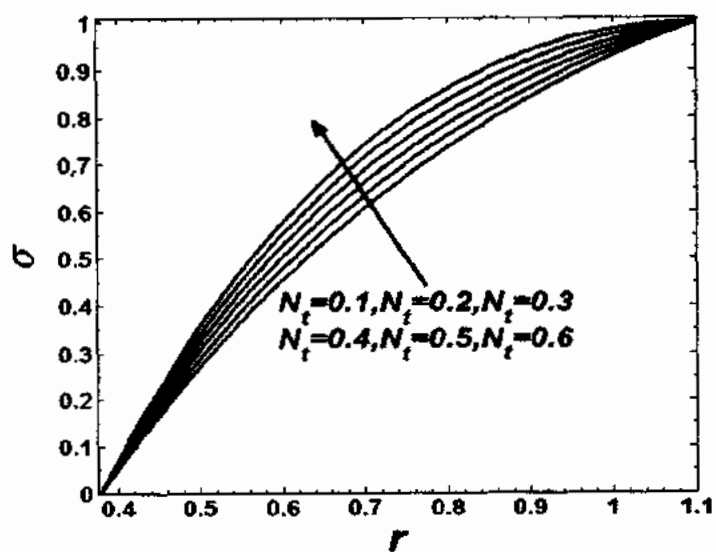


(a)

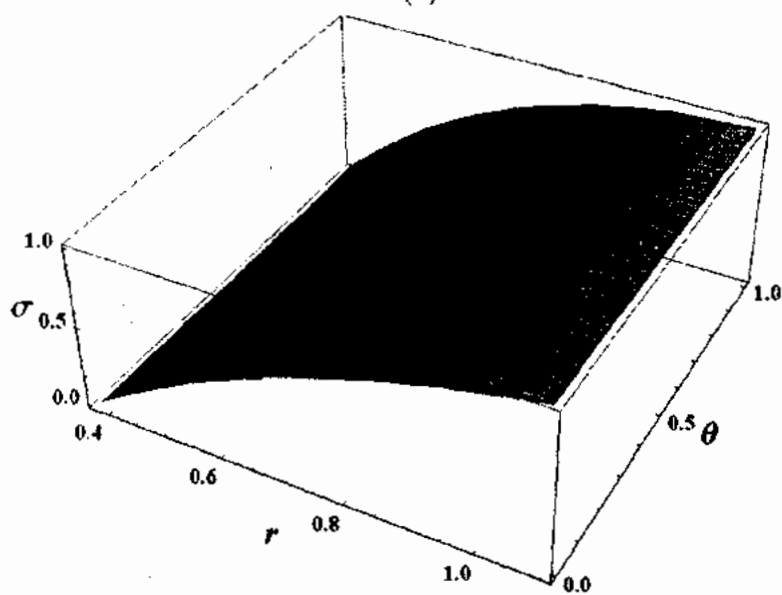


(b)

Fig. 6.16: Variation of nanoparticles phenomenon  $\sigma$  with  $N_b$  for fixed values of  $\delta = 0.1$ ,  $\epsilon = 0.2$ ,  $N_t = 0.1$ ,  $V_1 = 0.1$ ,  $z = 0$ ,  $\theta = 0.8$ ,  $\phi = 0.1$ , (a) for 2-dimensional, (b) for 3-dimensional.



(a)



(b)

Fig. 6.17: Variation of nanoparticles phenomenon  $\sigma$  with  $N_t$  for fixed values of  $\delta = 0.1$ ,  $\epsilon = 0.4$ ,  $N_b = 0.5$ ,  $V_1 = 0.1$ ,  $z = 0$ ,  $\theta = 0.8$ ,  $\phi = 0.1$ , (a) for 2-dimensional, (b) for 3-dimensional.



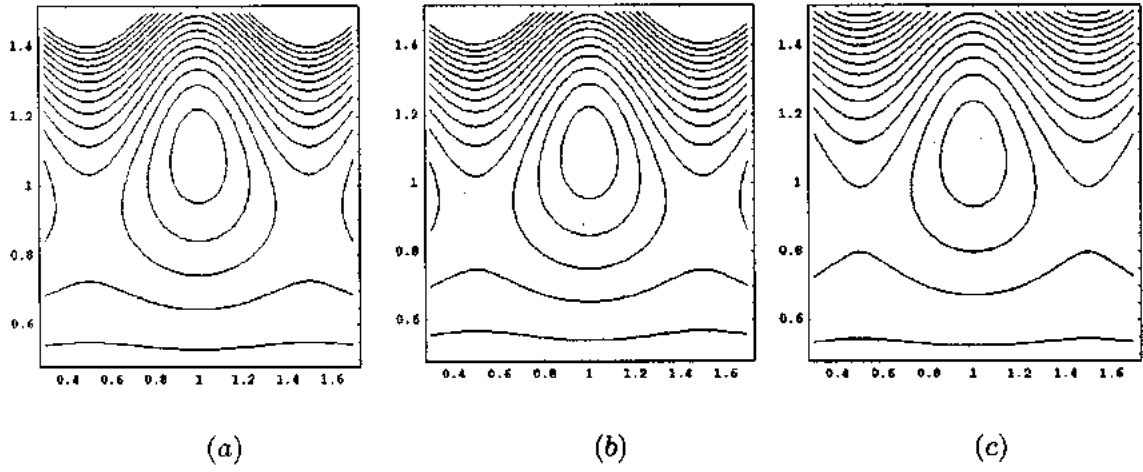


Fig. 6.18: Stream lines for different values of  $B_r$ , (a) for  $B_r = 0.1$ , (b) for  $B_r = 0.5$ , (c) for  $B_r = 0.9$ . The other parameters are  $\epsilon = 0.2$ ,  $V_1 = 0.3$ ,  $\theta = 0.1$ ,  $\phi = 0.1$ ,  $Q = 0.6$ ,  $\delta = 0.1$ ,  $N_t = 0.8$ ,  $N_b = 0.1$ ,  $G_r = 2$ .

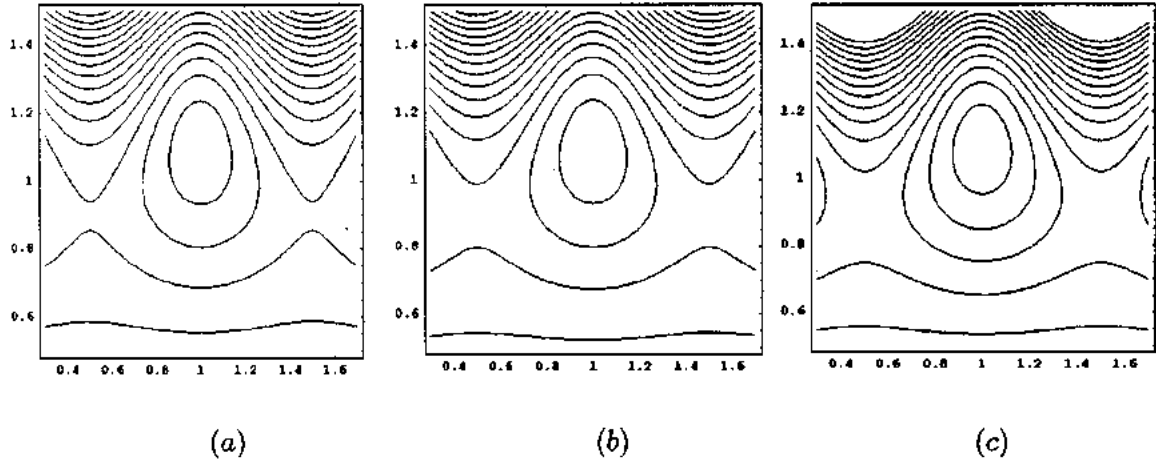


Fig. 6.19: Stream lines for different values of  $G_r$ , (a) for  $G_r = 1$ , (b) for  $G_r = 2$ , (c) for  $G_r = 3$ . The other parameters are  $\epsilon = 0.2$ ,  $V_1 = 0.3$ ,  $\theta = 0.1$ ,  $\phi = 0.1$ ,  $Q = 0.6$ ,  $\delta = 0.1$ ,  $N_t = 0.8$ ,  $N_b = 0.1$ ,  $B_r = 0.9$ .

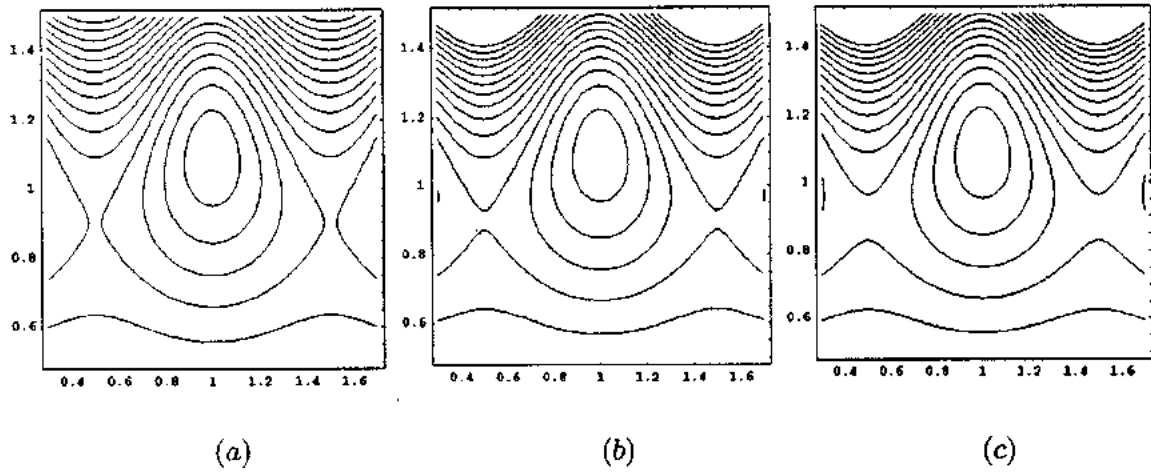


Fig. 6.20: Stream lines for different values of  $N_b$ , (a) for  $N_b = 0.1$ , (b) for  $N_b = 0.5$ , (c) for  $N_b = 0.9$ . The other parameters are  $\epsilon = 0.1$ ,  $V_1 = 0.3$ ,  $\theta = 0.1$ ,  $\phi = 0.1$ ,  $Q = 0.6$ ,  $\delta = 0.1$ ,  $N_t = 1$ ,  $G_r = 2$ ,  $B_r = 0.2$ .

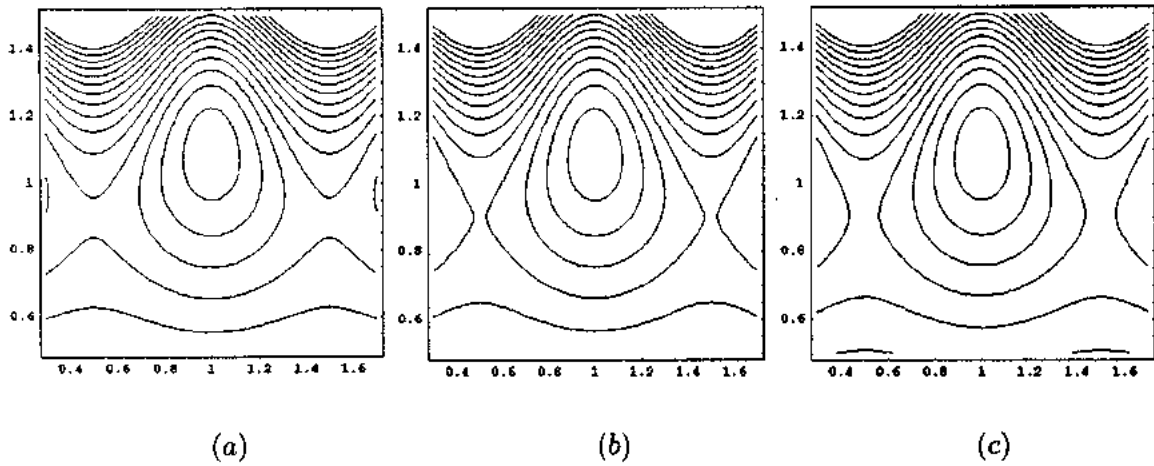


Fig. 6.21: Stream lines for different values of  $N_t$ , (a) for  $N_t = 0.1$ , (b) for  $N_t = 0.3$ , (c) for  $N_t = 0.5$ . The other parameters are  $\epsilon = 0.1$ ,  $V_1 = 0.3$ ,  $\theta = 0.8$ ,  $\phi = 0.1$ ,  $Q = 0.6$ ,  $\delta = 0.1$ ,  $N_b = 0.5$ ,  $G_r = 1$ ,  $B_r = 0.3$ .

## Chapter 7

# Mathematical treatment for the peristaltic flow of nanofluid through eccentric tubes comprising porous medium

In the current chapter, mathematical model of peristaltic flow of nanofluid between eccentric tubes is investigated through a porous medium. Assumptions of long wave length and low Reynolds number are carried out to observe the intestinal flow. The flow is considered to be unsteady and incompressible. Analytical solutions are evaluated through homotopy perturbation method. The expression of pressure rise is obtained through numerical integration whose data is presented through table. The problems under consideration are made dimensionless to reduce the complication of the analysis and to merge the extra parameters. All the emerging parameters affecting the flow phenomenon are discussed graphically. Trapping bolus scheme is also presented through streamlines for various pertinent quantities. The contents of this work are published in the journal "*Applied Nanoscience*", 4 (2014) 733–743.

## 7.1 Mathematical formulation of the problem

Let us analyze the peristaltic pumping characteristics of an unsteady and incompressible nanofluid between two vertical eccentric tubes through a porous space (see Fig. 6.1). The dimensions of the geometry are similar to those mentioned in chapter 2. Here, the medium of the flow is considered as porous. The velocity vector for the current problem is described as  $\mathbf{V} = (V, 0, U)$ . We incorporate the dimensionless quantities as described in Eq. (6.2) in addition with the following new parameter

$$k' = \frac{k_1}{a^2}, \quad (7.1)$$

here  $k'$  is the porosity parameter. After including the non-dimensional parameters and considering the approximations of long wavelength ( $\lambda \rightarrow \infty$ ) and low Reynolds number ( $\text{Re} \ll 1$ ), the dimensionless form of governing Eqs. (1.15), (1.16) and (1.21) (after ignoring primes) for nanofluid in porous space take the concluding form as

$$\frac{\partial^2 U}{\partial R^2} + \frac{1}{R} \frac{\partial U}{\partial R} + \frac{1}{R^2} \frac{\partial^2 U}{\partial \theta^2} + B_r \sigma + G_r \bar{\theta} - \frac{U}{k} = \frac{\partial P}{\partial Z}, \quad (7.2)$$

$$\frac{\partial^2 \bar{\theta}}{\partial R^2} + \frac{1}{R} \frac{\partial \bar{\theta}}{\partial R} + \frac{1}{R^2} \frac{\partial^2 \bar{\theta}}{\partial \theta^2} + N_b \left( \frac{\partial \bar{\theta}}{\partial R} \frac{\partial \sigma}{\partial R} + \frac{1}{R^2} \frac{\partial \bar{\theta}}{\partial \theta} \frac{\partial \sigma}{\partial \theta} \right) + N_t \left( \left( \frac{\partial \bar{\theta}}{\partial R} \right)^2 + \frac{1}{R^2} \left( \frac{\partial \bar{\theta}}{\partial \theta} \right)^2 \right) = 0, \quad (7.3)$$

$$\frac{\partial^2 \sigma}{\partial R^2} + \frac{1}{R} \frac{\partial \sigma}{\partial R} + \frac{1}{R^2} \frac{\partial^2 \sigma}{\partial \theta^2} + \frac{N_t}{N_b} \left( \frac{\partial^2 \bar{\theta}}{\partial R^2} + \frac{1}{R} \frac{\partial \bar{\theta}}{\partial R} + \frac{1}{R^2} \frac{\partial^2 \bar{\theta}}{\partial \theta^2} \right) = 0. \quad (7.4)$$

The related dimensionless boundary conditions for above partial differential equations are described in Eqs. (2.20), (2.21), (6.7) and (6.8).

## 7.2 Solution of the problem

We use homotopy perturbation method to solve the above non-linear, nonhomogeneous and coupled partial differential Eqs. (7.2) to (7.4). The deformation equations for the given problems are described as

$$\tilde{H}(\tilde{u}, q) = (1 - q) (\mathcal{L}_5[\tilde{u}] - \mathcal{L}_5[\tilde{u}_0]) + q \left( \mathcal{L}_5[\tilde{u}] + \frac{1}{R^2} \frac{\partial^2 \tilde{u}}{\partial \theta^2} + B_r \tilde{\sigma} + G_r \tilde{\theta} - \frac{\tilde{u}}{k} - \frac{\partial P}{\partial Z} \right) = 0, \quad (7.5)$$

$$(1-q) \left( \mathcal{L}_5 [\tilde{\theta}] - \mathcal{L}_5 [\tilde{\theta}_0] \right) + q \left( \mathcal{L}_5 [\tilde{\theta}] + \frac{1}{R^2} \frac{\partial^2 \tilde{\theta}}{\partial \theta^2} + N_b \left( \frac{\partial \tilde{\theta}}{\partial R} \frac{\partial \tilde{\sigma}}{\partial R} + \frac{1}{R^2} \frac{\partial \tilde{\theta}}{\partial \theta} \frac{\partial \tilde{\sigma}}{\partial \theta} \right) + N_t \left( \left( \frac{\partial \tilde{\theta}}{\partial R} \right)^2 + \frac{1}{R^2} \left( \frac{\partial \tilde{\theta}}{\partial \theta} \right)^2 \right) \right) = 0 \quad (7.6)$$

$$(1-q) (\mathcal{L}_5 [\tilde{\sigma}] - \mathcal{L}_5 [\tilde{\sigma}_0]) + q \left( \mathcal{L}_5 [\tilde{\sigma}] + \frac{1}{R^2} \frac{\partial^2 \tilde{\sigma}}{\partial \theta^2} + \frac{N_t}{N_b} \left( \frac{\partial^2 \tilde{\theta}}{\partial R^2} + \frac{1}{R} \frac{\partial \tilde{\theta}}{\partial R} + \frac{1}{R^2} \frac{\partial^2 \tilde{\theta}}{\partial \theta^2} \right) \right) = 0. \quad (7.7)$$

We assume

$$\mathcal{L}_5 = \frac{1}{R} \frac{\partial}{\partial R} \left( R \frac{\partial}{\partial R} \right), \quad (7.8)$$

as a linear operator. Let us consider the following initial guesses for  $U$ ,  $\bar{\theta}$  and  $\sigma$

$$\tilde{u}_0 = \frac{V (\ln R - \ln r_2)}{\ln r_1 - \ln r_2}, \quad \tilde{\theta}_0 = \frac{\ln r_1 - \ln R}{\ln r_1 - \ln r_2} = \tilde{\sigma}_0. \quad (7.9)$$

Now using the same procedure as adopted in last chapter (see Eqs. (6.14) to (6.16)), we have the following two systems of differential equations along with corresponding boundary conditions.

#### Zeroth order system

$$\mathcal{L}_5 [u_0] - \mathcal{L}_5 [\tilde{u}_0] = 0, \quad (7.10)$$

$$u_0 = 0, \quad \text{at } R = r_2, \quad u_0 = V_1, \quad \text{at } R = r_1, \quad (7.11)$$

$$\mathcal{L}_5 [\bar{\theta}_0] - \mathcal{L}_5 [\tilde{\theta}_0] = 0, \quad (7.12)$$

$$\bar{\theta}_0 = 1, \quad \text{at } R = r_2, \quad \bar{\theta}_0 = 0, \quad \text{at } R = r_1, \quad (7.13)$$

$$\mathcal{L}_5 [\sigma_0] - \mathcal{L}_5 [\tilde{\sigma}_0] = 0, \quad (7.14)$$

$$\sigma_0 = 1, \quad \text{at } R = r_2, \quad \sigma_0 = 0, \quad \text{at } R = r_1. \quad (7.15)$$

#### First order system

$$\frac{1}{R} \frac{\partial}{\partial R} \left( R \frac{\partial u_1}{\partial R} \right) + \frac{1}{R^2} \frac{\partial^2 u_0}{\partial \theta^2} + B_r \sigma_0 + G_r \bar{\theta}_0 - \frac{u_0}{k} = \frac{\partial P}{\partial Z}, \quad (7.16)$$

$$u_1 = 0, \quad \text{at } R = r_2, \quad u_1 = 0, \quad \text{at } R = r_1, \quad (7.17)$$

$$\frac{1}{R} \frac{\partial}{\partial R} \left( R \frac{\partial \bar{\theta}_1}{\partial R} \right) + \frac{1}{R^2} \frac{\partial^2 \bar{\theta}_0}{\partial \theta^2} + N_b \left( \frac{\partial \bar{\theta}_0}{\partial R} \frac{\partial \sigma_0}{\partial R} + \frac{1}{R^2} \frac{\partial \bar{\theta}_0}{\partial \theta} \frac{\partial \sigma_0}{\partial \theta} \right) + N_t \left( \left( \frac{\partial \bar{\theta}_0}{\partial R} \right)^2 + \frac{1}{R^2} \left( \frac{\partial \bar{\theta}_0}{\partial \theta} \right)^2 \right) = 0, \quad (7.18)$$

$$\bar{\theta}_1 = 0, \quad \text{at } R = r_2, \quad \bar{\theta}_1 = 0, \quad \text{at } R = r_1, \quad (7.19)$$

$$\frac{1}{R} \frac{\partial}{\partial R} \left( R \frac{\partial \sigma_1}{\partial R} \right) + \frac{1}{R^2} \frac{\partial^2 \sigma_0}{\partial \theta^2} + \frac{N_i}{N_b} \left( \frac{\partial^2 \bar{\theta}_0}{\partial R^2} + \frac{1}{R} \frac{\partial \bar{\theta}_0}{\partial R} + \frac{1}{R^2} \frac{\partial^2 \bar{\theta}_0}{\partial \theta^2} \right) = 0, \quad (7.20)$$

$$\sigma_1 = 1, \quad \text{at } R = r_2, \quad \sigma_1 = 0, \quad \text{at } R = r_1. \quad (7.21)$$

Now from Eqs. (7.16) to (7.21), the final solutions for velocity  $U$ , temperature  $\bar{\theta}$  and concentration  $\sigma$  can be directly written as

$$\begin{aligned} U = & \frac{V_1 \ln(R/r_2)}{\ln(r_1/r_2)} + \frac{1}{8kr_1^2 r_2^3} (6B_r k r_{11} + 6G_r k r_{11} + 4B_r k r_{22} - 4k \frac{\partial P}{\partial Z} r_{22} + 4G_r k r_{22} \\ & + 4k \frac{\partial P}{\partial Z} R^2 r_{23} - 4B_r k R^2 r_{24} - 4G_r k R^2 r_{24} + 6B_r k r_{25} + 6G_r k r_{25} + 6r_{11} V_1 + \\ & 4R^2 r_{23} V_1 - 4R^2 r_{24} V_1 + 6r_{25} V_1 - 12B_r k R^2 r_{12} \delta^2 - 12G_r k R^2 r_{12} \delta^2 + 4B_r \\ & k R^2 r_{15} \delta^2 + 4G_r k R^2 r_{15} \delta^2 - 12k \frac{\partial P}{\partial Z} R^2 r_{15} \delta^2 - 12R^2 r_{12} V_1 \delta^2 - 8R^2 r_{15} V_1 \\ & \delta^2 - \frac{1}{4(r_2 - \delta)} (16B_r k r_{13} + 16G_r k r_{13} - 16k \frac{\partial P}{\partial Z} r_{13} - 16B_r k r_{17} - 16G_r k r_{17} \\ & + 16k \frac{\partial P}{\partial Z} r_{17} + 16k \frac{\partial P}{\partial Z} r_{14} r_2 - 16k \frac{\partial P}{\partial Z} r_{18} r_2 - 24B_r k r_2^2 r_{20} - 24G_r k r_2^2 r_{20} + \\ & 24B_r k r_2 r_{21} + 24G_r k r_2 r_{21} + 24B_r k r_2 r_{30} + 24G_r k r_2 r_{30} - 24B_r k r_2^2 r_{31} \\ & - 24G_r k r_2^2 r_{31} + 16r_{14} r_2 V_1 - 16r_{18} r_2 V_1 - 24r_2^2 r_{20} V_1 + 24r_2 r_{21} V_1 + \\ & 24r_2 r_{30} V_1 - 24r_2^2 r_{31} V_1 + 48B_r k r_{12} r_2^2 \delta^3 + 48G_r k r_{12} r_2^2 \delta^3 - 48B_r k r_{15} \\ & r_2^2 \delta^3 - 48G_r k r_{15} r_2^2 \delta^3 + 48k \frac{\partial P}{\partial Z} r_{15} r_2^2 \delta^3 + 48B_r k r_{16} r_2^2 \delta^3 + 48G_r k r_{16} r_2^2 \\ & \delta^3 - 48k \frac{\partial P}{\partial Z} r_{16} r_2^2 \delta^3 + 48r_{12} r_2^2 V_1 \delta^3 - 48B_r k r_{12} r_2 \delta^4 - 48G_r k r_{12} r_2 \delta^4 - \\ & 48k \frac{\partial P}{\partial Z} r_{15} r_2 \delta^4 + 48k \frac{\partial P}{\partial Z} r_{16} r_2 \delta^4 - 48r_{12} r_2 V_1 \delta^4 - 48r_{15} r_2 V_1 \delta^4 + 48r_{16} \\ & r_2 V_1 \delta^4) - 4B_r k r_{11} \ln R - 4G_r k r_{11} \ln R - 4r_{11} V_1 \ln R + 8B_r k R^2 r_{12} \delta^2 \ln R \\ & + 8G_r k R^2 r_{12} \delta^2 \ln R + 8R^2 r_{12} V_1 \delta^2 \ln R + \frac{1}{4(r_2 - \delta)} R r_{29} (16k \frac{\partial P}{\partial Z} r_{21} + 16 \\ & B_r k r_2^2 r_{26} + 16G_r k r_2^2 r_{26} - 16k \frac{\partial P}{\partial Z} r_2^2 r_{26} + 24B_r k r_{27} + 24G_r k r_{27} - 24 \\ & B_r k r_2^2 r_{28} - 24G_r k r_2^2 r_{28} + 16k \frac{\partial P}{\partial Z} r_{30} + 16B_r k r_2^2 r_{32} + 16G_r k r_2^2 r_{32} - \\ & 16k \frac{\partial P}{\partial Z} r_2^2 r_{32} - 24B_r k r_{33} - 24G_r k r_{33} + 16r_{21} V_1 + 24r_{27} V_1 - 24r_2^2 r_{28} \\ & V_1 + 16r_{30} V_1 - 24r_{33} V_1 - 32B_r k r_{12} r_2^2 \delta^2 - 32G_r k r_{12} r_2^2 \delta^2 - 32r_{12} V_1 \\ & \delta^4 + 24B_r k r_2^2 \delta^2 \ln r_1 + 24G_r k r_2^2 \delta^2 \ln r_1 + 32k \frac{\partial P}{\partial Z} r_{12} r_2^2 \delta^2 + 24r_2^2 \\ & V_1 \delta^2 \ln r_1) - 8B_r k r_{11} \ln r_2 - 8G_r k r_{11} \ln r_2 + 12k \frac{\partial P}{\partial Z} r_{11} \ln r_2 + 4r_{11} V_1 \ln r_2) \end{aligned} \quad (7.22)$$

$$\bar{\theta} = \frac{\ln(r_1/R)}{\ln(r_1/r_2)} - \left( \ln \frac{R}{r_2} \ln \frac{R}{r_1} \left( (N_b + N_t) \epsilon^2 (\ln R)^2 + (4 - 3N_b - 3N_t) \epsilon^2 \ln R \ln r_2 + \right. \right. \\ \left. \left. 12(N_b + N_t) \delta^2 (\ln r_2)^2 + (9N_b + 9N_t - 8 - 4 \ln R) \epsilon^2 (\ln r_2)^2 + 8\epsilon^2 (\ln r_2)^3 + 4 \right. \right. \\ \left. \left. \delta \epsilon \cos \theta \left( \ln \frac{r_2}{r_1} \right)^2 (6N_b + 6N_t - \ln(R) + 2 \ln r_2 - \ln r_1) - 4\epsilon^2 \ln R \ln(\delta + \epsilon \cos \theta) \right. \right. \\ \left. \left. + (N_b + N_t) \epsilon^2 \ln R \ln r_1 - 24(N_b + N_t) \delta^2 \ln r_2 \ln r_1 + (12 - 15N_b - 15N_t) \epsilon^2 \ln r_2 \right. \right. \\ \left. \left. \ln r_1 + (8 \ln R - 20 \ln r_2) \epsilon^2 \ln R \ln r_2 \ln r_1 + 12(N_b + N_t) \delta^2 (\ln r_1)^2 + (7N_b + \right. \right. \\ \left. \left. 7N_t - 4) \epsilon^2 (\ln r_1)^2 + (16 \ln r_2 - 4 \ln R r_1) \epsilon^2 (\ln r_1)^2 \epsilon^2 \cos 2\theta ((N_b + N_t) \right. \right. \\ \left. \left. (\ln R)^2 - (8 + 3N_b + 3N_t) (\ln r_2)^2 + 3(4 + 3N_b + 3N_t) \ln r_2 \ln r_1 - (4 + \right. \right. \\ \left. \left. 5N_b + 5N_t) (\ln r_1)^2 + \ln R((4 - 3N_b - 3N_t) \ln r_2 + (-4 + N_b + N_t) \times \right. \right. \\ \left. \left. \ln r_1) \right) \right) / \left( 24(r_1)^2 \left( \ln \left( \frac{r_2}{r_1} \right) \right)^4 \right) \quad (7.23)$$

$$\sigma = \frac{1}{6N_b r_1^2 (\ln r_2 - \ln r_1)^3} \left( (N_b + N_t) \epsilon (\ln R - \ln r_2) (\epsilon (\cos 2\theta - 1) + (\epsilon + \delta \cos \theta)) \right. \\ \left. (\ln r_2 - \ln r_1) (\ln R - \ln r_1) (\ln R - 2 \ln r_2 + \ln r_1) + \frac{\ln(r_1/R)}{\ln(r_1/r_2)} \right) \quad (7.24)$$

Now we can evaluate pressure gradient  $\partial P/\partial Z$  by solving Eqs. (2.38) and (2.39) and is elaborated as

$$\frac{\partial P}{\partial Z} = \left( -24B_r k \pi r_1^3 r_{12} - 24G_r k \pi r_1^3 r_{12} + 21B_r k \pi r_1^4 r_{12} + 21G_r k \pi r_1^4 r_{12} - 96kQ \right. \\ \left. r_{15} + 12B_r k \pi r_1^4 r_{15} + 12G_r k \pi r_1^4 r_{15} - 12B_r k \pi r_1^4 r_{16} - 12G_r k \pi r_1^4 r_{16} + 36B_r k \pi r_1^2 \right. \\ \left. r_{12} r_2 + 36G_r k \pi r_1^2 r_{12} r_2 - 21B_r k \pi r_1^4 r_{12} r_2 - 21G_r k \pi r_1^4 r_{12} r_2 + 96kQ r_{15} r_2 - \right. \\ \left. 12B_r k \pi r_1^4 r_{15} r_2 - 12G_r k \pi r_1^4 r_{15} r_2 + 12B_r k \pi r_1^4 r_{16} r_2 + 12G_r k \pi r_1^4 r_{16} r_2 - 36B_r \right. \\ \left. k \pi r_1^2 r_{12} r_2^2 - 36G_r k \pi r_1^2 r_{12} r_2^2 + 24B_r k \pi r_1^3 r_{12} r_2^2 + 24G_r k \pi r_1^3 r_{12} r_2^2 + 24B_r k \pi r_1^2 \right. \\ \left. r_{15} r_2^2 + 24G_r k \pi r_1^2 r_{15} r_2^2 - 16B_r k \pi r_1^3 r_{15} r_2^2 - 16G_r k \pi r_1^3 r_{15} r_2^2 - 12B_r k \pi r_{12} r_2^3 \right. \\ \left. - 12G_r k \pi r_{12} r_2^3 + 15B_r k \pi r_{12} r_2^4 + 15G_r k \pi r_{12} r_2^4 - 12B_r k \pi r_{15} r_2^4 - 12G_r k \pi r_{15} r_2^4 \right. \\ \left. - 3B_r k \pi r_{12} r_2^5 - 3G_r k \pi r_{12} r_2^5 + 4B_r k \pi r_{15} r_2^5 + 4G_r k \pi r_{15} r_2^5 - 12k \pi r_1^2 r_{34} + 12k \pi \right. \\ \left. r_1^2 r_2 r_{34} + 12k \pi r_2^2 r_{34} - 12k \pi r_2^3 r_{34} + 24k \pi r_1^2 r_{35} - 24k \pi r_1^2 r_2 r_{35} + 24B_r k \pi r_{36} \right. \\ \left. + 24G_r k \pi r_{36} - 24B_r k \pi r_2^2 r_{36} - 24G_r k \pi r_2^2 r_{36} + 24k \pi r_1^2 r_{37} - 24k \pi r_1^2 r_2 r_{37} \right. \\ \left. - 36B_r k \pi r_1^2 r_{38} - 36G_r k \pi r_1^2 r_{38} + 21B_r k \pi r_1^4 r_{38} + 21G_r k \pi r_1^4 r_{38} + 12k \pi r_1^2 r_{39} \right. \\ \left. - 12k \pi r_1^2 r_2 r_{39} - 12k \pi r_2^2 r_{39} + 12k \pi r_2^3 r_{39} - 21B_r k \pi r_{40} - 21G_r k \pi r_{40} + 36B_r \right. \\ \left. k \pi r_1^2 r_{41} + 36G_r k \pi r_1^2 r_{41} + 12B_r k \pi r_{42} + 12G_r k \pi r_{42} - 15B_r k \pi r_{43} - 15G_r k \pi \right. \\ \left. r_{43} + 3B_r k \pi r_{44} + 3G_r k \pi r_{44} - 96kQ r_{46} - 24B_r k \pi r_1^2 r_{47} - 24G_r k \pi r_1^2 r_{47} \right) \quad (7.25)$$

$$\begin{aligned}
& +16B_r k \pi r_1^3 r_{47} + 16G_r k \pi r_1^3 r_{47} + 12B_r k \pi r_{48} + 12G_r k \pi r_{48} - 4B_r k \pi r_{49} \\
& - 4G_r k \pi r_{49} - 72k \pi r_1^2 r_{50} + 16\pi r_1^3 r_{50} + 16k \pi r_1^3 r_{50} - 12\pi r_1^4 r_{50} + 8\pi r_2^3 r_{50} \\
& + 8k \pi r_2^3 r_{50} - 48k \pi r_1^2 r_{12} V_1 - 24\pi r_1^3 r_{12} V_1 + 32k \pi r_1^3 r_{12} V_1 + 21\pi r_1^4 r_{12} V_1 + \\
& 120k \pi r_1^2 r_{15} V_1 - 16\pi r_1^3 r_{15} V_1 - 16k \pi r_1^3 r_{15} V_1 + 24\pi r_1^4 r_{15} V_1 - 72k \pi r_1^2 r_{16} V_1 \\
& - 12\pi r_1^4 r_{16} V_1 + 36\pi r_1^2 r_{12} r_2 V_1 - 21\pi r_1^4 r_{12} r_2 V_1 + 24\pi r_1^2 r_{15} r_2 V_1 - 96k \pi r_1^2 r_{15} r_2 \\
& V_1 - 24\pi r_1^4 r_{15} r_2 V_1 + 72k \pi r_1^2 r_{16} r_2 V_1 + 12\pi r_1^4 r_{16} r_2 V_1 - 36\pi r_1^2 r_{12} r_2^2 V_1 + \\
& 24\pi r_1^3 r_{12} r_2^2 V_1 - 12\pi r_{12} r_2^3 V_1 + 16k \pi r_{12} r_2^3 V_1 - 8\pi r_{15} r_2^3 V_1 - 8k \pi r_{15} r_2^3 V_1 \\
& + 15\pi r_{12} r_2^4 V_1 - 3\pi r_{12} r_2^5 V_1 + 24\pi r_{36} V_1 - 32k \pi r_{36} V_1 - 24\pi r_2^2 r_{36} V_1 - 36 \\
& \pi r_1^2 r_{38} V_1 + 48k \pi r_1^2 r_{38} + 21\pi r_1^4 r_{38} V_1 - 21\pi r_{40} V_1 + 24k \pi r_{41} V_1 + 36\pi r_1^2 \\
& r_{41} V_1 + 12\pi r_{42} V_1 - 40k \pi r_{42} V_1 - 15\pi r_{43} V_1 + 3\pi r_{44} V_1 - 24\pi r_1^2 r_{46} V_1 + \\
& 48k \pi r_1^2 r_{46} V_1 + 12\pi r_1^4 r_{46} V_1 + 192k \pi (r_2 - 1) r_{45} \phi \cos 2\pi(z - t) + 48k \pi \\
& (r_2 - 1) r_{45} \phi^2 \cos 4\pi(z - t) + 96k Q (\ln r_2)^3 / (4k \pi (r_1 - r_2)^2 (-1 + r_2) \\
& (3r_1^2 + 2r_1(-2 + r_2) + (-2 + r_2)r_2) \ln \frac{r_1}{r_2} (\ln r_2)^2)
\end{aligned} \tag{7.25}$$

The parameters used in above expression are defined as

$$\begin{aligned}
& r_{11} = R^2 \delta^2 (\ln r_1)^2, r_{12} = \ln r_1 r_2, r_{13} = r_2^2 \delta^3 (\ln r_2)^3, r_{14} = \delta^4 (\ln r_2)^3, \\
& r_{15} = \ln r_1 (\ln r_2)^2, r_{16} = (\ln r_1)^2 \ln r_2, r_{17} = r_2^2 \delta^3 (\ln r_1)^3, r_{18} = \delta^4 (\ln r_1)^3, \\
& r_{19} = \delta^3 (\ln r_1)^3, r_{20} = \delta^3 (\ln r_2)^2, r_{21} = \delta^4 (\ln r_2)^2, r_{22} = R^2 \delta^2 (\ln r_1)^3, \\
& r_{23} = \delta^2 (\ln r_2)^3, r_{24} = \delta^2 \ln R (\ln r_2)^2, r_{25} = R^2 \delta^2 (\ln r_2)^2, r_{26} = \delta^2 (\ln r_2)^2, \\
& r_{27} = \delta^4 \ln r_2, r_{28} = \delta^2 \ln r_2, r_{29} = \ln \left( \frac{r_2}{r_1} \right), r_{30} = \delta^4 (\ln r_1)^2, r_{31} = \delta^3 (\ln r_1)^2, \\
& r_{32} = \delta^2 (\ln r_1)^2, r_{33} = \delta^4 \ln r_1, r_{34} = V_1 \ln r_1, r_{35} = V_1 (\ln r_1)^2, \\
& r_{36} = r_1^3 (\ln r_2)^2, r_{37} = V_1 (\ln r_1)^3, r_{38} = r_2 (\ln r_2)^2, r_{39} = V_1 \ln r_2, \\
& r_{40} = r_1^4 (\ln r_2)^2, r_{41} = r_2^2 (\ln r_2)^2, r_{42} = r_2^3 (\ln r_2)^2, r_{43} = r_2^4 (\ln r_2)^2, \\
& r_{44} = r_2^5 (\ln r_2)^2, r_{45} = \left( \ln \frac{r_1}{r_2} \right) (\ln r_2)^2, r_{46} = r_2 (\ln r_2)^3, r_{47} = r_2^2 (\ln r_2)^3, \\
& r_{48} = r_2^4 (\ln r_2)^3, r_{49} = r_2^5 (\ln r_2)^3, r_{50} = V_1 (\ln r_2)^3
\end{aligned} \tag{7.26}$$

The pressure rise  $\Delta P$  in non-dimensional form is defined in Eq. (2.41) and is found by numerical integration with the help of a mathematical software *Mathematica*.



### 7.3 Graphical results and discussion

To establish the nanofluid characteristics through a porous space, we analyzed the unsteady and incompressible peristaltic flow of nano fluid between two eccentric tubes having different radii enclosing the porous medium. Analytical solutions are carried out with the help of homotopy perturbation technique. The expression for pressure rise is evaluated numerically to examine peristaltic pumping whose variation can be observed from given Table 7.1. All the parameters in the problem are made dimensionless by suitable transformations. This section discussed the physical behavior of all the pertinent parameters on the distributions of velocity, temperature and nano particles concentration. Figs. 7.1 to 7.4 represents the pressure rise variation for various emerging parameters. The pressure gradient profiles are displayed in Figs. 7.5 to 7.8. The effects of various physical quantities on the profiles of velocity, temperature and nano particles phenomenon is discussed through Figs. 7.9 to 7.15. Trapping bolus behavior of the intestinal flow is described through streamlines sketched in Figs. 7.16 to 7.18.

Fig. 7.1 indicates that pressure rise  $\Delta P$  is decreasing with local temperature Grashof number  $G_r$  while it increases for the amplitude ratio  $\phi$  in the retrograde pumping ( $\Delta P > 0, Q < 0$ ) and gives reverse variation in the peristaltic pumping ( $\Delta P > 0, Q > 0$ ) and augmented pumping ( $\Delta P < 0, Q > 0$ ) regions. One can observe from Fig. 7.2 that pressure rise is increasing with the increase in local nano particle Grashof number  $B_r$  and peristaltic pumping occurs in the region  $Q \in [0, 0.5)$ . From Fig. 7.3, it can be noticed that peristaltic pumping rate is directly varying with the porosity parameter  $k$ . Fig. 7.4 suggests that pumping rate is inversely proportional to the radius  $\delta$ .

Fig. 7.5 reveals the pressure gradient variation  $\partial P/\partial Z$  for the porosity parameter  $k$  and flow rate  $Q$ . It can be seen that pressure gradient is increasing with the increase in the magnitude of  $k$  but opposite relation is observed with the flow rate  $Q$ . It is also noted here that pressure gradient curves are varying uniformly with both the porosity of the space and the flow rate. From Fig. 7.6, we found that there is inverse change in pressure profile with local nano particle Grashof number  $B_r$  and local temperature Grashof number  $G_r$ . Fig. 7.7 implies that increase in the velocity  $V_1$  results in decreasing the pressure gradient curves while there is a direct relation between the distance parameter  $\epsilon$  and the change in pressure  $\partial P/\partial Z$ . One can explain the variation of pressure gradient  $\partial P/\partial Z$  for the amplitude ratio  $\phi$  and the radius  $\delta$  from Fig.

7.8. It is very obvious from this figure that pressure gradient is decreasing with the radius  $\delta$  throughout the flow domain but have opposite behavior with the amplitude ratio in the regions  $Z \in [0, 0.3) \cup (0.8, 1]$ .

The profile of velocity  $U$  for the parameters  $k$  and  $Q$  can be analyzed from Fig. 7.9. It can be observed here that velocity profile is diminished with the increase in porosity parameter  $k$  but it rises up with the flow rate  $Q$ . It can be predicted from Fig. 7.10 that velocity is changing directly with the increase in local nano particle Grashof number  $B_r$ , and local temperature Grashof number  $G_r$ , and also it remains uniform throughout the flow. Fig. 7.11 denotes that axial velocity distribution  $U$  is increasing with the increase in constant velocity  $V_1$  of the inner annulus but for distance parameter  $\epsilon$ , it gives same behavior in the domain  $R \in (0.6, 1.1)$  and reverse variation in the remaining part.

The variation of temperature distribution  $\theta$  against the amplitude ratio  $\phi$  and distance  $\epsilon$  is displayed in Fig. 7.12. It is depicted here that temperature curves are getting lower with  $\epsilon$  and  $\phi$ . Fig. 7.13 concludes that temperature profile is rising up with the increase in Brownian motion parameter  $N_b$  and thermophoresis parameter  $N_t$ . It can be declared from Fig. 7.14 that concentration of the nanoparticles gets the same variation with  $\epsilon$  and  $\phi$  as that of observed in the case of temperature profile. Fig. 7.15 discloses that nanoparticles concentration is increasing with thermophoresis parameter  $N_t$  but decreases with Brownian motion parameter  $N_b$ .

Trapping bolus phenomenon for local nano particle Grashof number  $B_r$  can be discussed through Fig. 7.16. It is illustrated here that circulating boluses are reduced in the sense of numbers but expanded in size with the increase in  $B_r$ . The variation of trapping boluses with the local temperature Grashof number  $G_r$  is visualized in Fig. 7.17 and it is measured from this graph that the behavior of boluses is similar as that experienced in the previous figure. However, the influence of porous space on the variation of trapping bolus phenomenon can be examined through Fig. 7.18 and it is derived that number of boluses is increasing with the increase in numerical values of porosity parameter  $k$  while boluses are contracted in dimensions

which indicates that more the medium is porous the bolus reduces its volume to pass through.

$Q$	$\Delta P$ for $k = 0.5, \phi = 0.1$	$\Delta P$ for $k = 1, \phi = 0.1$	$\Delta P$ for $k \rightarrow \infty, \phi = 0.1$
-1.0	0.527163	0.797414	1.067660
-0.9	0.450834	0.721085	0.991332
-0.8	0.374505	0.644755	0.915003
-0.7	0.298175	0.568426	0.838674
-0.6	0.221846	0.492096	0.762344
-0.5	0.145516	0.415767	0.686015
-0.4	0.069187	0.339438	0.609685
-0.3	-0.00714	0.263108	0.533356
-0.2	-0.08347	0.186779	0.457027
-0.1	-0.15980	0.110450	0.380697
0.0	-0.23613	0.034120	0.304368
0.1	-0.31246	-0.04220	0.228039
0.2	-0.38878	-0.11853	0.151709
0.3	-0.46511	-0.19486	0.075379
0.4	-0.54144	-0.27119	-0.00094
0.5	-0.61777	-0.34752	-0.07727
0.6	-0.69410	-0.42385	-0.15360
0.7	-0.77043	-0.50018	-0.22993
0.8	-0.84676	-0.57651	-0.30626
0.9	-0.92309	-0.65284	-0.38259
1.0	-0.99942	-0.72917	-0.45892

Table 7.1: Variation of pressure rise  $\Delta P$  for fixed values of  $\theta = 0.8$ ,  $\delta = 0.1$ ,  $B_r = 0.2$ ,  $G_r = 0.1$ ,  $t = 0.3$ ,  $N_b = 0.5$ ,  $N_t = 0.2$ ,  $\epsilon = 0.1$ ,  $V_1 = 0.3$ .

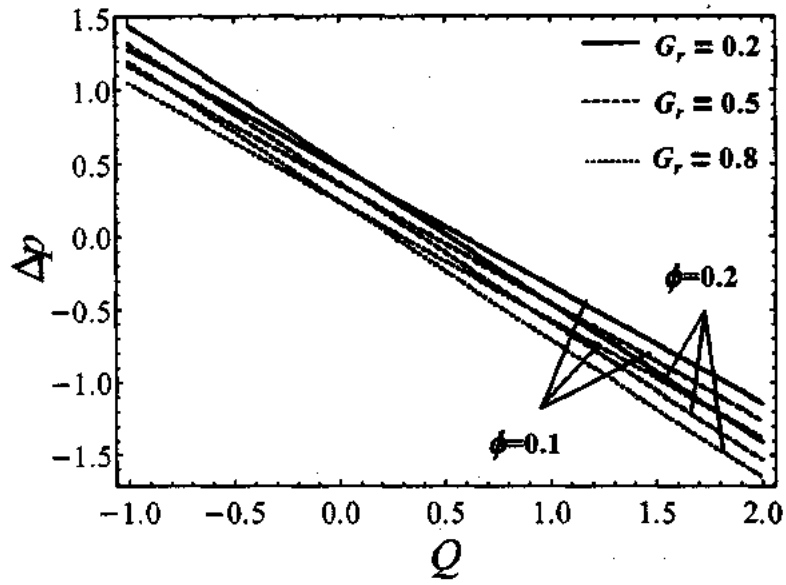


Fig. 7.1: Variation of pressure rise  $\Delta P$  with  $\phi$  and  $G_r$  for fixed values of  $\theta = 0.8$ ,  $\delta = 0.1$ ,  $B_r = 0.1$ ,  $k = 0.5$ ,  $t = 0.3$ ,  $N_b = 0.5$ ,  $N_t = 0.2$ ,  $\epsilon = 0.3$ ,  $V_1 = 0.1$ .

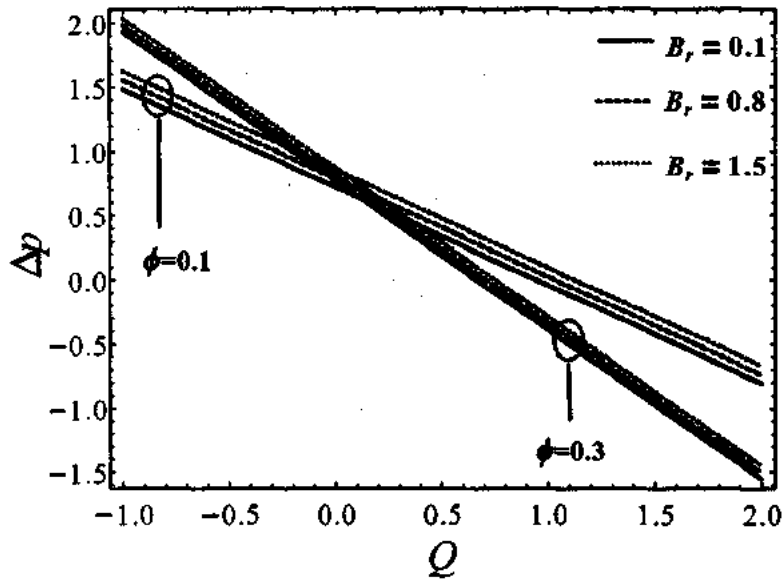


Fig. 7.2: Variation of pressure rise  $\Delta P$  with  $\phi$  and  $B_r$  for fixed values of  $\theta = 0.8$ ,  $\delta = 0.1$ ,  $G_r = 1$ ,  $N_b = 0.1$ ,  $k = 0.5$ ,  $t = 0.3$ ,  $N_t = 0.5$ ,  $\epsilon = 0.3$ ,  $V_1 = 0.1$ .

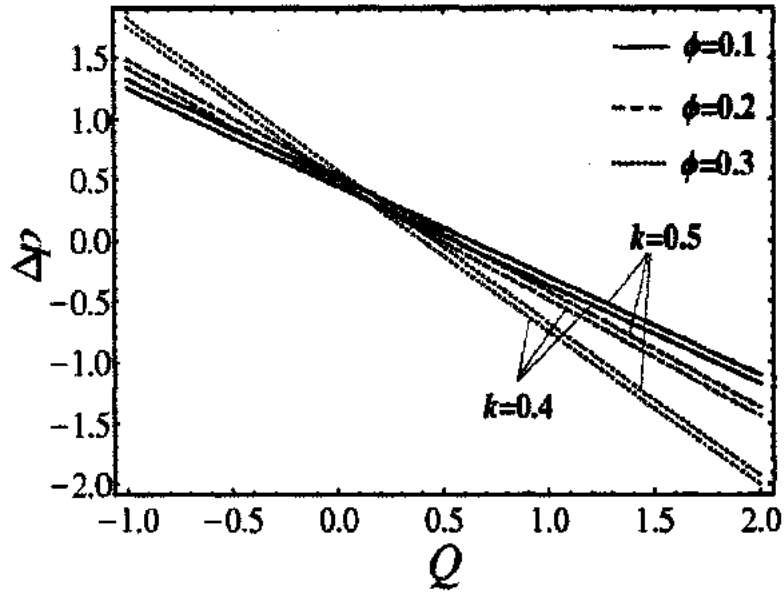


Fig. 7.3: Variation of pressure rise  $\Delta P$  with  $\phi$  and  $k$  for fixed values of  $\theta = 0.8$ ,  $\delta = 0.1$ ,  $G_r = 0.1$ ,  $N_b = 0.1$ ,  $B_r = 0.1$ ,  $t = 0.3$ ,  $N_t = 0.5$ ,  $\epsilon = 0.3$ ,  $V_1 = 0.1$ .

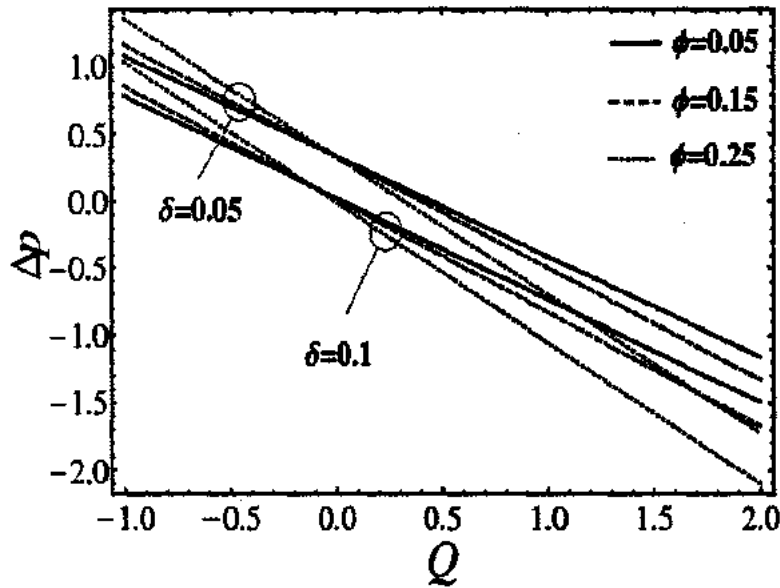


Fig. 7.4: Variation of pressure rise  $\Delta P$  with  $\phi$  and  $\delta$  for fixed values of  $\theta = 0.8$ ,  $B_r = 0.1$ ,  $G_r = 2$ ,  $N_b = 0.1$ ,  $k = 0.5$ ,  $t = 0.3$ ,  $N_t = 0.5$ ,  $\epsilon = 0.3$ ,  $V_1 = 0.2$ .

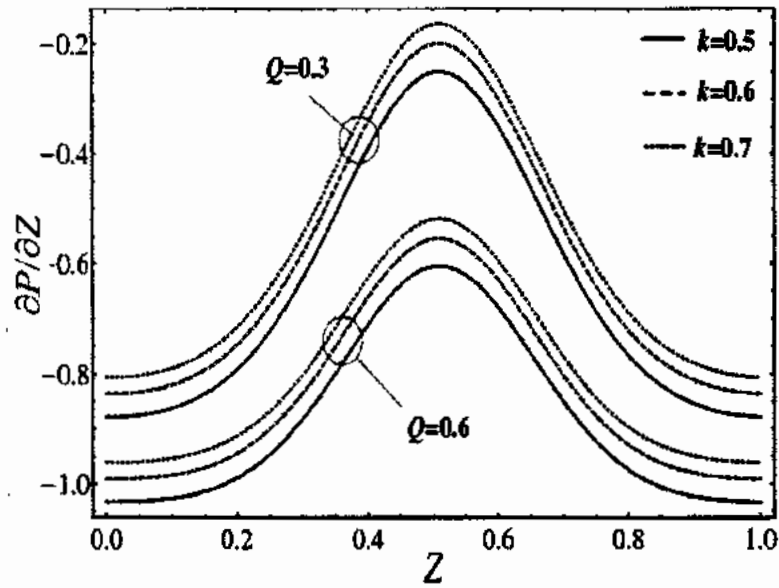


Fig. 7.5: Variation of pressure gradient  $\partial P/\partial Z$  with  $k$  and  $Q$  for fixed values of  $\epsilon = 0.3$ ,  $t = 0.01$ ,  $B_r = 0.3$ ,  $\delta = 0.1$ ,  $V_1 = 0.1$ ,  $\theta = 0.8$ ,  $\phi = 0.1$ ,  $G_r = 0.5$ ,  $N_b = 0.1$ ,  $N_t = 0.5$ .

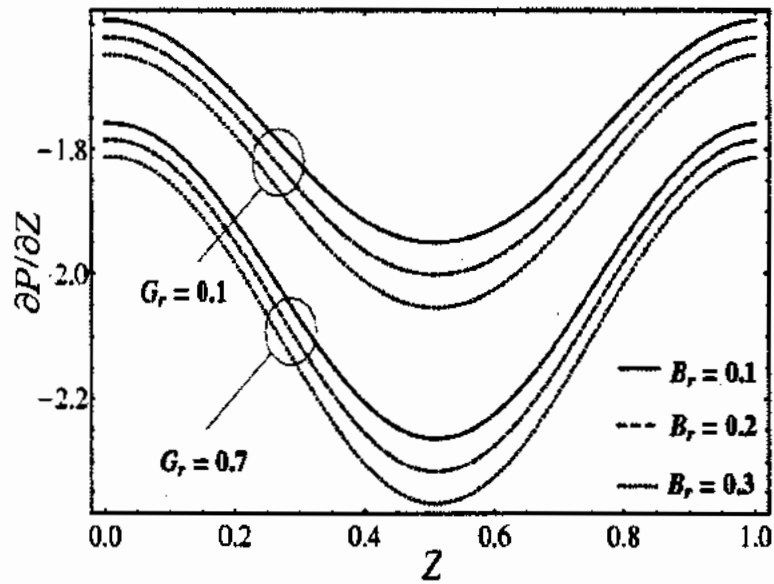


Fig. 7.6: Variation of pressure gradient  $\partial P/\partial Z$  with  $B_r$  and  $G_r$  for fixed values of  $\epsilon = 0.3$ ,  $t = 0.01$ ,  $k = 0.5$ ,  $\delta = 0.1$ ,  $V_1 = 0.1$ ,  $\theta = 0.8$ ,  $\phi = 0.1$ ,  $Q = 2$ ,  $N_b = 0.1$ ,  $N_t = 0.5$ .

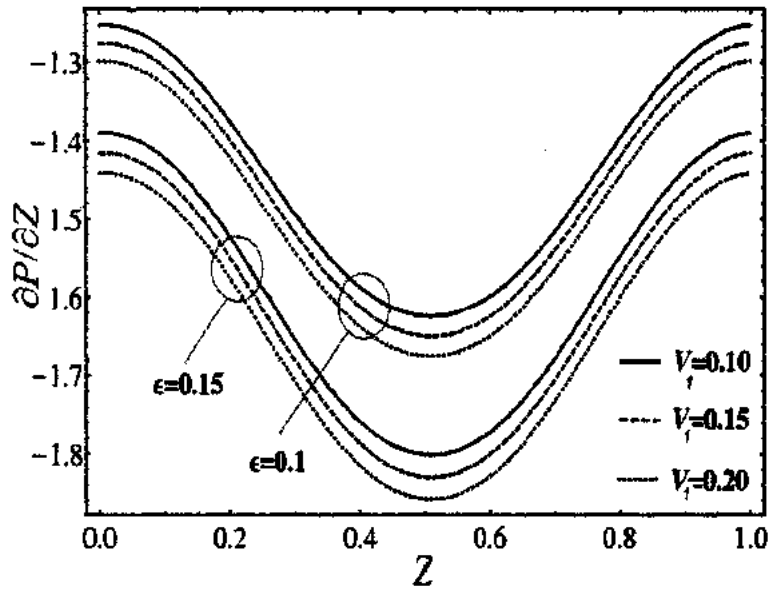


Fig. 7.7: Variation of pressure gradient  $\partial P/\partial Z$  with  $\epsilon$  and  $V_1$  for fixed values of  $k = 0.5$ ,  $t = 0.01$ ,  $B_r = 0.1$ ,  $\delta = 0.1$ ,  $Q = 2$ ,  $\theta = 0.8$ ,  $\phi = 0.1$ ,  $G_r = 1$ ,  $N_b = 0.1$ ,  $N_t = 0.5$ .

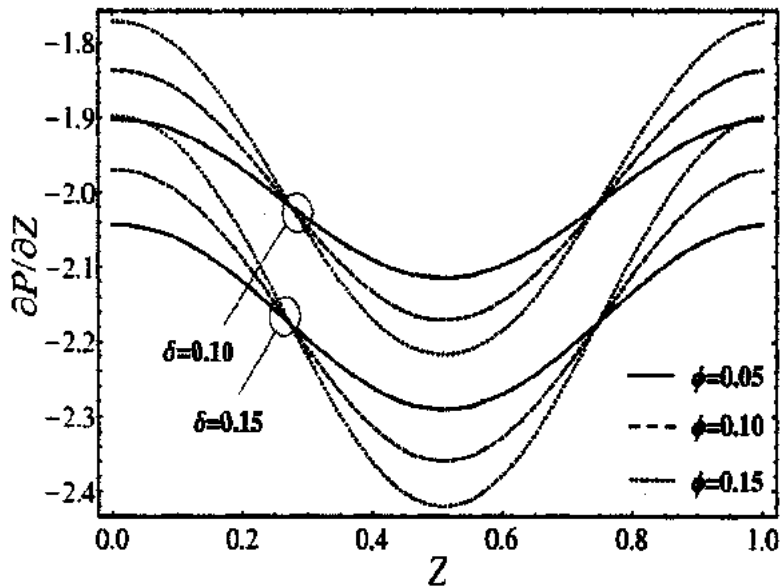


Fig. 7.8: Variation of pressure gradient  $\partial P/\partial Z$  with  $\phi$  and  $\delta$  for fixed values of  $\epsilon = 0.3$ ,  $t = 0.01$ ,  $B_r = 0.1$ ,  $Q = 2$ ,  $V_1 = 0.2$ ,  $\theta = 0.8$ ,  $k = 0.5$ ,  $G_r = 0.2$ ,  $N_b = 0.1$ ,  $N_t = 0.5$ .

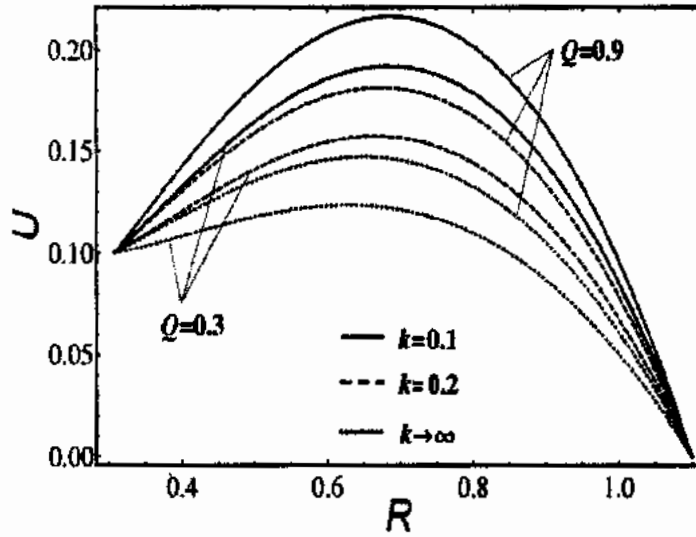


Fig. 7.9: Variation of velocity profile  $U$  with  $k$  and  $Q$  for fixed values of  $\epsilon = 0.3$ ,  $N_t = 0.5$ ,  $N_b = 0.1$ ,  $t = 0.3$ ,  $\delta = 0.1$ ,  $B_r = 0.3$ ,  $G_r = 1$ ,  $Z = 0$ ,  $V_1 = 0.1$ ,  $\theta = 0.8$ ,  $\phi = 0.1$ .

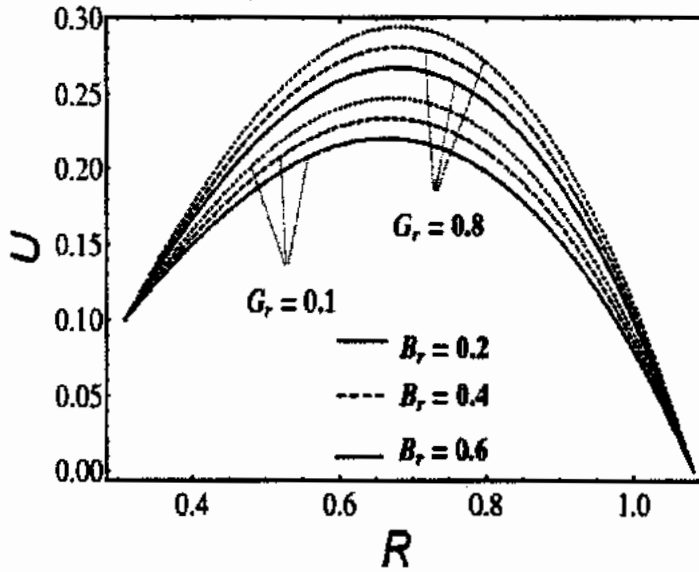


Fig. 7.10: Variation of velocity profile  $U$  with  $G_r$  and  $B_r$  for fixed values of  $\epsilon = 0.3$ ,  $N_t = 0.5$ ,  $N_b = 0.1$ ,  $t = 0.1$ ,  $\delta = 0.1$ ,  $k = 0.1$ ,  $Q = 2$ ,  $Z = 0$ ,  $V_1 = 0.1$ ,  $\theta = 0.8$ ,  $\phi = 0.1$ .



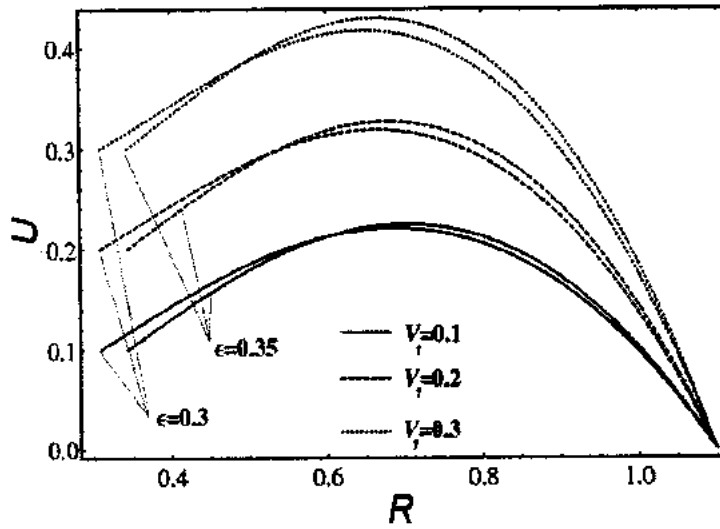


Fig. 7.11: Variation of velocity profile  $U$  with  $\epsilon$  and  $V_1$  for fixed values of  $G_r = 1$ ,  $N_t = 0.5$ ,  $N_b = 0.1$ ,  $t = 0.3$ ,  $\delta = 0.1$ ,  $k = 0.1$ ,  $Q = 1$ ,  $Z = 0$ ,  $B_r = 0.3$ ,  $\theta = 0.8$ ,  $\phi = 0.1$ .

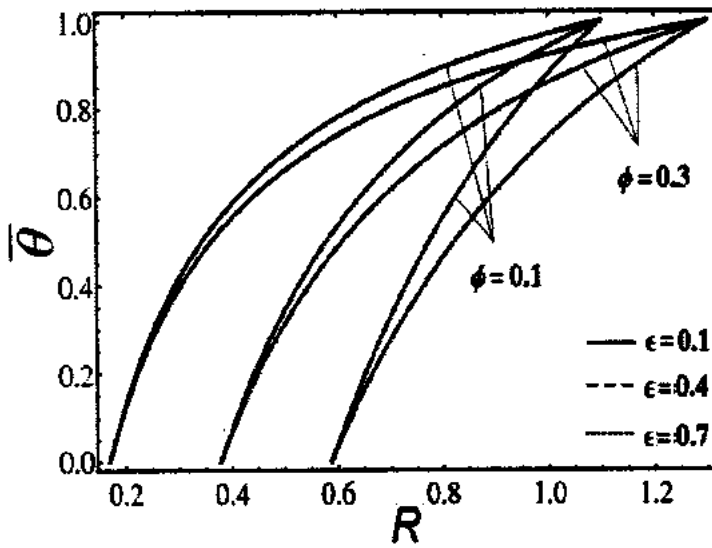


Fig. 7.12: Variation of temperature profile  $\bar{\theta}$  with  $\epsilon$  and  $\phi$  for fixed values of  $\delta = 0.1$ ,  $t = 0.3$ ,  $N_b = 0.4$ ,  $N_t = 0.2$ ,  $Z = 0$ ,  $\theta = 0.8$ ,  $k = 0.1$ .

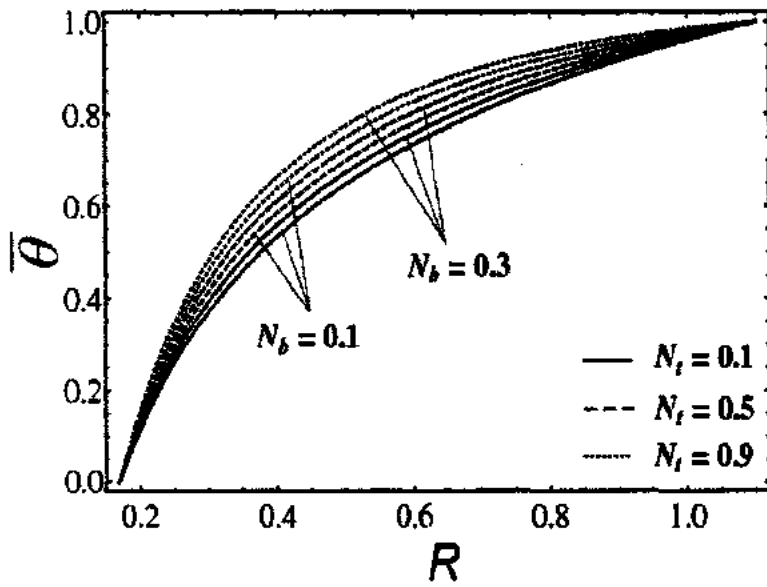


Fig. 7.13: Variation of temperature profile  $\bar{\theta}$  with  $N_b$  and  $N_t$  for fixed values of  $\delta = 0.1$ ,  $t = 0.3$ ,  $\epsilon = 0.1$ ,  $\phi = 0.1$ ,  $Z = 0$ ,  $\theta = 0.8$ ,  $k = 0.1$ .

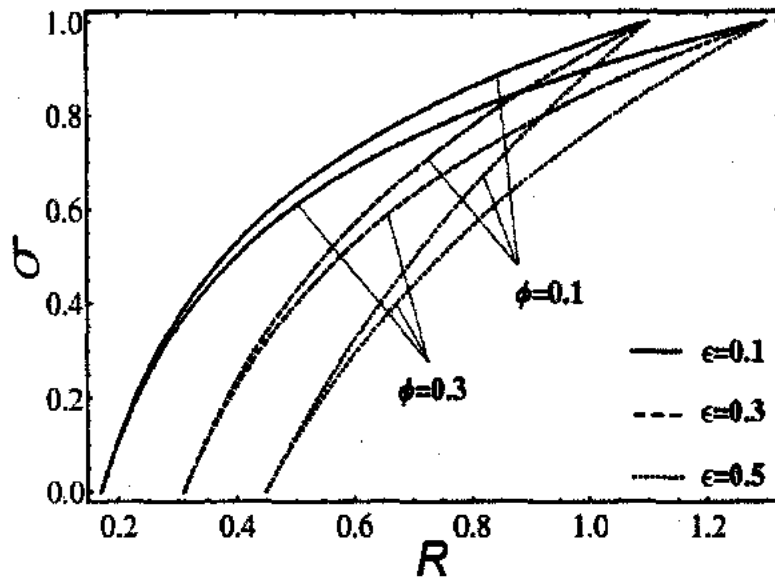


Fig. 7.14: Variation of nano particles concentration  $\sigma$  with  $\phi$  and  $\epsilon$  for fixed values of  $\delta = 0.1$ ,  $N_b = 0.4$ ,  $N_t = 0.2$ ,  $Z = 0$ ,  $\theta = 0.8$ ,  $t = 0.3$ ,  $k = 0.1$ .

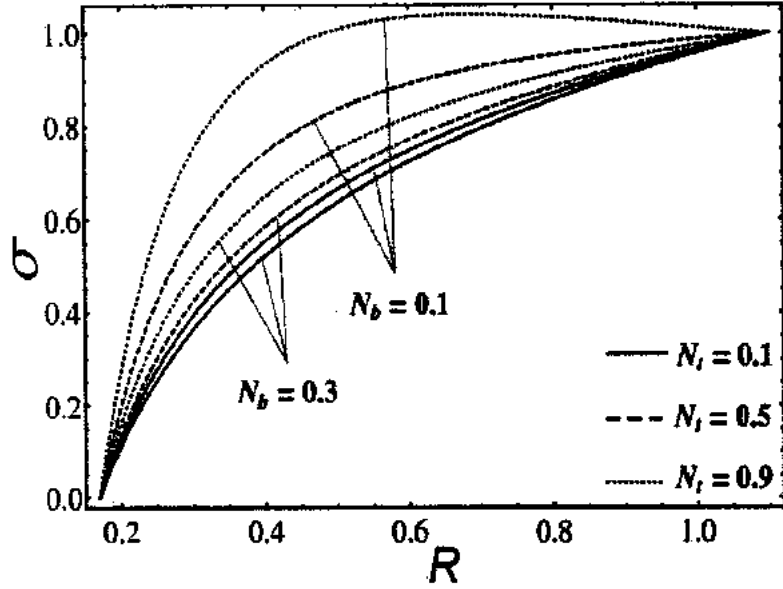


Fig. 7.15: Variation of nano particles concentration  $\sigma$  with  $N_b$  and  $N_t$  for fixed values of  $\delta = 0.1$ ,  $\epsilon = 0.1$ ,  $\phi = 0.1$ ,  $Z = 0$ ,  $\theta = 0.8$ ,  $t = 0.3$ ,  $k = 0.1$ .

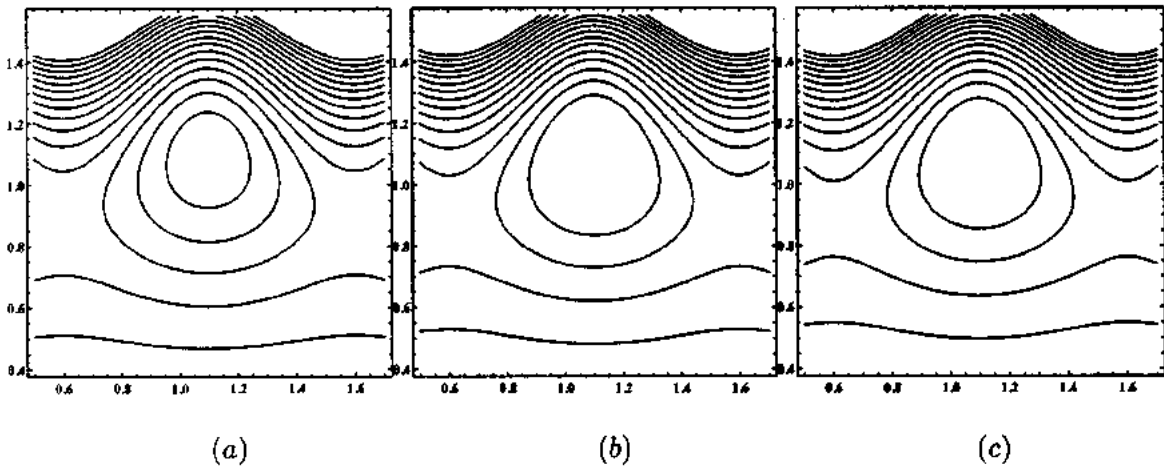


Fig. 7.16: Stream lines for different values of  $B_r$ , (a) for  $B_r = 0.3$ , (b) for  $B_r = 0.9$ , (c) for  $B_r = 2$ . The other parameters are  $\epsilon = 0.1$ ,  $V_1 = 0.1$ ,  $t = 0.1$ ,  $k = 0.3$ ,  $\theta = 0.8$ ,  $\phi = 0.1$ ,  $Q = 1$ ,  $\delta = 0.1$ ,  $N_t = 0.5$ ,  $N_b = 0.1$ ,  $G_r = 0.6$ .

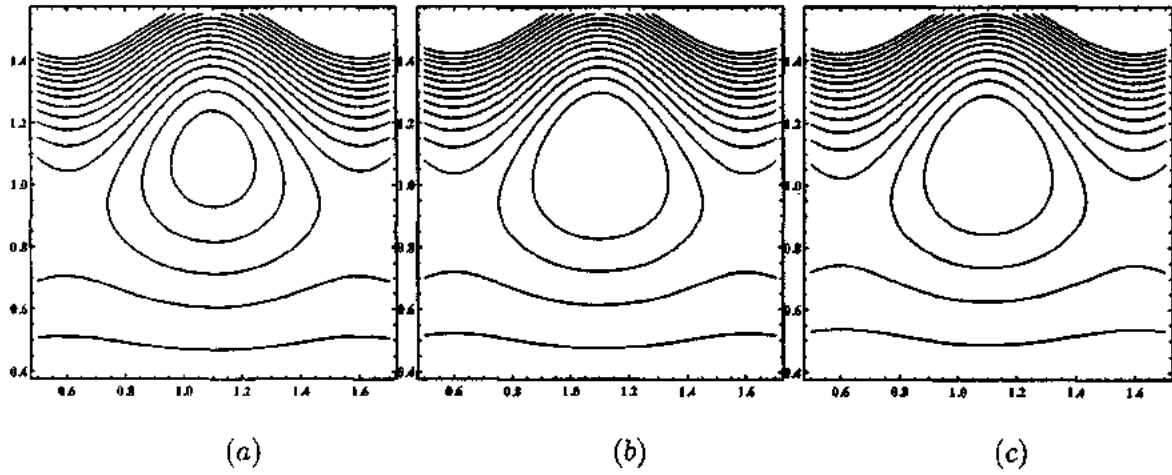


Fig. 7.17: Stream lines for different values of  $G_r$ , (a) for  $G_r = 0.6$ , (b) for  $G_r = 0.9$ , (c) for  $G_r = 1.5$ . The other parameters are  $\epsilon = 0.1$ ,  $V_1 = 0.1$ ,  $t = 0.1$ ,  $k = 0.3$ ,  $\theta = 0.8$ ,  $\phi = 0.1$ ,  $Q = 1$ ,  $\delta = 0.1$ ,  $N_t = 0.5$ ,  $N_b = 0.1$ ,  $Br = 0.3$ .

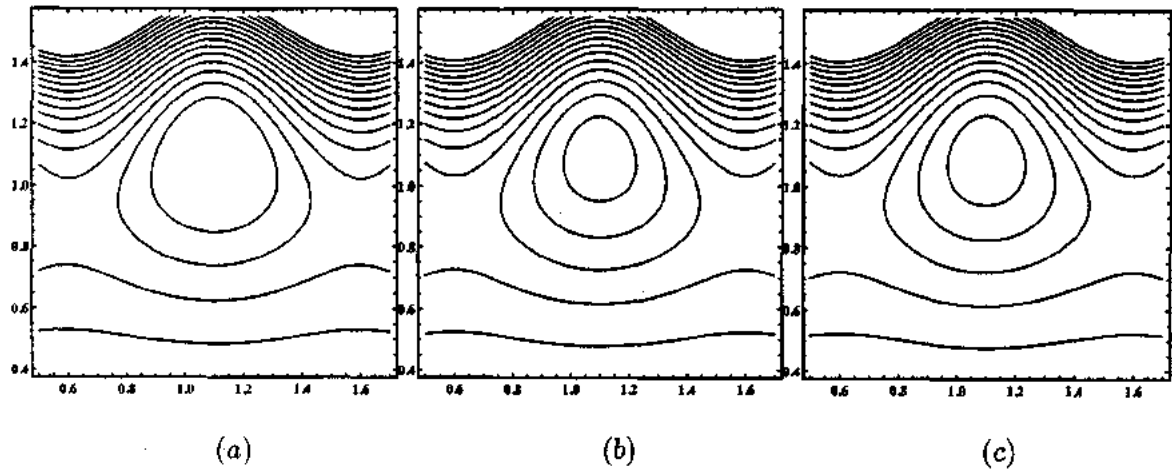


Fig. 7.18: Stream lines for different values of  $k$ , (a) for  $k = 0.1$ , (b) for  $k = 0.4$ , (c) for  $k = 0.9$ . The other parameters are  $\epsilon = 0.1$ ,  $V_1 = 0.1$ ,  $t = 0.1$ ,  $Br = 0.3$ ,  $\theta = 0.8$ ,  $\phi = 0.1$ ,  $Q = 1$ ,  $\delta = 0.1$ ,  $N_t = 0.5$ ,  $N_b = 0.1$ ,  $G_r = 1$ .

## Chapter 8

# Conclusions

This chapter is prepared to discuss the major findings of the whole study and arranged as follows:

### 8.1 Concluding remarks of chapter two

In chapter two, the series solutions for the peristaltic flow of Jeffrey fluid have been analyzed in between two eccentric tubes under the effects of MHD. The problem is formulated under the implementation of long wavelength and low Reynolds number. All the results are described graphically by observing the variation of various physical parameters. The main results evaluated from the above discussion are summarized as follow:

1. It is found that peristaltic pumping rate increases with  $\epsilon$ ,  $M$ ,  $\delta$ ,  $\phi$  and  $V_1$  but decreases with  $\theta$  and  $\lambda_1$ .
2. It is observed that pressure gradient profile is varying directly with  $M$ ,  $\delta$ ,  $\epsilon$ ,  $\phi$  and  $V_1$  while inversely proportional to  $\lambda_1$  in the centre of the channel, however, the behavior is quite opposite at the corners.
3. It is measured that velocity distribution is an increasing function of  $\delta$ ,  $\epsilon$ ,  $\phi$  and  $V_1$  but decreasing with  $M$ ,  $Q$  and  $t$  both for two and three dimensions.
4. It is seen that number of bolus is increasing but size is decreasing when someone varies the values of  $\lambda_1$  and inverse attitude is reported with the variation of  $M$ ,  $\phi$  and  $Q$ .

5. It is also observed that HPM and perturbation solutions [78] match closely with each other and presence of MHD results in suppressing the velocity profile.

## 8.2 Concluding remarks of chapter three

In chapter three, the peristaltic flow of Jeffrey fluid in a rectangular channel having compliant walls has been presented under the assumptions of long wavelength and low Reynolds number. The series solution is found with the help of eigen function expansion method. The graphs of all the results are presented and discussed for all pertinent parameters. Following main points from the graphical behavior are evaluated as:

1. It is seen that velocity profile is rising with  $E_3$  and  $E_4$ .
2. It is found that velocity profile is declining with  $\beta$ ,  $E_1$  and  $E_2$  both for two and three dimensions.
3. It is noted that size of the bolus is increasing on right half of the plane while decreasing on left side with the variation of  $\beta$ ,  $\phi$  and  $E_3$ .
4. It is observed that streamlines behavior is quite opposite for  $\lambda_1$ ,  $E_1$  and  $E_2$ .

## 8.3 Concluding remarks of chapter four

Chapter four gives an account of peristaltic flow in a duct for a Jeffrey fluid with partial slip effects. The equations are modeled and simplified using long wavelength and low Reynold's number approximations. The effects of various parameters on velocity  $u$ , pressure rise  $\Delta p$ , pressure gradient  $dp/dx$  and trapping are discussed through graphs. We have concluded the following observations:

1. The velocity field increases with the increase in  $\lambda_1$  and  $Q$  and decreases with the increase in  $\beta$ ,  $\beta_1$  and  $\phi$ .
2. The rise in pressure gradient is observed with increase in  $\beta_1$  and  $\lambda_1$  and a reduction is observed with increase in  $\beta$ ,  $\phi$  and  $Q$ .

3. Maximum resistance to the flow is observed at  $x = 0.5$ , where as, a small pressure gradient is observed at  $x < 0.2$  and  $x > 0.8$ .
4. A linear dependence of pressure rise per unit wavelength is observed, pressure rise increases with increase in  $\beta$  and  $\phi$  and suppresses in magnitude is observed for  $\beta_1$  and  $\lambda_1$ .
5. In size of bolus formed above and below  $y = 0$  there is an increase with increase in  $\beta$  and  $\phi$  while decrease with the flow rate  $Q$ .
6. The major role of the slip conditions is observed to slow down the flow velocity and increase the peristaltic pumping rate.

## 8.4 Concluding remarks of chapter five

In chapter five, analytical series solutions are presented for the peristaltic flow of Carreau fluid in gap between two eccentric tubes. The problem is measured under the assumptions of long wave length and low Reynolds number. The comparison of present analysis is also made with the existing literature. The main findings of the above work are as listed below:

1. It is measured that in peristaltic pumping, the pressure rise curves rise up with  $\delta$  but fall down with  $We$  and  $n$ .
2. It is observed that pressure rise is a decreasing function of  $We$ ,  $n$  and  $\theta$  while increasing function of radius  $\delta$ .
3. From graphical results, it is seen that velocity profile is decreasing with the increase in  $We$  and  $n$  in left half of the domain but reverse attitude is measured in the right half while it increases with  $\delta$  throughout the region.
4. It is depicted that the number of bolus is changing inversely with  $We$  and  $Q$  but dimensions of the bolus increase.
5. It is also concluded that if we put  $We = n = 0$  in the present analysis we get the results of previous work done in [78].

## 8.5 Concluding remarks of chapter six

The authors have found the effects of heat and mass transfer on the peristaltic flow of nanofluid in a rectangular channel in chapter six. The equations of motion are evaluated in dimensionless form in a wave frame of reference. The obtained partial differential equations are solved with the help of well known homotopy perturbation method. The effects of all pertinent parameters are measured through graphs for velocity, temperature and nano particles concentration both in two and three dimensions. From the above analysis, following major points are evaluated:

1. The pressure rise increases with the increase in local nano particle Grashof number  $B_r$  but opposite attitude is seen for local temperature Grashof number  $G_r$  and radius of the inner tube  $\delta$ .
2. Pressure gradient reduces with  $Q$ ,  $G_r$ ,  $\delta$ ,  $B_r$ ,  $V_1$  and  $\epsilon$  while increases with the amplitude ratio  $\phi$ .
3. The presence of porous medium affects in decreasing the velocity of the nanofluid while the more values of flow rate  $Q$ ,  $G_r$ ,  $B_r$  and  $V_1$  results in rising up the profile of velocity. However, the distance parameter  $\epsilon$  reduces the velocity of the flow in left part of the domain and lifts up in the remaining area.
4. Temperature distribution decreases with  $\epsilon$  and  $\phi$  but increases with the Brownian motion parameter  $N_b$  and thermophoresis parameter  $N_t$ .
5. The effect of  $N_t$ ,  $\epsilon$  and  $\phi$  on nano particles concentration is similar to that of temperature profile but  $N_b$  leaves the inverse impact on the nano particles concentration.
6. Trapping boluses are reduced in numbers but enlarge their dimensions with the numerical increase in  $B_r$  and  $G_r$ .

## 8.6 Concluding remarks of chapter seven

The mathematical model of peristaltic flow of an unsteady nanofluid between eccentric tubes having porous space has been analyzed in chapter seven. All the results are obtained analytically



and discussed the contribution of various emerging parameters graphically. However, the data for the pressure rise is obtained by numerical treatment whose variation have been prescribed through table. Following are the main results evaluated in this investigation:

1. The peristaltic pumping rate increases with the increase in porosity parameter  $k$ .
2. With the increase in values of porosity parameter  $k$ , change in pressure becomes large but it diminishes with  $Q$ ,  $G_r$ ,  $\delta$ ,  $B_r$ ,  $V_1$  and  $\epsilon$  while direct relation is seen between pressure gradient and amplitude ratio  $\phi$  at the corners as compared with the central part of the domain.
3. The presence of porous medium affects in decreasing the velocity of the nanofluid while the more values of flow rate  $Q$ ,  $G_r$ ,  $B_r$  and  $V_1$  results in rising up the profile of velocity. However, the distance parameter  $\epsilon$  reduces the velocity of the flow in left part of the domain and lifts up in the remaining area.
4. Temperature distribution is varying inversely with  $\epsilon$  and  $\phi$  but direct relation is seen for Brownian motion parameter  $N_b$  and thermophoresis parameter  $N_t$ .
5. The effect of  $N_t$ ,  $\epsilon$  and  $\phi$  on nano particles concentration remains same as for temperature profile.
6. Trapping boluses are increased in numbers but reduced in their dimensions with the increase in numerical values of porosity parameter  $k$ .

## Bibliography

1. W. M. Bayliss, E. H. Starling, The movements and innervation of the small intestine, *J. Physiol.*, **24** (1899) 99–143.
2. W. C. Tan, M. Takashi, Stokes' first problem for an Oldroyd-B fluid in a porous half-space, *Phys. Fluids*, **17** (2005) 23–101.
3. W. C. Tan, M. Takashi, Stability Analysis of a Maxwell fluid in a porous medium heated from below, *Phys. Lett. A.*, **360** (2007) 454–460.
4. W. C. Tan, M. Xu, Plane surface suddenly set in motion in a viscoelastic fluid with fractional Maxwell model, *Acta Mech. Sinica*, **18** (2002) 342–349.
5. C. Fetecau, A. U. Awan, C. Fetecau, Taylor-Couette flow of an Oldroyd-B fluid in a circular cylinder subject to a time-dependent rotation, *Bull. Math. Soc. Sci. Math. Roumanie*, **52** (2009) 117–128.
6. C. Fetecau, A. U. Awan, M. Athar, A note on Taylor-Couette flow of a generalized second grade fluid due to a constant couple, *Nonlinear Anal. Model. cont.*, **15** (2010) 155–158.
7. C. Fetecau, F. L. Buzescu, A. U. Awan, C. Fetecau, Exact solutions for some oscillating motions of Oldroyd-B fluids, *Int. J. Liq. State Sci.*, **1** (2009) 43–52.
8. M. Hameed, M. Siegel, Y. N. Young, J. Li, M. R. Booty, D. T. Papageorgiou, Influence of insoluble surfactant on the deformation and breakup of a bubble or thread in a viscous fluid, *J. Fluid Mech.*, **594** (2008) 307–340.
9. A. M. Siddiqui, M. Hameed, B. M. Siddiqui, Q. K. Ghori, Use of Adomian decomposition method in the study of parallel plate flow of a third grade fluid, *Commun. Nonlinear Sci. Numer. Simul.*, **15** (2010) 2388–2399.
10. A. H. Kara, C. M. Khalique, Conservation laws and associated symmetries for some classes of soil water motion equations, *Int. J. NonLinear Mech.*, **36** (2001) 1041–1045.
11. P. D. Ariel, Flow of viscoelastic fluids through a porous channel-I, *Int. J. Numer. Meth. Fluids*, **17** (1993) 605–633.

12. P. D. Ariel, Axisymmetric flow of a second grade fluid past a stretching sheet, *Int. J. Eng. Sci.*, **39** (1997) 1335–1357.
13. M. A. Hossain, M. Wilson, Natural convection flow in a fluid saturated porous medium enclosed by non-isothermal walls with heat generation, *Int. J. Therm. Sci.*, **41** (2002) 447–454.
14. M. Khan, K. Maqbool, T. Hayat, Influence of Hall current on the flows of generalized Oldroyd-B fluid in a porous space, *Acta Mech.*, **184** (2006) 1–13.
15. M. Khan, T. Hayat, S. Asghar, Exact solution for MHD flow of a generalized Oldroyd-B fluid with modified Darcy's law, *Int. J. Eng. Sci.*, **44** (2006) 333–339.
16. N. H. Ibragimov, G. Unal, C. Jogleus, Approximate symmetries and conservation laws for Ito and Stratonovich dynamical systems, *J. Math. Anal. Appl.*, **297** (2004) 152–168.
17. A. M. Siddiqui, M. Hameed, B. M. Siddiqui, B. S. Babcock, Adomian decomposition method applied to study nonlinear equations arising in non-Newtonian flows, *Appl. Math. Sci.*, **6** (2012) 4889–4909.
18. M. I. A. Othman, Effect of rotation on plane waves in generalized thermo-elasticity with two relaxation times, *Int. J. Solids Struct.*, **41** (2005) 2939–2956.
19. M. I. A. Othman, Effect of rotation and relaxation time on thermal shock problem for a half-space in generalized thermovisco-elasticity, *Acta Mech.*, **174** (2005) 129–143.
20. M. I. A. Othman, B. Singh, The effect of rotation on generalized micropolar thermoelasticity for a half-space under five theories, *Int. J. Solids Struct.*, **44** (2007) 2748–2762.
21. P. D. Ariel, Analysis of axisymmetric flow of second order fluid near a stagnation point, *Trans. CSME.*, **25** (2001) 125–135.
22. T. Hayat, F. M. Mahomed, S. Asghar, Peristaltic flow of a magnetohydrodynamic Johnson-Segalman fluid, *Nonlinear Dyn.*, **20** (2005) 375–385.
23. F. M. Mahomed, P. G. L. Leach, The linear symmetries of a nonlinear differential equation, *Quaest. Math.*, **8** (1985) 241–274.

24. P. D. Ariel, Rayleigh-Taylor instability of compressible fluids in the presence of a vertical magnetic field, *Appl. Scient. Res.*, **24** (1971) 294–304.
25. M. A. Hossain, D. A. S. Rees, Natural convection flow of a viscous incompressible fluid in a rectangular porous cavity heated from below with cold sidewalls, *Heat Mass Trans.*, **39** (2003) 657–663.
26. T. Mahmood, J. H. Merkin, Similarity solutions in axisymmetric mixed-convection boundary-layer flow, *J. Engg. Math.* **22** (1988) 73–92.
27. A. H. Kara, F. M. Mahomed, G. Unal, Approximate symmetries and conservation laws with applications, *Int. J. Theor. Phy.*, **38** (1999) 2389–2399.
28. S. Asghar, M. R. Mohyuddin, T. Hayat, Effects of Hall current and heat transfer on flow due to a pull of eccentric rotating disks, *Int. J. Heat Mass Trans.*, **48** (2005) 599–607.
29. V. A. Baikov, C. M. Khalique, Some invariant solutions for unsaturated flow models with plant root extraction, *Quaes. Math.*, **24** (2001) 9–19.
30. R. Naz, F. M. Mahomed, D. P. Mason, Comparison of different approaches to conservation laws for some partial differential equations in fluid mechanics, *Appl. Math. Comput.*, **205** (2008) 212–230.
31. M. A. Hossain, M. Z. Hafiz, D. A. S. Rees, Buoyancy and thermocapillary driven convection flow of an electrically conducting fluid in an enclosure with heat generation, *Int. J. Therm. Sci.*, **44** (2005) 676–684.
32. G. Unal, Symmetries of Ito and stratonovich dynamical systems and their conserved quantities, *Nonlinear Dynam.*, **32** (2003) 417–426.
33. C. M. Khalique, F. M. Mahomed, Soil water redistribution and extraction flow models: Conservation laws, *Nonlinear Anal. Real World Appl.*, **10** (2009) 2021–2025.
34. F. Yin, Y. C. Fung, Peristaltic waves in circular cylindrical tubes, *J. Appl. Mech.* **36** (1969) 579–587.
35. J. C. Burns, T. Parkes, Peristaltic motion, *J. Fluid Mech.*, **29** (1967) 731–743.

36. L. M. Srivastava, V. P. Srivastava, Peristaltic transport of a particle-fluid suspension, *J. Biomech. Engg.*, **111** (1989) 157–65.
37. N. A. S. Affi, N. S. Gad, Interaction of peristaltic flow with pulsatile magneto-fluid through a porous medium, *Acta Mech.*, **149** (2001) 229–237.
38. J. C. Misra, S. K. Pandey, Peristaltic transport of blood in small vessels: study of a mathematical model, *Comput. Math. Appl.*, **43** (2002) 1183–1193.
39. Kh. S. Mekheimer, Peristaltic flow of blood under effect of a magnetic field in a non-uniform channels, *Appl. Math. Comput.*, **153** (2004) 763–777.
40. S. Nadeem, N. S. Akbar, Effects of heat transfer on the peristaltic transport of MHD Newtonian fluid with variable viscosity: application of Adomian decomposition method, *Commun. Nonlinear Sci. Numer. Simul.*, **14** (2009) 3844–3855.
41. M. V. Subba Reddy, M. Mishra, S. Sreenadh, A. R. Rao, Influence of lateral walls on peristaltic flow in a rectangular duct, *Int. Fluids Engg.*, **127** (2005) 824–827.
42. V. Aranda, R. Cortez, L. Fauci, Stokesian peristaltic pumping in a three-dimensional tube with a phase shifted asymmetry, *Phys. Fluids*, **23** (2011) 081901–10.
43. Kh. S. Mekheimer, S. Z. A. Husseny, A. I. Abd el Lateef, Effect of lateral walls on peristaltic flow through an asymmetric rectangular duct, *Appl. Bionics Biomech.*, **8** (2011) 295–308.
44. S. Akram, Kh. S. Mekheimer, S. Nadeem, Influence of lateral walls on peristaltic flow of a couple stress fluid in a non-uniform rectangular duct, *Appl. Math. Info. Sci.*, **8** (2014) 11–27.
45. T. W. Latham, Fluid motion in a peristaltic pump, M.Sc, Thesis, M.I.T, Cambridge, (1966).
46. S. Srinivas, M. Kothandapani, Peristaltic transport in an asymmetric channel with heat transfer, *Int. Commun. Heat. Mass. Trans.*, **35** (2008) 514–522.

47. S. Maiti, J. C. Misra, Peristaltic flow of a fluid in a porous channel: A study having relevance to flow of bile within ducts in a pathological state, *Int. J. Engg. Sci.*, **49** (2011) 950–966.
48. S. Srinivas, R. Gayathri, Peristaltic transport of a Newtonian fluid in a vertical asymmetric channel with heat transfer and porous medium, *Appl. Math. Comput.*, **215** (2009) 185–196.
49. S. Jothi, A. R. Prasad, M. V. S. Reddy, Peristaltic flow of a Prandtl fluid in a symmetric channel under the effect of a magnetic field, *Adv. Appl. Sci. Res.*, **3** (2012) 2108–2119.
50. O. Eytan, D. Elad, Analysis of intra-uterine fluid motion induced by uterine contractions, *Bull. Math. Biol.*, **61** (1999) 221–238.
51. S. K. Pandey, M. K. Chaube, Peristaltic flow of a micropolar fluid through a porous medium in the presence of an external magnetic field, *Commun. Nonlinear Sci. Numer. Simul.*, **16** (2011) 3591–3601.
52. N. S. Akbar, S. Nadeem, Z. H. Khan, Numerical simulation of peristaltic flow of a Carreau nanofluid in an asymmetric channel, *Alex. Engg. J.*, **53** (2014) 191–197.
53. N. S. Akbar, S. Nadeem, Endoscopic effects on peristaltic flow of a nanofluid, *Commun. Theor. Phys.*, **56** (2011) 761–768.
54. Kh. S. Mekheimer, Y. Abdelmaboud, Peristaltic flow of a couple stress fluid in an annulus: Application of an endoscope, *Physica A*, **387** (2008) 2403–2415.
55. Y. A. Elmaboud, Influence of induced magnetic field on peristaltic flow in an annulus, *Commun. non-linear Sci. Numer. Simul.*, **17** (2011) 685–698.
56. M. H. Haroun, Non-linear peristaltic flow of a fourth grade fluid in an inclined asymmetric channel, *Comput. Mater. Sci.*, **39** (2007) 324–333.
57. Kh. S. Mekheimer, Y. A. Elmaboud, Peristaltic flow through a porous medium in an annulus: application of an endoscope, *Appl. Math. Info. Sci.*, **2** (2008) 103–121.

58. C. Vasudev, U. R. Rao, G. P. Rao, M. V. S. Reddy, Peristaltic flow of a Newtonian fluid through a porous medium in a vertical tube under the effect of a magnetic field, *Int. J. Current Scientific Res.*, **1** (2011) 105–110.
59. S. R. Mahmoud, N. A. S. Affi, H. M. Al-Isede, Effect of porous medium and magnetic field on peristaltic transport of a Jeffrey fluid, *Int. J. Math. Anal.*, **5** (2011) 1025–1034.
60. O. Manca, S. Nardini, D. Ricci, A numerical study of nanofluid forced convection in ribbed channels, *Appl. Therm. Engg.*, **37** (2012) 280–292.
61. X. Wang, A. S. Mujumdar, Heat transfer characteristics of nanofluids: a review, *Int. J. Therm. Sci.*, **46** (2007) 1–19.
62. S. Nadeem, E. N. Maraj, The mathematical analysis for peristaltic flow of nanofluid in a curved channel with compliant walls, *Appl. Nanosci.*, **4** (2014) 85–92.
63. N. S. Akbar, S. Nadeem, T. Hayat, A. A. Hendi, Peristaltic flow of a nanofluid in a non-uniform tube, *Heat Mass Trans.*, **48** (2012) 451–459.
64. J. Buongiorno, Convective transport in nanofluids, *J. Heat Trans.*, **128** (2006) 240–250.
65. M. Kothandapani, S. Srinivas, Peristaltic transport of a Jeffrey fluid under the effect of magnetic field in an asymmetric channel, *Int. J. Nonlinear. Mech.*, **43** (2008) 915–924.
66. S. Nadeem, S. Akram, T. Hayat, A. A. Hendi, Peristaltic flow of Carreau fluid in a rectangular duct, *J. Fluids Engg.*, **134** (2012) 7 pages.
67. K. Vafai, *Handbook of porous media*, Taylor and Francis e-Library (2005).
68. T. Hayat, A. A. Khan, S. Asghar, Peristaltic transport of a third order fluid under the effect of a magnetic field, *Comput. Math. App.*, **53** (2007) 1074–1087.
69. H. Alfven, Existence of electromagnetic-hydrodynamic waves, *Nature*, **150** (1942) 405–406.
70. R. Ellahi, A. Zeeshan, *Analytical solutions for non-linear partial differential equations: Basics, concepts and methods*, Lap Lambert academic publishing (2012).

71. M. O. Ahmad, R. M. Corless, The Method of Modified Equations in Maple. Electronic Proceedings 3rd International IMACS Conference on Application of Computer Algebra, Maui, USA. (1997) July 24–26.
72. Z. J. Wu, J. Q. Ye, J. G. Cabrera, 3D analysis of stress transfer in the micromechanics of fiber reinforced composites by using an eigen-function expansion method, *J. Mech. Phys. Solids*, **48** (2000) 1037–1063.
73. J. H. He, Homotopy perturbation method for solving boundary value problems, *Phys. Lett. A*, **350** (2006) 87–88.
74. J. H. He, A note on the homotopy perturbation method, *Therm. Sci.*, **14** (2010) 565–568.
75. J. H. He, An elementary introduction to the homotopy perturbation method, *Comput. Math. App.*, **57** (2009) 410–412.
76. D. D. Ganji, A. Sadighi, Application of He's homotopy perturbation method to nonlinear coupled systems of reaction diffusion equations, *Int. J. Nonlinear Sci. Numer. Simul.*, **7** (2006) 411–418.
77. A. H. Shapiro, M. Y. Jaffrin, S. L. Weinberg, Peristaltic pumping with long wavelengths at low Reynolds number, *J. Fluid Mech.*, **37** (1969) 799–825.
78. Kh. S. Mekheimer, Y. Abdelmaboud, A. I. Abdellateef, Peristaltic transport through an eccentric cylinders: Mathematical model, *Appl. Bionics Biomech.*, **10** (2013) 19–27.
79. S. Nadeem, S. Akram, Peristaltic flow of a Jeffrey fluid in a rectangular duct, *Nonlinear Anal. Real World Appl.*, **11** (2010) 4238–4247.
80. E. F. El-Shehawy, N. T. El-Dabe, I. M. El-Desoky, Slip effects on the peristaltic flow of a non-Newtonian Maxwellian fluid, *Acta Mech.*, **186** (2006) 141–159.